NASA CR-121108
R73AEG282

AERO-ACOUSTIC DESIGN AND TEST OF A MULTIPLE SPLITTER EXHAUST NOISE SUPPRESSOR FOR A 0.914m DIAMETER LIFT FAN

by

D. L. STIMPERT AND W. R. UHL

GENERAL ELECTRIC COMPANY

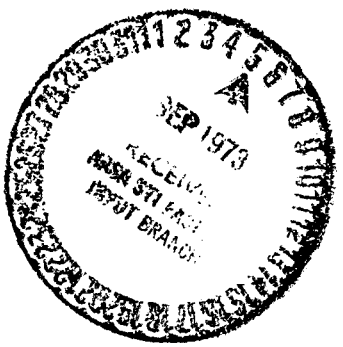

prepared for

NATIONAL AERONAUTICS AND SPACE ADMINISTRATION

NASA-Lewis Research Center

CONTRACT NAS3-15556

IRVIN J. LOEFFLER - PROJECT MANAGER

1. Report No.	2. Government Accession No.	3. Recipient's Catalog No.
NASA CR-121108		

4. Title and Subtitle	5. Report Date
Aero-Acoustic Design Test of a Multiple Splitter Exhaust Noise Suppressor for a 0.914m Diameter Lift Fan	January 1973
	6. Performing Organization Code
7. Author(s)	8. Performing Organization Report No.
D.L. Stimpert and W.R. Uhl	73AEG282
	10. Work Unit No.
9. Performing Organization Name and Address	11. Contract or Grant No.
General Electric Company Aircraft Engine Group Cincinnati, Ohio 45215	NAS 3-15556
	13. Type of Report and Period Covered
12. Sponsoring Agency Name and Address	Contractor Report
National Aeronautics and Space Administration Washington, D.C. 20546	14. Sponsoring Agency Code

15. Supplementary Notes

Project Manager, Irvin J. Loeffler
NASA Lewis Research Center, Cleveland, Ohio

16. Abstract

A lift fan exhaust suppression system representative of that which is required to meet future VTOL aircraft noise goals was designed and tested. The test vehicle was a 1.3 pressure ratio, 36 inch (91.44 cm) diameter lift fan with two chord rotor to stator spacing.

A two splitter fan exhaust suppression system thirty inches (76.2 cm) long achieved 10 PNdB exhaust suppression in the aft quadrant compared to a design value of 20 PNdB. It was found that a broadband noise floor limited the realizable suppression. An analytical investigation of broadband noise generated by flow over the treatment surfaces provided very good agreement with the measured suppression levels and noise floor sound power levels.

A fan thrust decrement of 22% was measured for the fully suppressed configuration of which 11.1% was attributed to the exhaust suppression hardware.

17. Key Words (Suggested by Author(s))	18. Distribution Statement
Propulsion, Lift Fan, VTOL, Noise Tip Turbine, Acoustic, Noise Suppression Multiple Exhaust Splitter	Unclassified - Unlimited

19. Security Classif. (of this report)	20. Security Classif. (of this page)	21. No. of Pages	22. Price*
Unclassified	Unclassified	278	

* For sale by the National Technical Information Service, Springfield, Virginia 22151

TABLE OF CONTENTS

TABLE OF CONTENTS - Concluded

LIST OF TABLES

LIST OF FIGURES

LIST OF FIGURES (Cont'd)

LIST OF FIGURES (Cont'd)

LIST OF FIGURES (Cont'd)

LIST OF FIGURES (Cont'd)

LIST OF FIGURES (Cont'd)

LIST OF FIGURES (Cont'd)

LIST OF FIGURES (Cont'd)

LIST OF FIGURES (Cont'd)

LIST OF FIGURES (Cont'd)

LIST OF FIGURES (Cont'd)

LIST OF FIGURES (Cont'd)

LIST OF FIGURES (Cont'd)

SECTION I

SUMMARY

A test program sponsored by NASA Lewis was conducted at the General Electric Flight Test Center acoustic test site. The test vehicle was the LF336/B lift fan which is a 36 inch (91.44 cm) diameter fan with two chord rotor to stator spacing. Design pressure ratio was 1.3 at a tip speed of 950 feet per second (290 m/sec).

Test objectives were to: (1) design and test a highly suppressed lift fan exhaust suppression system representative of that required to achieve future noise goals; (2) determine the variation in noise reduction with exhaust splitter length; (3) determine the magnitudes and directivity of the inlet and exhaust radiated fan noise levels, and (4) determine the jet noise floor level with coplanar annular jets of different temperature levels.

A two splitter fan exhaust suppression system 30 inches (76.2 cm) long achieved 10 PNdB suppression at the 110 degree microphone (relative to the fan inlet) at 5300 RPM fan speed (87.7% design fan speed). This was less than the design predicted suppression of 20 PNdB. Pure tone suppression of 28 dB was realized for the same configuration compared to a design estimate of 32 dB. The lack of fan broadband noise reduction was the principal difference between measured and design estimated suppression.

Analytical investigations indicated that the apparent lack of broadband suppression was due to a broadband noise floor generated by flow over the treatment surfaces. This analysis also indicated that the primary factor in reducing the flow-generated broadband noise would be to lower the flow Mach number over the treatment surfaces. Suppressor geometry changes are a secondary factor in lowering this noise floor.

Fan inlet radiated noise was successfully suppressed by a massive, acoustically treated inlet box which allowed fan exhaust radiated levels and directivity patterns to be measured. In the forward quadrant at the 50 degree microphone position, the unsuppressed fan exhaust radiated noise was 8 PNdB below the unsuppressed inlet radiated noise. Directivity indices were obtained

for both the total of the inlet and exhaust radiated fan noise levels and the fan exhaust radiated noise levels which will allow the evaluation of separate inlet and exhaust suppression effects.

Predictions of jet noise and core noise were made which indicated that the observed broadband floor was not jet noise and/or core noise above 1000 Hz.

Fan performance was poorer than expected because of the fan discharge exit conditions which were established by the 2 inch (5.08 cm) wide acoustic splitter bases. The exit conditions resulted in considerably below ambient static pressures at the splitter bases and at the fan hub. These adverse static pressure gradients were alleviated by the addition of eight radial U-channels at the fan and tip turbine exit plane. The two-splitter, 30 inches (76.2 cm) long fan exhaust suppression system and the acoustically treated fan inlet box exhibited a 22.0 percent fan thrust deficiency at a corrected fan speed of 5200 RPM. However, the thrust loss attributable to the exhaust suppressor (adapter section and treated section) was estimated to be 11 percent.

SECTION II

INTRODUCTION

In order for vertical takeoff and landing (VTOL) aircraft to have a viable position in the commercial aviation fleets of the future, the aircraft will probably have to meet noise limits even more stringent than those applied to conventional takeoff and landing aircraft. Extensive research has been conducted on the generation of lift fan noise and its alleviation by judicious selections of fan geometry using the LF336 lift fan as a test vehicle. The specific objectives of previous test programs as reported in References 1 through 5 were: to better understand the sources of propagation of lift fan noise; to substantiate analytical noise prediction methods; and to evaluate noise reduction potentials for lift fans due to changes in stator configuration and rotor-stator spacing. In addition to these fan design modifications, it will be necessary to install acoustically treated ducts and splitters in the fan exhaust to meet the anticipated noise goals for advanced VTOL commercial aircraft. Advanced study programs on both integral and remote lift fan systems (References 6 and 7) showed that multi-splitter arrangements are usually required to suppress exhaust radiated fan noise. Due to length limitations associated with lift fan engine installation, these splitters should become an integral part of the fan exhaust flowpath. This requires detailed information to achieve the desired noise reduction with minimum weight and performance penalties.

In order to provide some of this design information, a program sponsored by the NASA Lewis Research Center was conducted at the General Electric Flight Test Center to:

1. Design and test a highly suppressed lift fan exhaust system representative of that required to achieve noise goals for future lift fan applications, thus providing both acoustic and aerodynamic design data.

2. Determine the variation in achievable noise reduction with exhaust duct/splitter length.

3. Determine the separate far field magnitudes and directivity of the inlet and exhaust radiated fan noise levels to allow an evaluation of separate suppression requirements.

4. Determine the jet noise floor level with coplanar annular jets having different temperature levels to establish a maximum level of PNdB suppression with treated fan exhaust.

Testing began June 20, 1972, and was completed August 11, 1972. One-third octave band data and narrowbands from the current test are documented and tabulated in Reference 8.

Of the three LF336 configurations available for testing, the LF336/B fan was selected as the test vehicle. It is a 1.3 pressure ratio fan with two chord spacing thus representing the cycle and geometry favored for advanced lift fan designs. Further noise reduction devices, such as optimized vane-blade number and vane lean, are not present on this fan but are thought to have a secondary effect on the fan inlet and exhaust noise split at two chord spacing.

Included in this report are details of the hardware, data acquisition equipment, and test schedule to meet the test objectives presented above. Both performance and acoustic data are analyzed in light of the test objectives. To account for an apparent lack of suppression with increasing treatment length, a study was conducted which indicated the presence of a noise floor generated by flow over the treatment surfaces.

SECTION III

TEST CONFIGURATION

A. Test Set-Up

The LF336/B Lift Fan Discharge Noise Suppression Test set-up was similar to that used in previous LF336/B and LF336/C testing at General Electric Edwards Flight Test Center (EFTC), California. The fan axis was mounted parallel to the ground and at a height of 10 feet (3.05 m). Also the J85 engine was installed parallel to the ground at 90° to the fan axis. All fan hardware and exhaust suppressors were mounted on the active portion of the thrust frame. Figure 1 shows the test site set-up with the un-suppressed fan installed on the thrust frame and the J85 attached to the fan scroll inlet. The instrumentation used for this test is listed in Table I.

B. Lift Fan

The LF336/B, S/N 002, lift fan, (P/N 4013057-173) is a single-stage 36 inch diameter (91.44 cm) tip turbine driven fan designed to achieve a 1.3-pressure-ratio. The fan is driven by the full flow of one dry J85-5 turbojet engine. A fan cross section is shown in Figure 2. Fan design point definition is presented in Table II. There are 42 rotor blades, with a fundamental blade passing frequency of 4230 Hz at 100% RPM. There are 45 stator vanes with a rotor-stator axial spacing of 2.0 blade chords.

C. Inlet Suppressor

Three components were used to form the fan inlet flowpath and provide sufficient front end radiated noise suppression. An inlet adapter locates a large jet engine bellmouth (GE4) and an acoustic plenum so as to minimize their line of sight interference between the far field microphones and the test vehicle. Figure 3 shows a sketch of the acoustic plenum, the GE4 bellmouth and the inlet adapter installed to the fan inlet plane.

The acoustic plenum which was positioned on the ground in front of the inlet duct was fabricated from 0.75 inch (1.91 cm) plywood and lined with a bulk absorber acoustic material. Figure 4 shows a view of the inlet suppressor. The acoustic plenum is 10 feet (3.05 m) x 10 feet (3.05 m) x 20 feet (6.1 m). The edges of the 10 feet (3.05 m) x 10 feet (3.05 m) inlet to the plenum (Figure 5) were well rounded with a 10 inch (25.4 cm) radius to reduce losses and preclude flow separation at the inlet. The bulk suppressor, Scottfelt 3-900, was attached to the inside of the plenum with 3M77 spray adhesive. Scottfelt thickness was 1 inch (2.54 cm) on the sides and 2 inches (5.08 cm) on the end opposite the fan inlet. A 40 mesh steel wire screen 0.010 inch (0.025 cm) diameter wire covered the Scottfelt to prevent erosion. A wooden frame positioned the inlet plenum in front of the fan.

The GE4 bellmouth was bolted to the inlet plenum through a flanged 85 inch (215.9 cm) diameter hole in the end of the plenum. The bellmouth was fabricated from fiberglass, honeycomb, aluminum rings and fittings, and had a 111.44 inch (283.1 cm) diameter inlet contoured to a cylindrical duct diameter of 60.56 inch (153.8 cm). Figure 6 shows a front end view of the bellmouth. Tufts were added to the inner surface to provide visual observation of the inlet flow condition during fan operation.

The inlet adapter (Figure 7) was slip-fitted to the GE bellmouth and fastened to the thrust stand. In the figure, the adapter and bellmouth were wrapped with a lead-vinyl blanket. The adapter had Scottfelt squeezed between its aft flange and the fan bellmouth to provide the necessary aerodynamic and acoustic seal between the fan and adapter. Since this was not a bolted attachment, it precluded adverse loads being applied to the fan. The adapter was fabricated from a 60.56 inch (153.8 cm) diameter aluminum cylinder flanged at both ends and covered with a lead-vinyl blanket.

The entire inlet suppression system as shown in Figure 8 was designed to produce a minimal total pressure drop from the entrance of the inlet box to the entrance to the fan inlet plane. The dimensions of the inlet suppressor were selected to be 10 feet (3.05 m) x 10 feet (3.05 m) x 20 feet (6.1 m) because its massive size would exhibit a very small total pressure loss and

its size would allow it to be moved about the test site without much difficulty. Analysis of the total pressure loss through the inlet system revealed a total pressure loss coefficient of,

$$\bar{\omega}_{INLET} = \Delta P_t/\rho V^2/2 = 0.0052 \quad (1)$$

where $\Delta P_t = P_{T_o} - P_{T_{fan\ inlet}}$

ρ = Fan inlet density

V = Fan inlet velocity

The equations and assumptions that were used for this estimate are discussed in the aerodynamic performance section under estimated losses.

D. Exhaust Suppressor

Figure 9 is a sketch of the exhaust suppression hardware concept showing its relative size compared with the lift fan. The dashed lines indicate surfaces that were acoustically treated. The untreated exhaust adapter between the fan and exhaust suppressor section provided the smooth diameter changes necessary to allow for the added area of the two treated splitters in the fan flow annulus. Figure 10 shows the entire exhaust suppressor assembly.

1. Adapter

Figure 11 shows the flowpath dimensions for the exhaust adapter and the lift fan rear frame to which it was attached. The adapter was fabricated from AISI 1010 steel having 0.030 inch (0.0762 cm) thickness for the flowpath surfaces which were rolled and welded together, positioned by three equally spaced struts. Figure 12 shows the transition assembly.

Figure 13 is a photograph looking into the front of the adapter which shows the wiggle strip that separates the outer fan and the inner turbine flowpaths. This allowed the hot turbine flowpath to grow thermally relative to the cold fan flowpath. Fifteen turnbuckles were used to attach the outer turbine shell to the rear frame. This attachment was only for sealing. Three

hollow struts provided access for pressure lines to pass through to the static pressure taps along the flowpath surfaces. The weight of the adapter and the three exhaust suppressors was transferred to the thrust stand by tie rods to the overhead structure (Figure 14).

The aerodynamic design criterion for the exhaust adapter revolved about the acoustic design of the suppression system which required two exhaust splitters that divided the fan stream exhaust into three equally spaced passages with each splitter being 2 inches (5.08 cm) wide. The boundary layer thickness along each passage wall was taken into account so that a constant effective area could be maintained for each passage, which resulted in 0.060 inches (0.152 cm) being added to the radii of the three passages. A one-dimensional analysis provided an estimated total pressure loss of 0.8% or 0.1528 psi (1.05 kN/m^2) across the inlet adapter which was based on an inlet Mach number of 0.622 and an exit static pressure equal to 14.96 psia (101.3 kN/m^2). A wake behind each splitter base was understood to occur but no base suck down was anticipated.

2. Suppressor Description

The three identical exhaust suppressors (Figure 9 & 10) were designed to have co-planar exhausts for both the fan and turbine streams. All fan and turbine flowpath surfaces were acoustically treated. Acoustic treatment consisted of one inch (2.54 cm) of Scottfelt 3-900 for each splitter and the inner fan flowpath surface, and one inch (2.54 cm) of Cerafelt 400 for each surface of the turbine and outer fan flowpath. All treated surfaces were covered with a perforated sheet of 0.030 inch (0.076 cm) AISI 1010 material (Figure 15). Perforation diameter was 0.063 inches (0.16 cm) with a porosity of 30%. Each splitter had a 0.030 inch (0.076 cm) septum which separated each side and precluded flow through the splitter (Figure 9). Three 0.25 inch (0.635 cm) wide by 4 inch (10.16 cm) AISI 1010 struts rigidly connected the rings together as shown in Figure 15. One section of the exhaust suppressors contained hollow struts (Figure 16) which allowed the base pressure instrumentation to pass through. Figure 14 shows the fan system in its fully suppressed configuration,i.e., with exhaust adapter and three ten inch (25.4 cm) suppressor sections. Six quick disconnect latches on each exhaust duct provided easy assembly and disassembly during test operation. Figure 17 shows the exhaust section barrel assembly.

3. Acoustic Design

Peak suppression values (estimated suppression amplitude corresponding to the design frequency) for combinations of treated length-to-duct height and height-to-wavelength ratios are given in Figure 18. These suppression values are based on theoretical predictions and measured engine and duct data. Several data points are given for both engine and acoustic duct configurations that were treated with the bulk type absorption materials, Scottfelt 3-900 and Cerafelt 400. The suppression values were used to obtain the predicted peak suppression values as a function of treatment length as shown in Figure 19. $H/\lambda_o = 0.90$, corresponding to the configuration in Figure 20 and to a tuning frequency of 4000 Hz was used. To define the required treatment material thickness Figures 21 and 22 were used. Scottfelt 3-900, a bulk-type absorber material, was selected because of its superior suppression bandwidth characteristics and low cost relative to single-degree-of-freedom and multi-degree-of-freedom resonator systems. Figure 21 gives the required reactance for a treatment system as a function of the acoustic parameter, H/λ_p, where $\lambda_p = (1 + M)\ \lambda_o$. Thus, for a given duct height, Mach number, and tuning frequency the required reactance can be defined. The data points shown in Figure 21 were obtained as follows. First the H/λ_p parameters were defined based on acoustic duct test results for various configurations. Next the acoustic reactance corresponding to the peak attenuation frequency was defined using acoustic impedance tube data results with a flow correction for each treatment configuration. Since the range of data in Figure 21 did not include the design point, ($H/\lambda_p = 0.64$), an extrapolation of the "best fit" curve for the data was required. Having defined the required reactance, Figure 22, (which gives the reactance as a function of λ_p at a Mach number of 0.4 for various treatment thicknesses) was used to define the required treatment thickness. The reactance values as shown in Figure 22 were obtained from acoustic impedance tube data with a flow correction factor included.

The required treatment thickness as indicated in Figure 22 is approximately one inch (2.54 cm). A face sheet having 30 percent open area which offers very little acoustic resistance was selected for both splitters and the hub wall to serve as a protector for the Scottfelt. Given in Figure 23 are

the measured transmission loss values for 1.0 inch (2.54 cm) thick Scottfelt 3-900 at a flow Mach number of 0.4. The data shows that the peak attenuation occurs at approximately 4000 Hz. The duct height was four inches (10.2 cm) for this particular treatment configuration. Cerafelt 400 was the suppression material used in the turbine flowpath and the outer fan wall because of its ability to withstand higher temperatures. The acoustic properties of Cerafelt 400 are very similar to those of Scottfelt 3-900, both having approximately the same density and both being bulk-type absorber materials. A comparison of measured acoustic reactance values for both Scottfelt 3-900 and Cerafelt 400 is given in Figure 24.

Suppression bandwidth characteristics for Scottfelt 3-900 based on acoustic duct and engine data are given in Figure 25. The data corresponds to a Mach number range of 0.3 to 0.4 and a H/λ_o range of from 1.0 to 2.0. The bandwidth is given in terms of the peak suppression amplitude which corresponds to the tuning frequency of $f = f_p$. Thus, knowing the peak suppression value as predicted from Figure 18, the suppression level versus frequency was calculated using the results in Figure 25. The maximum Mach number used in this design study was 0.40. It was assumed that for higher Mach number values the peak attenuation level would be slightly reduced but that the acoustic bandwidth would be increased. The peak attenuation frequency was assumed not to change for an increase in Mach number.

E. Test Site and Test Facility

The test program was conducted at an outdoor test facility designed and constructed for testing full scale lift fans and engines. The site (Figure 26) is in an area free of buildings and obstructions located at the General Electric Edwards Flight Test Center at Edwards Air Force Base, California. The area surrounding the acoustic test site consists of desert sand and brush. Figure 26 is a photograph taken across the top of the control room which extends only 30 inches (76.2 cm) above the ground. The photograph shows the GE4 bellmouth positioned in front of the LF336 fan and shows the J85 with its inlet suppressor removed. To the right in the photograph is the concrete apron around the original LF336 test site which had a previously committed test program in operation during this test period.

The test stand is attached to four concrete columns which protruded above the asphalt apron. The fan was mounted 10 feet (3.05 m) above the ground with the fan flow parallel to the ground. Flexure plates transfer the fan thrust from the thrust stand to a single loadcell. One J85-5 engine supplies the driving gas to the fan through a "Y" duct that distributes the flow equally to each half of the 360° scroll. A sound suppressor (Figure 27) was mounted to the J85 inlet to eliminate the engine compressor as a source of noise during these tests. The lead-vinyl blanket shown around the suppressor and inlet to the J85 was required to preclude noise transmission from the J85 bellmouth.

SECTION IV

INSTRUMENTATION & TEST

A. Performance

1. Thrust & Airflow

The fan axial thrust was measured by a calibrated load cell, one end being mounted on the static section of the test frame and the other end mounted to the active portion of the frame. A GE4 bellmouth was fitted to the fan inlet so that the inlet suppression box could be utilized. A transition section was attached to the fan inlet and the GE4 bellmouth was fitted over it and attached to the inlet box. Between the transition section and the GE4 bellmouth, a slip seal, shown in Figure 28, was utilized to minimize effects of friction and any movement since the bellmouth was not attached to the active portion of the thrust frame. For this reason, the momentum across the bellmouth was calculated and included in the thrust measurement. The momentum term was calculated from the measured static pressure in the bellmouth and its cross sectional area. The correction that was calculated was derived from the basic thrust equation, i.e.,

$$F = \dot{m}V + (P_e - P_o)\,A \qquad (2)$$

where

F	=	force
$\dot{m}$	=	mass flow rate
V	=	Velocity
P_e	=	exit static pressure
P_o	=	inlet static pressure
A	=	GE4 bellmouth area

Since the inlet velocity is relatively low, incompressible relations may be used such that

$$\dot{m}V = \rho V^2 A = 2 q_B A \qquad (3a)$$

and $$P_o - P_e = q_B \quad (3b)$$

Then,

$$F = 2q_BA - q_BA = q_BA \quad (4)$$

where, F = Force on GE4 Bellmouth

q_B = GE4 bellmouth dynamic pressure

The dynamic pressure was measured directly in the duct by the GE4 bellmouth static pressure taps, since the static pressure was referenced to barometric pressure. The GE4 bellmouth static pressure tap location is shown in Figure 28.

The fan inlet airflow was measured only when the GE4 bellmouth and the transition section were mounted to the fan inlet with the inlet suppressor. The same static pressure measurement used for the thrust correction was used to calculate the airflow. The airflow was calculated as follows:

$$\dot{m} = [2\, g\, \rho\, q_B]^{1/2} C_f\, A \quad (5)$$

where, $\rho = (P_o - q_B)/(RT_o)$ = GE4 bellmouth air density

$q_B = (P_o - P_B)$ = GE4 bellmouth static pressure reading

A = GE4 bellmouth area

C_f = 0.985 = GE4 bellmouth flow coefficient.

2. Suppressor Pressure Taps

Figure 29 shows the static pressure tap locations in the 12 inch (30.5 cm) adapter transition section. These taps were located at two circumferential locations 90° apart in case a non-uniform flow distribution occurred. Figure 29 also shows the location of the exit plane static pressure taps. One 10 inch (25.4 cm) exhaust suppressor section was instrumented for these static pressure taps and that section was used in each configuration that utilized

exhaust suppression so that an exit static pressure distribution could be obtained. All of the static pressures were channeled into the data acquisition system by the use of scani-valves which resulted in each static pressure being read individually.

3. Traverse Probe

Fan exhaust total and static pressure and total temperature profiles were obtained for each test from non-nulling exhaust traversing probe. The traverse probe which is shown in Figures 30 and 31 contained 2 elements, one for total and static pressure, the second for total temperature. The transducers used to measure the total and static pressures were mounted directly on the traverse probe actuator to keep the leads from the probe to the transducer as short as possible in order to minimize response time. The actuation system containing the traverse probe was mounted on a bracket, designed so that changes in the axial direction could readily be made as different lengths of exhaust suppression were added. The axial distance between the fan exit plane and the traverse probe was about 1/2 inch (1.27 cm). The speed at which the traverse probe moved averaged 0.22 inch per second (0.56 cm/sec). Figure 32 shows the traverse probe mounted at the fan discharge plane.

4. Calibration

Prior to testing, all instrumentation was calibrated using calibration standards traceable to the National Bureau of Standards. All calibrations were assumed to be a straight line, i.e., counts versus measured parameter, and the error introduced by this assumption was calculated for each device that was calibrated. All data from each calibration was entered into a computer program which calculated the slope and intercept of the straight line and the full scale error. Then each measured parameter was related to an equation of the form;

$$MP = K1\ (counts) + K2 \qquad (6)$$

where,

MP = Measured Parameter (thrust, temperature, etc)

K1 = Slope = $\Delta MP/\Delta$ counts

counts = digitized output of transducers, load cells, etc.

K2 = intercept = value of measured parameter at zero counts

The maximum error introduced into this test from any instrumentation device was 0.9%. Figures 33, 34 and 35 show the instrumentation recording equipment in the test site control room

5. Test Run Summary

The test runs and configurations investigated during the LF336 Discharge Noise Suppression tests are summarized in chronological order in Table III. The test series began on June 20, 1972 and was completed on August 11, 1972. Total operating time on the fan was 9.3 hours. The changes in the fan configuration which occurred are discussed in detail in the aerodynamic performance section.

B. Acoustic Data Acquisition and Calibration

Acoustic data was recorded from seventeen microphones located on a 150 foot (45.7 m) arc and in a horzontal plane through the fan centerline. The microphones were positioned at ten degree increments with 0 degrees at the fan inlet as shown in the sketch in Figure 36. All data acquisition was made using the Bruel-Kjaer model 4133 microphone system. The 0.5 inch diameter (1.27 cm) microphone cartridges were oriented at zero degree incidence to the noise source. Bruel-Kjaer UA 027 windscreens were used for Test 2 and all successive tests. An AR200 type tape recorder operating at sixty inches per second (152.4 cm per second) was used for data recording. A schematic representation of the total data acquisition system is shown in Figure 37, while Figure 35 shows the recording equipment in the control room.

Prior to the initiation of acoustic testing and also during the test program, a frequency response of each data channel (minus microphone head) was made by the insertion of a Hewlett-Packard Psuedo-Random Pink Noise Generator into each cathode follower and recorded on magnetic tape. Pink noise is composed of all frequencies and shaped for equal energy in each 1/3 octave band.

The free field frequency response of each individual microphone head was derived from a pressure response curve recorded automatically by the electrostatic actuator method traceable to the Bureau of Standards. Free field characteristics are given by the microphone manufacturer.

Individual microphone head sensitivities are determined by the insertion of a Bruel-Kjaer pistonphone on the cartridge mounted to a standard microphone. Windscreen response characteristics are determined from the manufacturer's published curves.

Prior to and subsequent to each day's testing an absolute calibration of each microphone was made by the insertion of a pistonphone and recorded on tape. A barometric correction was made to the pistonphone output per manufacturer's specifications and any microphone whose output voltage deviated more than $\pm$1.5 dB from laboratory standards was replaced.

During test operations, sound was recorded continuously for a period of two minutes except in those cases where marginal winds necessitated completing the runs as soon as possible. In such cases, the recording time was reduced to one minute.

SECTION V

DATA PROCESSING

A. Performance

All performance parameters are recorded simultaneously on a high speed recording system known as the Pulse Code Modulated System or PCM. The PCM system has the capability of recording digital and analog data and data from stepping or switching devices. The switching devices used for pressure measurements are known as scani-valves. The scani-valves are designed to record up to 48 different pressures at the rate of 10 per second so that every pressure is recorded every 4.8 seconds. All straight-through parameters, that is, all parameters not recorded through scani-valves, are recorded continuously at the rate of 100 times per second.

The PCM system receives data from the various instrumentation devices in the form of counts or millivolts and this data is converted to an octal counting system by the PCM before being recorded on magnetic tape. A data reduction program reads the tape, averages each parameter after making several passes through the data, deleting data that is a specified limit away from the mean, converts each parameter to engineering units and performs other programed calculations. For data processing and reduction purposes, each averaged reading consists of data sampled at a 100 per second rate over a specified 60 second time period. During the same time period, traverse probe data is reduced at a 10 per second rate and plotted using the Calcomp plotter.

B. Acoustic

All 1/3 octave band data processing was performed at the Edwards Flight Test Center using a General Radio real time analyzer in conjunction with a Honeywell 316 and SDS 930 computer. Thirty-two second averaging time was used for data processing with data for each angle sampled from the same period of time for each data point.

Data processing included the total system response for each 1/3 octave band, corrections for non-uniformity in the pink noise generator itself, the microphone cartridge corrections, and windscreen corrections (where applicable).

Sound pressure levels at all angles and at frequencies from 50 to 10,000 Hz were corrected to standard day conditions (59° F (288° K) 70% relative humidity) on the 150 feet (45.7m) microphone arc using the results of References 9 and 10. Other acoustic data obtained included the following:

1. Overall sound pressure levels
2. Directivity indices
3. Perceived noise levels
4. Extrapolated 1/3 octave band sound pressure levels, overall sound pressure levels, and perceived noise levels at sideline distances of 100, 200, 300, 500, 750, and 1000 feet (30.5, 61.0, 91.5, 152.4, 228.6, and 304.8 meters).
5. One-third octave band sound power levels corrected to the source and with 150 foot (45.7m) absorption and extra ground attenuation corrections not included.

Repeatability of data was insured by taking one repeat and sometimes two repeat data points at each speed point for a given test configuration. The speed points investigated and number of repeat points for each are given in Table IV. Throughout this report, the perceived noise levels, PNL suppression levels, and 1/3 octave band sound pressure levels represent an average of the original data point and its repeat(s), while the narrowband spectra and SPL suppression levels presented are for specific data points.

Narrowband analysis was done in Evendale using a Federal Scientific UA-6A Ubiquitous Spectrum Analyzer and a 129B Digital Averager. All data was processed using a 20 Hz filter and an averaging time of 12.8 seconds. No humidity or acquisition/reduction response corrections were made to these narrowbands.

Some narrowband analysis was done while testing at Edwards Flight Test Center. These narrowbands (primarily in Appendices C and D) were obtained by using a Spectral Dynamics Analyzer model SD101A which is capable of various bandwidths and which sampled a ten second tape loop.

SECTION VI

ACOUSTIC PERFORMANCE

A. Fan Inlet Noise Suppression

A massive inlet suppressor was designed to eliminate inlet radiated fan noise and permit measurement of exhaust radiated fan noise. Details of the inlet suppressor were discussed in a previous section.

The effect of massive fan inlet suppression on perceived noise level directivity at 5300 RPM fan speed is shown in Figure 38. At the maximum unsuppressed noise forward quadrant angle (50°), a reduction of 7.5 PNdB is realized. Aft quadrant angles show an increase in level as fan inlet suppression is installed indicating that there may be increased turbulence or distortion in the flow to the fan due to the fan inlet suppressor. Similar results are noted for fan speeds of 4200 and 4800 RPM in Figures 39 and 40 respectively. For both these speeds, an increase in aft quadrant level is observed. At 4200 RPM, the reduction at the maximum forward quadrant angle is 7.0 PNdB and at 4800 RPM, it is 8.0 PNdB. Figure 41 compares the unsuppressed and inlet suppressed perceived noise levels at the forward quadrant angle of maximum unsuppressed noise as a function of corrected fan speed. Suppression is seen to be fairly constant with fan speed.

In Figure 42 the effect of the fan inlet suppression on sound pressure levels is shown at the 40 degree microphone location for a fan speed of 5300 RPM. This angle is normally assumed to be controlled by fan inlet radiated noise when dealing with lift fan spectra. There is a 5 to 7 dB reduction in fan broadband levels. Similar fan broadband suppression is noted in Figure 43 at 4800 RPM while at 4200 RPM in Figure 44 the fan broadband reduction is 8 to 10 dB. At all three speeds there is a reduction of 10 to 13 dB in the 1/3 octave band which contains the BPF.

Although the preceding figures have shown that there is substantial fan pure tone and fan broadband reduction due to fan inlet suppression, it remains to be established whether or not the fan inlet radiated noise has been suppressed to the point where fan exhaust radiated noise is now the controlling

noise source at the forward angles. If the levels were controlled by fan inlet radiated noise, fan exhaust treatment would have no effect. Thus, to determine if the 1/3 octave band containing the BPF is exhaust radiated noise, the directivity of that band was compared in Figure 45 for the unsuppressed fan, fan with inlet suppression only, and the fan with inlet suppression plus ten inches (25.4 cm) of exhaust treatment at a fan speed of 5300 RPM. Fan exhaust suppression is seen to suppress the levels at all angles with the possible exception of 0 degrees. Similar results are observed for fan speeds of 4200 and 4800 RPM in Figures 46 and 47, respectively. For these two speeds, all angles but the 0 degree microphone are reduced by fan exhaust treatment and possibly the 10 degree microphone at 4200 RPM. Note also that the level of pure tone suppression is nearly the same for the forward and aft angles. This means, therefore, that at least the 1/3 octave band containing the BPF is controlled by fan exhaust radiated noise at all angles except zero degrees.

To determine if the fan broadband sound pressure levels are exhaust radiated, the suppression (relative to the fan with massive inlet suppression) realized at the 40 and 110 degree microphones with ten inches (25.4 cm) of exhaust treatment are compared in Figure 48 at fan speeds of 4800 and 5300 RPM. If the fan broadband levels at the forward angles with massive fan inlet suppression installed were still controlled by fan inlet radiated noise, then one would expect to see no or little suppression as ten inches (25.4 cm) of exhaust treatment is added. However, the suppression realized at 40 degrees is the same as the 110 degree suppression for frequencies above 1000 Hz. This indicates that these levels are controlled by exhaust radiated noise.

The fan noise portion of the spectrum obtained at any far field microphone during the unsuppressed fan test (Test 1) may be thought of as the sum of two separate and distinct spectra, i.e., the fan inlet radiated spectrum and the exhaust radiated spectrum. It was shown in the preceding discussion that massive fan inlet suppression was successful in eliminating fan inlet radiated noise which resulted in the measurement of exhaust radiated fan noise (Test 2). While the fan inlet radiated noise spectrum was not measured directly, it may easily be found by subtracting the exhaust radiated spectrum from the total unsuppressed fan spectrum.

B. Fan Exhaust Noise Suppression

After eliminating fan inlet radiated noise, fan exhaust treatment was installed to determine the effect of treatment length on suppression and to ultimately suppress the fan exhaust radiated noise enough that the jet noise floor would be dominant at all frequencies up to 4000 Hz.

The effect of various splitter lengths on perceived noise levels are shown in Figure 49 for a fan speed of 5300 RPM. For these comparisons, the fan configuration which had massive inlet suppression and an unsuppressed exhaust (Test 2) was used as a baseline. It is apparent from Figure 49 that the initial ten inches (25.4 cm) of exhaust treatment achieved most of the suppression at all angles. Also evident is a rearward shift in angle of maximum noise as suppression was added. Lower fan speeds of 4800 and 4200 RPM, Figures 50 and 51 respectively, show that most of the suppression is again achieved with the first ten inch (25.4 cm) section and that there is a rearward shift in angle of maximum noise. In Figure 52, perceived noise levels at the unsuppressed exhaust angle of maximum noise are shown as a function of corrected fan speed for the various exhaust configurations. The suppression realized at this angle of max noise varies from 7.5 PNdB at 4200 RPM to 10 PNdB at 5300 RPM. The peak-to-peak suppression is shown in Figure 53 as a function of corrected fan speed and varies from 9.0 PNdB at 5300 RPM to 7.0 PNdB at 4200 RPM.

The perceived noise level suppression realized as a function of treatment length at the unsuppressed exhaust angle of maximum noise for 5300 RPM fan speed is shown in Figure 54. Also shown on this figure is the peak-to-peak suppression realized and the predicted PNL. The realized suppression was not as effective as expected.

Advanced study programs on the integral and remote lift fan systems (References 6 and 7) had as an objective a perceived noise level of 95 PNdB on a 500 foot (152.4 m) sideline for a 120,000 pound (54,432 kg) airplane at the noise rating point (80 percent power). The measured LF336 levels for the fan with unsuppressed exhaust and fully suppressed exhaust are shown in Figure 55 for a single engine. The noise rating point power occurs at 5300 RPM for the unsuppressed fan and would require 27 fans to generate the 120,000

pound (53,380 kN) of thrust required to be compatible with the advanced study lift fans. Correcting the 95 PNdB goal for 27 fans to a single fan means that the PNL would have to be 95 - 10 $\log_{10}$ 27 or 80.6 PNdB at the noise rating point. This level is shown on Figure 55, and indicates that more noise suppression (10.5 PNdB) is necessary to meet this goal with this fan. Also shown on Figure 55 are the estimated design perceived noise levels on a 500 foot (152.4 m) sideline. At the noise rating point the PNL of the fan with unsuppressed exhaust was 101.0 PNdB. The design estimate for the fully suppressed configuration was 83.0 PNdB compared to the measured level of 89.0 PNdB at the noise rating point.

C. Suppression Details

Figure 56 shows the effect of various splitter lengths on far field 20 Hz bandwidth sound pressure levels at a fan speed of 5300 RPM at the 110° microphone. Most of the suppression on these 20 Hz narrowbands was achieved with the initial ten inches (25.4 cm) of treatment. This is apparent for the pure tone at 3700 Hz and the fan broadband noise at higher frequencies. At 5300 RPM at least 28 dB pure tone suppression was realized. There is a tone evident at 8300 Hz in the fully suppressed case which is the BPF of the core engine compressor first stage. Similar results are observed for fan speeds of 4200 and 4800 RPM in Figures 57 and 58, respectively.

Figures 59, 60, and 61 show the fan broadband suppression realized at 5300 RPM for the three exhaust treatment lengths. The levels were obtained from 20 Hz narrowbands and are compared to predicted suppression levels. A faired curve has been drawn through the measured fan broadband suppression. Fan pure tone suppression with ten inches (25.4 cm) of exhaust treatment is greater than predicted. With twenty inches (50.8 cm) of treatment the measured and predicted pure tone suppression are the same. With thirty inches (76.2 cm) of treatment the pure tone suppression is less than predicted; however, the pure tone is no longer identifiable in the narrowband spectrum. With the exception of the high frequency fan broadband suppression attained with ten inches (25.4 cm) of treatment, the achieved levels are less than predicted.

Similar results are attained for a fan speed of 4800 RPM in Figures 62, 63, and 64. As before a faired broadband suppression curve has been drawn through the measured levels.

In Figure 65, the realized fan suppression levels for 4800 and 5300 RPM are compared for all treatment lengths. These curves indicate that the initial ten inches (25.4 cm) of treatment provide most of the realized fan broadband suppression.

Forward quadrant narrowband spectra for various treatment lengths are shown in Figure 66 at 5300 RPM. The results are similar to those observed on the aft quadrant curves with the initial ten inches (25.4 cm) of treatment providing most of the suppression. Figure 67 shows the suppression levels obtained at the 60 degree microphone for ten inches (25.4 cm) of exhaust treatment at 5300 RPM fan speed. The broadband suppression at this forward angle is very similar to that shown in Figure 59 for the aft quadrant except that BPF suppression is about 6 dB less. In Figure 68, the suppression at the 60 degree microphone with thirty inches (76.2 cm) of exhaust treatment is similar to but less than that shown in Figure 61 for the 110 degree microphone.

Examination of Figure 66 indicates that the pure tone does not decrease further with increased treatment length beyond ten inches (25.4 cm). This may mean that the pure tone is controlled by inlet radiated noise at this point. However, fan broadband levels actually increase 3 to 4 dB over the ten inch (25.4 cm) treatment length when twenty (50.8 cm) and thirty (76.2 cm) of treatment were tested. If the fan broadband levels were controlled by inlet radiated noise, then further addition of exhaust treatment would not raise the levels. Instead, an increase is noted which indicates the presence of a broadband floor which is caused by the addition of treatment length.

Similar results are observed at the 60 degree microphone at 4800 RPM in Figure 69. Fan broadband levels for the 20 and 30 (50.8 and 76.2 cm) inches of treatment length are generally above the levels with only ten (25.4 cm) inches of treatment.

D. Treatment Effectivity

The following analysis of treatment effectivity and flow noise generation was made by H.W. Hehmann to gain an understanding of the less than predicted exhaust system noise suppression.

A recent paper (Reference 11) by J.E. Ffowcs Williams indicates that the apparent lack of broadband suppression may be due to broadband noise generated by flow over the treatment surface. The analysis is shown in Appendix A.

General Electric design curves are based on flow duct data and show the influence of flow noise implicitly by bending and essentially flattening the peak suppression curves of Figure 18 as L/H >> 1. However, the point of inflection and the achievable peak suppression plateau depend upon a unique relationship of source to flow generated noise as will be shown below.

For the LF336 at 4000 Hz, the effective porosity is

$$\frac{4\,a\,N}{k} \simeq 10 >> 1 \qquad (7)$$

where a = hole diameter = 1.6×10^{-3} m

N = number of holes per unit area = 1.16×10^{5} holes/m^2

k = wave number = 74 m^{-1}

λ = wavelength (m)

Thus, we have a surface-scattered field which is due to a system of aerodyanmic dipoles.

Appendix A presents expressions for flow generated power spectra, Equation 24, and radiated power spectra, Equation 25, as well as attainable attenuation, Equation 27. Calculations based on these equations were made for the LF336 noise suppressor with the following input data. Mach number and boundary layer thickness values are given in Table V. The attenuation constant, β, of Scottfelt 3-900 is based on GE duct measurements where flow effects are negligible. The power, W, of the unsuppressed (Test 2) fan was measured to be 60.2 watts at 5300 RPM and 21.0 watts at 4800 RPM for the third octave band containing the BPF. The respective measured values for a 20 Hz bandwidth are 20 and 6.4 watts.

For both speedpoints considered, the cut-off frequency (Equation 23) is above the blade passing frequency (BPF). For the 5300 RPM case, $\bar{U}$ based on exhaust probe measurements is 186 meters per second and δ is 1.47×10^{-2} meter. Thus, the cut-off frequency (per eq. 23) f_o = 12,650 Hz which is greater than the BPF of 3700 Hz. Similarly, for the 4800 RPM case $\bar{U}$ = 173 meters per second and $\delta = 1.53 \times 10^{-2}$ meters which results in a cut-off frequency of 11,300 Hz compared to the BPF of 3350 Hz.

Calculated attenuation based on the above analysis is compared with measured far field attenuation for the 1/3 octave band containing the BPF and the BPF with a 20 Hz bandwidth. Agreement is good for both the 20 Hz and 1/3 octave bandwidth analysis at 5300 RPM. (See Figure 70). In Figure 71, good agreement is also achieved between the calculated BPF attenuation for the 1/3 octave band and 20 Hz bandwidth at the speed of 4800 RPM. The noise spectra due to flow generated power plus attenuated fan power can be estimated using Equation 25. Reasonable agreement is shown in Figures 72 and 73 between the measured and predicted power level spectra. The discrepancies are probably due to the assumption that P = constant below cutoff. Better high frequency agreement with measured data is found if the cutoff frequency is assumed to be

$$f_0' = 0.4\,\bar{U}/\delta = 0.4\,f_0 \tag{8}$$

The calculations over the frequency range shown are based on duct measured attenuation constant β for Scottfelt 3-900 and the measured power level of the LF336 with aft unsuppressed and front fully suppressed (Test 2).

A recent empirical formulation on self generated noise by I.L. Ver (Reference 12) relates the octave band sound power level re 10^{-12} watts as

$$PWL_{OB} \simeq 121 + 55 \log_{10} M + 10 \log_{10} A - 45 \log_{10} POA/100 + 7.5 \log_{10} \frac{460 + T}{530} \tag{9}$$

where M = Mach number

A = scrubbing area = (98 ft^2, 9.1 m^2)

POA = percent open area = (30%)

T = gas temperature = (95° F, 308° K)

The Mach numbers for the 30" (.762 m) long treated 4800 and 5300 RPM speed points are shown in Table V. Mr. Ver implicitly assumes that the source is completely attenuated and the flow noise generated floor is reached.

The predicted octave band spectrum is assumed to be flat over the entire frequency range. The calculated 1/3 octave band power level is approximately 20 dB higher than the measured LF336 levels as shown in Figures 72 and 73. Although the levels from this formulation are not in agreement with measured levels, the flat shape predicted by Ver's analysis is consistent with the observed shape. There are several similarities between Ver's Equation 9 and Equation 24 viz., the Mach number conclusion, area dependence, and open area dependence. Although Ver shows a 5.5 flow power dependence while a 6 (for dipoles or 4 (for monopoles) power dependence is indicated by the Williams analysis.

The important result from the above discussion is that there is an exhaust suppression ceiling. It was shown in Figures 70 and 71 that the initial ten to twenty inches (25.4 to 50.8 cm) of treatment provided most of the suppression in the 20 Hz and 1/3 octave bands which contain the BPF. This result plus examination of Equations 24 and 27 suggests that better suppression levels could be obtained by shortening duct treatment length to reduce treatment generated broadband noise, but still allow enough length to suppress fan noise. Decreasing the passage flow velocity should also reduce treatment generated broadband noise due to the sixth power dependence on flow.

Transformation of Equation 27 for an infinitely long duct leads to the following expression

$$ATT_{max} \simeq 10 \log_{10} \left[\frac{2W\beta}{P}\right] \qquad (10)$$

which shows that for a given β (suppression material constant), the maximum attainable attenuation as seen in the near plateau (Figure 19) is a function of the ratio of source noise (W) to flow noise (P). While the source noise used in the GE duct test (50 watts) on which the acoustic design is based is of the same order of magnitude as the LF336 source, the flow noise is not. Furthermore, the treatment scrubbing area in the GE flow duct is 2 ft^2 (.185 m^2) vs 98 ft^2 (9.1 m^2) for the LF336. Based on scrubbing area alone at the same Mach number, the duct test should yield about 16.9 dB more attenuation than the LF336. Finally, it is unlikely that the attenuation of Scottfelt changes drastically between 0.4M (duct) and 0.51 - 0.57M (for a fully suppressed LF336). Indeed, 9 dB broadband suppression (Figure 70) was obtained for the first 10 inches (.254 m) of treatment at an average flow of 0.59M.

Thus the flow noise generating mechanism which had not been quantized prior to Williams' paper can be used to explain the lack of attenuation obtained in the LF336 test series.

E. Other Acoustic Results

Other areas investigated included the predicted effect of core and jet noise on the far field levels, observed fan exhaust tones, core engine tones, and far field directivity patterns. These topics are discussed in more detail in Appendices B, C, D, and E, respectively.

SECTION VII

AERODYNAMIC PERFORMANCE

The initial testing that began on June 20, 1972 was run with the exhaust adapter installed on the fan exit. The exhaust adapter was a 12 inch (30.48 cm) long acoustically untreated section which transitions from the fan exit flowpath to the flowpath of the acoustic suppression system. Figure 74 shows an aft view of the fan with the exhaust adapter installed. The fan inlet contained no acoustic inlet suppression. The test was run to a maximum fan speed of 5304 RPM (87.7% design) and acoustic and performance data were recorded at spot points.

A. Splitter Inlet Pressure

During the initial run, a performance problem was observed as indicated by low static pressure, high flow conditions within the fan. The significant aerodynamic performance data recorded during the initial test were surface pressures along the exhaust adapter section and a traverse probe profile at the exit plane of the system. Figure 75 shows the measured adapter section static pressures recorded for the initial run. The measured pressure levels identify the low static pressure, high flow conditions. This data shows that these pressures were as low as -4.75 psig (-32.7 kN/m^2) at the 5304 RPM conditions at the mid-passage inlet. This low level of pressure was very significant, considering that the fan was pumping about 4 psig (27.56 kN/m^2). This indicated that the adapter section acted like a diffuser, thus causing the flow rate through the inner passage of the adapter section to be larger than the fan design flow. Figure 76 shows the average static pressure distribution through the adapter section which confirms diffuser action.

The second test run was made with the fan configuration changed by the addition of a 10 inch (25.4 cm) suppressor section downstream of the adapter and the wing simulation surface removed. The addition of this section increased the transition section wall static pressures as indicated in Figure 77. The two sets of curves in Figure 77 are for the two circumferential locations and at a corrected fan speed of 2870 RPM. Only idle speed data was available because of a data acquisition problem.

The fan configuration was again changed for Run 3 by the addition of blockage in the exhaust plane of the 10 inch (25.4 cm) suppressor section. The blockage was designed to establish ambient pressure at the fan exit plane and was produced by mounting eight radial U-channels at the exhaust plane of the section as shown in Figure 78. Four of these channels, one inch by one-half inch (2.54 cm by 1.27 cm) commercial channel iron, extended across all three fan and the turbine passages. The other four channels did not extend across the inner flowpath annulus. Figure 79 shows the splitter wall static pressure distribution with the added blockage installed. Comparison of the data with and without blockage shows increased adapter section static pressures with blockage. Without blockage, the fan mid-passage pressure was 0.4 psi (2.76 kN/m^2) to 0.5 psi (3.44 kN/m^2) below ambient. With blockage, the pressure was 0.1 psi (0.689 kN/m^2) to 0.2 psi (1.38 kN/m^2) below ambient. This change in pressure is quite large for the added blockage which was about 10 percent for each passage.

Figure 80 shows a comparison of the fan stage back pressure for the first three configurations, which was taken to be the static pressure at Plane A, 2 inches aft of the fan stator exit. At a corrected fan speed of 4000 RPM, the average static pressure was -1.0 psi (-6.895 kN/m^2) with the adapter section only, -0.83 psi (-5.71 kN/m^2) with the adapter plus 10 inches (25.4 cm) of exhaust suppression, and -0.03 psi (-0.206 kN/m^2) with the adapter, 10 inches (25.4 cm) of exhaust suppression and the U-channel blockage. From this comparison, the added blockage which reduced the exit area of the adapter section 10 percent, was effective in reducing the high flow conditions through the adapter section.

B. Base Pressure (Venting)

Figures 81 and 82 show pressure traverses at the exit plane of the suppressor and at an angular position midway between two of the blockers. Figure 81 is for the run without U-channel blockage, and Figure 82 is a similar set of data after installation of the blockage. The radial temperature distribution with the blockage installed is also shown in Figure 83.

For the case without blockage (Figure 81), the base pressures or pressures in the wakes behind the inner and outer splitters were substantially below

ambient pressure. This low pressure effectively increased the velocity through the passage and produced an effective area for the passage that appeared greater than the physical area. This high velocity, low pressure then fed forward into the passage and caused a high flow through the fan. The hub and midbox passages were not much below ambient and were of a level experienced in previous fan tests. The extremely low base pressures were not anticipated in the design of the splitter section.

The data in Figure 82 clearly shows the effects of the added blockage. Note in Figure 76 that the traverse station was about 22 1/2 degrees from the nearest blockage channel. For this configuration, the base and stream pressure for the two splitters has increased significantly over the case without blockage. Pressures had increased from 0.4 to 0.5 psi (2.76 to 3.44 kN/m^2) below ambient to 0.15 to 0.20 psi (1.03 to 1.38 kN/m^2) below ambient.

Figures 84, 85, and 86 show the static pressure distribution at the bases of the inner splitter, the outer splitter, and the midbox, respectively, for five test configurations. They were, the adapter plus 10 inches (25.4 cm) of suppression, the adapter plus 10 inches (25.4 cm) of suppression plus airfoiled blockage, and the adapter plus U-channel blockage with 10 inches (25.4 cm), 20 inches (50.8 cm) and 30 inches (76.2 cm) of suppression. Figure 84 shows that the U-channeled blockage increased the inner splitter base static pressure at 4000 RPM fan speed from -0.88 psi (-6.06 kN/m^2) to -0.24 psi (-1.63 kN/M^2). Figure 85 shows that the outer splitter base static pressure increased from -0.73 psi (-5.01 kN/m^2) to -0.34 psi (-2.34 kN/m^2) at 4000 RPM with the addition of the U-channel blockage, and Figure 86 shows that the midbox base static pressure distribution remained the same throughout all the configuration changes.

A reasonable explanation for the large pressure change due to the U-channeled blockage was base venting, i.e., the U-channeled blockage became a path for turbine stream gas and some ambient air to reach the low pressure regions along the splitter bases. The fact that base venting occurred was seen in the temperature profile in Figure 83. The air temperature behind both of the splitters and the hub showed a temperature greater than the fan stream temperature. The only possible source for this hot air to come from was the hot turbine exhaust gas. It was surprising that a 20 to 40° F (11.1 to 22.2° K)

temperature rise was possible when consideration was given to the distance the air must travel in open-vented channels and bases. Another portion of the data that showed how high the venting flow must have been was in the midbox static pressures. Before the U-channels were added, the midbox pressure was approximately 0.1 psi (0.689 kN/m^2) below ambient; with venting, the pressure went down to 0.22 (1.52 kN/m^2) psi. This indicated that the U-channel blockage ejected flow from the midbox section as well as from ambient or outside air. Figure 87 shows a sketch of the indicated base venting process.

C. Fan Alone

The possibility that the radial U-channel blockage may have been a noise generator warranted the design of an acoustically more desirable form of blockage. It was decided that the U-channel should be faired at both the leading and trailing edges. While these airfoiled blockage components were being fabricated, testing resumed with the clean fan configuration, that is, Test 1, no inlet or exhaust suppression.

The measured test results for Test 1 are shown in Figures 88 to 99. The measured results presented are corrected thrust versus corrected fan speed (Figure 87), corrected engine speed versus corrected fan speed (Figure 88), and fan exhaust total and static pressure and total temperature profiles (Figures 89 thru 99) for five fan speeds. Since the GE4 bellmouth and the transition duct were not used for this test, no airflow calculations were made.

Examination of the exhaust total pressure profiles for Test 1, revealed a decrease in total pressure at about 11.5 inches (29.31 cm) radius. This dip in the profile was caused by the traverse probe pssing through a fan stream stator wake. This problem was corrected before continuing with the testing by moving the total and static pressure probe until it was clear of the fan stators.

Figure 100 is a fan thrust comparison of the LF336/B used for the suppression tests, a LF336/B fan used for acoustic tests in February, 1969 (Reference 3) and a LF336/A fan used for acoustic tests in January, 1969 (Reference 2). The difference between the /A and /B configuration was that the /A had a rotor to outlet guide vane spacing of 15% of the rotor chord while the /B had

a spacing of 200%, or 2 times, the rotor chord. The comparison shows that the LF336/B performed as expected and as tested previously, and it was assumed that it performed on its proper operating line.

Before continuing testing, it was decided to replace the J85 engine (S/N 230-729) with another J85 (S/N 231-232) because of excessive turbine frame vibrations. The highest levels recorded for engine (S/N 230-729) were 3.6 mils (0.009 cm), while the replacement engine (S/N 231-232) experienced only 1.1 mils (0.003 cm). The replacement engine had lower vibrations but exhibited poorer performance. Further tests revealed that almost a 2% increase in engine speed was necessary to obtain the same fan speed when comparing fan speed-engine speed relationships of the replacement engine to the engine with high vibrations.

D. Fan with Inlet Box

The configuration for Test 2 included the fan inlet box without exhaust suppression. Figure 4 shows the inlet box system mounted to the fan inlet. Figures 101 thru 111 present the measured performance from Test 2. Data presented include thrust variation with fan speed (Figure 101), engine speed versus fan speed (Figure 102), and fan inlet airflow variation with fan speed (Figure 103). Presented in Figures 104 thru 111 are the exhaust total and static pressure and total temperature profiles for a range of fan speeds. The total and static pressure profiles show that the traverse probe was moved out of the fan stator wake by the absence of the dip in the total pressure profile near 11.5 inches (29.31 cm) radius.

E. Fan with Suppressor Ducts

1. 10 Inch (25.4 cm) Duct

The initial Test 3 configuration consisted of the inlet box, the exhaust transition adapter and the 10 inch (25.4 cm) acoustically treated exhaust section with the airfoiled blockage. Figure 112 shows the airfoiled blockage mounted to the exhaust section. The measured performance data are shown in Figures 113 thru 124. Data presented include thrust variation with fan speed (Figure 113), engine speed versus fan speed (Figure 114), fan inlet airflow

variation with fan speed (Figure 115), and adapter section average wall static pressure distribution (Figure 116). Figures 117 thru 124 are the exhaust total and static pressure and total temperature profiles for several fan speeds.

Analysis of the Test 3 data revealed that the airfoiled blockage failed to vent the splitter bases and the hub as did the U-channeled blockage. Figure 116 reveals that the previous high flow phenomena reappears with the airfoiled blockage because of the low wall static pressure distribution in the adapter section. At 5300 RPM fan speed the static pressure in Plane A, 2 inches (5.08 cm), was -0.996 psi (-6.86 kN/m^2) in the middle passage and -0.80 psi (-5.51 kN/m^2) in the outer passage.

Also the total and static pressure profile in Figure 117 shows static pressures of 0.6 to 1.0 psig (4.14 to 6.89 kN/m^2) below ambient at the inner and outer splitters and 0.4 to 0.5 psig (2.76 to 3.44 kN/m^2) below ambient at the midbox which agreed with the data containing no blockage. The total temperature profile in Figure 118 likewise failed to show any temperature rise behind the splitters and the hub which was another indication that the airfoiled blockage failed to vent the splitter's bases and the hub. The airfoiled blockage obviously reduced the effective blockage area of the fan by preventing radial flow and eliminating the wake behind the added blockage, thus increasing the velocity through the fan stream.

After the initial Test 3 indicated that the airfoiled blockage failed to vent the splitter bases and the hub, it was decided to remount the eight radial U-channel blockages for the remaining tests. Test 3 was then rerun with the airfoiled blockage removed and the U-channel blockage installed. The measured results are shown in Figures 125 thru 136. Data presented include thrust variation with fan speed (Figure 125), engine speed versus fan speed (Figure 126), fan inlet airflow variation with fan speed (Figure 127), and the adapter section average wall static pressure distribution (Figure 128). Presented in Figures 129 thru 136 are the total and static pressure and total temperature profiles from the traversing probe at several fan speeds.

Analysis of the data revealed results similar to the previous test with U-channeled blockage. The adapter section wall static pressure distribution

increased to previous accepted levels (Figure 128), and the total and static pressure profile at the suppressor exit plane (Figure 129) indicated increased static pressures along the splitter bases and the hub. Also the pressure profile showed lower midbox static pressures, which again indicated that the U-channel blockage ejected flow from the midbox region as well as from the ambient outside air. Likewise, the total temperature profile (Figure 130) showed an increase in temperature behind the splitter bases and the hub which indicated that the U-channel blockage had vented as desired.

2. 20 Inch (50.8 cm) Duct

The configuration for Test 4 included the fan inlet box, exhaust adapter section and 20 inches (50.8 cm) of exhaust suppression with the U-channeled blockage. The measured test results are presented in Figures 137 thru 148. Data presented include thrust variation with fan speed (Figure 137), engine speed versus fan speed (Figure 138), fan inlet airflow variation with fan speed (Figure 139) and adapter section average wall static pressure distribution (Figure 140). Presented in Figures 141 thru 148 are the exhaust total and static pressure and total temperature profiles for several fan speeds.

3. 30 Inch (76.2 cm) Duct

The final configuration for Test 5 included the fan inlet box, the exhaust adapter section and 30 inches (76.2 cm) of exhaust suppression with the U-channeled blockage. Measured test results are presented in Figures 149 thru 162. Data presented include thrust variation with fan speed (Figure 149), engine speed versus fan speed (Figure 150), fan inlet airflow versus fan speed (Figure 151), and adapter section average wall static pressure distribution (Figure 152). Presented in Figures 153 thru 162 are the exhaust total and static pressure and total temperature profiles at various fan speeds.

F. Thrust Variations

1. Measured Data

Figure 163 shows the measured fan thrust comparison for each fan configuration, and the percent thrust difference from the base fan is shown in Figure 164. The fully suppressed fan, 30 inches (76.2 cm) of exhaust suppression,

exhibited a 22 percent difference, with 20 inches (50.8 cm) and 10 inches (25.4 cm) of suppression, a 20 percent difference was measured, and with the inlet suppressor only configuration a 2 percent thrust decrement was observed.

Figure 165 shows the average static fan back pressure which was assumed to be at Plane A of the adapter section, i.e., 2 inches (5.08 cm) aft of the fan stator exit plane. An above ambient back pressure will increase the rotor stage pressure ratio and decrease the fan airflow while a below ambient back pressure decreases the pressure ratio and increase the airflow. The estimated effect of the measured fan back pressure will be discussed in the estimated loss section.

2. Estimated Losses

The 22% thrust decrement which was measured for the fully suppressed fan configuration warranted an analysis of estimating the thrust loss due to components of the specific fan configurations. Three sources of losses were identified which were:

- Losses due to acoustic hardware
  i.e., splitter supporting struts, adapter and suppressor sections, splitter bases.
- Losses due to test set-up
  i.e., inlet suppressor, GE4 Bellmouth, inlet transition section, hub and midbox bases, and U-channel blockage.
- Losses due to change in fan operating point
  i.e., fan stage back pressure.

The losses associated with the acoustic hardware consisted of the aerodynamic drag of the splitter supporting struts (Figure 16), of the adapter and suppressor sections (Figures 12 and 17), and of the splitter bases. With 10 inches (25.4 cm) of suppression 6 support struts were present in the configuration, 9 with 20 inches (50.8 cm) and 12 with 30 inches (76.2 cm).

The strut drag was calculated from the equation (Reference 13)

$$\text{Drag} = \frac{C_f \rho V^2 A_w}{2g} \qquad (11)$$

where C_f = Average skin friction coefficient based on the profile drag coefficient, C_{ds}, for a thickness ratio (t/c) of 6.25% and $C_f = C_{ds}/2 = 0.005/2 = 0.0025$

ρ = Air density

V = Velocity

A_w = Wetted area of the support struts

The values of the strut drag which were calculated were 3.75 pounds (0.017 kN), 5.3 pounds (0.024 kN) and 7.1 pounds (0.032 kN) for 10 inches (25.4 cm), 20 inches (50.8 cm) and 30 inches (76.2 cm) of suppression, respectively, at a corrected fan speed of 5200.

One of the major losses from the exhaust suppression system was the skin friction drag from the flow over the acoustic splitters and adjacent walls. The average skin friction coefficient based on the Reynolds Number through each passage was calculated to be 0.0029 which is similar to the skin friction coefficient for a smooth plate. However, it was assumed that the skin friction coefficient for the acoustic splitters was 37.5 percent greater because of the porous acoustic treatment surface.

Several tests have been conducted in order to measure the difference in the drag between a smooth plate and an acoustically treated section. The results indicated that the ratio of the drag of the treated surface to a smooth surface was between 1.22 and 1.72. Based on these numbers plus similar ratios from several airframe manufacturers, a 37.5 percent increase in the average skin friction coefficient for acoustic treatment with a porous plate surface was adopted as a General Electric standard.

The skin friction drag over the suppression system was calculated from the equation (Reference 13)

$$\text{Drag} = \frac{C_f\ (1.375)\ \rho\ V^2\ A_w}{2g} \qquad (12)$$

where,

C_f = Average skin friction coefficient

ρ = Air density

V = Velocity

A_w = Total wetted area of splitters and adjacent walls

The skin friction drag that was calculated for each suppressed configuration at 5200 corrected fan speed was 183 pounds (0.816 kN), 241 pounds (1.07 kN) and 328 pounds (14.6 kN) for 10 inches (25.4 cm), 20 inches (50.8 cm) and 30 inches (76.2 cm) of exhaust suppression, respectively.

The final loss associated with the acoustic hardware was the splitter base drag. It was calculated as

$$\text{Drag} = (\Delta PA)_{\substack{\text{inner}\\\text{splitter}}} + (\Delta PA)_{\substack{\text{outer}\\\text{splitter}}} \qquad (13)$$

where

ΔP = $P_o - P_s$, with P_s = Static Pressure at base of splitters

A = Base Area

The calculated values for a fan speed of 5200 were 159 pounds (0.71 kN), 148 pounds (0.66 kN) and 130 pounds (0.58 kN) for exhaust suppression of 10 inches (25.4 cm), 20 inches (50.8 cm) and 30 inches (76.2 cm), respectively.

The second source of performance losses were those due to the test set-up, i.e., the fan inlet suppression system, the hub and midbox, and the U-channeled blockage which was required to alleviate the below ambient static pressure at the splitter bases.

Analysis of the total pressure loss of the inlet suppression system, which consisted of the inlet box, the GE4 Bellmouth and inlet transition section, was based on the equation (Reference 14)

$$\Delta P = \frac{K_1 \rho V_1^2}{2g} + \frac{K_2 \rho V_1^2}{2g} + \frac{K_3 \rho V_2^2}{2g} \qquad (14)$$

where

ΔP = Total Pressure loss

K_1 = 0.23 for the slightly rounded entrance to the inlet box

K_2 = 1.20 for the 90° mitered corner in the box

K_3 = 0.20 for the inlet to the GE4 Bellmouth

V_1 = Air velocity in inlet box

V_2 = Air velocity in GE4 Bellmouth

ρ = Air density

For the configurations with inlet suppression, a total pressure loss coefficient of 0.0052 ($\Delta P/q$) was calculated which corresponded to a total pressure loss of 0.009 psi (0.062 kN/m^2) from the inlet of the box to the inlet of the fan. Previously published values for the effect of a change in fan inlet total pressure on fan thrust indicated a fan inlet total pressure derivative of 4.0 percent. The 0.009 psi (0.062 kN/m^2) loss was a 0.1 percent change in fan inlet total pressure so therefore, a 0.4 percent loss was present for each configuration with inlet suppression.

The base drag of the hub and midbox was calculated from the equation

$$\text{Drag} = (\Delta PA)_{\text{Hub}} + (\Delta PA)_{\text{Midbox}} \qquad (15)$$

where

ΔP = $P_o - P_s$, with P_s = Static Pressure at base of Hub or Midbox

A = Base Area

Results of the calculations were 130 pounds (0.591 kN), 138 pounds (0.615 kN) and 154 pounds (0.687 kN) for 10 inches (25.4 cm), 20 inches (50.8 cm) and 30 inches (76.2 cm) of exhaust suppression, respectively, at 5200 corrected fan speed.

The U-channeled blockage which was added to the fan exit plane caused additional losses. These losses appeared as forebody drag and rod-splitter interference drag. The forebody drag was estimated from the equation (Reference 13)

$$\text{Drag} = \frac{C_D \rho V^2 A_f}{2g} \tag{16}$$

where

C_D = 0.8 = forebody drag coefficient
ρ = Air density
V = Air velocity
A_f = Wetted frontal area of U-channels

The calculated values were 153 pounds (0.681 kN), 161 pounds (0.718 kN) and 162 pounds (0.723 kN) for 10 inches (25.4 cm), 20 inches (50.8 cm) and 30 inches (76.2 cm) of exhaust suppression, respectively, at 5200 corrected fan speed.

The interference drag from the junctions of U-channeled blockage and the splitter, hub and midbox bases was calculated using the equation (Reference 13)

$$\text{Drag/Joint} = \frac{C_{Dt} \rho V^2 t^2}{2g}$$

where

C_{Dt} = 1.0 = interference drag coefficient
ρ = Air density
V = Air velocity
t = thickness of U-channeled blockage at each joint

The values that were obtained were 139 pounds (0.62 kN), 139 pounds (0.62 kN) and 140 pounds (0.623 kN) for 10 inches (25.4 cm), 20 inches (50.8 cm) and 30 inches (76.2 cm) of exhaust suppression, respectively, for a corrected fan speed of 5200.

The final source of performance losses that was investigated were those due to the change in the fan operating point because of variations of fan stage back pressure. Figure 166 shows the thrust decrease for various levels of fan discharge static pressure which was derived from the CF336 fan map from Reference 15.

Determining the average fan discharge static pressure from Figure 128, 140 and 152, using Plane A as the back pressure station, resulted in -0.06 psi (-0.414 kN/m^2), 0.13 psi (0.896 kN/m^2) and 0.23 psi (1.58 kN/m^2) for 10 inches (25.4 cm), 20 inches (50.8 cm) and 30 inches (76.2 cm) of exhaust suppression, respectively, at 5200 corrected fan speed. From Figure 166, the thrust decrease was found directly to be 1.7 and 0.8 percent for 30 inches (86.2 cm) and 20 inches (50.8 cm) of exhaust suppression, respectively and an increase in thrust of 0.4 percent for 10 inches (25.4 cm) of suppression.

Table VI contains the summary of the estimated thrust losses from all sources for various amount of exhaust suppression. Comparing the estimated thrust losses to the measured thrust losses, reasonable agreement was indicated. For 10 inches (25.4 cm) of exhaust suppression, 18.2 percent was estimated versus 20 percent measured, for 20 inches (50.8 cm), 20.9 percent estimated versus 20 percent measured, and for 30 inches (76.2 cm), 24 percent estimated versus 22 percent measured.

SECTION VIII

CONCLUSIONS

This was a test of a long, two-splitter lift fan exhaust suppressor system designed to achieve noise goals for advanced lift fans. As a result of this program, it appears that advanced lift fan suppressor design considerations will have to be modified. Significant specific conclusions from this test are listed below:

1. Fan inlet radiated noise levels were suppressed sufficiently to allow determination of fan exhaust radiated levels. For a two-chord rotor-stator spacing configuration, unsuppressed inlet and exhaust radiated levels were approximately equal. In the forward quadrant (at the 50 degree microphone), the unsuppressed exhaust radiated noise was 8 PNdB below the inlet radiated noise.

2. The maximum exhaust treatment (30" (76.2 cm) length) realized 8 PNdB peak-to-peak suppression in the aft quadrant and 10 PNdB suppression at the 110 degree microphone position compared to a design suppression of 20 PNdB. Pure tone suppression of 28 dB was realized. The ten inch (25.4 cm) long exhaust suppressor provided a 6 PNdB suppression.

3. At the noise rating point on a 500 foot (152.4 m) sideline, the maximum PNL is 91.6 PNdB. Another 11.0 PNdB suppression will have to be realized to meet a single fan noise level of 80.6 PNdB, which is equivalent to an advanced lift fan design goal of 95 PNdB on a 500 foot sideline (152.4 m) for a 120,000 pound (54,432 kg) aircraft.

4. The difference between design and measured overall suppression was attributed primarily to the presence of flow-generated broadband noise from the treated surfaces. Analysis indicated that reduced flow Mach number is a primary factor, and suppressor geometry changes are a secondary factor, in reducing the flow-generated broadband noise floor.

5. Predicted core and jet noise levels indicated that these sources did not contribute to the broadband noise floor at frequencies above 1000 Hz.

6. Fan exhaust tones observed in the spectra appeared to be due to vortex shedding off the blunt splitter bases. At the maximum fan speed tested, these tones only contributed 0.5 PNdB to the perceived noise levels.

7. An overall fan thrust decrement of 22.0 percent was measured at maximum fan speed for the complete suppressed test configuration. However, the thrust loss attributable to the exhaust suppressor configuration (adapter section and treated sections) was estimated to be 11.1 percent.

8. The blunt based acoustic splitters intensified the below-ambient static pressure condition at the fan exit which resulted in reduced fan thrust (base pressure effect). Future acoustic splitter designs should incorporate design changes to alleviate the lower-than-ambient conditions at the fan discharge plane.

9. When splitter rings are used, the transition section between the fan discharge and the treated rings should be carefully designed to avoid local flow accelerations or decelerations in the passages.

SECTION IX

SYMBOLS

SYMBOL		UNITS
A, A_w or A_f	Wetted surface area, GE4 bellmouth area, or base area	$in^2 ft^2$ (cm^2, m^2)
a	Treatment hole diameter	in (cm)
ATT_{max}	Attenuation	dB
ATT_{duct}	Duct attenuation	dB
BPF	Blade passing frequency	Hz
BVO	Engine bleed valve indicator	percent
C_D	Drag coefficient	-
C_{Dt}	Interference drag coefficient	-
C_{ds}	Strut drag coefficient	-
C_f	Average skin friction coefficient	-
C_f	GE4 bellmouth flow coefficient	-
c	Chord	in (cm)
d	Characteristic dimension	ft (m)
D.I.	Directivity index	dB
f	Frequency	Hz
f_p	Peak tuning frequency	Hz
f_0	Cutoff frequency	Hz
f_0'	Cutoff frequency (0.4 f_0)	Hz
F	Force	lb (kN)
F_n	Fan net thrust	lb (kN)
FG	Fan Thrust	lb (kN)
g	Gravitational Constant	32.174 ft/sec^2 (6.673×10^{-11} Nm^2/kg^2)

SYMBOL		UNITS
H	Duct height	in (cm)
k	Wave number	m^{-1}
K, K_1, K_2, K_3	Constants	-
ℓ	Space length of pressure pulse	m
L	Treatment length	in (cm)
M	Mach number	-
m	Number of holes	-
$\dot{m}$	Mass flow rate	lbm/sec (kg/sec)
N	Number of holes per unit area	m^{-2}
N_e	Engine Speed	RPM
NF or N_f	Fan Speed	RPM
OAT	Ambient temperature	°F (°K)
P,p	Pressure	psi (N/M^2)
P_a	Aerodynamic wall pressure	psia (N/m^2)
P, P(ω), P(f)	Generated power	Watts
P(f,δ(x))	Flow noise generated per unit length	Watts/Hz/m
P'(f)	Total radiated power	Watts/Hz
PCM	Pulse code modulated	-
P_e	Exit static pressure	psia (kN/M^2)
PNL	Perceived noise level	PNdB
P_o, PO	Ambient pressure	psia (kN/m^2)
POA	Percent open area	-
P_s	Static pressure at base of splitters	psia (kN/m^2)
PS2	Engine bellmouth static pressure	psia (kN/m^2)
PS10	Fan bellmouth static pressure	psig (kN/m^2)

SYMBOL		UNITS
PS11	Fan discharge static pressure	psig (kN/m^2)
PSA	Transition section static pressure	psig (kN/m^2)
PSB	Transition section static pressure	psig (kN/m^2)
PSBM	Fan bellmouth static pressure	psig (kN/m^2)
PSBN	Fan bulletnose static pressure	psig (kN/m^2)
PSC	Transition section static pressure	psig (kN/m^2)
PSD	Transition section static pressure	psig (kN/m^2)
PSE	Fan base static pressure	psig (kN/m^2)
P_t	Total pressure	psia (kN/m^2)
P_{t0}	Total pressure at fan inlet suppressor	psia (kN/m^2)
$P_{T_{\text{fan inlet}}}$	Fan inlet total pressure	psia (kN/m^2)
PT11	Fan discharge total pressure	psig (kN/m^2)
PWL	Sound power level re 10^{-13} watts except where noted	dB
PWL_{OB}	Octave band power level re 10^{-12} watts	dB
PWL_R	PWL - Δ	dB
q_B	Bellmouth dynamic pressure	psi (kN/m^2)
R	Radius	in, ft (cm, m)
R	Distance from dipole	(m)
R	Universal gas constant	53.35 ft-lb/lb/°R (8.312×10^3 J/k mole/° K)
S_N	Strouhal number	-
SPL, SPL_θ	Sound pressure level re 0.0002 dyne/cm^2, 1/3 octave band except where noted	dB
SPL'_θ	SPL without air attenuation	dB
$\overline{SPL}_S$	Space-averaged SPL	dB
S/V	Scani-valve	-

SYMBOL		UNITS
t	Thickness	in (cm)
T	Gas total temperature	°F (°K)
T5	Engine exhaust gas temperature	°C (°K)
TBB	Fan ball bearing temperature	°F (°K)
TL	Transmission loss due to treatment	dB
T_o	Ambient temperature	°F (°K)
TRB	Fan roller bearing temperature	°F (°K)
TT11	Fan discharge total temperature	°F (°K)
TWF	Engine fuel temperature	°F (°K)
$\overline{U}$	Mean flow velocity	ft/sec (m/sec)
V	Air velocity	mph (m/sec)
VO	Ambient wind velocity	MPH (m/sec)
V_j	Jet velocity	ft/sec (m/sec)
V1	Engine compressor vertical vibs	mils (cm)
V_1	Inlet box air velocity	ft/sec (m/sec)
V2	Engine turbine vertical vibs	mils (cm)
V_2	GE4 bellmouth air velocity	ft/sec (m/sec)
V3	Engine turbine horizontal vibs	mils (cm)
V4	Fan axial vibs	mils (cm)
V5	Fan horizontal vibs	mils (cm)
W	Sound power	watts
W(f)	Source power	Watts/Hz
W_{10}	Fan inlet airflow	lb/sec (kg/sec)
WF	Engine fuel flow	lb/hr (kg/sec)
x	Distance along treatment surface	ft (m)
X	Fan discharge traverse probe immersion	in (cm)

SYMBOL		UNITS
α	Ambient wind direction	degrees
β	Attenuation constant (0.23TL/L)	nepers/m
Δ	Total of air attenuation corrections	dB
δ	Boundary layer thickness	m
δ	Correction to standard pressure (PO/14.696)	-
θ	Angle from fan inlet or angle from normal	degrees
θ	Correction to standard temperature (TO/518.67)	-
λ	Wavelength	inches (m)
λ_o	Wavelength with zero media flow	inches (m)
λ_p	Phase wavelength	inches (m)
ρ	Density	lb/ft^3 (kg/m^3)
ω	Circular frequency	sec^{-1}
ω_0	Circular cutoff frequency	sec^{-1}
$\bar{\omega}_{inlet}$	Pressure loss coefficient	-

SECTION X

REFERENCES

1. McCann, E.O.: LF336/A and LF336/B Acoustic Tests Data Report. General Electric Company, TM 69-200, April 21, 1969

2. Kazin, S.B.: Results and Analysis of LF336/A Acoustic Test Data. General Electric Company, TM 69-223, April 30, 1969

3. Kazin, S.B.: Results and Analysis of LF336/B Acoustic Test Data, with Comparison to the LF336/A. General Electric Company TM 69-243, May 12, 1969

4. McCann, E.O.: Volk, L.J.: LF336C Modification and Acoustic Test Program Data Report (Three Volumes). General Electric Company, TM 70-729, September, 1970

5. Kazin. S.B. and Volk, L.J.: LF336 Lift Fan Modification and Acoustic Test Program. General Electric Company Final Report Contract No. NAS2-5462, April 16, 1971, CR-1934

6. Preliminary Design study of Quiet Integral Fan Lift Engines for VTOL Transport Application in the 80's. NASA CR-120969, August, 1971

7. Remote Lift Fan Study Program, Vol. I, II, and III, NASA CR-120970, 120971, and 120972, January 1972.

8. McCann, E.O.: Results of Discharge Noise Suppression Tests on the LF336/B Lift Fan at the Edwards Flight Test center. General Electric Company, TM 72-642, December 15, 1973

9. Standard Values of Atmospheric Absorption as a Function of Temperature and Humidity for Use in Evaluating Aircraft Flyover Noise. S.A.E. ARP 866, August 31, 1964.

10. Method of Calculating the Attenuation of Aircraft Ground to Ground Noise Propagation during Takeoff and Landing. Aerospace Information Report 923, Society of Automotive Engineers, Inc., August 15, 1966

11. Ffowcs Williams, J.E.: The Acoustics of Turbulence near Sound Absorbant Liners. Journal of Fluid Mechanics, Volume 51, Part 4, February 1972

12. Ver, I.L.: Prediction Scheme for the Self-Generated Noise of Silencers. P. 294, Inter-Noise 72 Proceedings, Washington, D.C., October 4-6, 1972.

13. Hoerner, S.F.: Fluid-Dynamic Drag, Published by author, 1965.

14. Aerospace Fluid Component Designer's Handbook, Vol. 1, TRW Systems Group, Redondo Beach, California, Feb. 1970, Prepared for Air Force Rocket Propulsion Laboratory, Edwards Air Force Base. RPL-TDR-64-25.

15. Volk, L.J.: LF336/A Lift Fan Final Report, General Electric Company, R69AEG180, April 1, 1969.

16. Skudrzyk, E.J.: Underwater Acoustics Seminar. Ordinance Research Laboratory, Pennsylvania State University, June 2-7, 1968

17. Lilley, G.M.: Pressure Fluctuations in an Incompressible Turbulent Boundary Layer. C. of A. Report 133 (1960)

18. Harrison, M.: Pressure Fluctuations on the Wall Adjacent to a Turbulent Boundary Layer. Hydromechanics Laboratory Research and Development Report, Department of the Navy, David Taylor Model Basin, Report 1260 (1958)

19. Bakewell, Jr., H.P.: The Longitudinal Space-Time Correlation Function in Turbulent Air Flow. Letter to the Editor, JASA Vol. 35, August 1963

20. Gardner, S.: On Surface Pressure Produced Boundary Layer Turbulence. Technical Research Group Report. 2 Aerial Way, Syosset, New York

21. Ingard, V.: Attention and Regeneration of Sound in Ducts and Jet Diffusers, JASA, Volume 31, Number 9, September, 1959.

22. Jet Noise Prediction. Aerospace Information Report No. 876, Society of Automotive Engineers, Inc., July 10, 1965

23. Beranek, L.L.: Noise Reduction, New York, McGraw-Hill Book Company, 1960.

APPENDIX A

FLOW GENERATION NOISE

According to J.E. Ffowcs Williams (Reference 11) either monopole or dipole radiated pressure fields are possible due to flow past treatment. If the effective porosity

$$4\ aN/k < 1 \tag{18}$$

where a = hole diameter (m)

N = number of holes per unit area (m^2)

k = $2\pi/\lambda$ = wavemumber (m^{-1})

λ = wave length

we have a surface-scattered field which is due to a system of aerodynamic monopoles radiating a pressure field of amplitude

$$P = \sum_{m} \frac{3\pi}{8} \frac{a}{|R|} P_a \tag{19}$$

where R = distance from monopole (m)

P_a = aerodynamic wall pressure (Newton/m^2)

m = number of holes

If the effective porosity is greater than 1, we have a surface-scattered field which is due to a system of aerodynamic dipoles radiating a pressure field of amplitude.

$$P = \sum_{m} \frac{k \cos \theta}{2\pi N |R|} P_a \tag{20}$$

where R = distance from dipole (m)

θ = angle from normal to wall (degrees)

A direct measurement of the aerodynamic wall pressure p_a, is not available; however, an estimate of the monopole or dipole radiated power can

be made using an estimate of p_a from Dr. E.J. Skudrzyk's lectures on flow noise (Reference 16)

$$P_a \simeq 1/2\ K\ \rho\ \bar{U}^2 \tag{21}$$

where $\bar{U}$ = mean velocity (m/sec)
ρ = density (kg/m^3)
K = 4 to 6 x 10^{-3} per References 17, 18, 19, and 20

Skudrzyk's second assumption is that the idealized power spectrum of the pressure referred to unit frequency is given by:

$$P\ (\omega) = \text{constant}\ \omega \leq \omega_0 \tag{22a}$$

$$P\ (\omega) = \text{constant}/\omega^3\ \ \omega > \omega_0 \tag{22b}$$

The cutoff frequency ω_0 is given by

$$\omega_0 = 2\pi\ \bar{U}/\delta \tag{23}$$

where δ is the boundary layer thickness (meters).

To solve Equation 20 for dipole radiation, the additional assumptions are made that $k = M/\ell$ and $\ell = \delta$, or that the space length of the pressure pulse ℓ is equal to the boundary layer thickness.

For frequencies less than the cutoff frequency, the flow generated power spectrum is

$$P\ (f) = 1.6\ M^3\ \bar{U}^3\ \rho\ A\ \ N^{-1}\ \delta^{-2}\ x\ 10^{-7}\ \frac{\text{watts}}{\text{Hz}} \tag{24}$$

where the variables not previously defined are

M = Mach number
A = scrubbing or treatment area (m^2)

F

For a monopole, Ffowcs Williams (Reference 11) estimates a flow generated power level per unit area to be in the order of $a^2 N \rho \bar{U}^3 M \times 10^{-6}$ watts/m^2.

For a one-dimensional duct of length L, the total radiated power spectrum P' (f) is the sum of the attentuated source power and the treatment generated noise following Ingard's (Reference 21) analysis.

$$P'(f) = W(f)\, e^{-\beta L} + \int_0^L \frac{P(f, \delta(x))}{2}\, e^{-\beta(L-x)}\, dx \ \frac{\text{watts}}{\text{Hz}} \qquad (25)$$

where
- $W(f)$ = source power (watts/Hz)
- $P(f, \delta(x))$ = flow noise/length (watts/Hz/m)
- β = attenuation constant (0.23 TL/L) (nepers/m)
- TL = transmission loss due to treatment (db)

The significance of Equation 21 may be explained by referring to the sketch in Figure 167. The power P' radiated at the exit plane is the sum of the aft radiated source power W attenuated over the length of the duct L and the power generated at some point x by the flow over the treatment surface radiated downstream (hence the 1/2 in the integral) and attenuated over the remaining length (L-x). The duct attenuation is then given by

$$ATT_{duct} = 10 \log_{10} \frac{W}{P'} \qquad (26)$$

Assuming that P is constant over the length of the treatment, integrating and combining Equations 25 and 26 gives

$$ATT_{duct} = TL - 10 \log_{10} \left[1 + \frac{P(f)\,(e^{\beta L} - 1)}{2\, W(f)\, \beta} \right] \qquad (27)$$

APPENDIX B

CORE AND JET NOISE

One of the conclusions of the preceding section was that the apparent lack of duct treatment suppression was due to flow-generated broadband noise. Other possible sources of a broadband floor could be jet noise or core noise. As a check for the possibility of this type of floor, predicted jet noise and core noise levels were compared with measured noise levels. A modified version of the SAE jet noise prediction technique as outlined in Reference 22 was used to calculate jet noise levels. In this method, the frequency of the jet noise peak is determined from the Strouhal relationship

$$S_N = fd/V_j \tag{28}$$

where S_N is the Strouhal number, f the frequency of the peak, V_j the jet velocity, and d is a characteristic dimension. There are some differences of opinion as to whether the characteristic dimension should be an effective diameter of the annulus area for coannular jets or the annulus height itself. Both characteristic dimensions were used in checking for the jet noise floor. Velocities and weight flows for the jet noise prediction are based on performance measurements.

Core (or internal) engine noise was estimated using an empirically developed prediction technique based on turbofan engine data. Core engine noise consists of low frequency combustor noise and low frequency tip turbine turbomachinery noise.

The following comparisons of estimated core and jet noise levels, were all made at the 110 degree microphone on a 150 foot (45.7 m) arc with fan inlet suppression installed and thirty (76.2 cm) m) of exhaust treatment. In Figure 168, jet and core noise predictions are compared to measured levels at 5300 RPM. For this comparison, the jet noise was determined by calculating the jet noise of each of the four annulus areas. Each area was individually referenced to its effective diameter. The resulting spectra were added to give the predicted jet noise levels. The total of the jet and core noise does not give a good comparison with the measured levels. Similar results are

achieved at 4800 RPM fan speed in Figure 169. The jet and core noise total is also above measured levels. It should be noted that neither the jet noise nor the core noise prediction technique attempts to model the ground null and reflection patterns.

In Figure 170, predicted jet and core noise are again compared to measured levels; however, for this comparison the jet noise was referenced to the annulus height of each coannular exhaust passage. As a result, the jet noise peak shifts to a higher frequency and does not result in a good comparison with measured levels. Similar results are noted at 4800 RPM in Figure 171.

The important result from these last four figures is that predicted jet and core noise levels regardless of the base (effective diameter or annulus height) are well below measured levels at frequencies greater than 1000 Hz. This means that neither jet noise nor core noise is contributing to the flow generated floor. Low frequency measured levels at various fan speeds are not predicted consistently by jet noise prediction techniques which are based on effective diameter or annulus height.

APPENDIX C

FAN EXHAUST TONES

During the initial mechanical checkout run with the exhaust adapter in place, it was noted that the fan performance was off the design operating line. For this and subsequent checkout runs, apparent fan exhaust tones were observed and investigated. The initial configuration tested is shown in Figure 74 and included the exhaust adapter on the fan exhaust and unsuppressed fan inlet. As previously stated, the exhaust adapter is a twelve inch (30.5 cm) long untreated section which transitions from the fan exit flowpath to the flowpath of the double ring suppression system. For this checkout run, selected far field microphones were used to record sound; however, no attempt was made to meet wind requirements of less than 5 mph (8 km/hr) since the test was primarily a mechanical check-out. During this test, two things were observed; first, low static pressure and high-flow conditions in the fan, and, second, the presence of a strong tone at low frequencies in the range of 500 to 800 Hz which varied with fan speed. Figure 172 shows this tone at the 120 degree microphone position at a fan speed of 4200 RPM. The exhaust adapter alone caused a radially outward flow in the outer fan flowpath annulus, and a radially inward flow condition through the middle annulus. For this reason, a second checkout run was made with ten inches (25.4 cm) of exhaust treatment to redirect the flow axially. In addition, the wing simulation surface was removed to eliminate that as a possible source of the observed tones. Figure 172 shows that the 750 Hz tone is down 11 dB in this second checkout run. Although redirecting the flow with the ten inches (25.4 cm) of exhaust treatment alleviated the low static pressures somewhat, eight radial U-channels were installed on the fan exhaust plane for blockage as shown in Figure 31. Addition of this blockage raised static pressures and vented the splitter bases. Acoustic results indicated that the 750 Hz tone so prominent in runs 1 and 2 was not present as Figure 172 shows. While the results of these three checkout runs were being analyzed, acoustic testing was initiated with the fan in an unsuppressed (inlet and exhaust) configuration since fan performance precluded operation with exhaust adapter only. In addition, Test 2 which had fan inlet suppression was completed.

During Tests 1 and 2, faired radial blockage to replace the ones shown in Figure 78 were designed and fabricated. These faired tabs are shown in Figure 112 and were designed to eliminate any wake noise that might be generated by flow over the radial blockage at higher speeds than those tested during the checkout runs. Figure 174 shows the resulting spectrum with faired radial blockage at 4200 RPM. Note that fan inlet suppression was installed and the wing simulation surface was also installed. The faired radial blockage was not acceptable from a performance viewpoint and Figure 174 shows a hump of noise near 750 Hz which is similar to that observed in checkout run 2 (Figure 172). U-Channel blockage was re-installed to regain fan performance and, simultaneously, the wing simulation surface was removed to provide the same exhaust configuration as checkout run 3. Figure 175 shows the 120 degree microphone spectrum at 4200 RPM for Test 3. There are two points to be noted here. The first is that there is a hump of noise centered on 750 Hz and, second, there is no appreciable difference between the faired blockage (Figure 174) and U-Channel blockage in the frequency range from 1000 to 2000 Hz. If wake generated noise from the U-Channels was radiating to the far field, one would expect to see a Strouhal type peak near 1200 to 1500 Hz based on the following assumptions of S_N = .20 to .25, $\bar{U}$ = 500 fps (152 m/sec), and d = 1 inch (2.54 cm). Equation 29 relates these variables

$$S_N = fd/\bar{U} \tag{29}$$

The fact that there is no difference between the U-Channel blockage and faired radial blockage in this frequency region indicates that the U-Channel blockage does not affect the far field noise levels.

The spectra of Figures 174 and 175 each have the 750 Hz hump and both configurations have exhaust splitters with blunt trailing edges as shown in Figures 78 and 112. If vortex shedding noise were being generated off these bases, one would expect for S_N = .2 to .25, $\bar{U}$ = 500 fps (152 m/

sec), and d = 2 inches (5.08 cm) to see a Strouhal peak near 600 to 750 Hz according to the relations of Equation 29.

Frequency spectra at higher fan speeds of 4800 and 5300 RPM are shown in Figures 176 and 177, respectively, for Test 3. Figure 175 has a slight hump near 900 Hz while Figure 177 shows a hump centered at 1000 Hz. The hump in Figure 176 occurs at the frequency where the second ground reflection null occurs and this may be why the hump is not as pronounced as another speeds. These three figures indicate that the hump varies or shifts with fan speed.

Velocities in the exit plane based upon the performance probe data are shown in Figure 178 for each flow passage for Tests 3, 4 and 5 which had ten inches (25.4 cm), twenty inches (50.8 cm), and thirty inches (76.2 cm) of exhaust treatment, respectively. Except for the fan inner passage, velocity varies linearly with fan (on the average). In Figure 178, the peak frequencies of the exhaust tones are seen to also very linearly with fan speed. Combining the results of Figures 178 and 179 indicates that the peak frequency varies linearly with the velocity. This is precisely the relationship given in equation 29 which for a given reference dimension d, indicates that frequency is directly proportional to velocity. These results suggest that the tones are vortex shedding noise off the blunt splitter bases. That these tones are exhaust radiated is verified by Figure 180, which is the 20 Hz bandwidth SPL directivity pattern of the tone at 4800 RPM fan speed. Figure 181 shows that the tone is present in 1/3 octave band data.

Perceived noise level calculations of an average curve through the data of Figure 181 with the tones gives a level of 108.2 PNdB. Fairing through the tone gives 107.7 PNdB which indicates that the tone only slightly affects the perceived noise levels achieved.

These tones appear to be a characteristic of lift fans which have blunt splitter bases and may necessitate some changes to existing design philosophies if they are to be removed from the spectra of future lift fans.

APPENDIX D

CORE ENGINE TONES

Previous LF336 lift fan testing (References 1 and 4) had revealed the presence of two low frequency tones near 100 Hz and 250 Hz. The tone near 250 Hz tracked with core engine speed and was found to be a one-per-rev signal from the J85 core engine. The source of the 100 Hz tone which did not vary with speed (engine or fan) was never identified. Since one of the goals of this test was to determine the low frequency jet noise spectrum, early test results were examined closely with the objective of identifying and eliminating these tones from the far field noise levels. During the checkout phase of testing, a hand-held near field microphone indicated a strong one-per-rev signal near the bellmouth and inlet suppressor of the J85 engine. Accordingly, these components were wrapped with a lead-vinyl blanket to reduce radiation at this point. Figure 27 shows the lead blanket in place. When the far field data of Test 1 (unsuppressed fan) revealed that both tones were still present, it was decided to replace the core engine with a different engine. The same core engine had been used for all previous LF336 testing and had a history of high turbine frame vibrations. The replacement engine had a history of low vibrations. Results of the engine change on narrowbands are shown in Figure 182. Comparing Test 1 and Test 2 at the 120 degree microphone at 4200 RPM fan speed shows that replacing the core engine eliminated the 100 Hz tone. The one-per-rev signal is still present; however, the tone-to-broadband ratio has decreased. Subsequent tests which have increasing lengths of exhaust treatment show no indications of either tone. The one-per-rev signal was not visible in the 20 Hz narrowbands at higher speeds at this 120 degree microphone location.

Further examination of 20 Hz bandwidth narrowbands at other angles revealed that the one-per-rev signal was present at the 30 degree microphone as shown in Figure 183 at 4800 RPM for unsuppressed and fully suppressed exhaust configurations. Also shown in Figure 183 is the 40 degree microphone spectrum for the same configuration which does not have the tone. Figure 184 shows the 250 Hz 1/3 octave band directivity pattern for the fully suppressed

exhaust configuration at 5300 RPM and 4800 RPM. At both speeds the forward quadrant levels at 30 degrees are being influenced by the core engine one-per-rev signal.

APPENDIX E

DIRECTIVITY PATTERNS

Directivity indices for Tests 1 and 2 were calculated as part of the normal data processing program. The directivity index is a valuable tool since it allows comparisons to be made without a dependence on the magnitude of the sound power level of the radiated source. The directivity index D.I. as defined in Equation 30 is similar to the definition given in Reference 23.

$$D.I._{\theta} = SPL_{\theta} - \overline{SPL}_{S} \tag{30}$$

The subscript θ denotes that the directivity index and sound pressure level are measured in the direction θ. $\overline{SPL}_{S}$ is the space averaged sound pressure level that would be produced by a nondirectional source at the same distance as the measured SPL's. For this test, the area used in the power level calculation was assumed to be a 3/4 sphere which is an estimate of the surface reflection characteristics. The 3/4 sphere assumption is an average of a fully reflecting surface and a fully absorbing surface. $\overline{SPL}_{S}$ is then

$$\overline{SPL}_{S} = PWL - 20 \log R - 9.74 \tag{31}$$

where the sound power level, PWL, is referenced to 10^{-13} watts and R is the radius in feet. Combining Equations 30 and 31 gives the following relationship:

$$PWL + D.I._{\theta} = SPL_{\theta} + 20 \log R + 9.74 \tag{32}$$

For a radius of 150 feet (45.7 m), Equation 32 is shown in Figure 185. The above relation does not include corrections for air absorption and extra ground attenuation effects. These corrections may easily be included by replacing SPL_{θ} in Equation 32 by SPL'_{θ} where

$$SPL'_{\theta} = SPL_{\theta} + \Delta \tag{33}$$

where Δ is the total attenuation correction for that distance.

Figure 186 shows the directivity indices from the unsuppressed fan configuration of Test 1 for the 1/3 octave band which contains the blade passing frequency. Although three speed points and their repeat points are shown on this figure, there is generally a collapse of the data to plus or minus two dB.

Directivity indices from the unsuppressed fan exhaust radiated spectrum of Test 2 are shown in Figure 187 again for the 1/3 octave band containing the BPF. This figure shows that the three speed points plus the two repeats at each speed collapse to plus or minus 1.5 dB. Similar results were observed for the fan broadband bands above and below the BPF band. This means that the directivity indices from the top two fan speeds for each of these two tests may be averaged (as indicated by the solid lines in Figures 186 and 187 to give representative directivity indices for the unsuppressed total and the unsuppressed fan exhaust radiated spectrum that are independent of fan speed. This was done for the five 1/3 octave bands above and below the BPF band plus the BPF band from Tests 1 and 2 and the results shown in Figures 188 thru 198.

The directivity indices presented in Figures 188 thru 198 may be used to estimate the far field sound pressure levels of similar lift fans. The only input needed is the source sound power level with air absorption and extra ground attenuation corrections for 150 foot (45.7 m).

For example, assume that the BPF sound pressure level of an unsuppressed lift fan is desired at the 120 degree microphone location on a 150 foot (45.7 m) arc and that the source power level has been estimated to be 130 dB. First, from Figure 193 the DI is read from the inlet and fan exhaust curve at 120 degrees to be 0 dB. Next, the sound power level and directivity index are used in Figure 185 to determine the sound pressure level desired. From Figure 185 the SPL at 120 degrees at 150 foot (45.7 m) is 77 dB.

For a second example showing the possible applications of Figures 188 thru 198, let us assume that we need to estimate the 70 degree microphone fan broadband noise three 1/3 octave bands below the pure tone for a fan which has 10 dB of exhaust suppression. For this "paper" fan, the unsuppressed fan power level corrected to 150 foot (45.7 m) has been estimated at 130 dB. From Figure 190, the DI for the unsuppressed fan is -0.5 dB which combined with the power level gives an unsuppressed fan SPL of 76.5 dB. Next, the unsuppressed exhaust radiated SPL is calculated. If the exhaust and inlet radiated PWL's are assumed equal, the PWL of the exhaust radiated spectrum will be 3 dB less than the total or 127 dB. From Figure 190, the exhaust radiated DI is -2 dB at 70 degrees which combined with the exhaust radiated PWL of 127 dB give a SPL is

72 dB using Figure 185. If the unsuppressed exhaust radiated SPL is 72 dB and the total is 76.5 dB, the inlet radiated level must be 74.6 dB. However, the fan exhaust was to have 10 dB of suppression which would lower it to 62 dB. The SPL at the 70 degree microphone is now the logarithmic sum of the inlet radiated SPL and the suppressed exhaust radiated SPL or 74.6 + 62.0 = 74.8 dB.

Both of the above examples were for specific angles on a 150 foot (45.7 m) radius. The calculations may be easily expanded to include all angles and all fan noise 1/3 octave bands. In addition, standard extrapolation procedures may be used to determine the sound pressure levels at any arc or sideline distance.

Table I. Instrumentation List.

Parameter	Symbol	No.	Range	Recorder
J85 RPM	NE	1	0-102%	Panel, PCM
J85 Fuel Flow	WF	1	0-6000 lb/hr (0-2722 kg/sec)	Panel, PCM
J85 EGT	T5	1	0-1000° C (0-1273° K)	Panel, PCM
J85 Oil Pressure		1	0-50 PSIG (0-344.7 kN/m^2)	Panel
J85 Vibs Comp. Vert.	V1	1	0-10 Mils (0-0.254 mm)	Panel
J85 Vibs Turb. Vert.	V2	1	0-10 Mils (0-0.254 mm)	Panel
J85 Vibs Turb. Horiz.	V3	1	0-10 Mils (0-0.254 mm)	Panel
J85 Bellmouth Static Pres.	PS2	2	-1.5-0 PSIG (-10.34-0 kN/m^2)	PCM
Fuel Temperature	TWF	1	0-150° F (256-339° K)	PCM
Bleed Valve Indicator	BVO	1	0-100%	PCM
LF336 RPM	NF	1	0-7000 RPM	Panel, PCM
LF336 Vibs Axial	V4	1	0-5 Mils (0-0.127 mm)	Panel
LF336 Vibs Horizontal	V5	1	0-5 Mils (0.0.127 mm)	Panel
LF336 Roller Bearing Temp.	TRB	2	0-500° F (256-533° K)	Panel, PCM
LF336 Ball Bearing Temp.	TBB	2	0-500° F (256-533° K)	Panel, PCM
Fan Total Thrust	FG	1	0-6000 lb (0-26.69 kN)	Panel, PCM
GE4 Bellmouth Static Press.	PS10	1	0-10 in. H_2O (0-2.49 kN/m^2)	Panel, PCM
Fan Discharge Trav. Temp	TT11	1	0-1000° F (256-811° K)	PCM
Fan Disc. Trav. Total Pres.	PT11	1	-5 to +5 PSIG (-34.47 to +34.47 kN/m^2)	PCM
Fan Disc. Trav. Static Pres.	PS11	1	-5 to +5 PSIG (-34.47 to +34.47 kN/m^2)	PCM
Fan Disc. Trav. Immersion	X	1	0-15 inch (0.38.1 cm)	PCM, Panel

Table I. Instrumentation List. - Concluded

Parameter	Symbol	No.	Range	Recorder
Ambient Wind Velocity	VO	1	0-50 MPH (0-22.35 m/sec)	Panel
Ambient Wind Direction	α	1	360°	Panel
Ambient Pressure	PO	1	0-15 PSIA (0-103.4 kN/m^2)	Panel, PCM
Ambient Air Temperature	OAT	1	0-150° F (256-533° K)	Panel, PCM
Fan Bellmouth Static Pres.	PSBM	12	-5 to 0 PSIG (-34.47 to 0 kN/m^2)	PCM - S/V
Fan Bulletnose Static Pres.	PSBN	12	-5 to 0 PSIG (-34.47 to 0 kN/m^2)	PCM - S/V
Trans. Section Static Pres.	PSA	12	-5 to +5 PSIG (-34.47 to +34.47 kN/m^2)	PCM - S/V
Trans. Section Static Pres.	PSB	12	-5 to +5 PSIG (-34.47 to +34.47 kN/m^2)	PCM - S/V
Trans. Section Static Pres.	PSC	12	-5 to +5 PSIG (-34.47 to +34.47 kN/m^2)	PCM - S/V
Trans. Section Static Pres.	PSD	12	-5 to +5 PSIG (-34.47 to +34.47 kN/m^2)	PCM - S/V
Base Static Pressure	PSE	22	-5 to +5 PSIG (-34.47 to +34.47 kN/m^2)	PCM - S/V

S/V is Scani-valve for pressure recording.

All other channels on PCM were straight through, i.e., continuous recording of one parameter.

Table II. LF336/B Lift Fan Description

Fan Pressure Ratio	1.30	
Fan Tip Diameter, inches, cm	36	91.44
Fan Radius Ratio	0.475	
Fan Flow*, lbs/sec, kg/sec	218	98.9
Bypass Ratio	5.0	
Fan Tip Speed*, ft/sec, m/sec	950	289.6
RPM*	6048	
Total Thrust *, Unvectored, lbs, N	5500	24,465
Blade Number	42	
Vane Number	45	
Blade-Vane Axial Spacing, expressed in Blade Tip Chords	2.0	

* Corrected Values

Table III. Test Run Summary
LF336 Discharge Noise Suppression Investigation

Run	Test	Date	Description
1		06-20-72	Engine and fan checkout with exhaust adapter only
2		06-21-72	Exhaust adapter and 10 inch (25.4 cm) exhaust suppression
			Wing simulation surface removed
3,4		06-23-72	Exhaust adapter and 10 inch (25.4 cm) exhaust suppression
			Wing simulation surface removed
			U-Channel blockage added
5		07-05-72	Exhaust adapter and 10 inch (25.4 cm) exhaust suppression removed
6	1	07-06-72	Unsuppressed Fan
7,8		07-10-72	Inlet Suppressor checkout
9		07-10-72	Replacement J85 (S/N 231-232) checkout
10	2	07-22-72	Inlet suppression only
11	3	07-25-72	Inlet suppression
			Exhaust adapter and 10 inch (25.4 cm) exhaust suppression
			Airfoiled blockage
			Wing simulation surface
12	3	07-27-72	Inlet suppression
			Exhaust adapter and 10 inch (25.4 cm) exhaust suppression
			U-Channel blockage
			Wing simulation surface removed
			Aborted due to high winds

Table III. Test Run Summary
LF336 Discharge Noise Suppression Investigation - Concluded

Run	Test	Date	Description
13	3	07-29-72	Same as Run 12
14	4	08-03-72	Exhaust Adapter and 20 inches (50.8 cm) exhaust suppression
			U-Channel blockage
			Wing simulation surface removed
15,16	5	08-04-72	Inlet suppression
			Exhaust adapter and 30 inches (76.2 cm) exhaust suppression
			U-Channel blockage
			Wing simulation surface removed
17	5	08-11-72	Same as Run 15, 16
			Idle speed points

Table IV. LF336 Tests.

Test	Fan Speed (Nominal) 50 (3024)	60 (3628)	70 (4233)	80 (4838)	87.7 % (5304) RPM
1	2*	2	2	2	2
2			3	3	3
3			3	3	3
4			3	3	3
5	2	2	3	3	3

* Denotes number of readings at each speed.

Table V. Flow-Noise Generation Parameters.

Speed Point	L (inch)	L (cm)	Area (m^2)	Average Flow Mach number	Boundary Layer Thickness δ (m)
4800 rpm	10	25.4	3.03	0.52	0.0084
	20	50.8	6.06	0.51	0.0149
	30	76.2	9.10	0.51	0.0153
5300 rpm	10	25.4	3.03	0.59	0.0090
	20	50.8	6.06	0.59	0.0116
	30	76.2	9.10	0.57	0.0147

Table VI. Estimated Thrust Losses for Various Amounts of Exhaust Suppression.

		10 Inches (25.4 cm)	20 Inches (50.8 cm)	30 Inches (76.2 cm)
Losses from Acoustic Hardware				
Support Strut Drag		0.1	0.1	0.2
Splitter Skin Friction Drag		4.3	5.7	7.8
Splitter Base Drag		3.8	3.5	3.1
	Total	8.2	9.3	11.1
Losses Due to Test Set-Up				
Inlet Box, GE4 Bellmouth & Inlet Adapter Section		0.4	0.4	0.4
Hub & Midbox Base Drag		3.1	3.3	3.7
Rod Forebody Drag		3.6	3.8	3.8
Rod Splitter Interference Drag		3.3	3.3	3.3
	Total	10.4	10.8	11.2
Losses from Fan Back Pressure		-0.4	0.8	1.7
Total Losses from all Sources		18.2	20.9	24.0

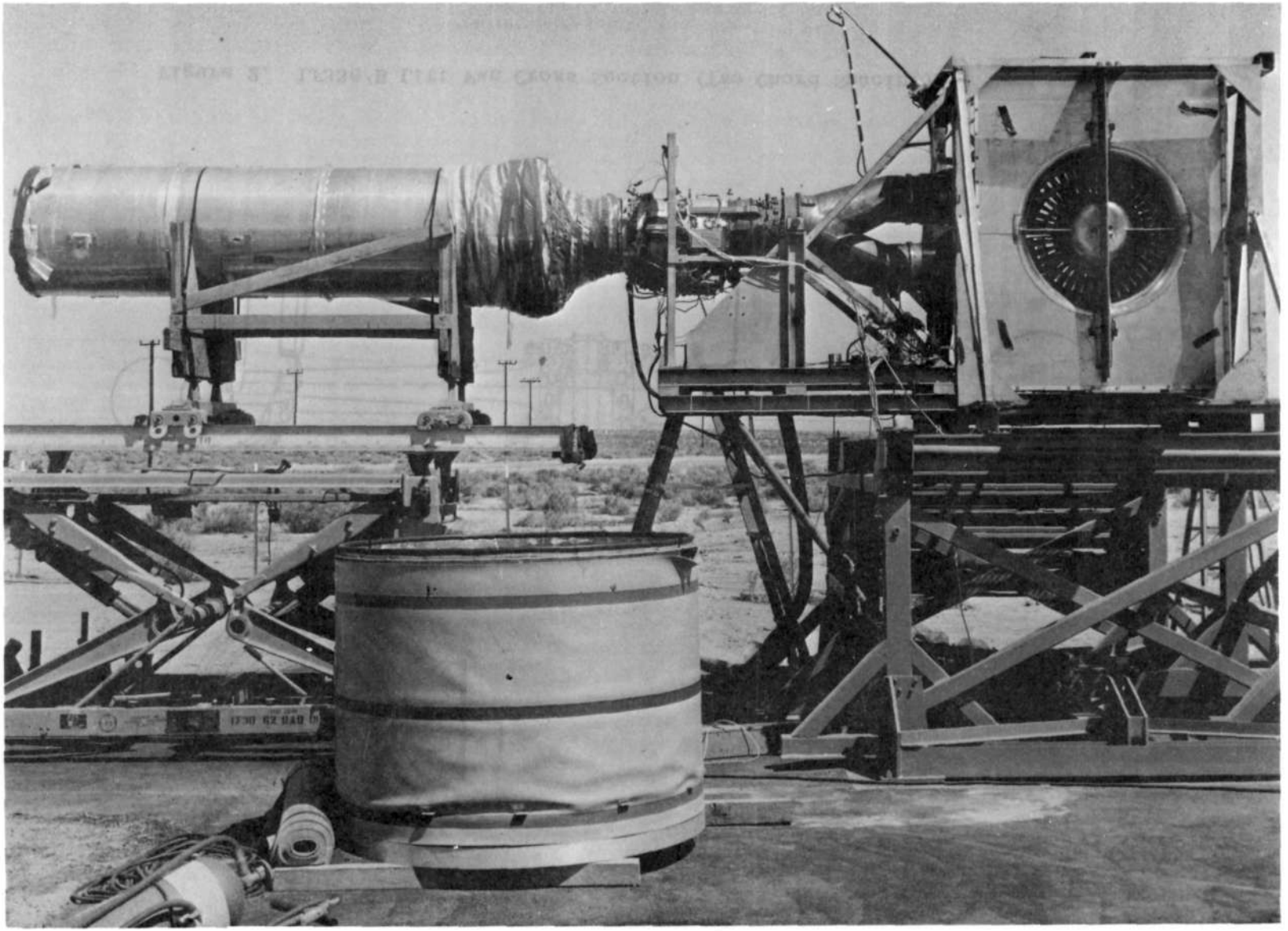

Figure 1. LF336/B Lift Fan without Inlet Noise Suppressor

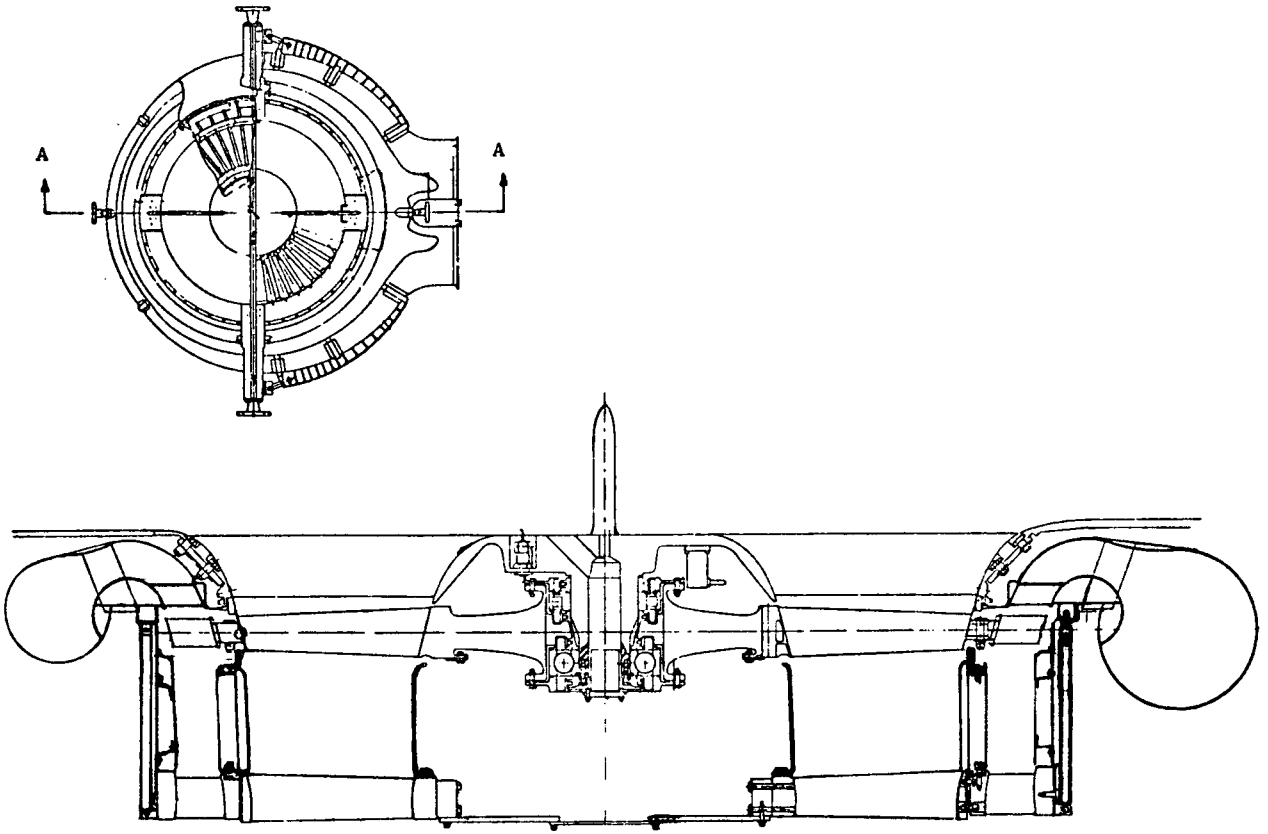

Figure 2. LF336/B Lift Fan Cross Section (Two Chord Spacing)

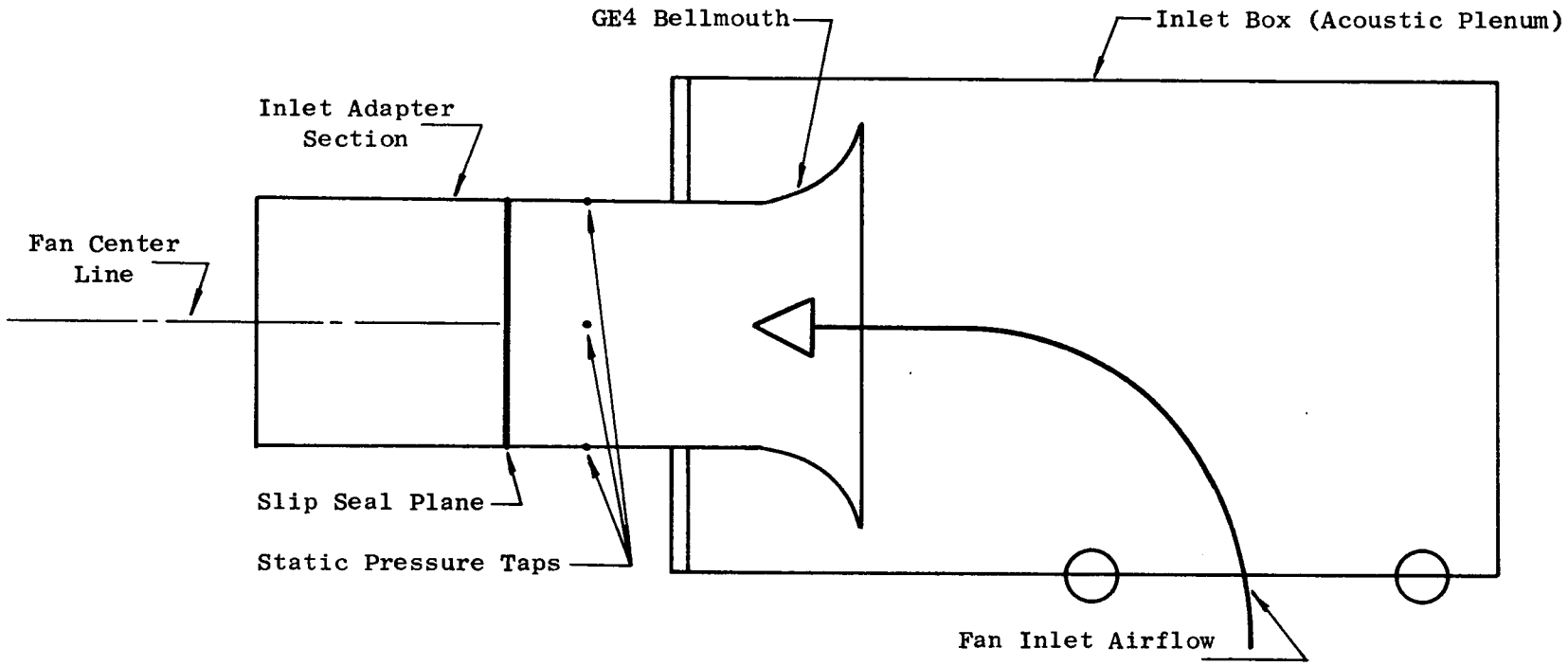

Figure 3. Inlet Suppressor System Components

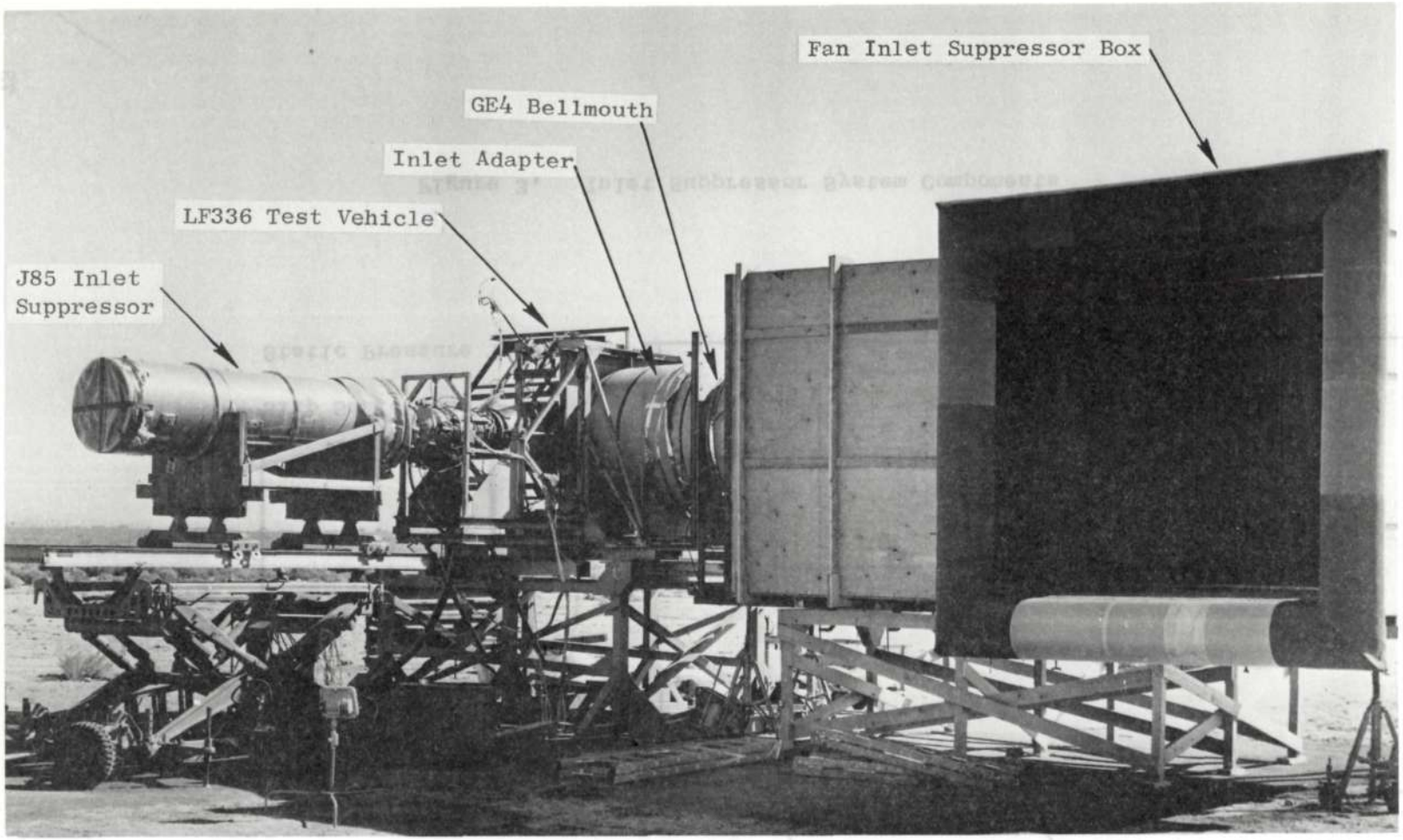

Figure 4. LF336/B Lift Fan with Inlet Noise Suppressor

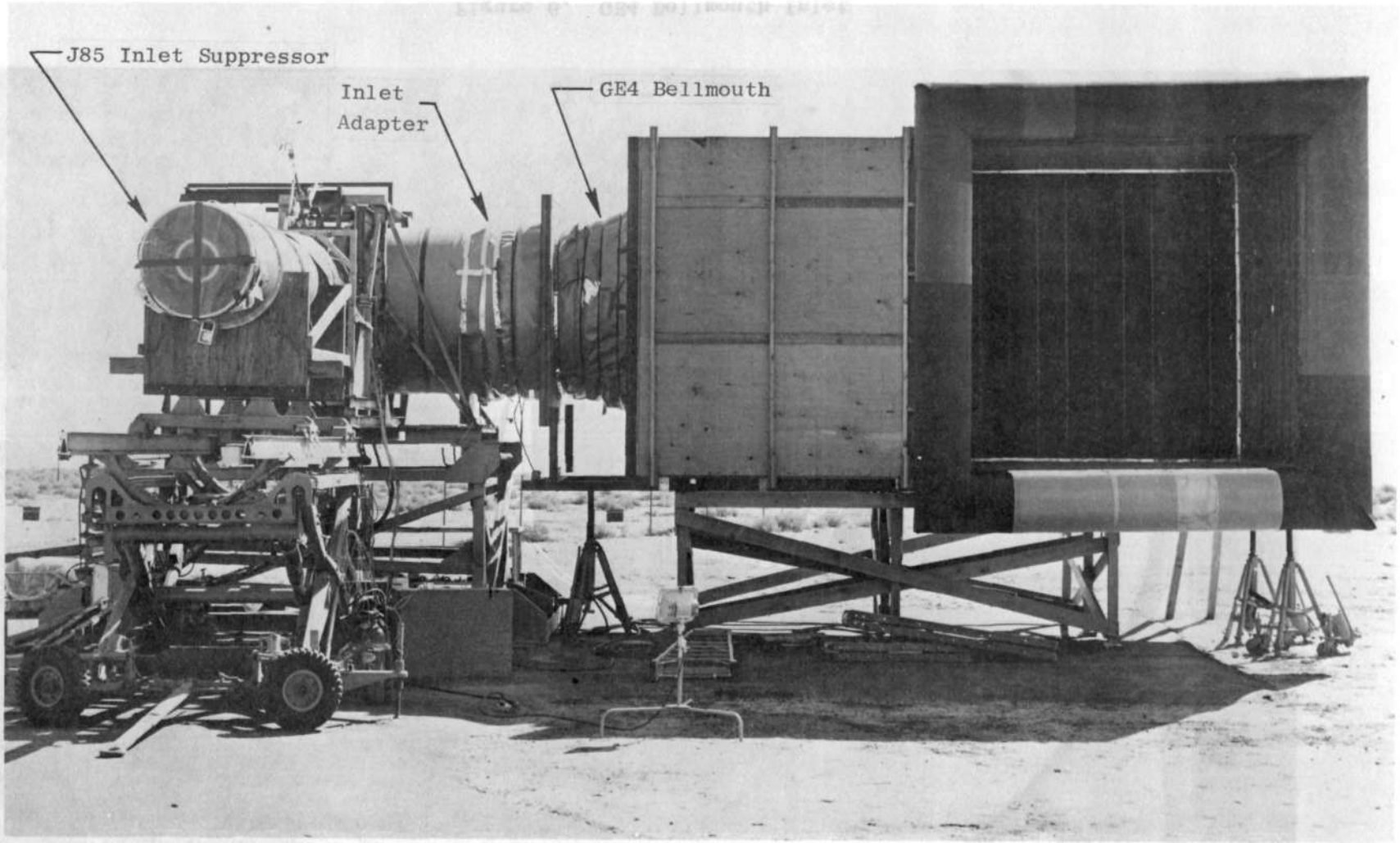

Figure 5. LF336/B Lift Fan Inlet Noise Suppressor - Inlet Side

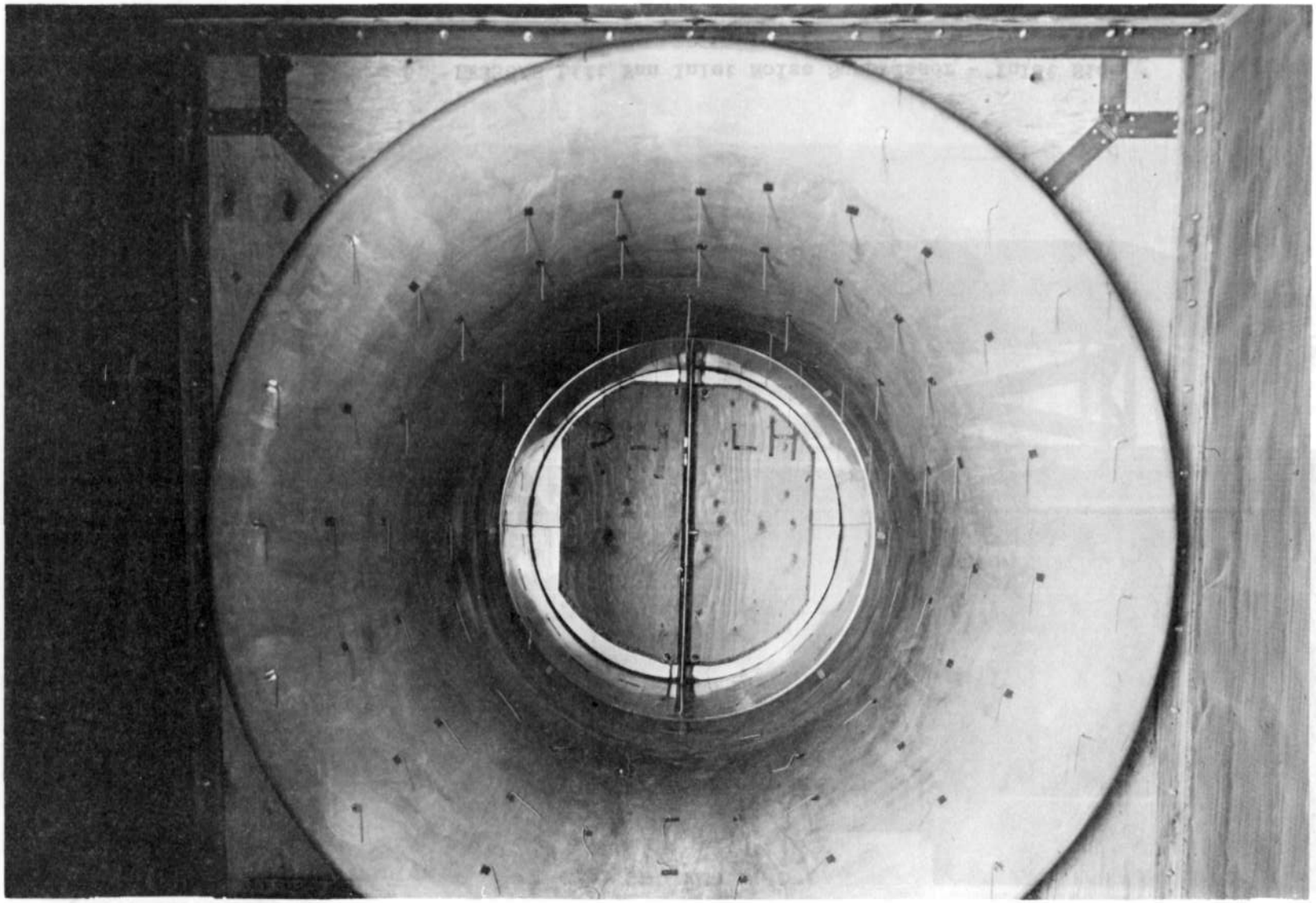

Figure 6. GE4 Bellmouth Inlet

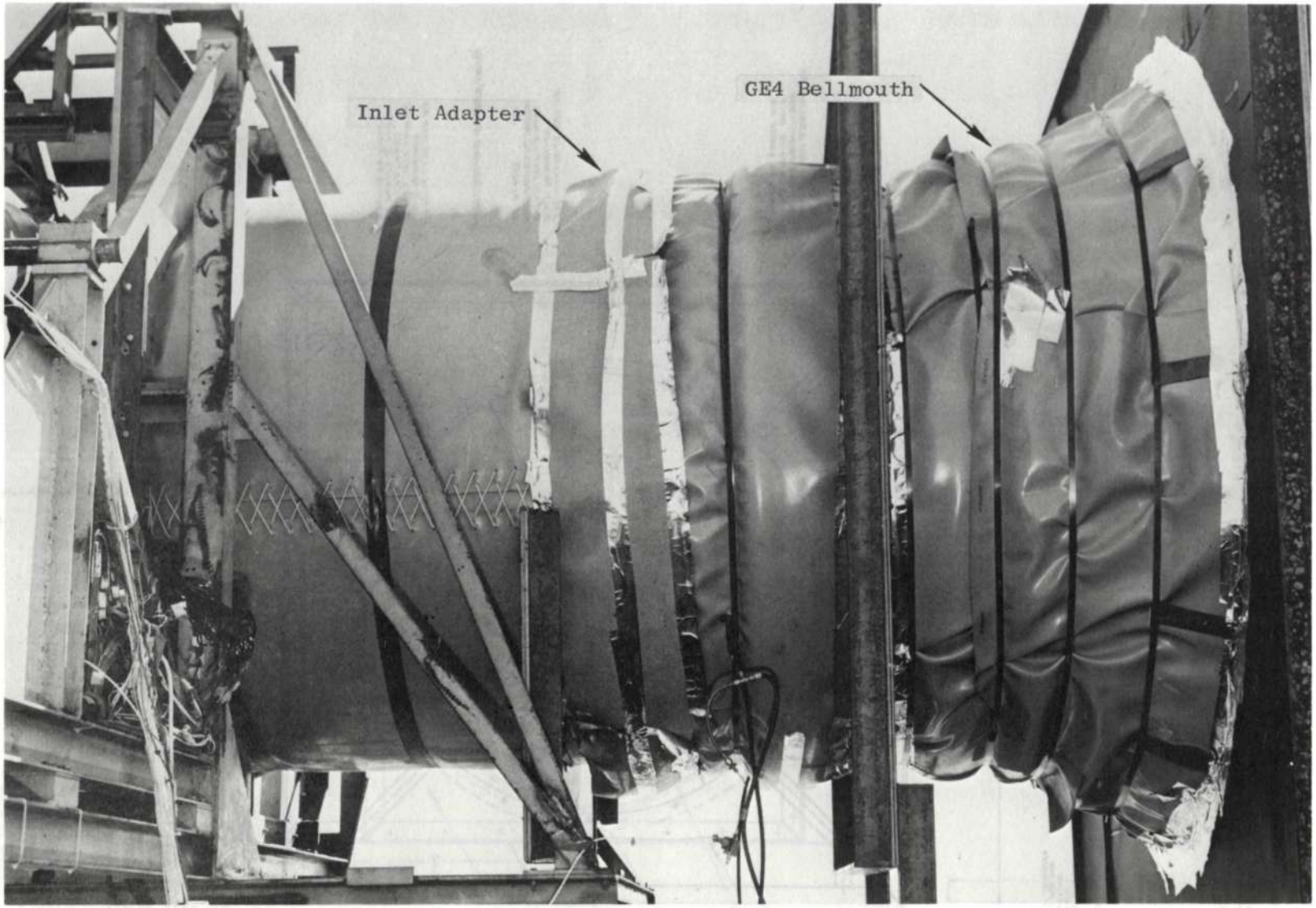

Figure 7. GE4 Bellmouth and Fan Inlet Duct

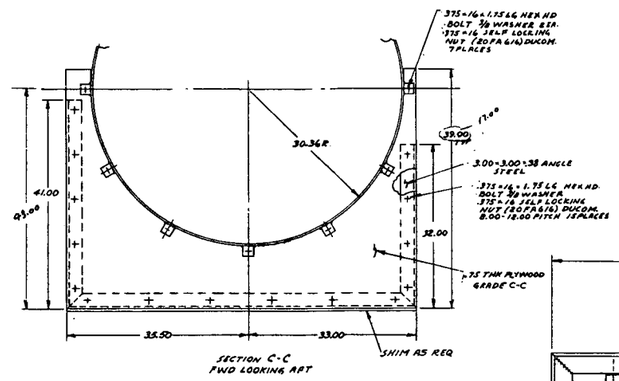

SECTION C-C
FWD LOOKING AFT

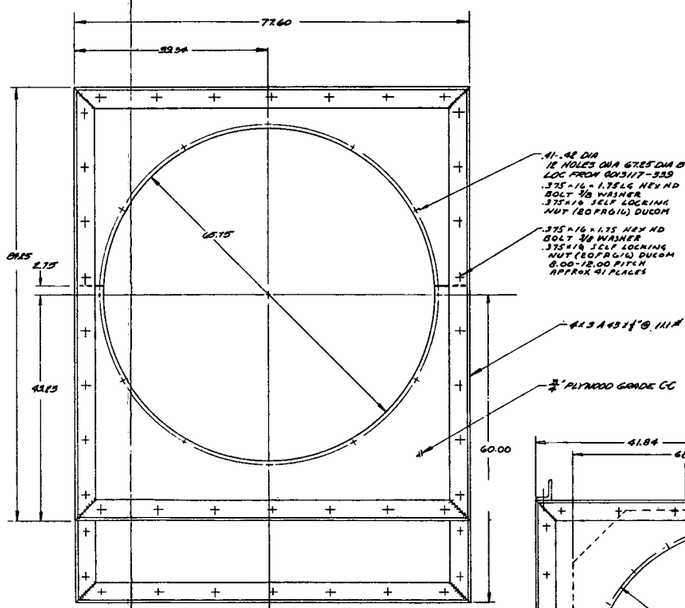

VIEW AT D-D
AFT LOOKING FWD

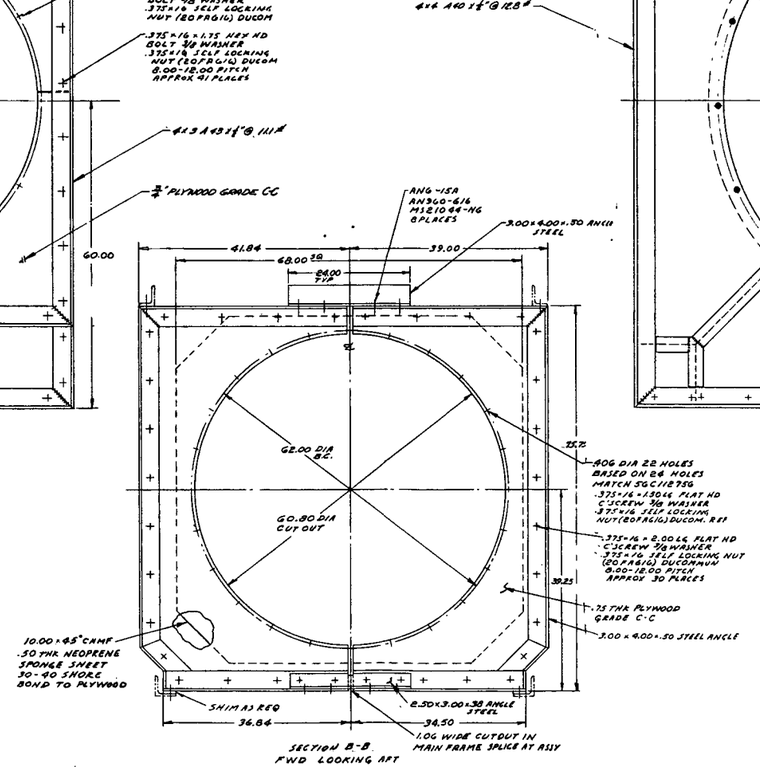

SECTION B-B
FWD LOOKING AFT

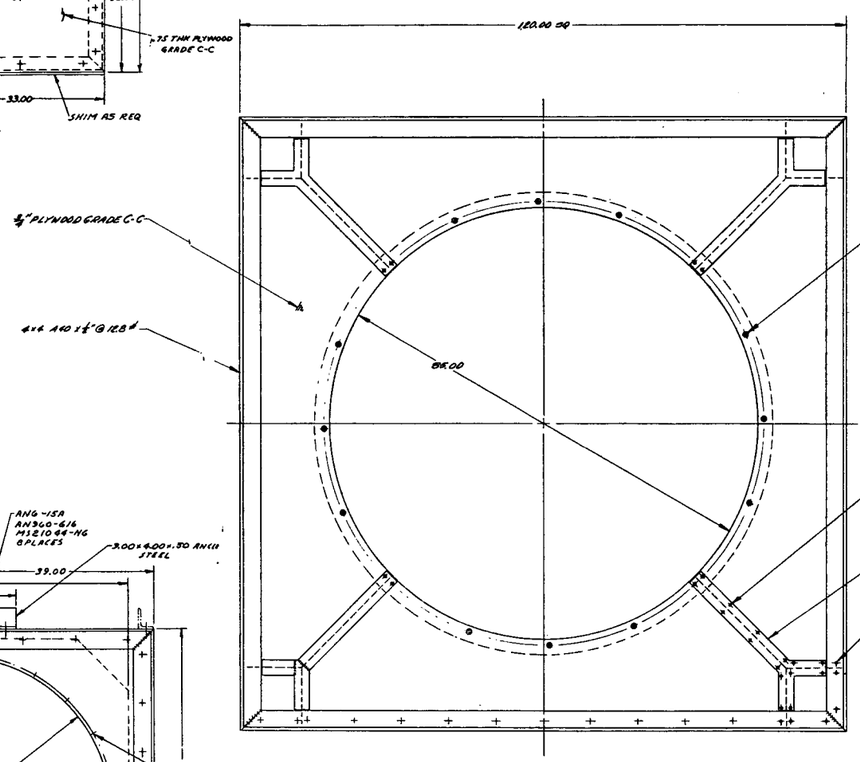

VIEW AT E-E
AFT LOOKING FWD

FOLDOUT FRAME 1

C2

FOLDOUT FRAME 2

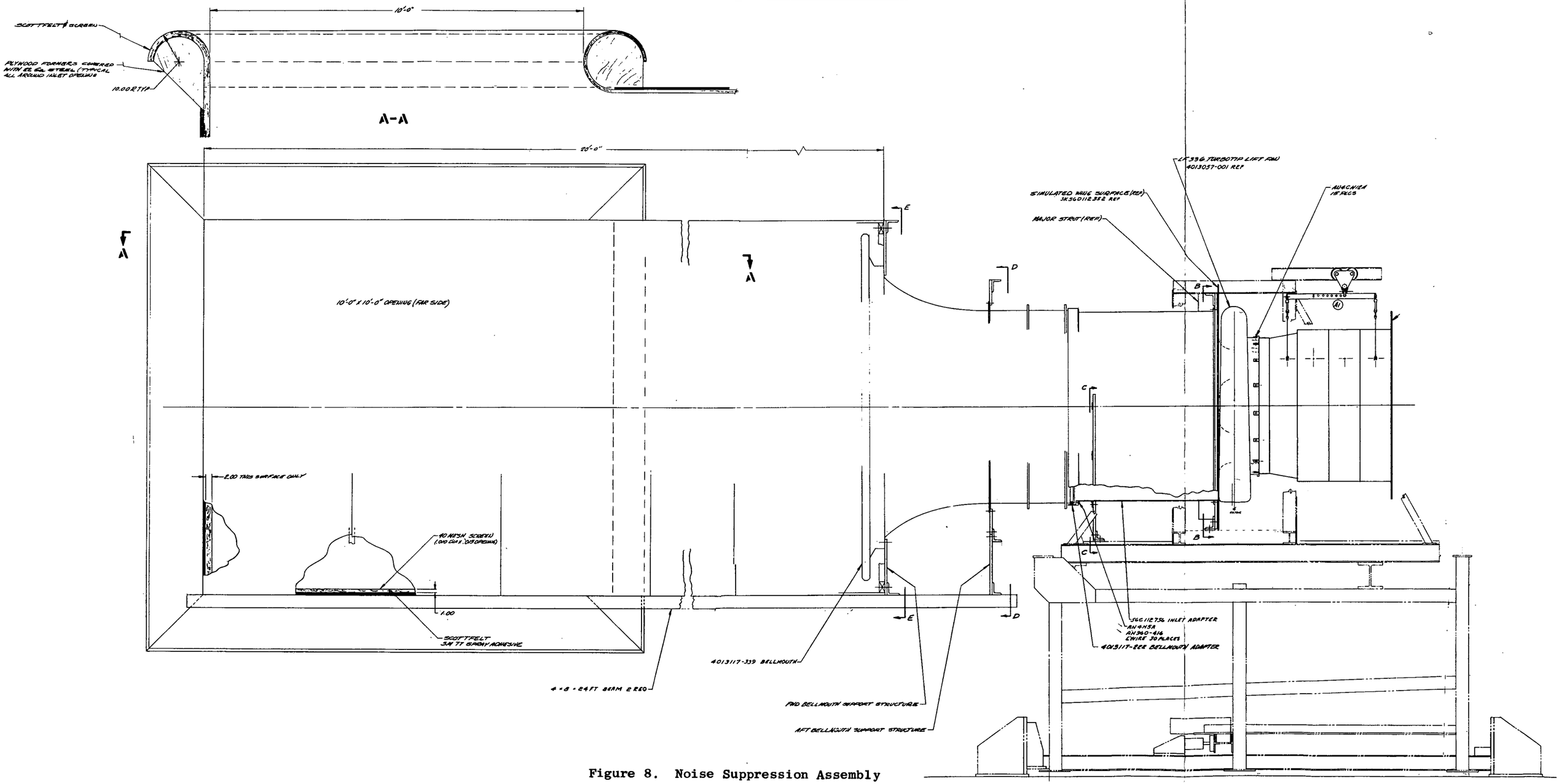

Figure 8. Noise Suppression Assembly

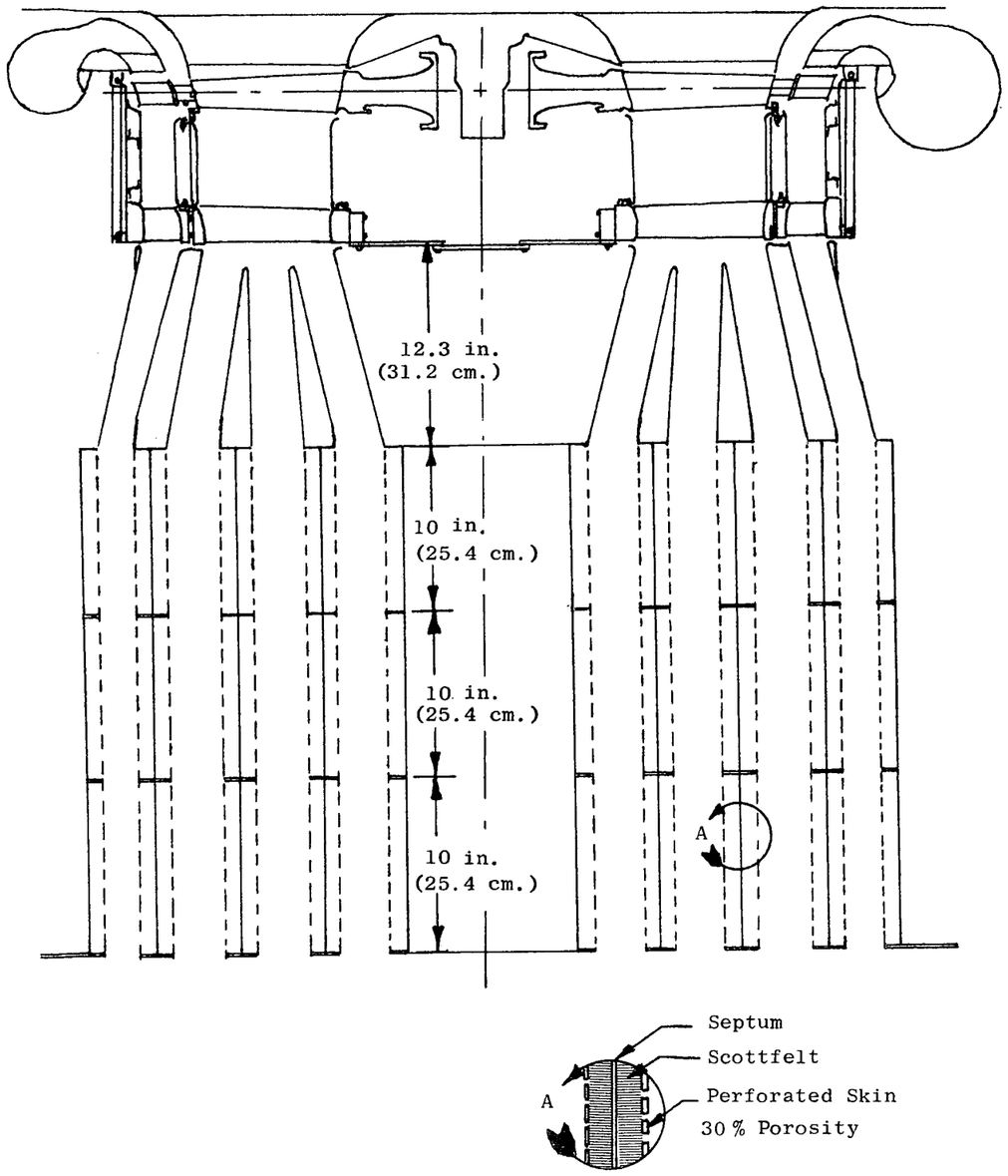

Figure 9. LF336/B with Exhaust Suppression Hardware

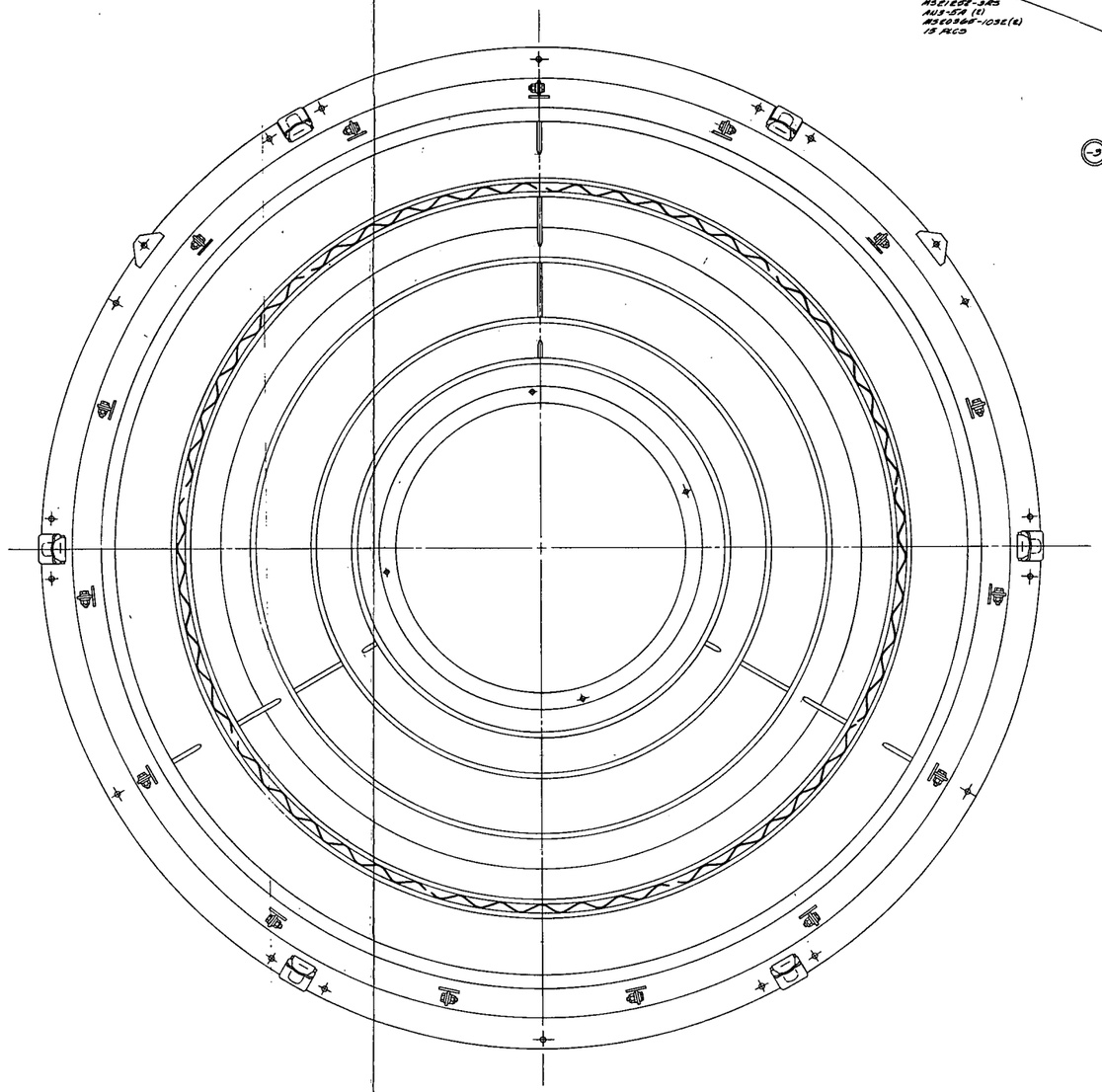

LKG AFT

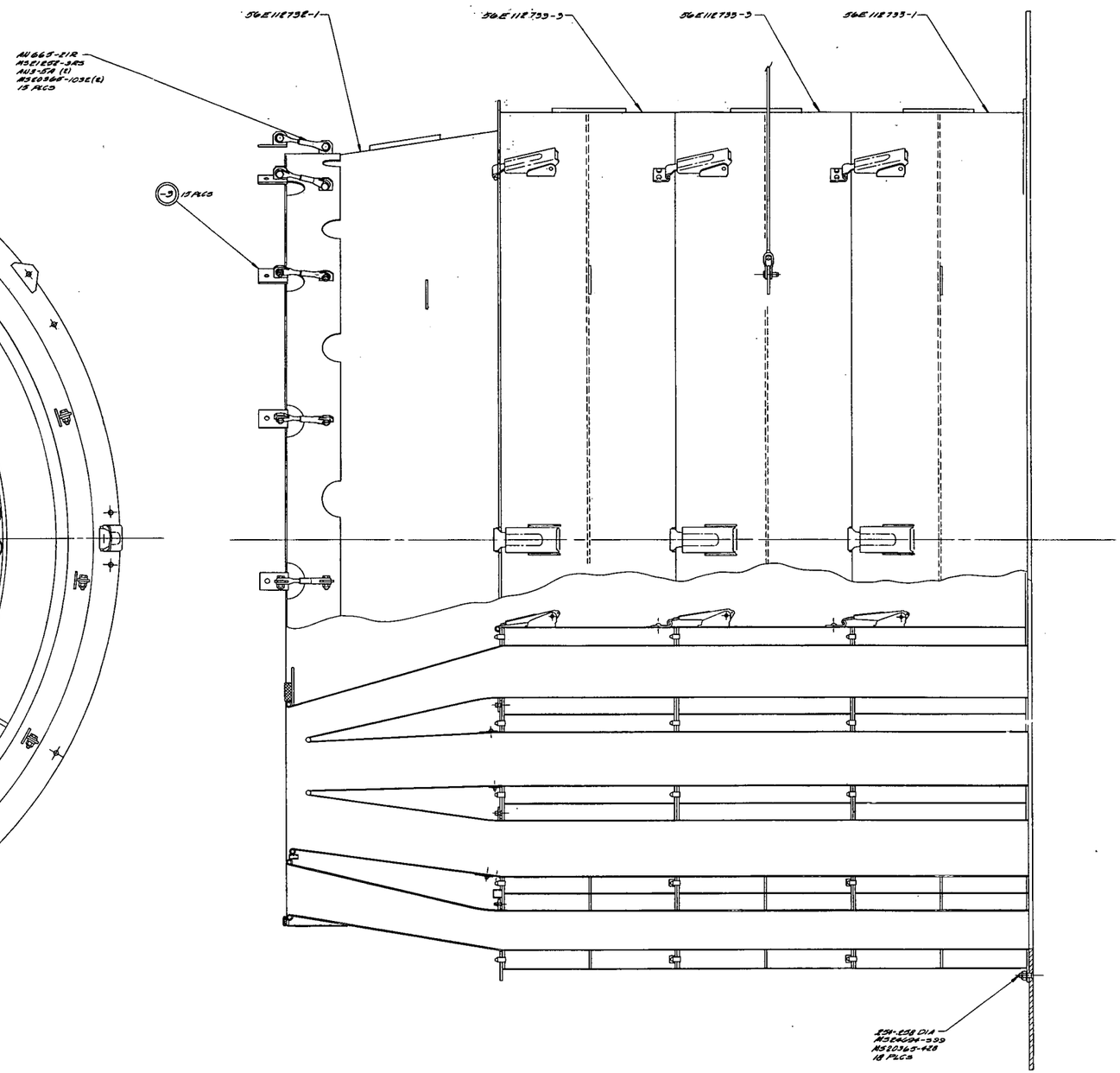

-1 ASSY

FOLDOUT FRAME 1

FOLDOUT FRAME 2

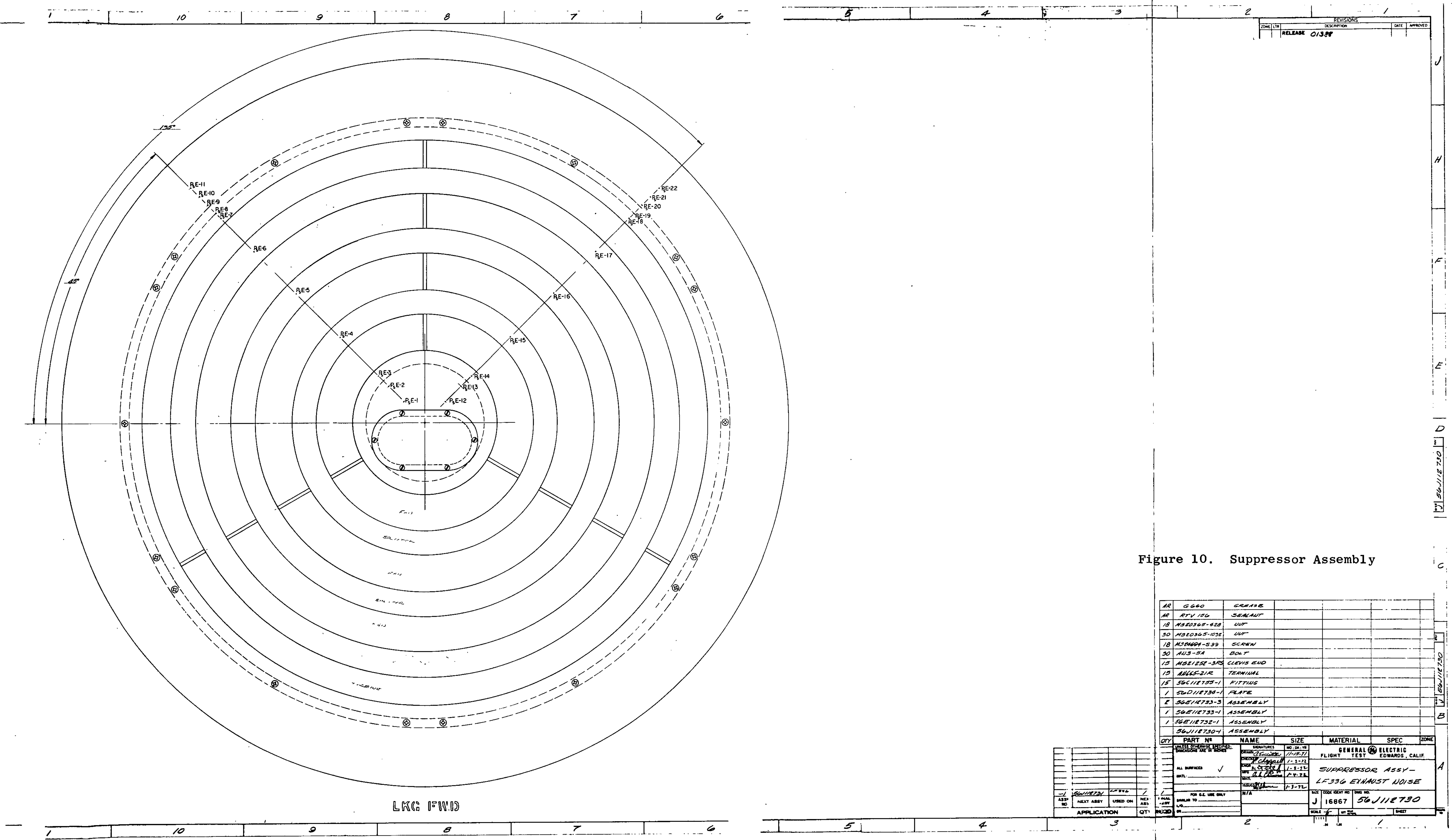

Figure 10. Suppressor Assembly

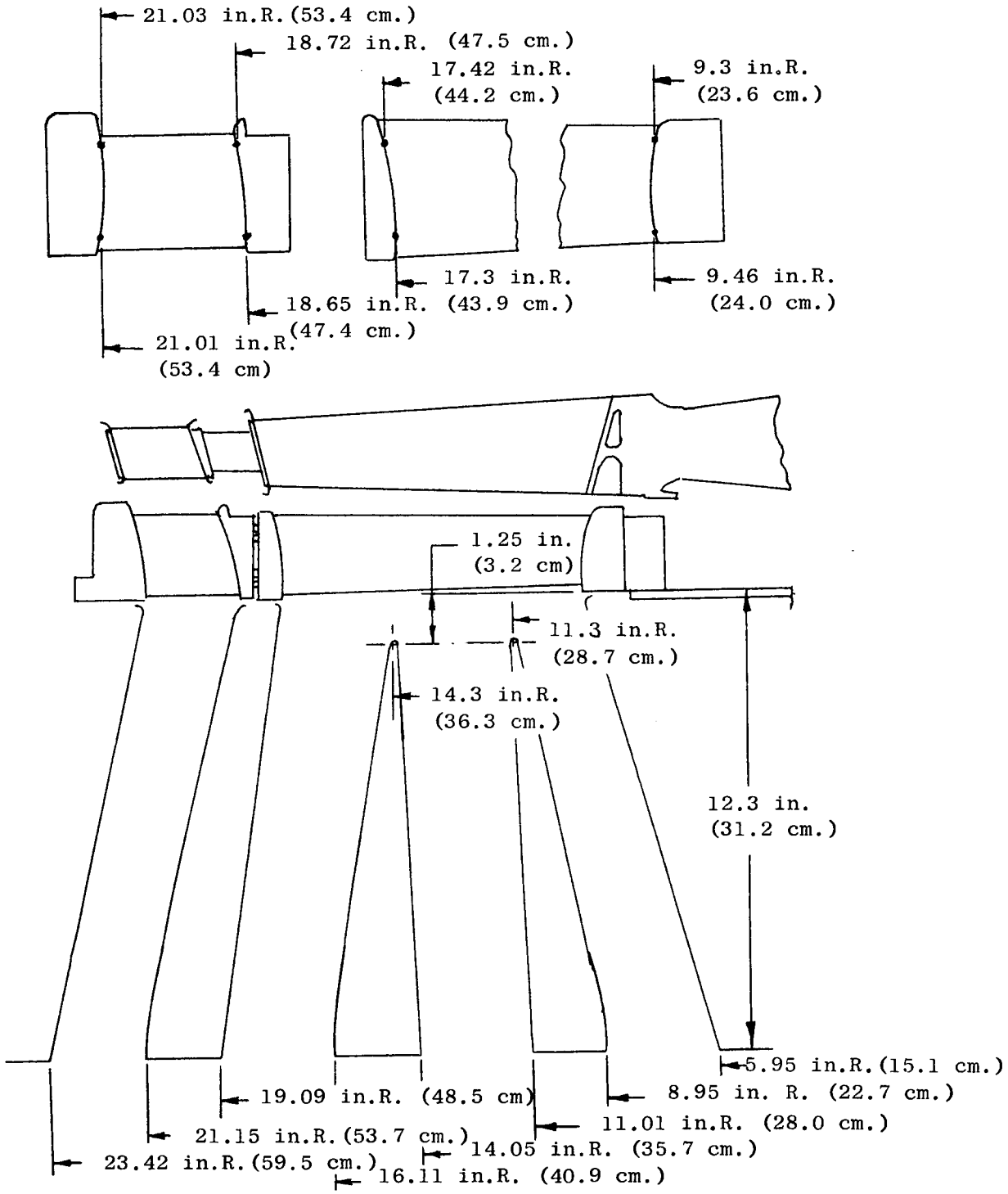

Figure 11. Exhaust Adapter - Flowpath Dimensions

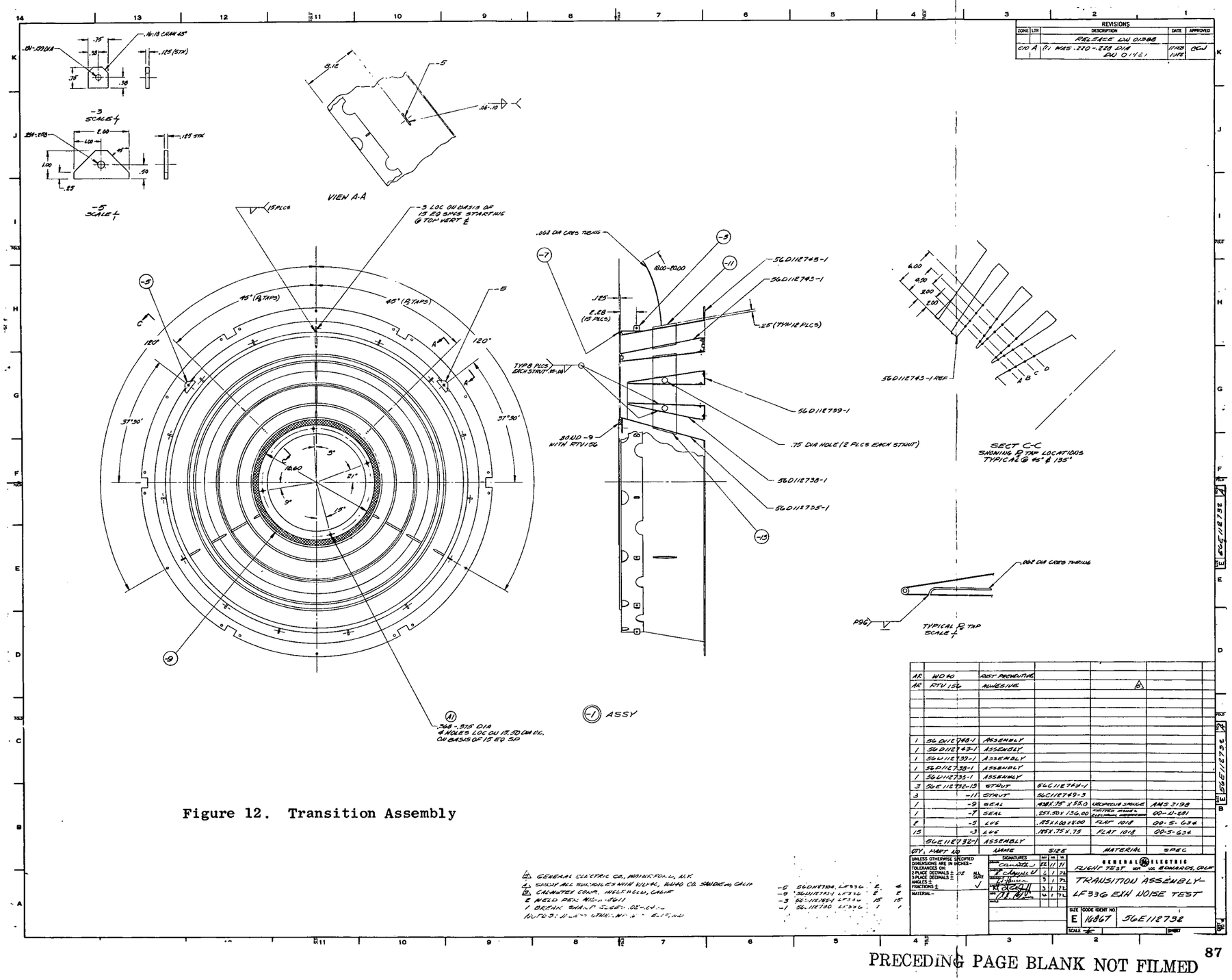

Figure 12. Transition Assembly

PRECEDING PAGE BLANK NOT FILMED

FOLDOUT FRAME 1

FOLDOUT FRAME 2

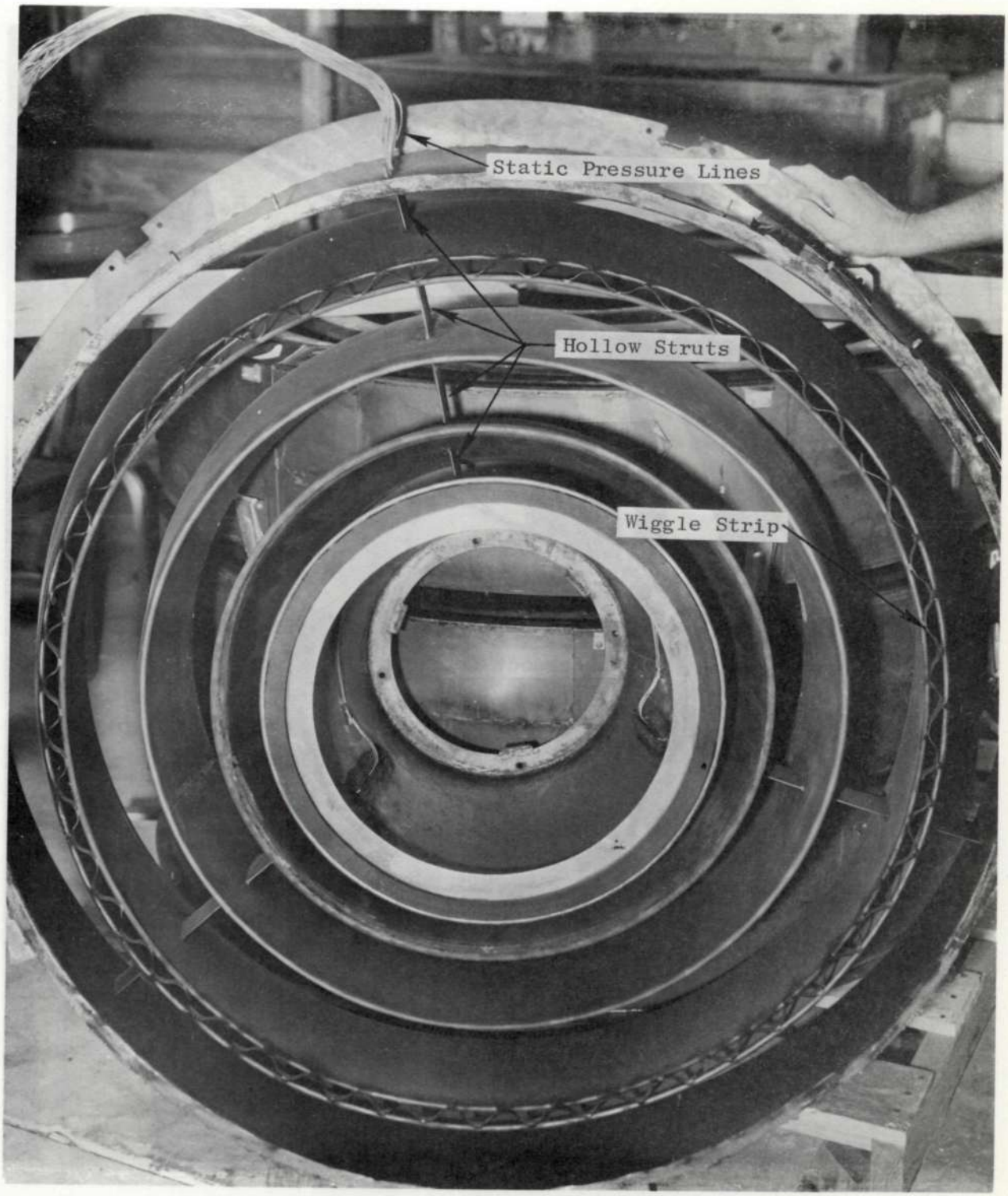

Figure 13. LC336/B Exhaust Adapter

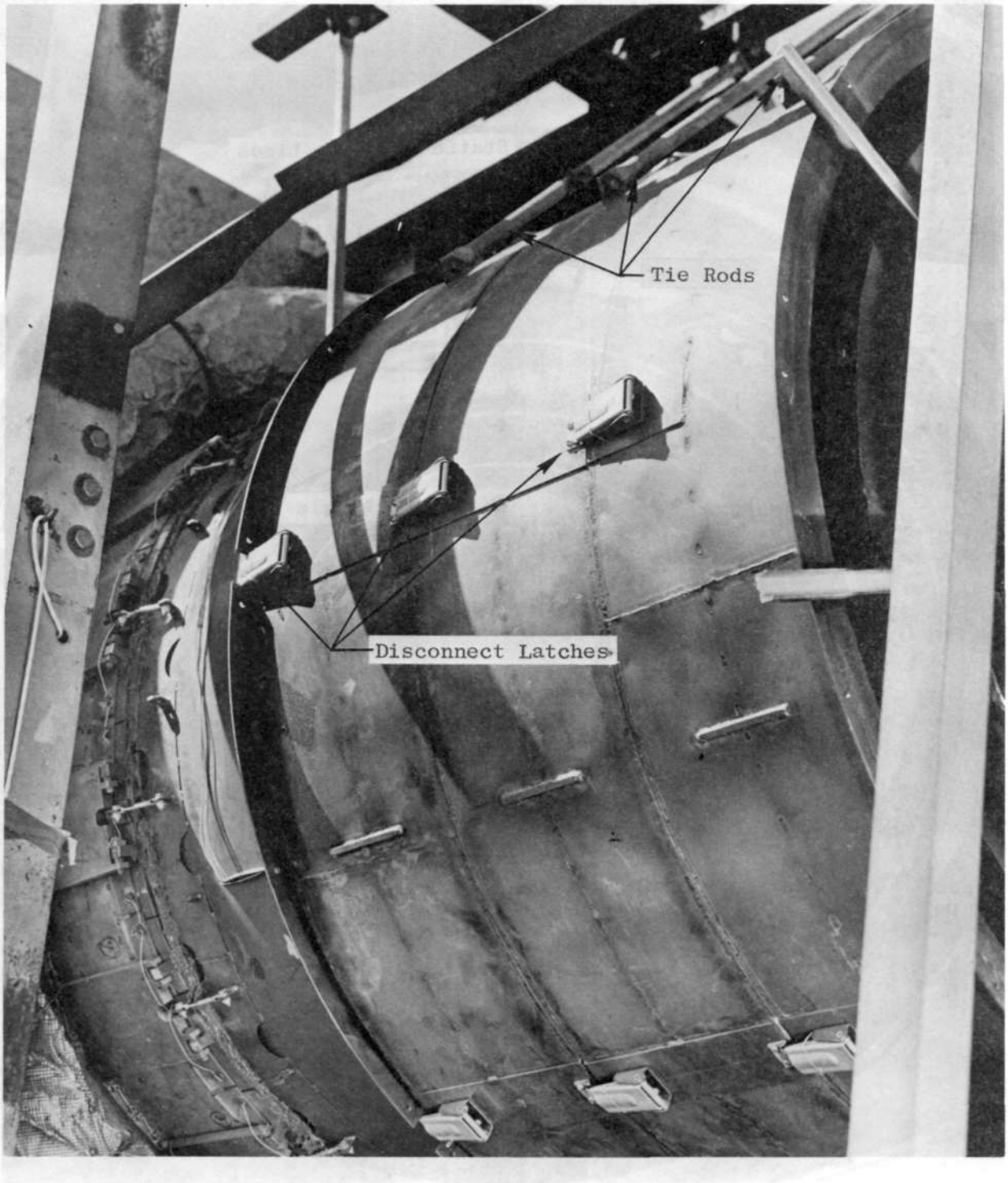

Figure 14. LF336/B with Exhaust Noise Suppressors and Adapter

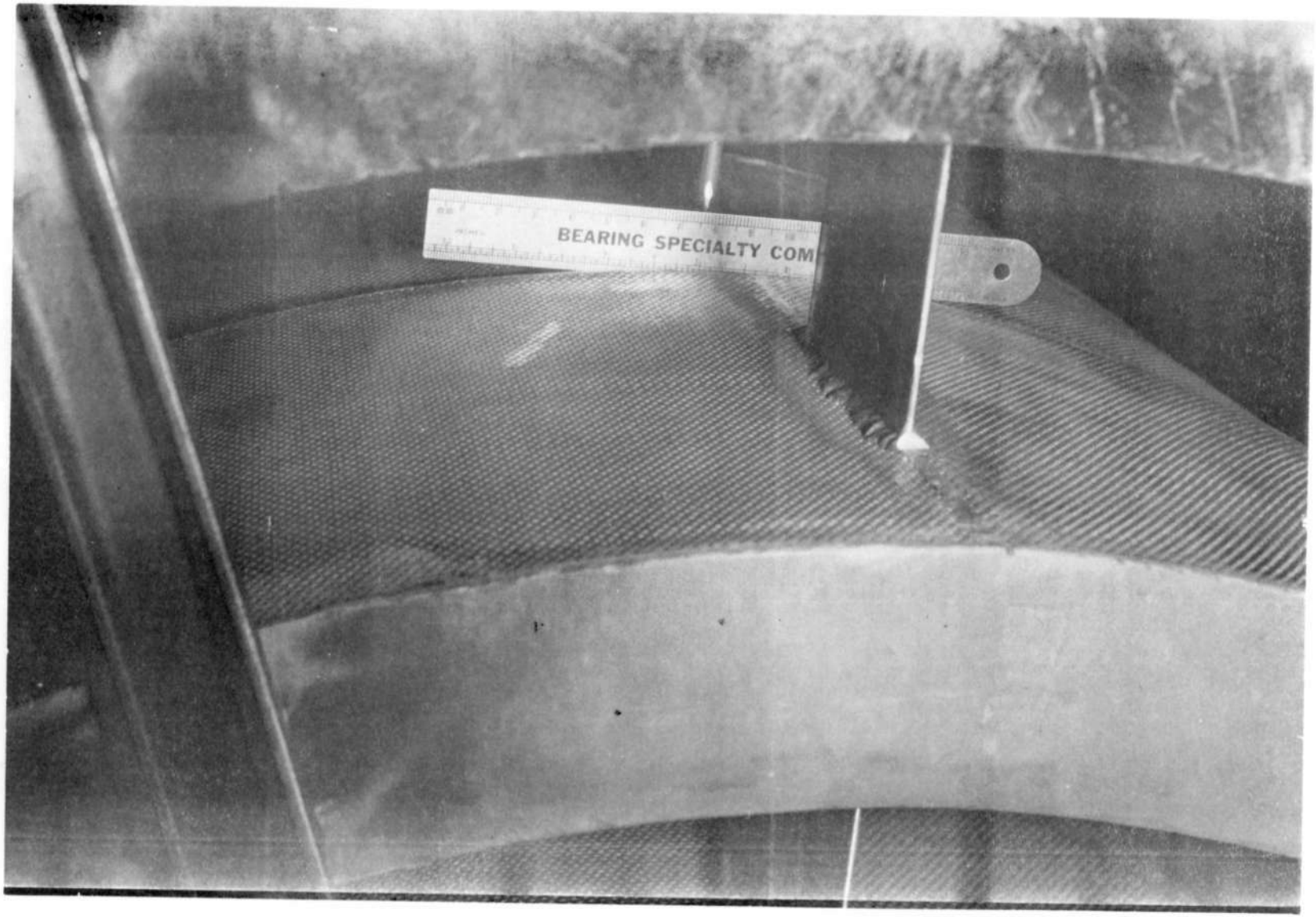

Figure 15. Exhaust Noise Suppressur - Perforated Skin

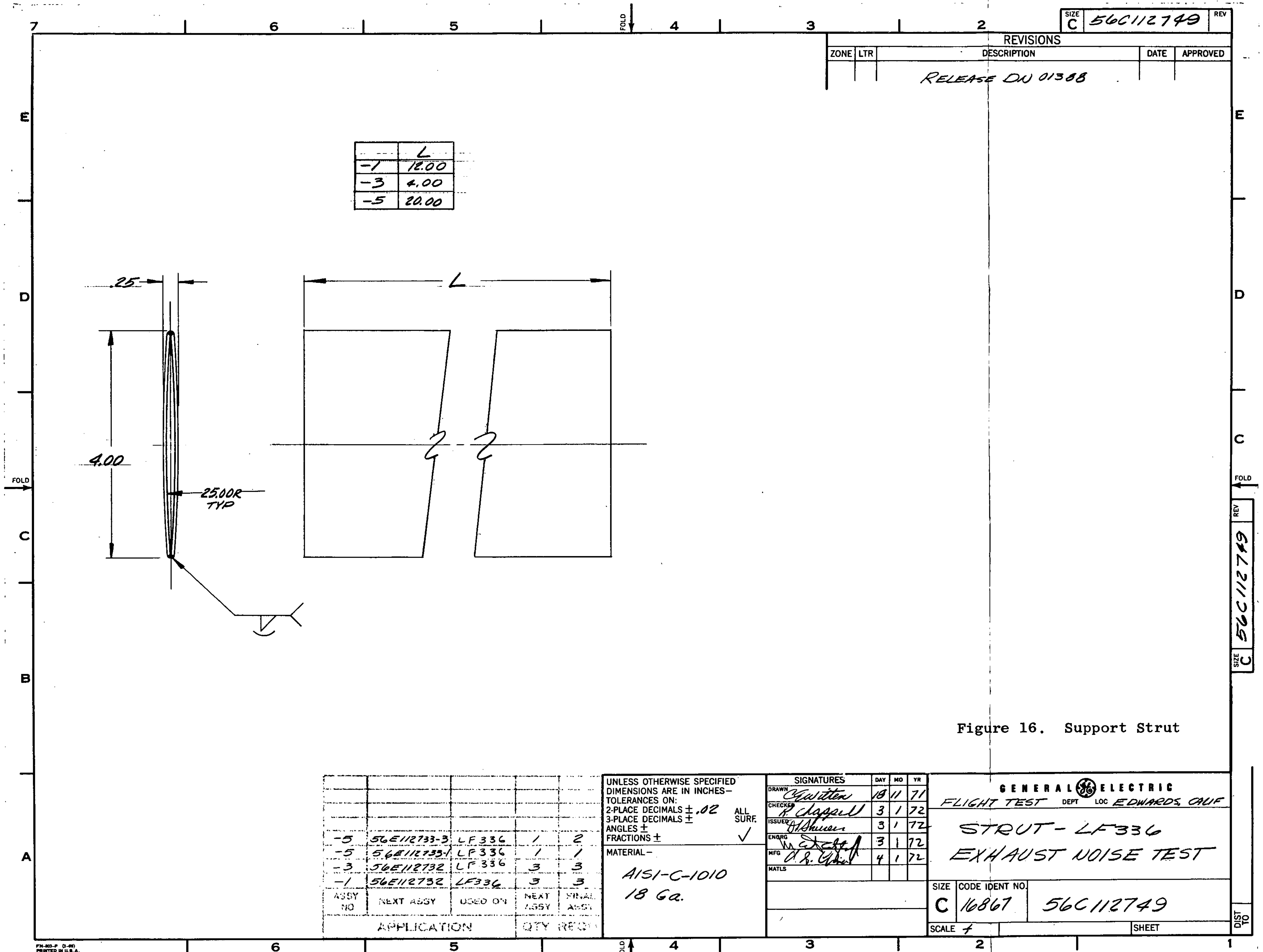

Figure 16. Support Strut

PRECEDING PAGE BLANK NOT FILMED

FOLDOUT FRAME 1

FOLDOUT FRAME 2

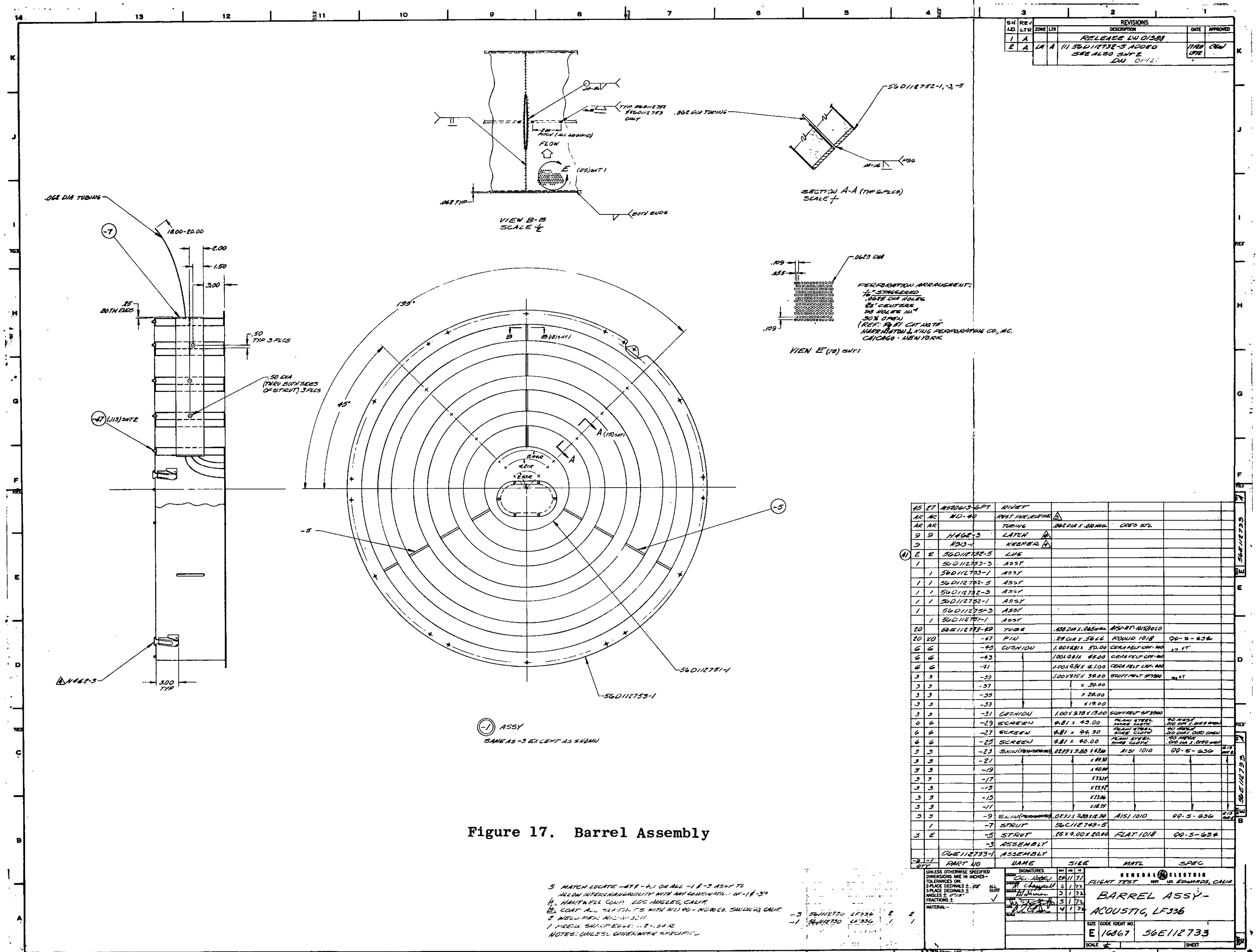

Figure 17. Barrel Assembly

PRECEDING PAGE BLANK NOT FILMED

FOLDOUT FRAME 1

FOLDOUT FRAME 2

DATA POINTS - ENGINE AND DUCT

CERAFELT CONFIGURATION

♦ DUCT DATA $H/\lambda_o = 1.9$

SCOTTFELT CONFIGURATIONS

▲ DUCT DATA $H/\lambda_o = 1.5$
● DUCT DATA $H/\lambda_o = 0.66$
■ ENGINE DATA TF39 $H/\lambda_o = 1.5$
▲ NASA-LEWIS FAN $H/\lambda_o = 1.5$
● CF6 D/V $H/\lambda_o = 1.65$

FLOW MACH NUMBER = 0.3 TO 0.4

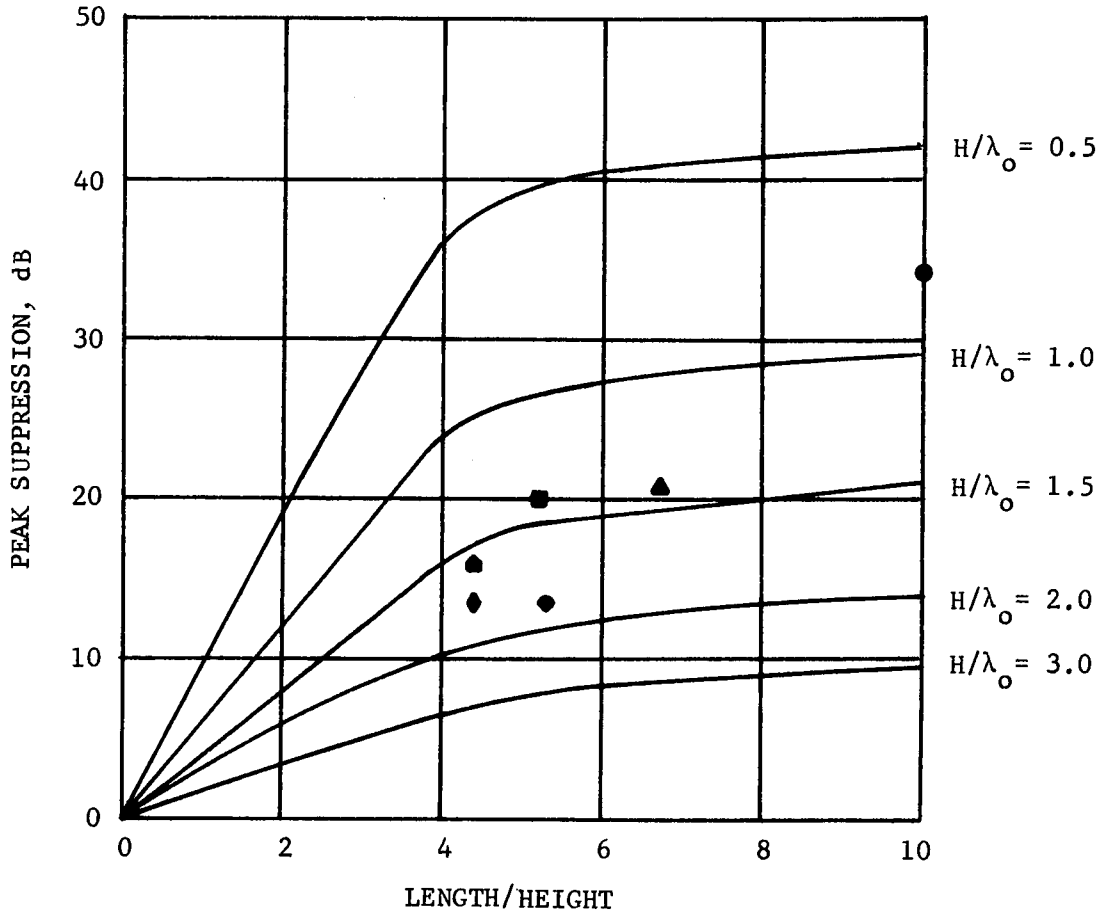

Figure 18. Peak Suppression Design Curves

PRECEDING PAGE BLANK NOT FILMED

- 2 SPLITTERS
- 4000 Hz PEAK FREQUENCY
- $H/\lambda_o = 0.9$
- MACH NUMBER = 0.3 TO 0.4

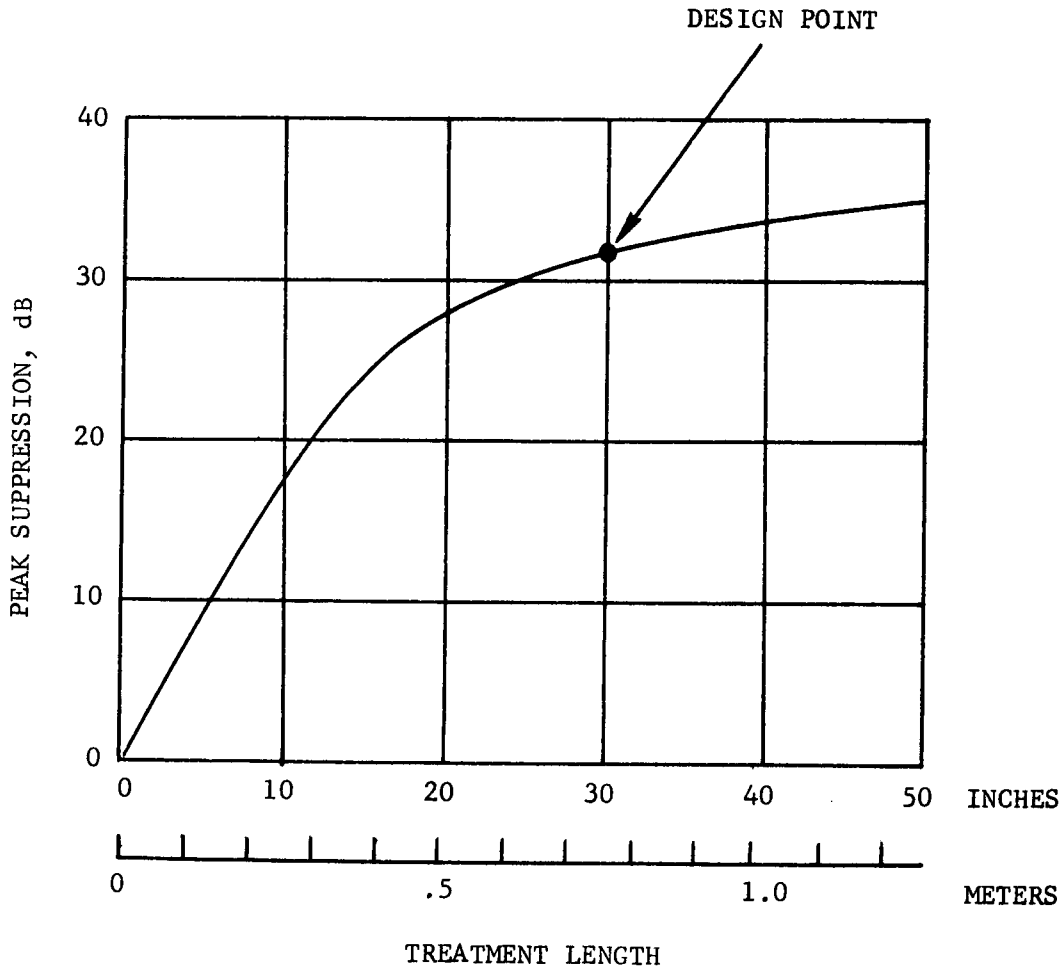

Figure 19. Peak Suppression as a Function of Treatment Length

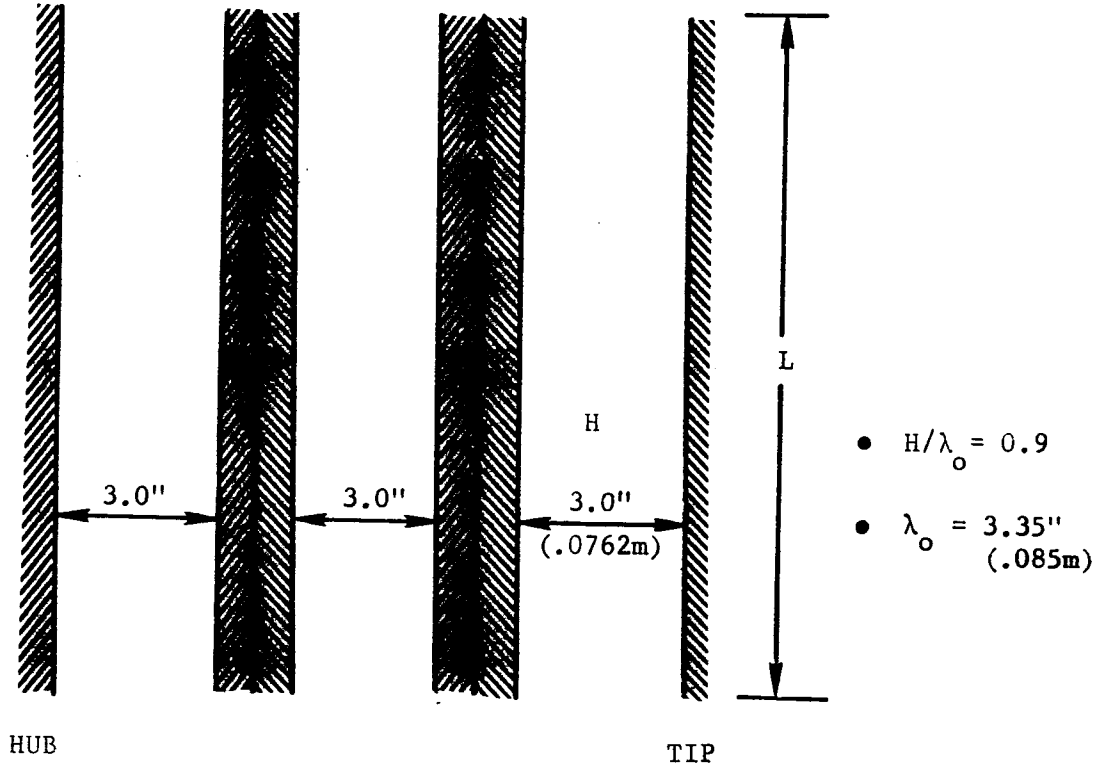

Figure 20. LF336 Splitter Configuration

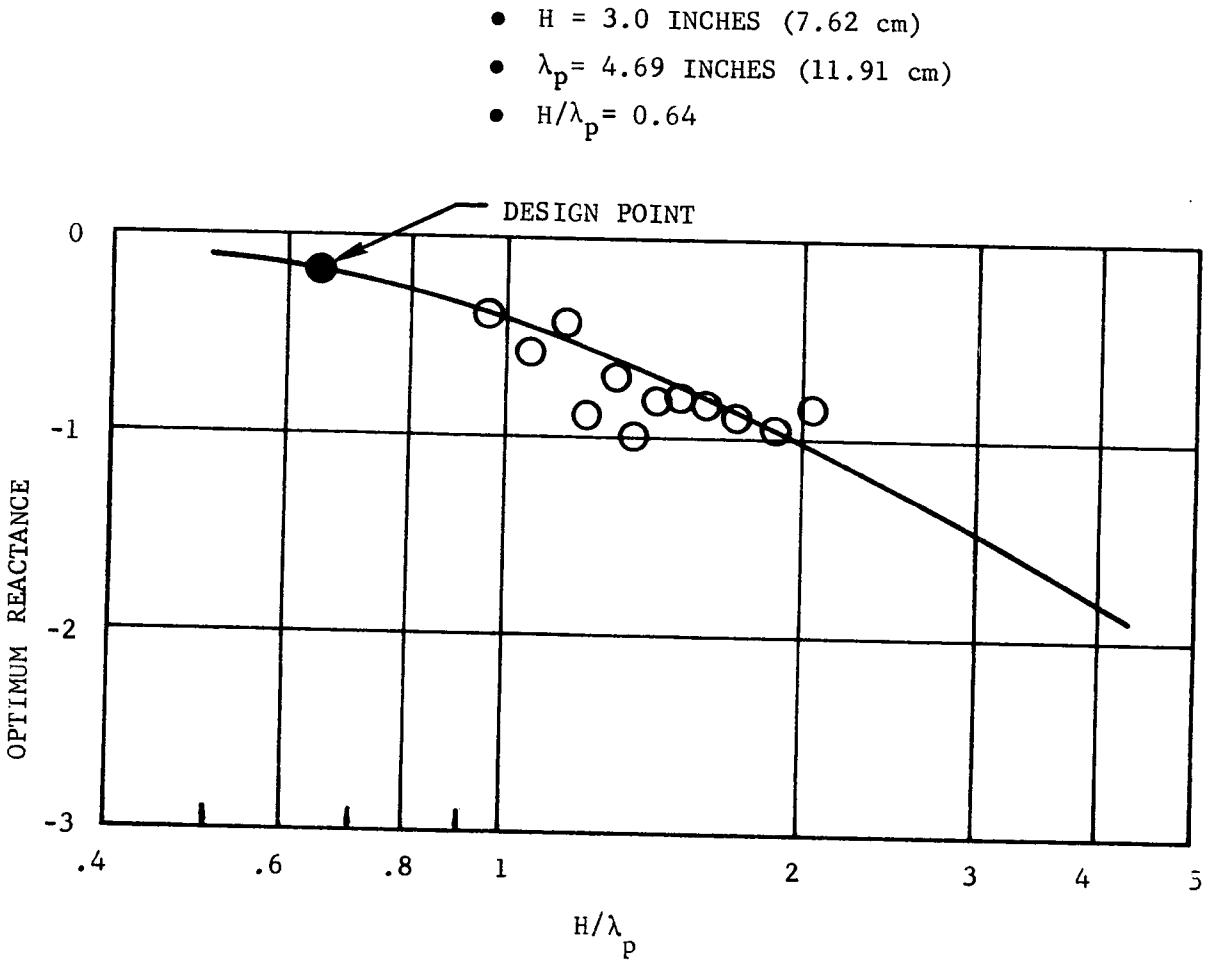

Figure 21. Optimum Acoustic Reactance versus H/λ_p

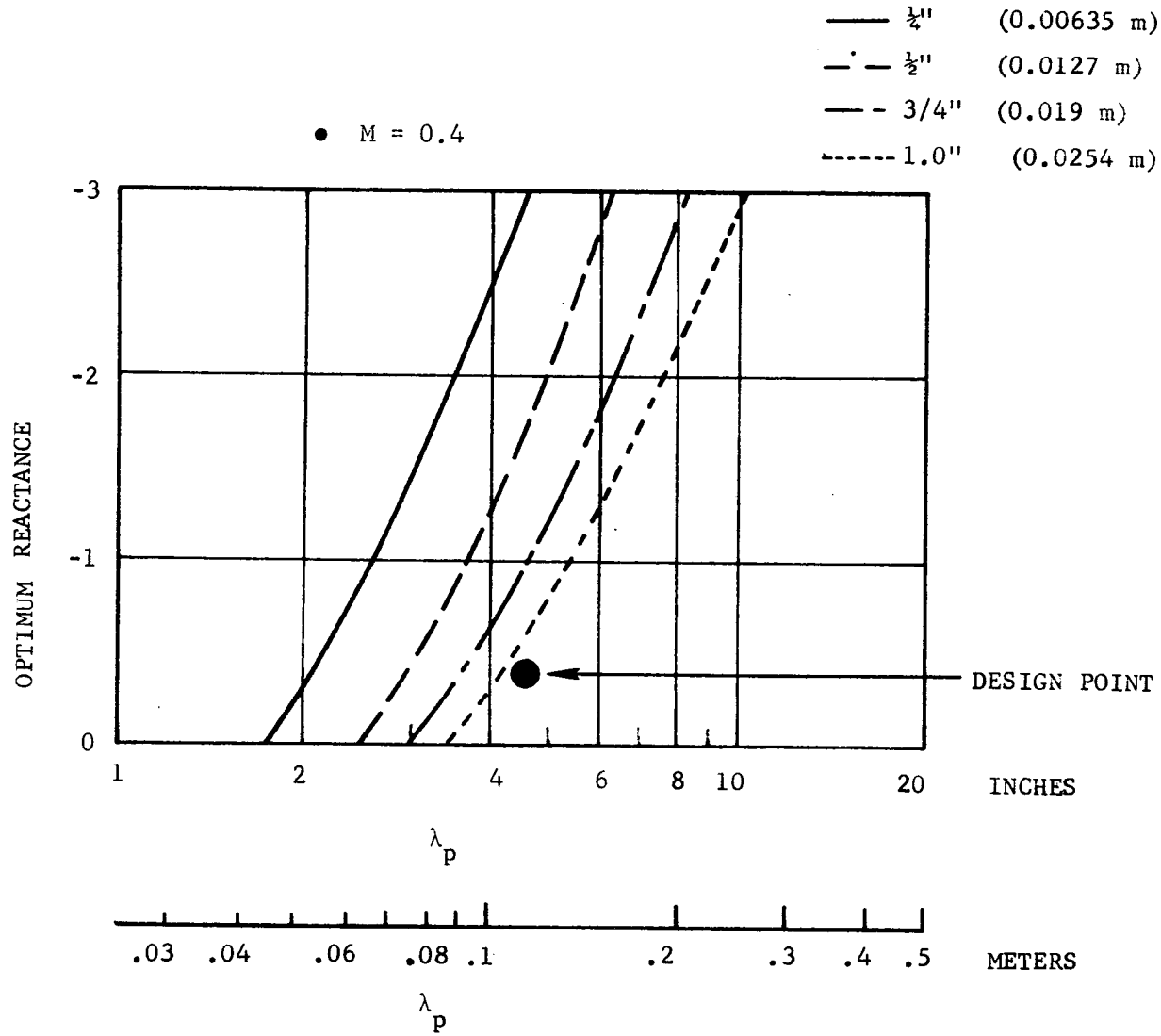

Figure 22. Scottfelt 3-900 Reactance versus Wavelength

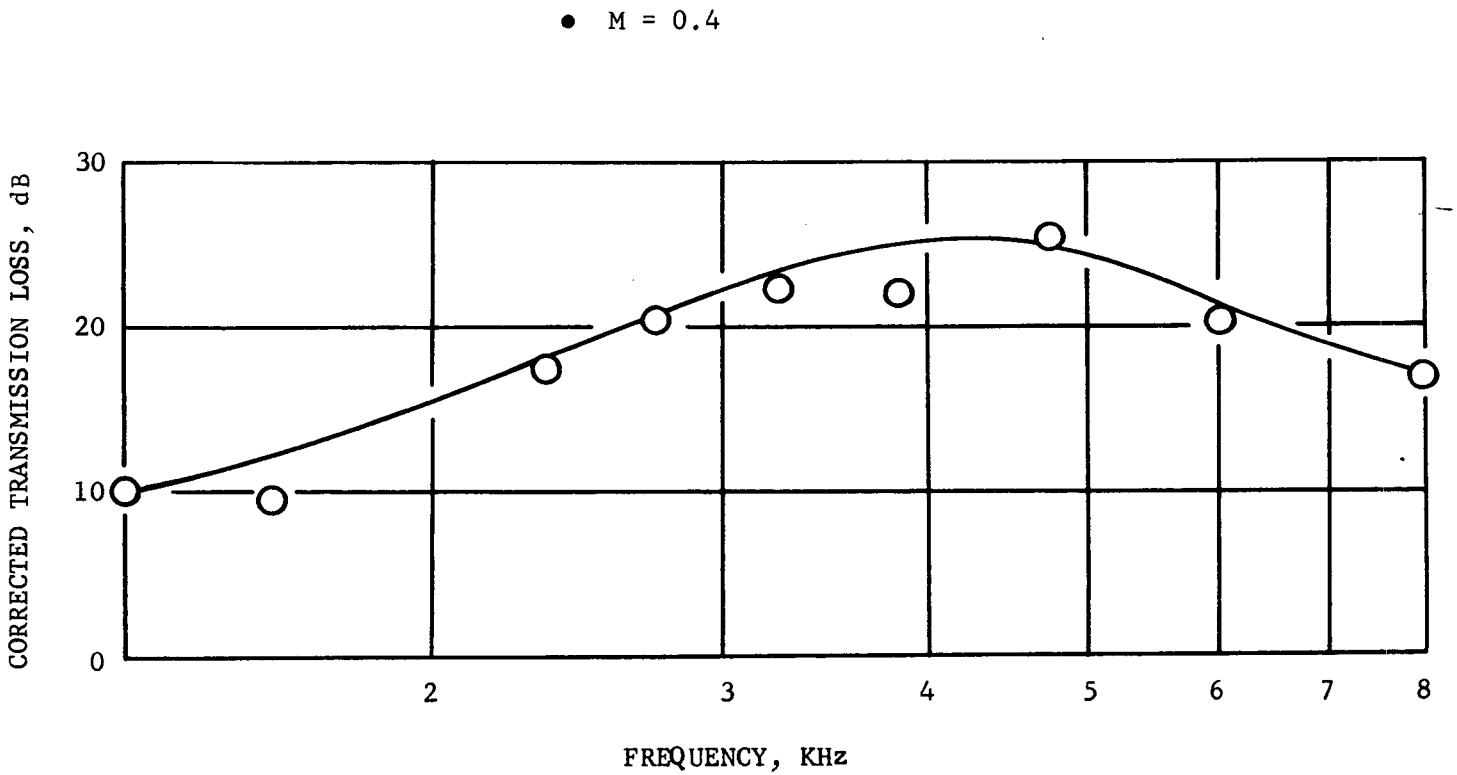

Figure 23. Corrected Transmission Loss, 1"(2.54 cm) SCOTTFELT 3-900

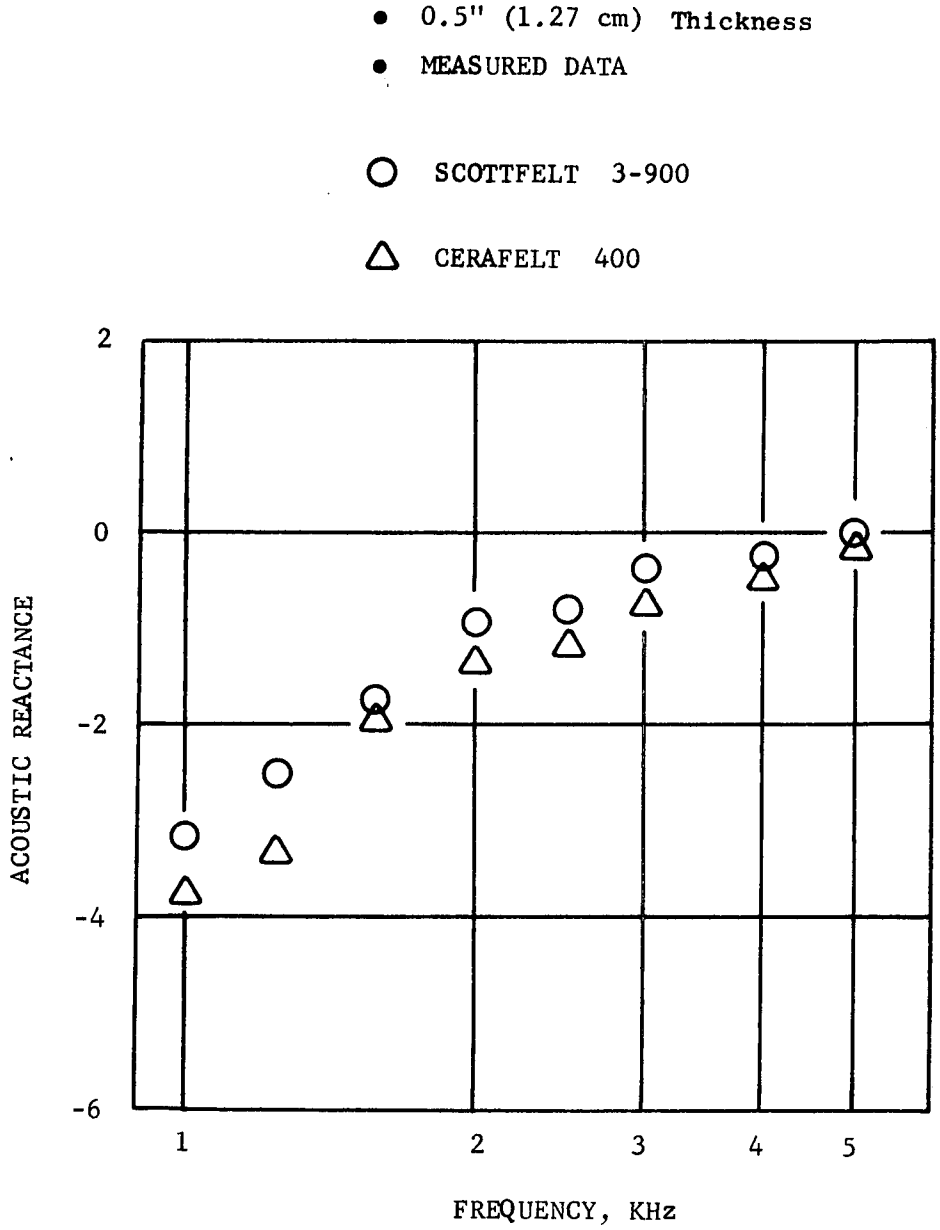

Figure 24. Comparison of SCOTTFELT 3-900 and Cerafelt 400 Reactance Values

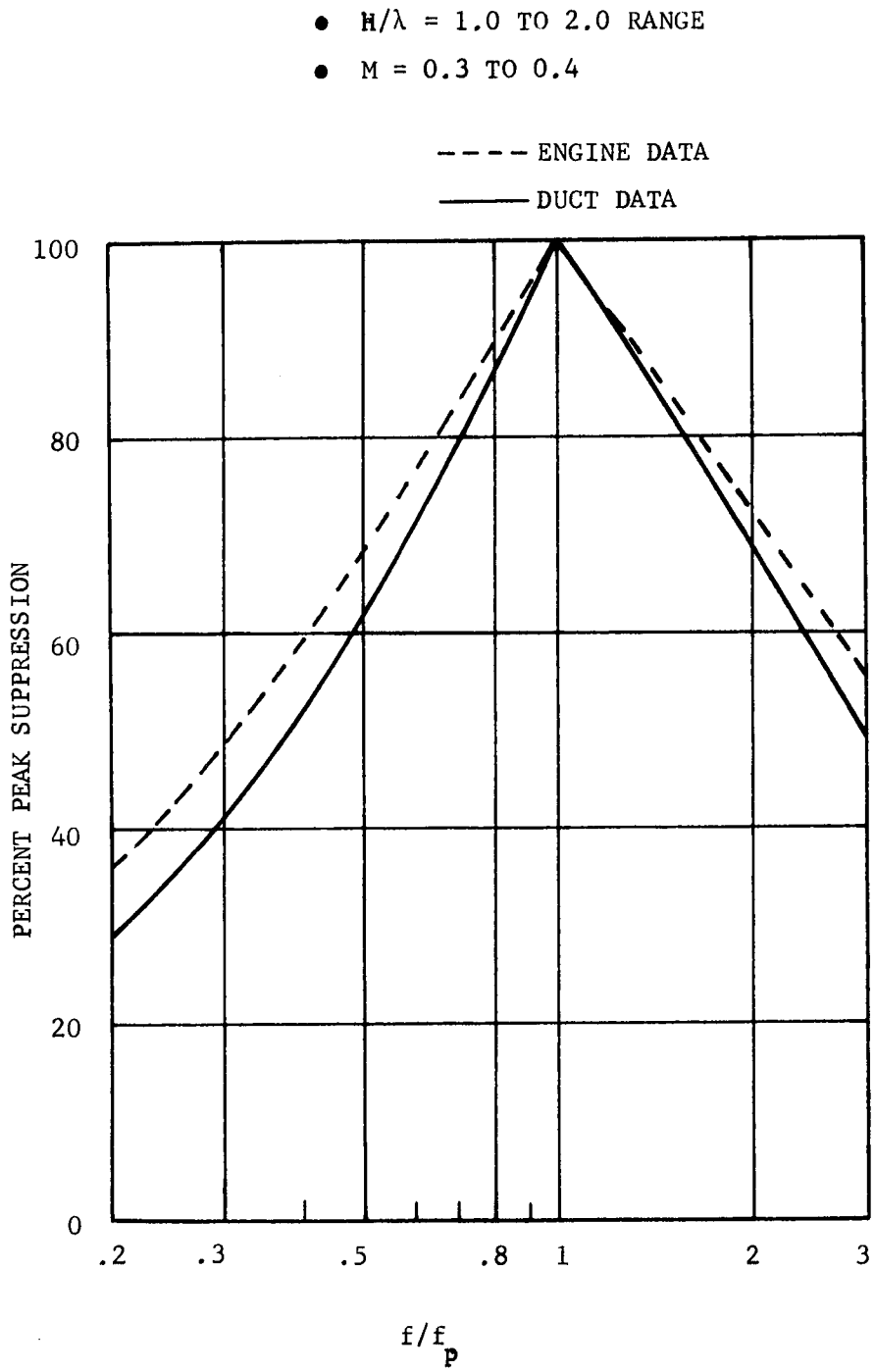

Figure 25. Percentage Bandwidth for Scottfelt 3-900

Figure 26. LF336 Lift Fan Test Site

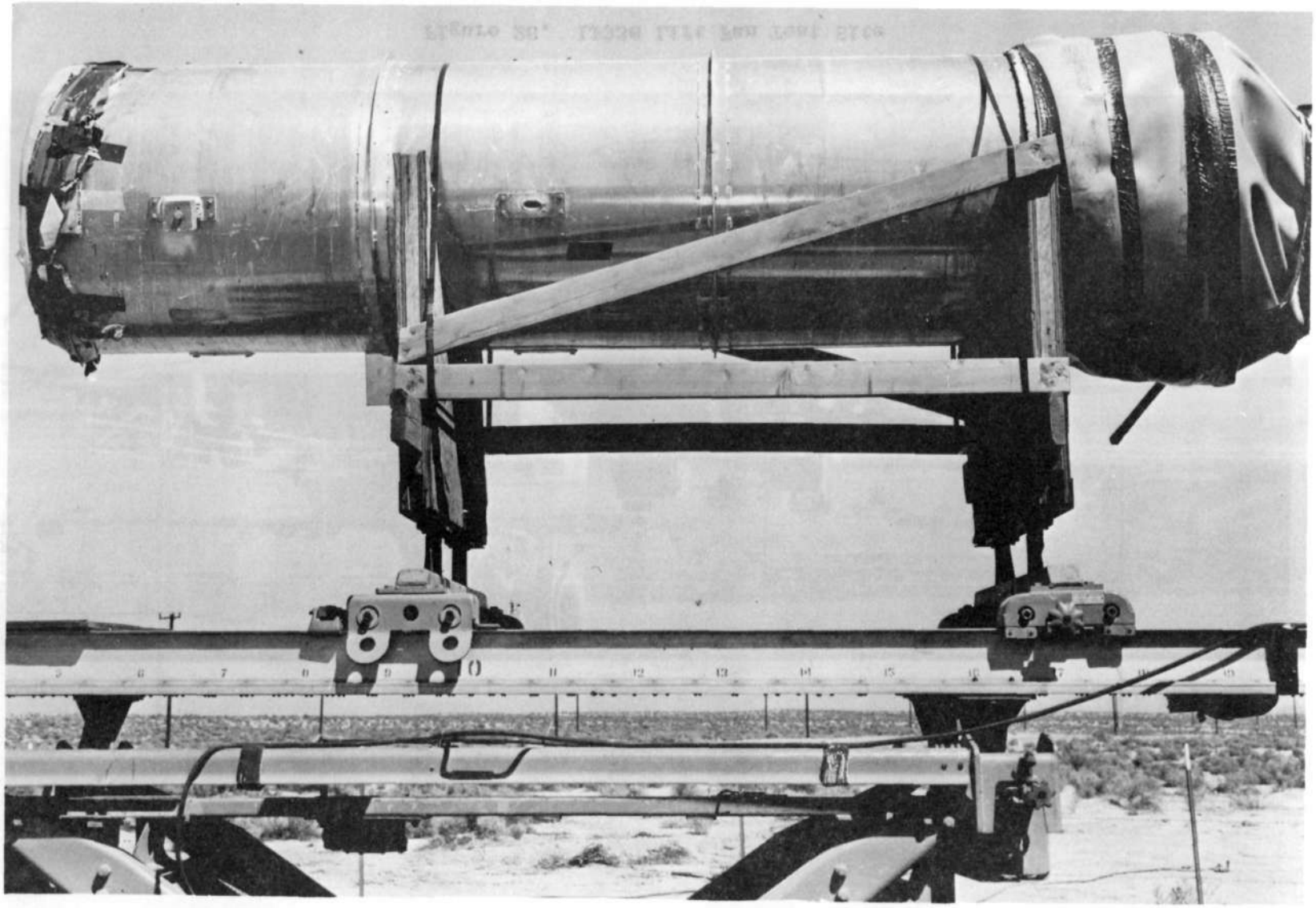

Figure 27. J85 Inlet Noise Suppressor

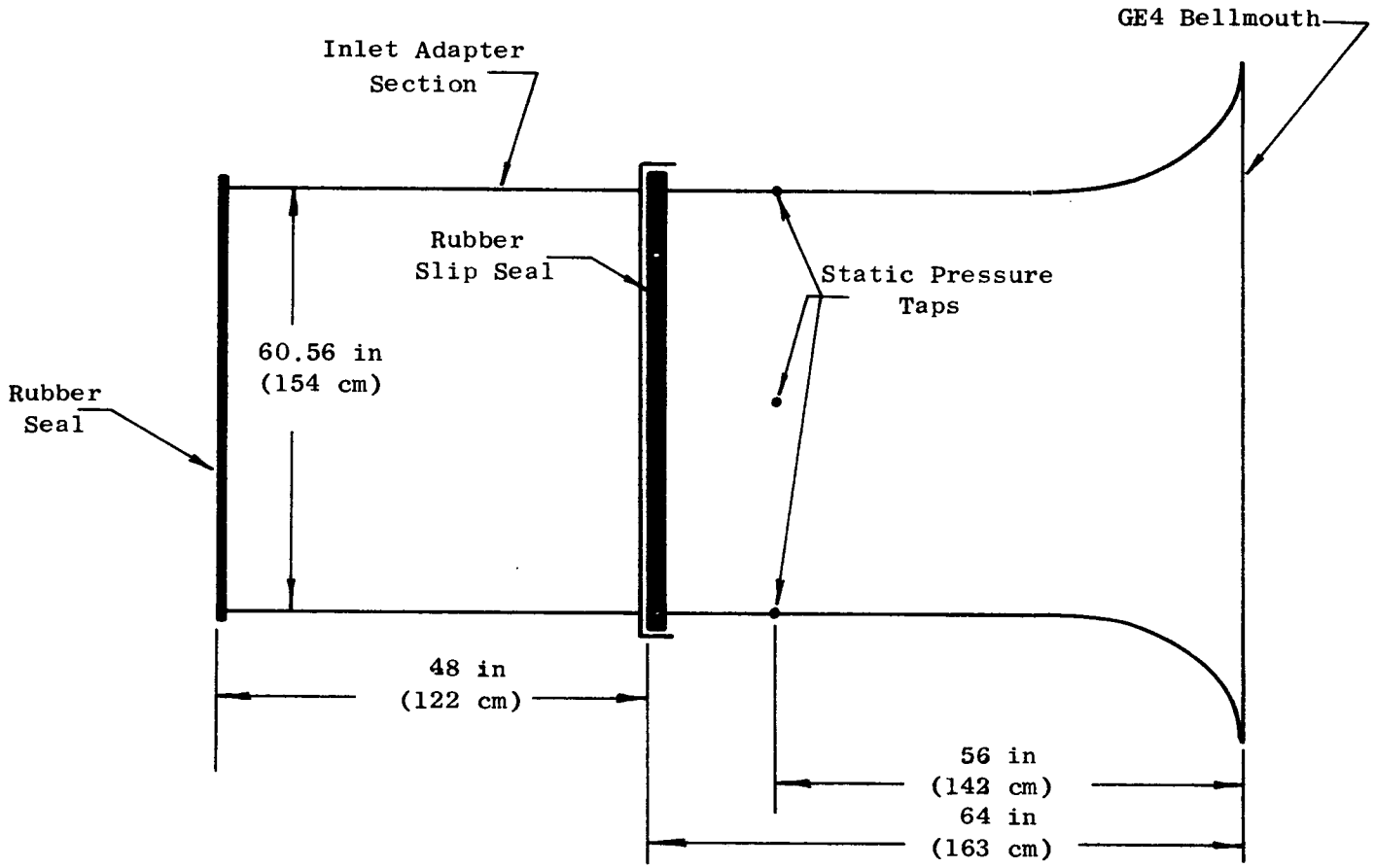

Figure 28. GE4 Bellmouth Slip Seal Arrangement

- 1-6 Planes A-D and 1-11 Plane E located @ $\theta = 45°$
- 7-12 Planes A-D and 12-22 Plane E located @ $\theta = 135°$
- Taps @ Plane E are typical for each Exhaust Section

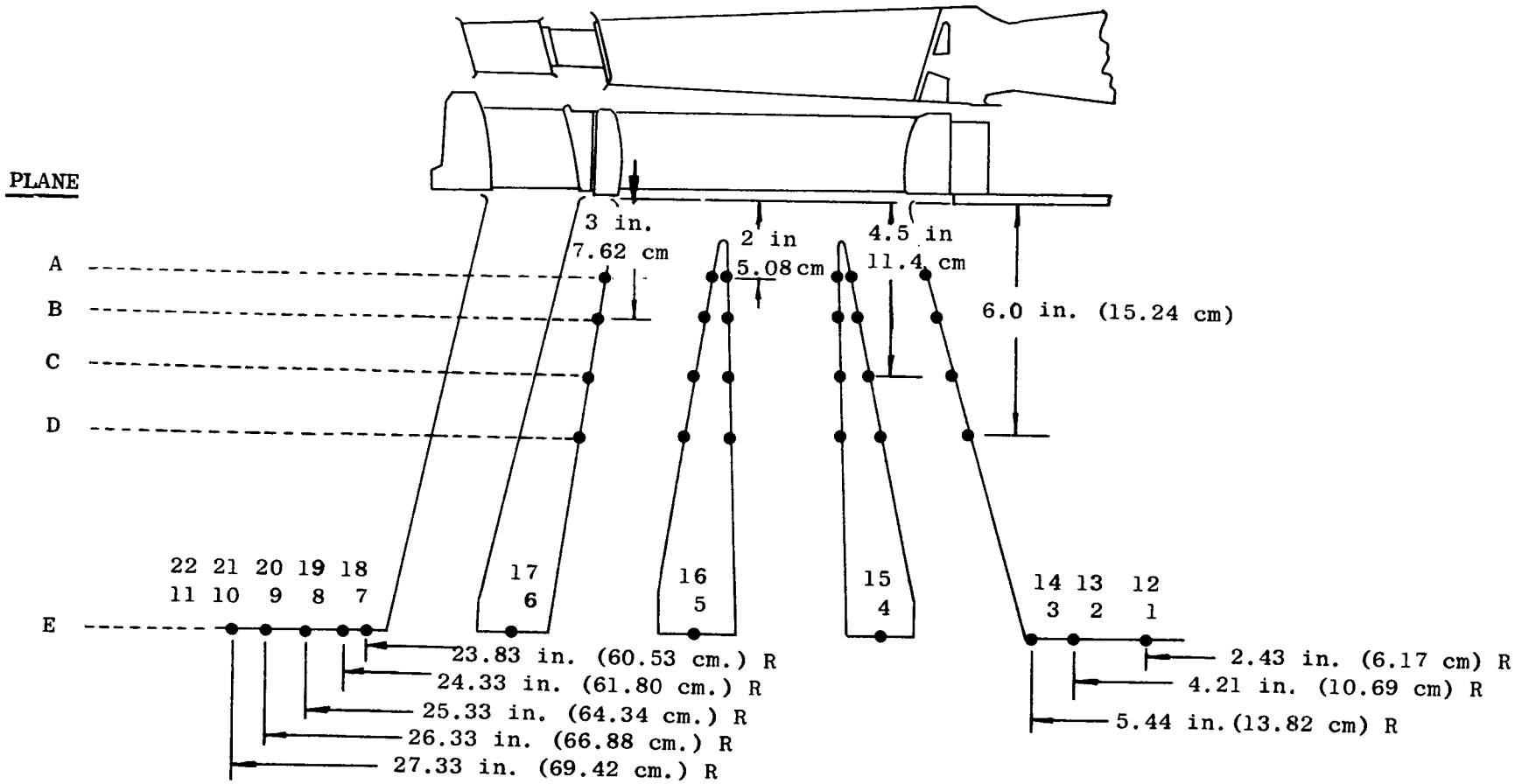

Figure 29. Static Pressure Tap Location

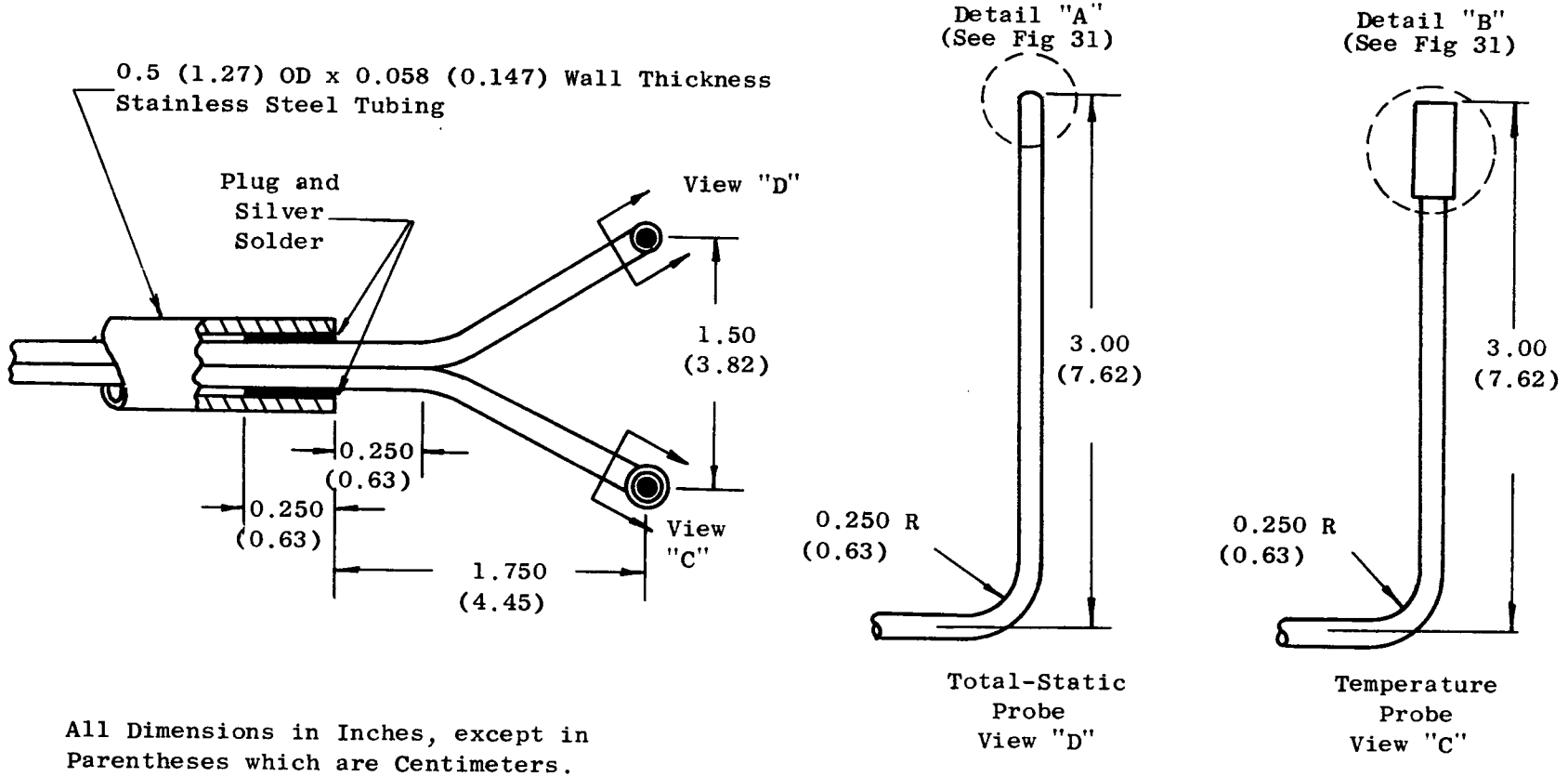

Figure 30. Exhaust Traversing Probe Detail

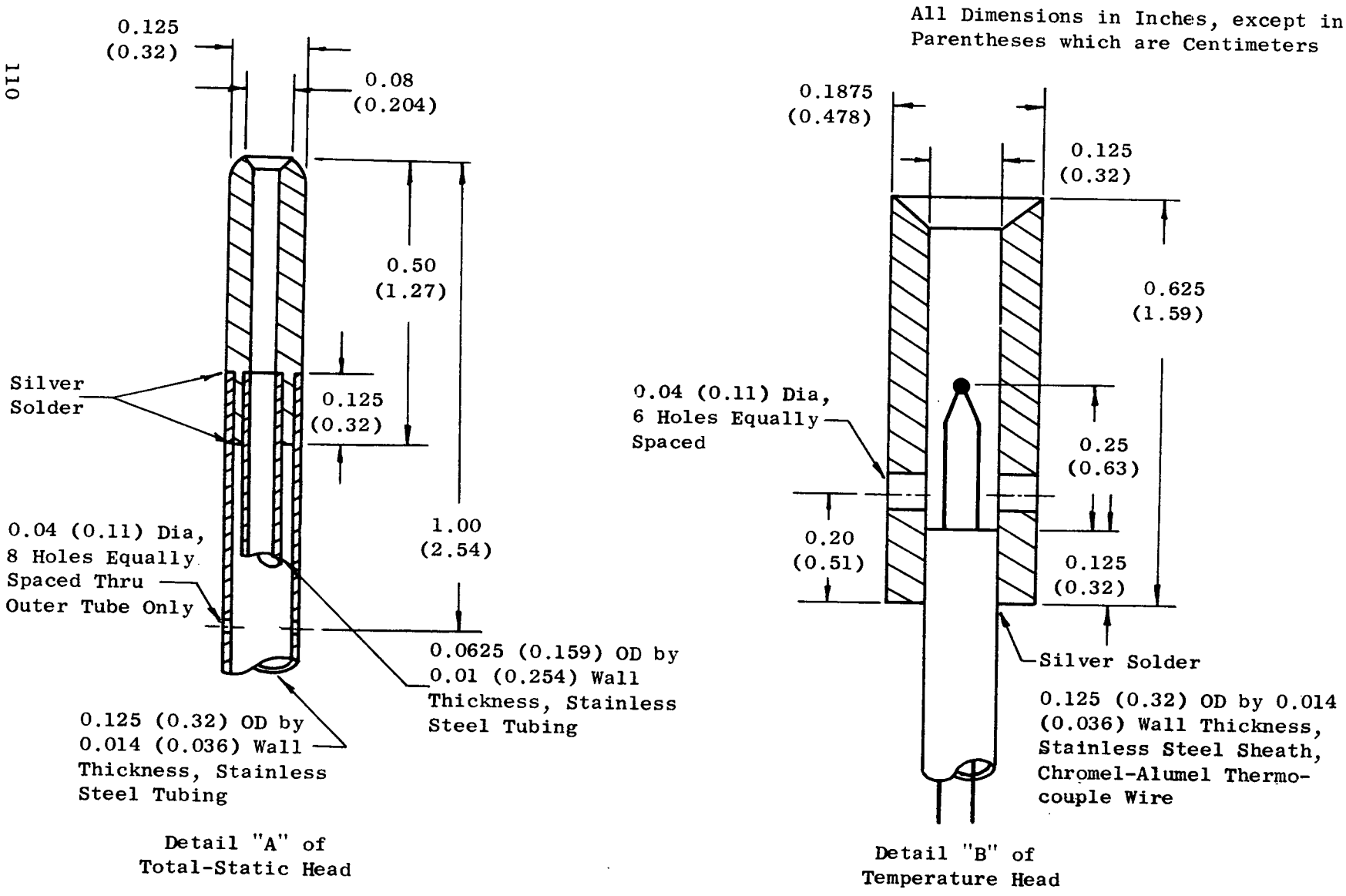

Figure 31. Exhaust Traversing Probe Total-Static and Temperature Head Detail

Figure 32. Traverse Probe Mounted at Fan Discharge

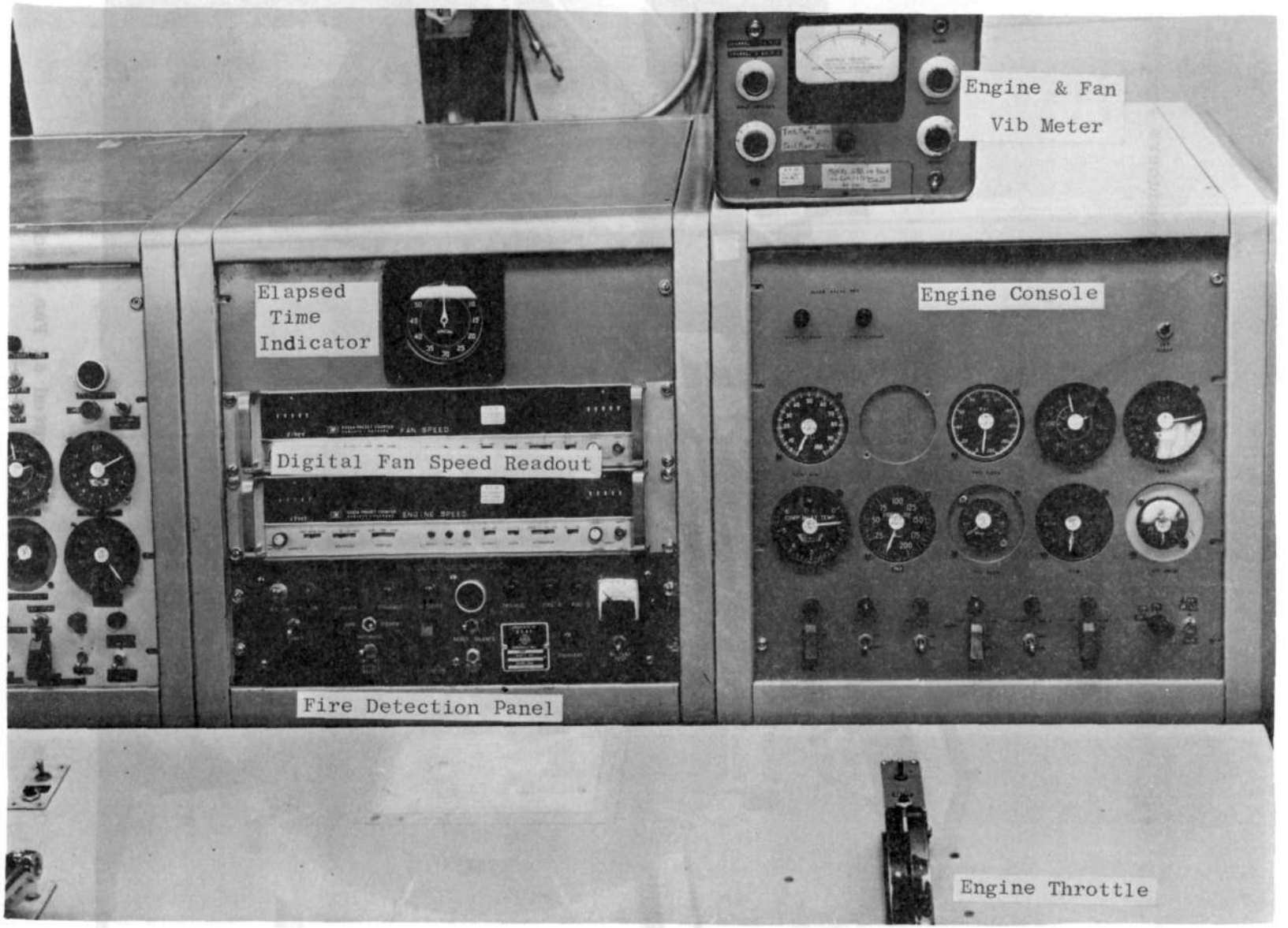

Figure 33. Engine and Fan Console

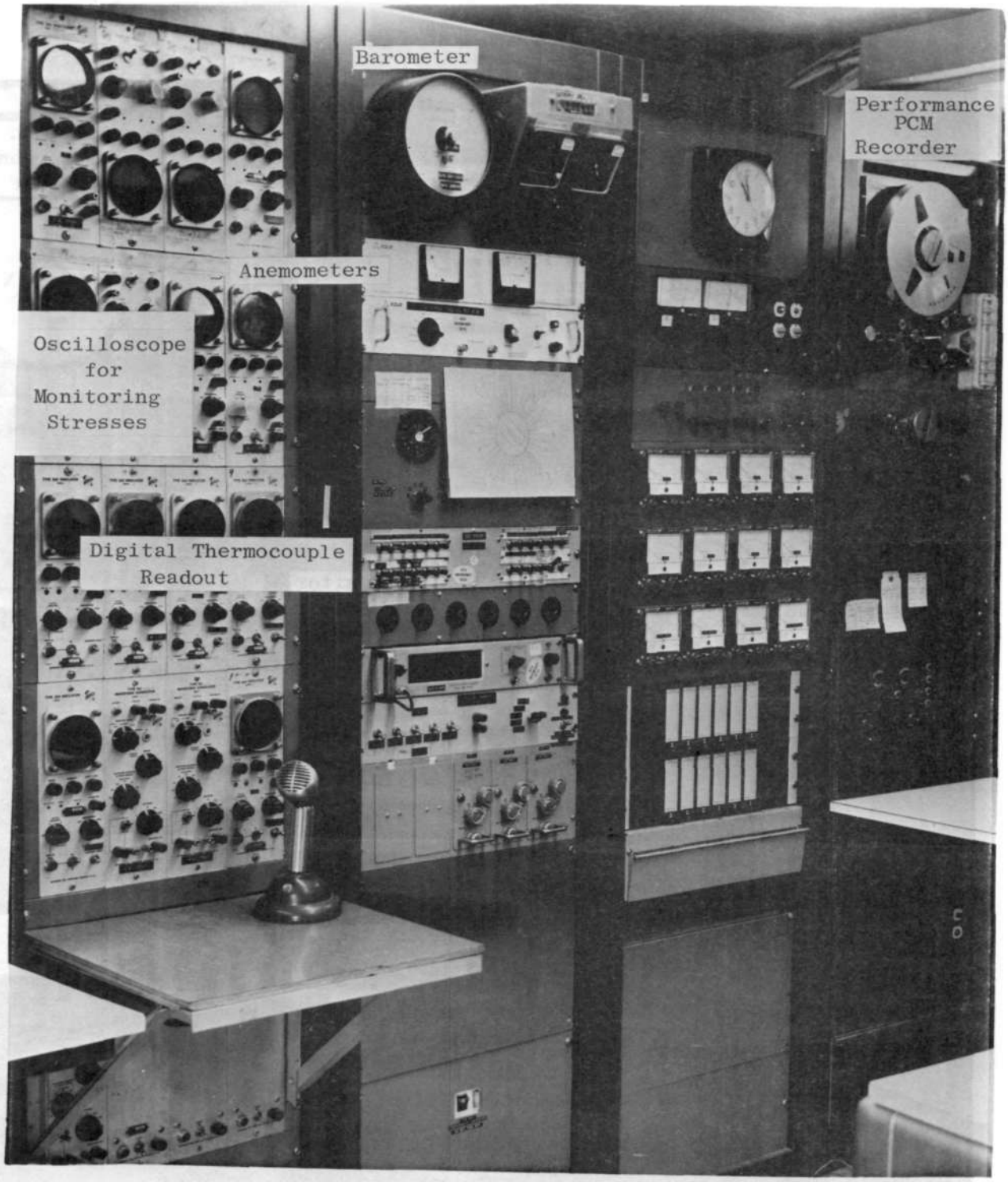

Figure 34. Fan and Engine Performance Recording Equipment

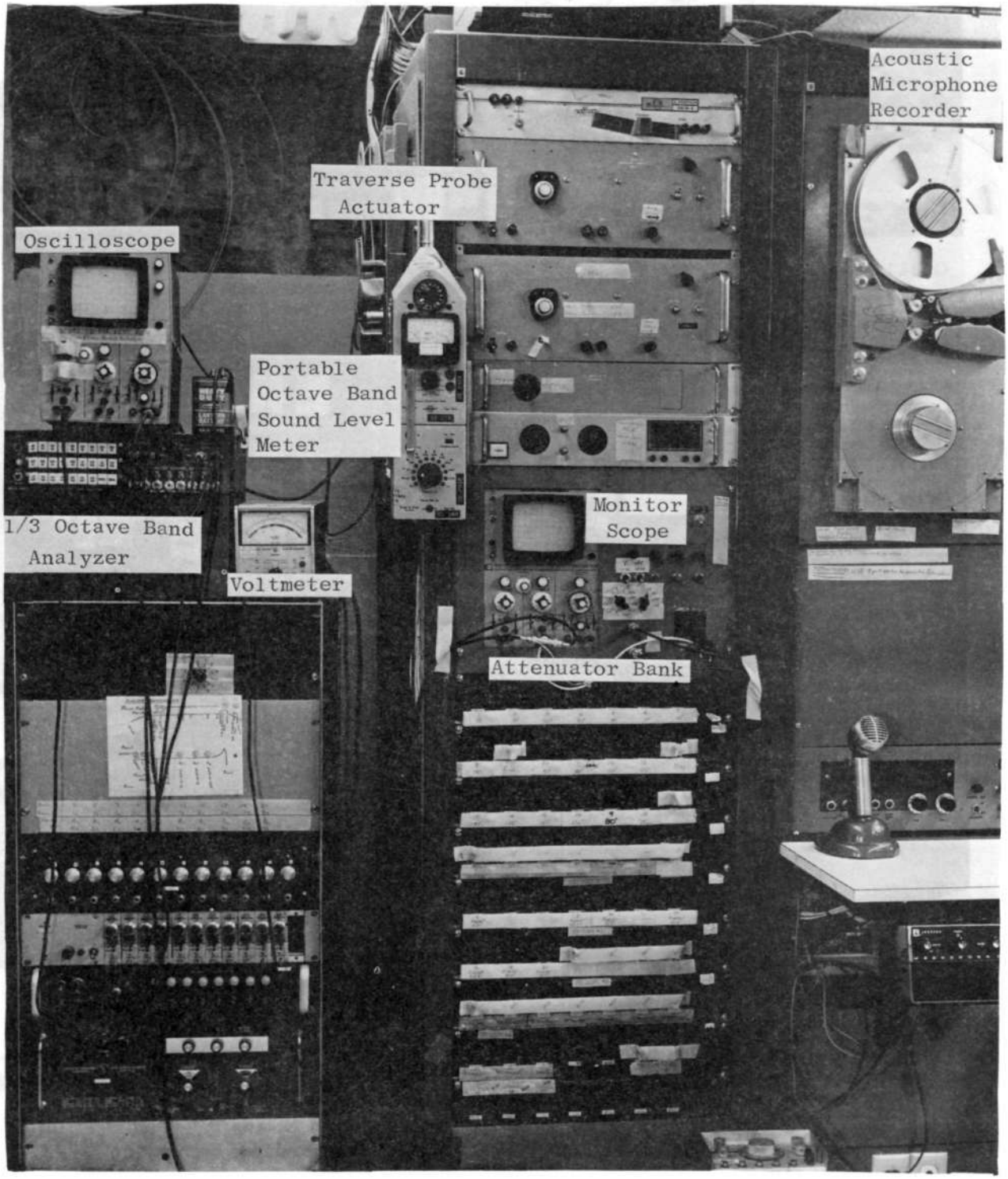

Figure 35. Acoustic Noise Measuring Equipment

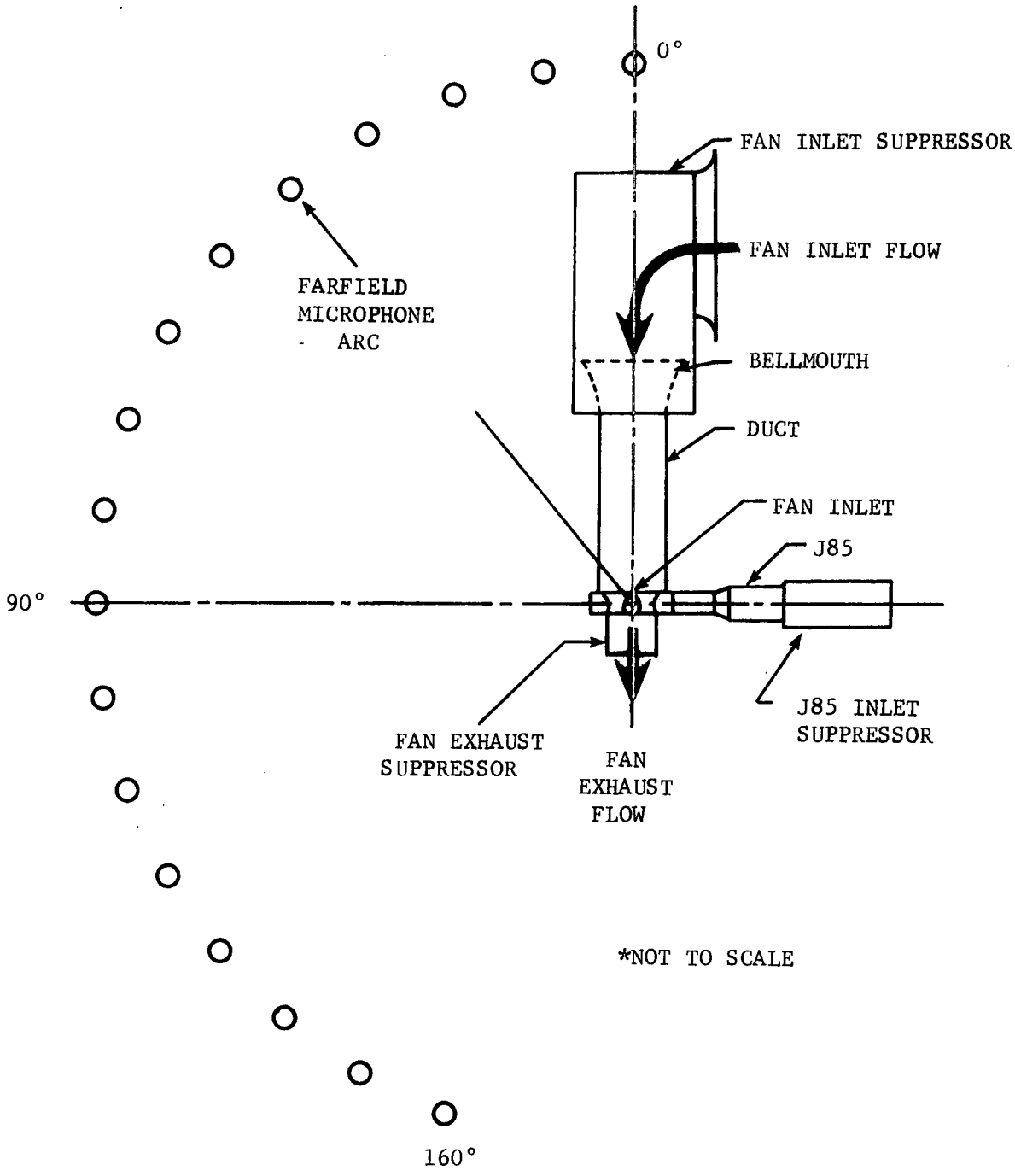

Figure 36. Schematic Representation of LF336 Test Site

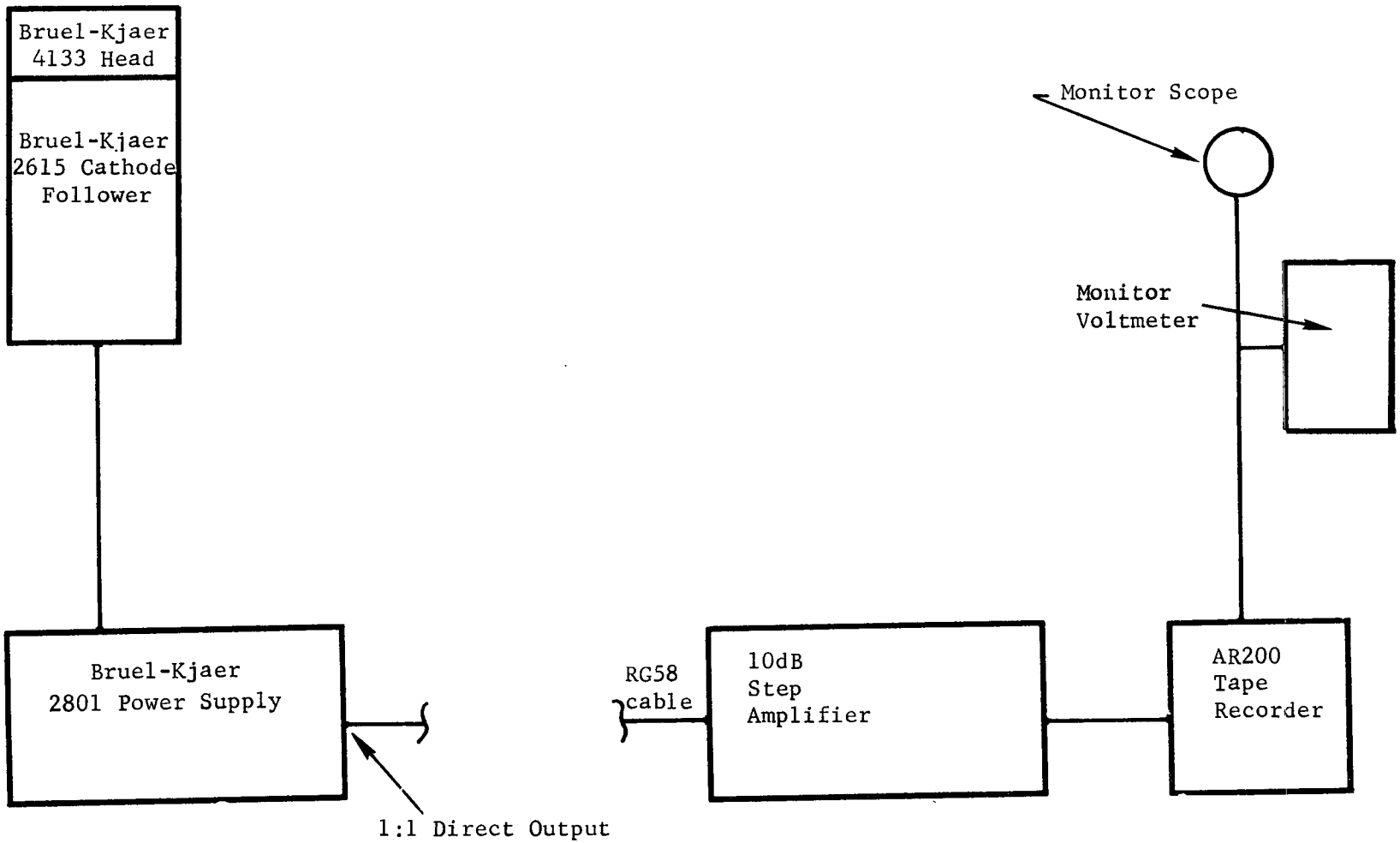

Figure 37. Data Acquisition Schematic Diagram

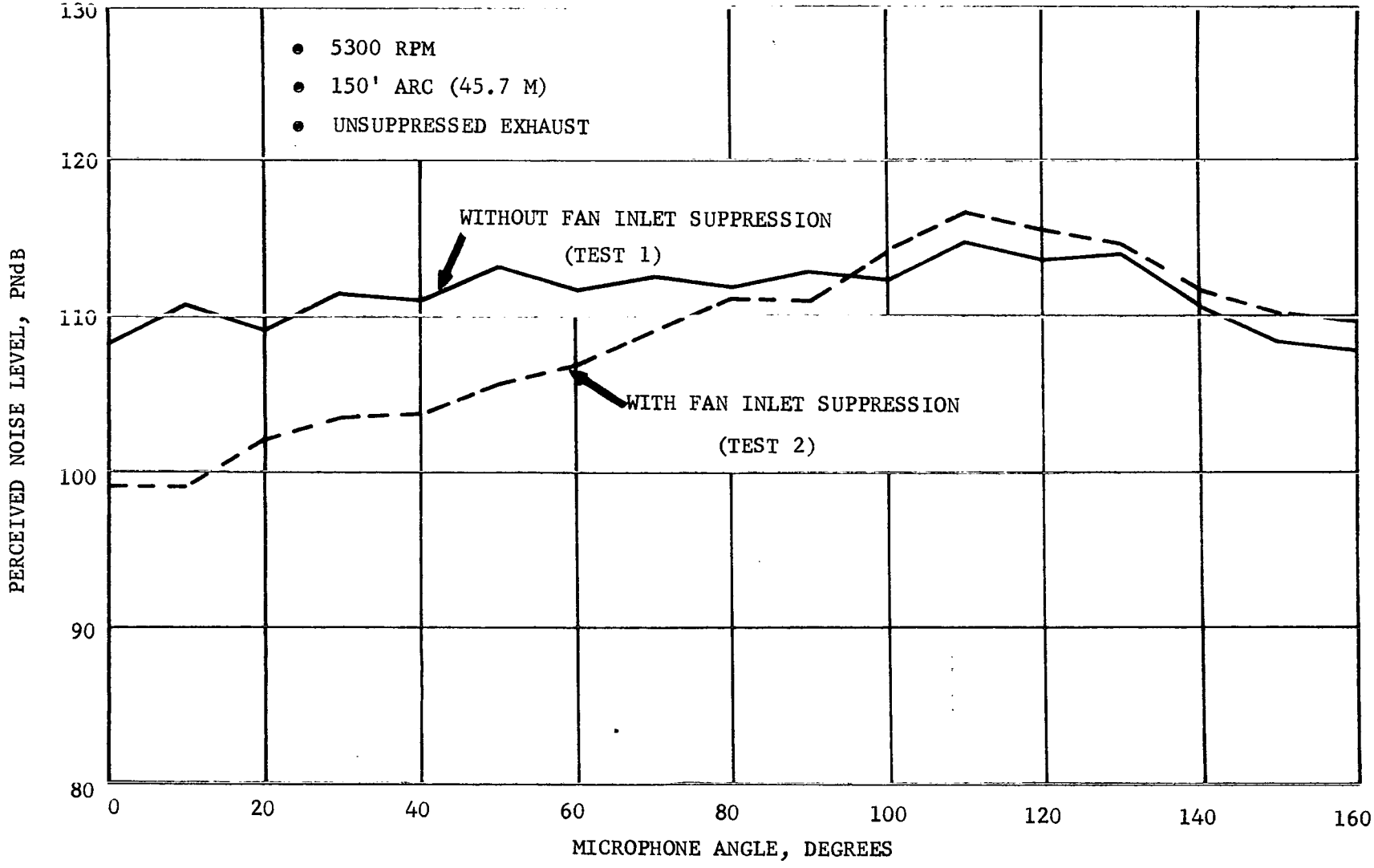

Figure 38. LF336/B Perceived Noise Level Directivity at 5300 RPM with and without Fan Inlet Suppression

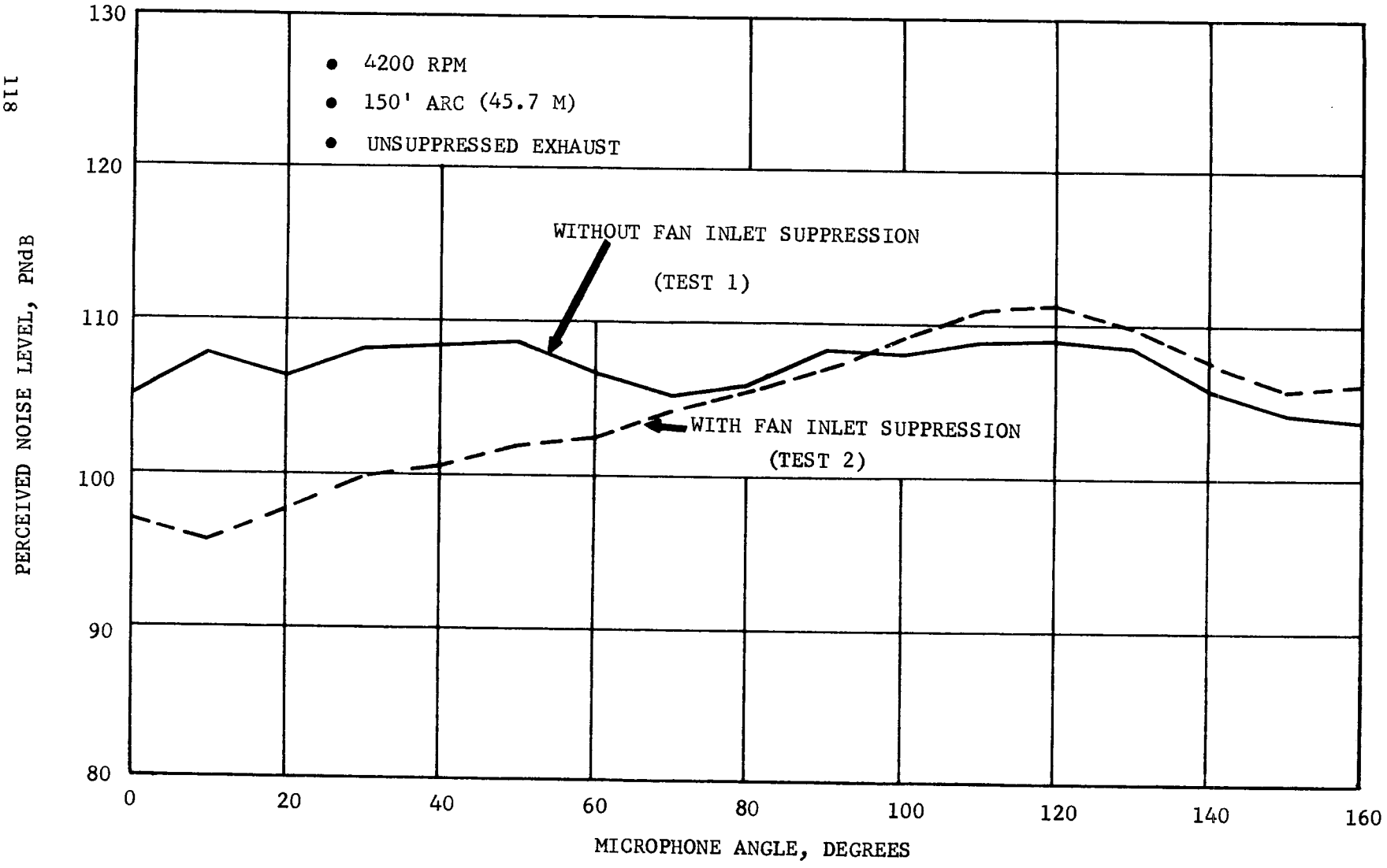

Figure 39. LF336/B Perceived Noise Level Directivity at 4200 RPM with and without Fan Inlet Suppression

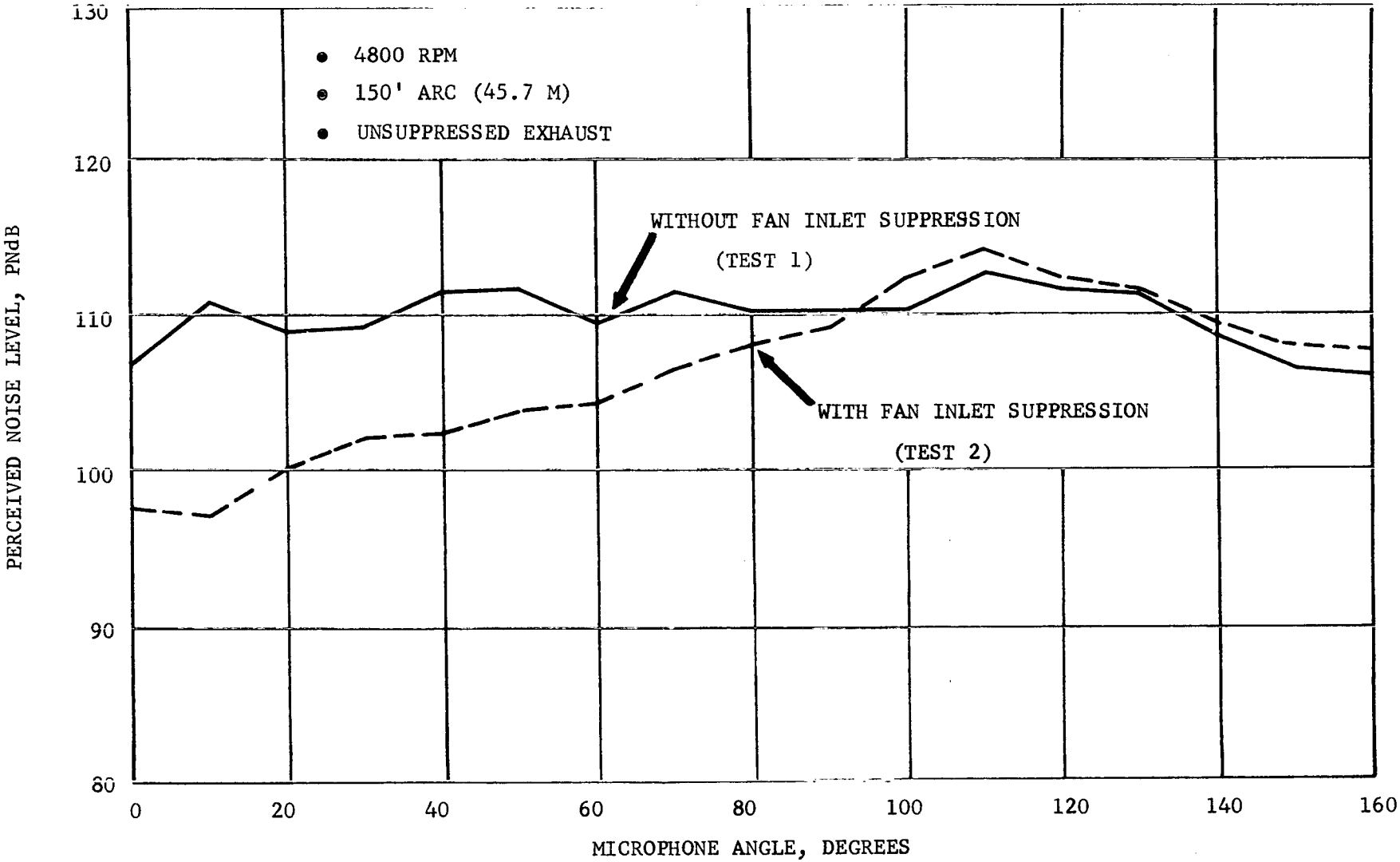

Figure 40. LF336/B Perceived Noise Level Directivity at 4800 RPM with and without Fan Inlet Suppression

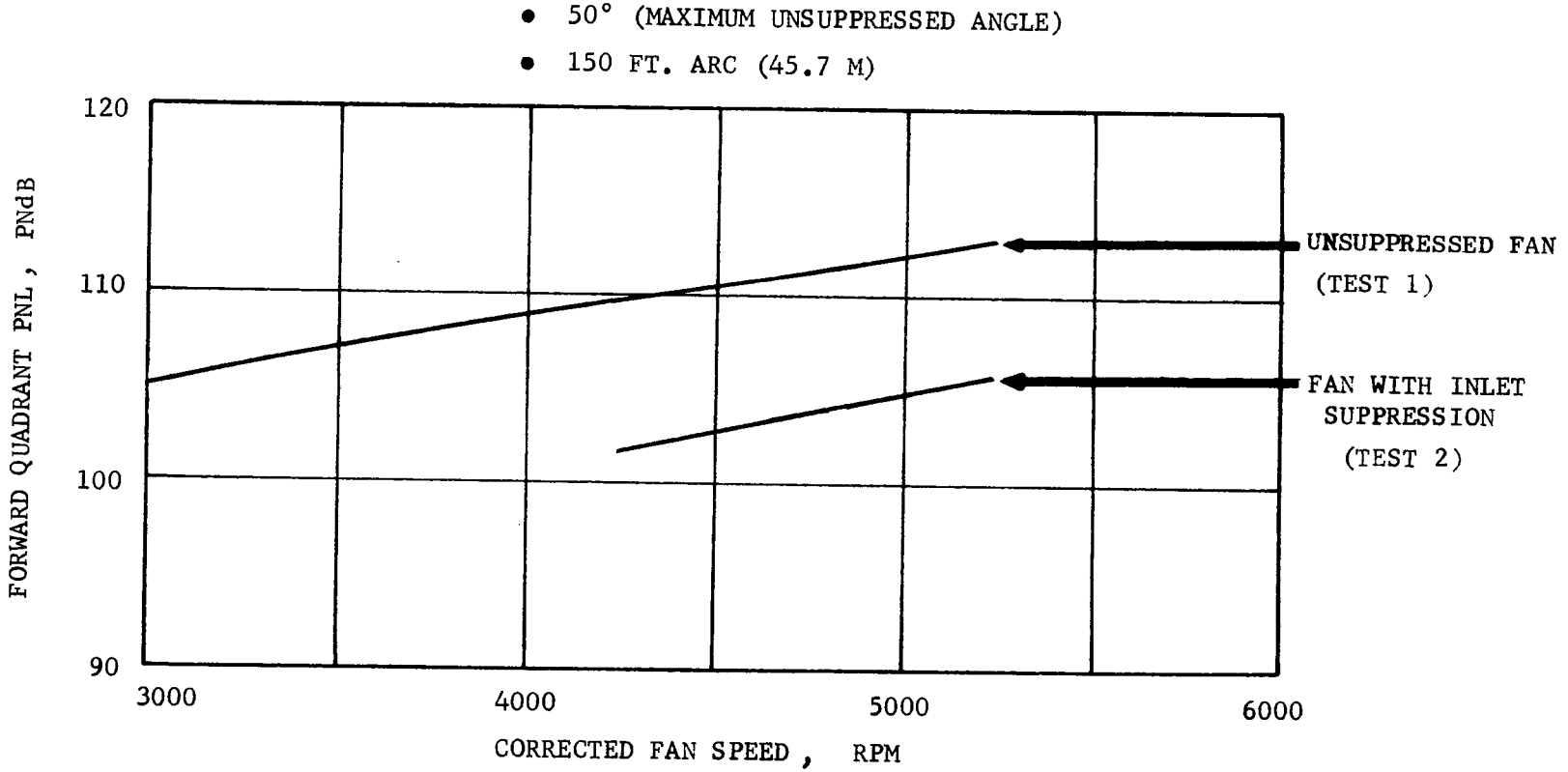

Figure 41. Effect of Fan Speed on Forward Quadrant Perceived Noise Levels

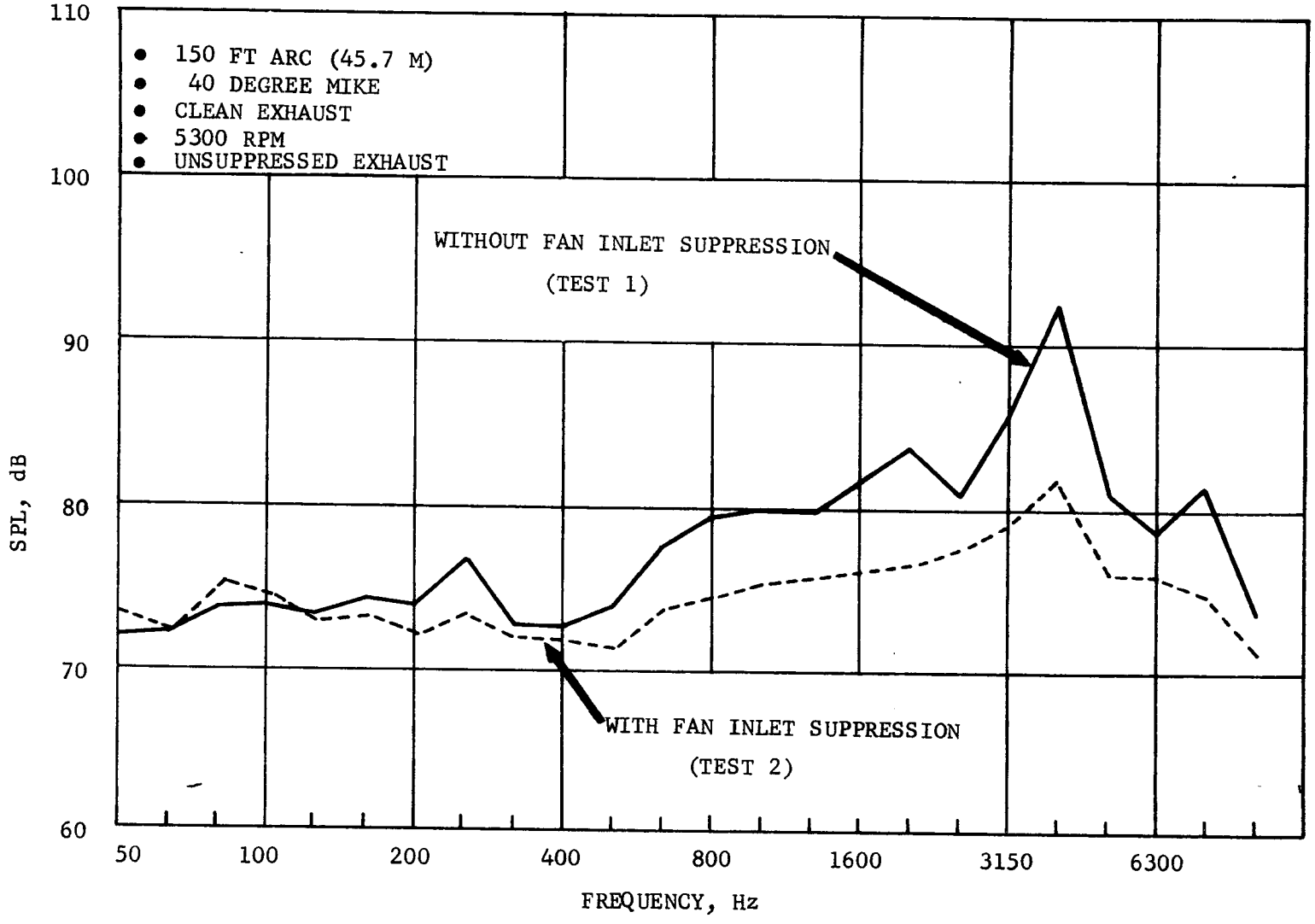

Figure 42. 40 Degree Microphone Sound Pressure Levels at 5300 RPM with and without Fan Inlet Suppression

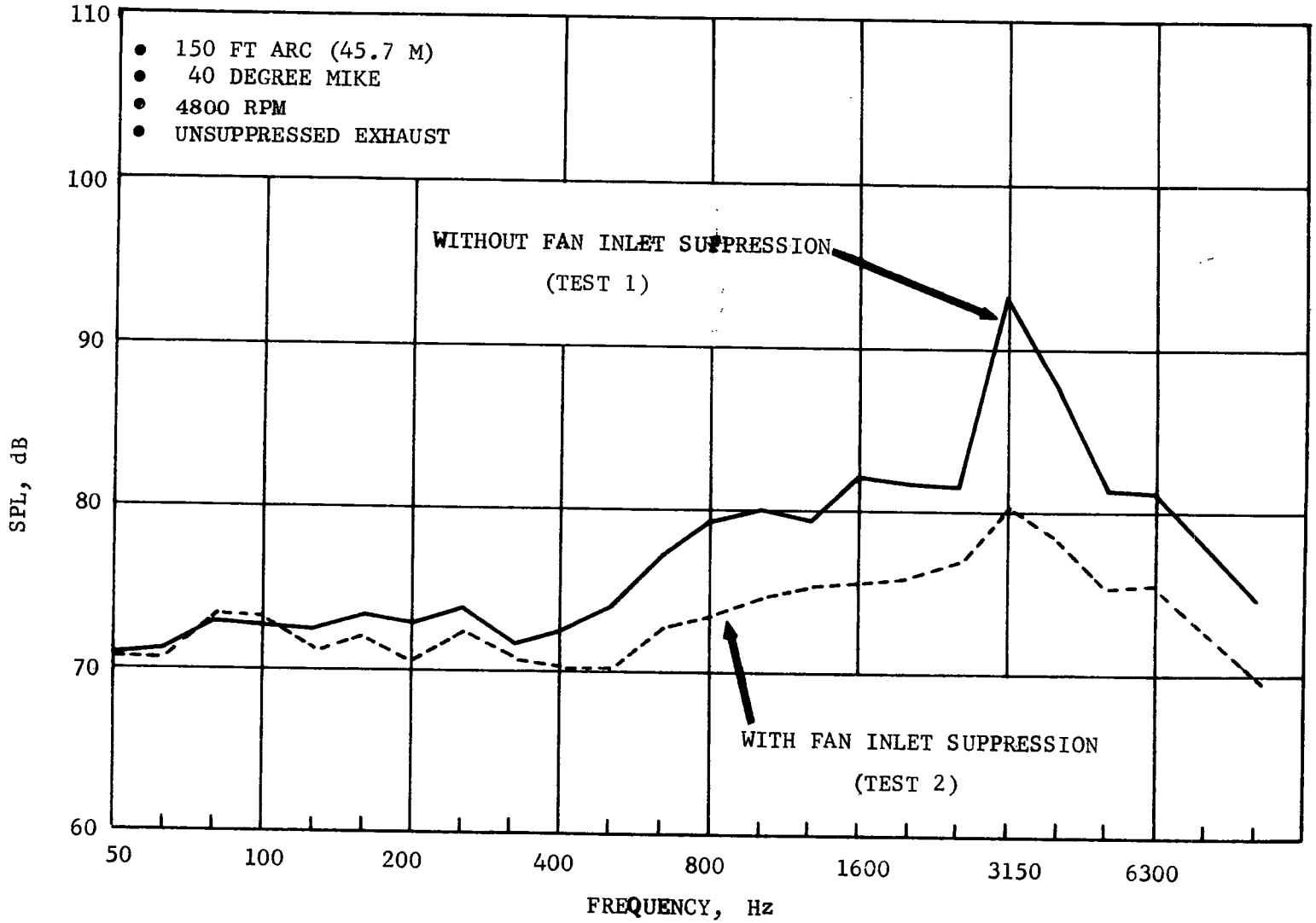

Figure 43. 40 Degree Microphone Sound Pressure Levels at 4800 RPM with and without Fan Inlet Suppression

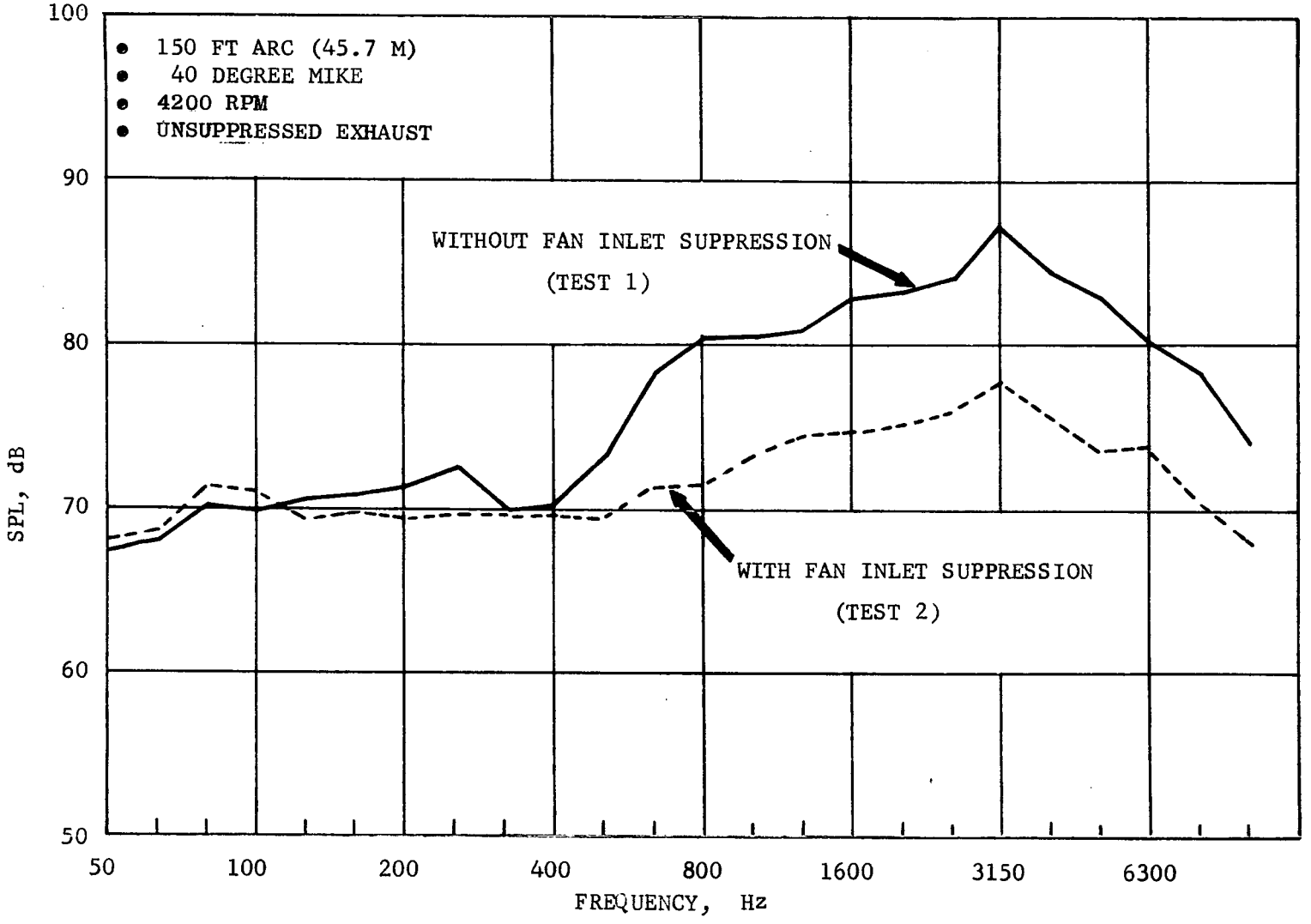

Figure 44. 40 Degree Microphone Sound Pressure Levels at 4200 RPM with and without Fan Inlet Suppression

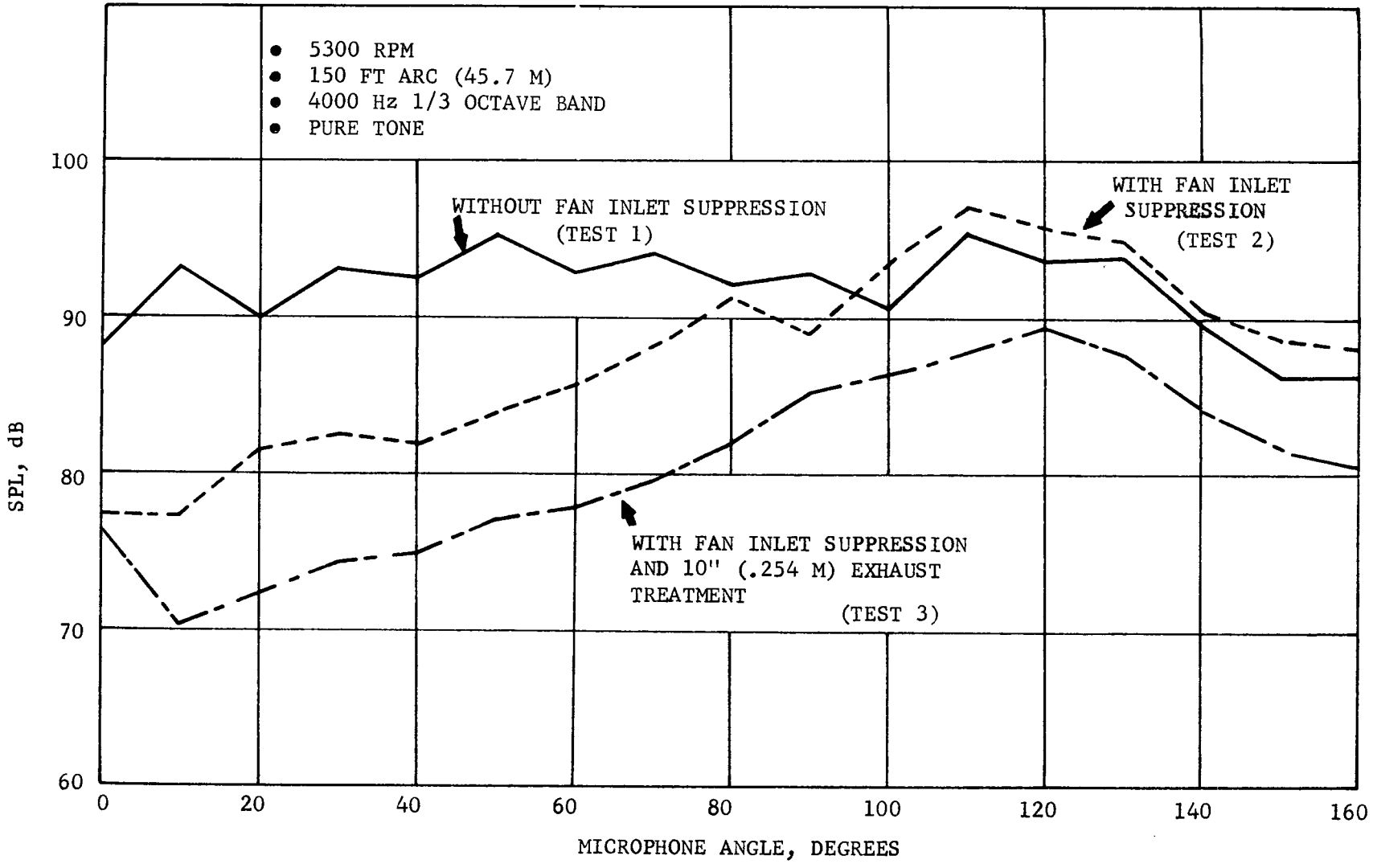

Figure 45. LF336/B Pure Tone Directivity Patterns at 5300 RPM for Tests 1, 2 and 3

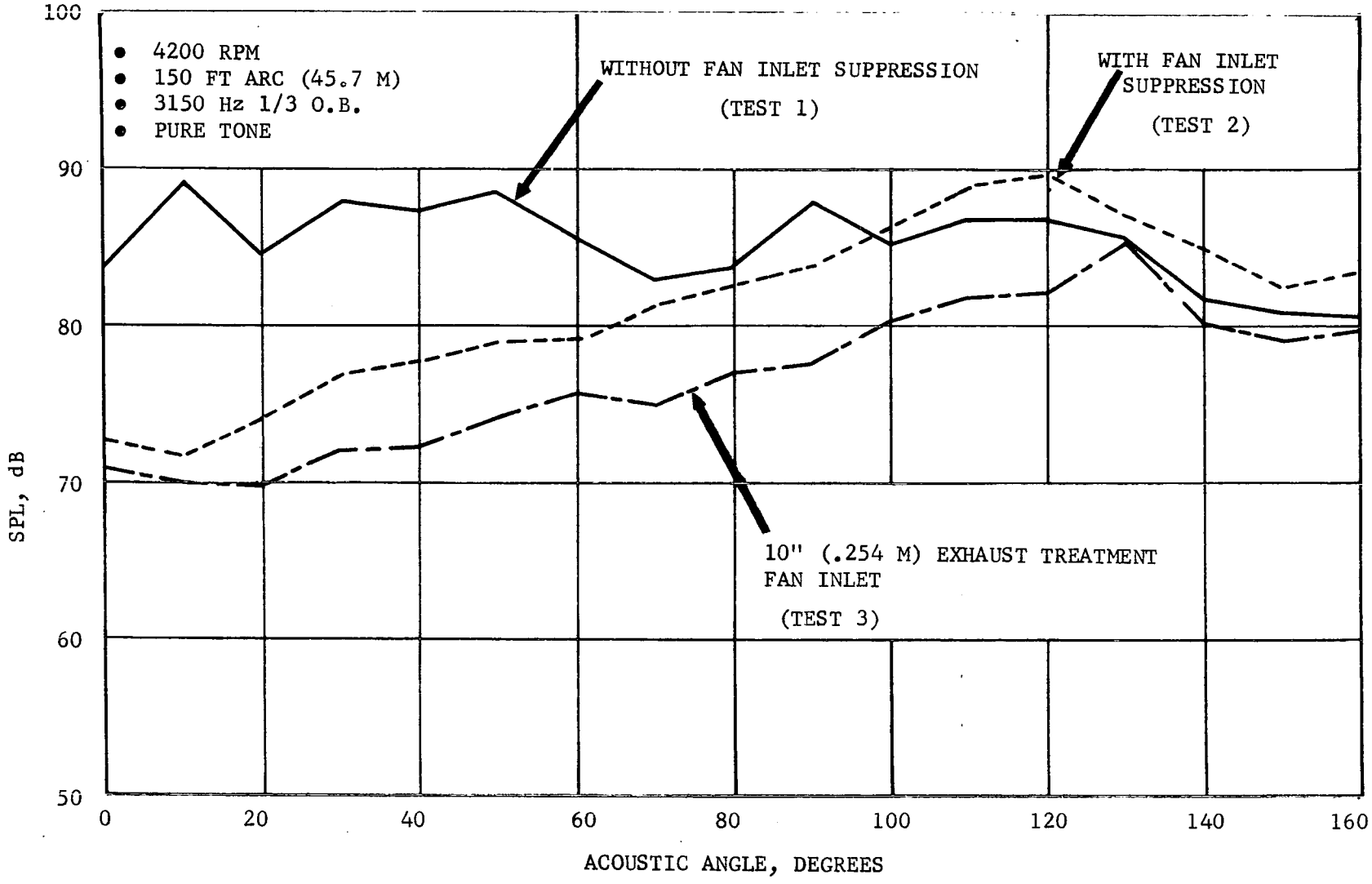

Figure 46. LF336/B Pure Tone Directivity Patterns at 4200 RPM for Tests 1, 2 and 3

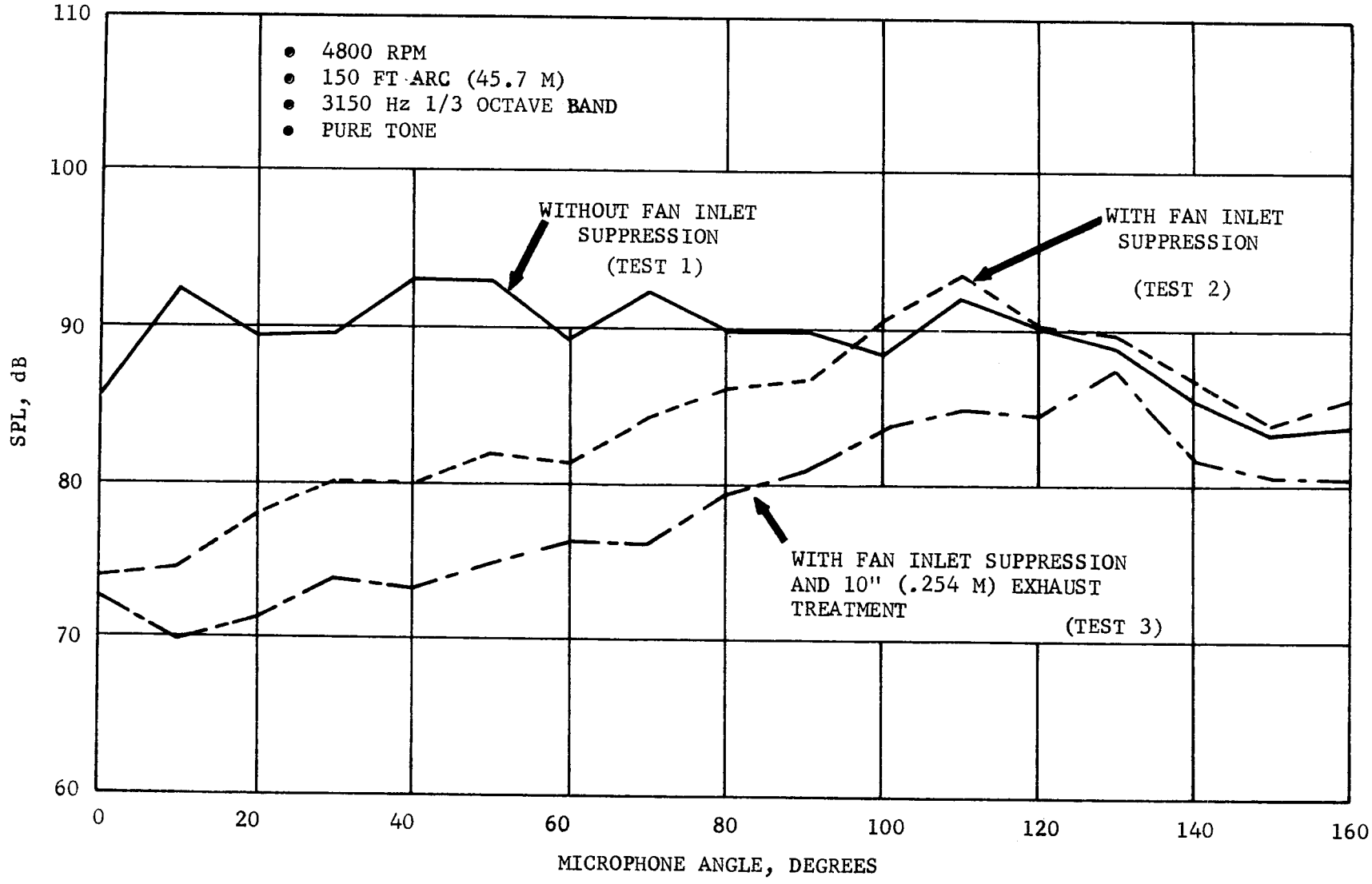

Figure 47. LF336/B Pure Tone Directivity Patterns at 4800 RPM for Tests 1, 2 and 3

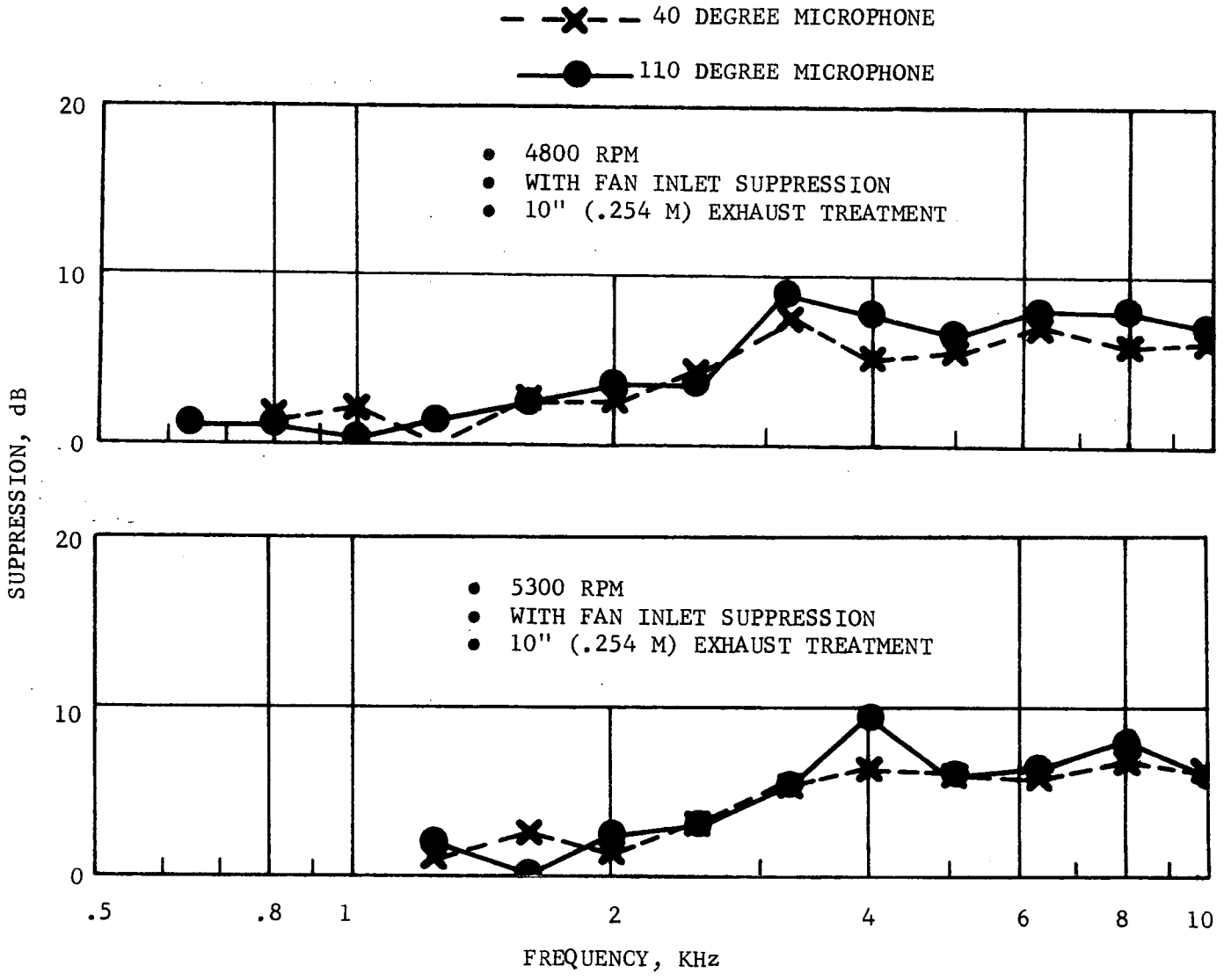

Figure 48. LF336/B Forward and Aft Suppression

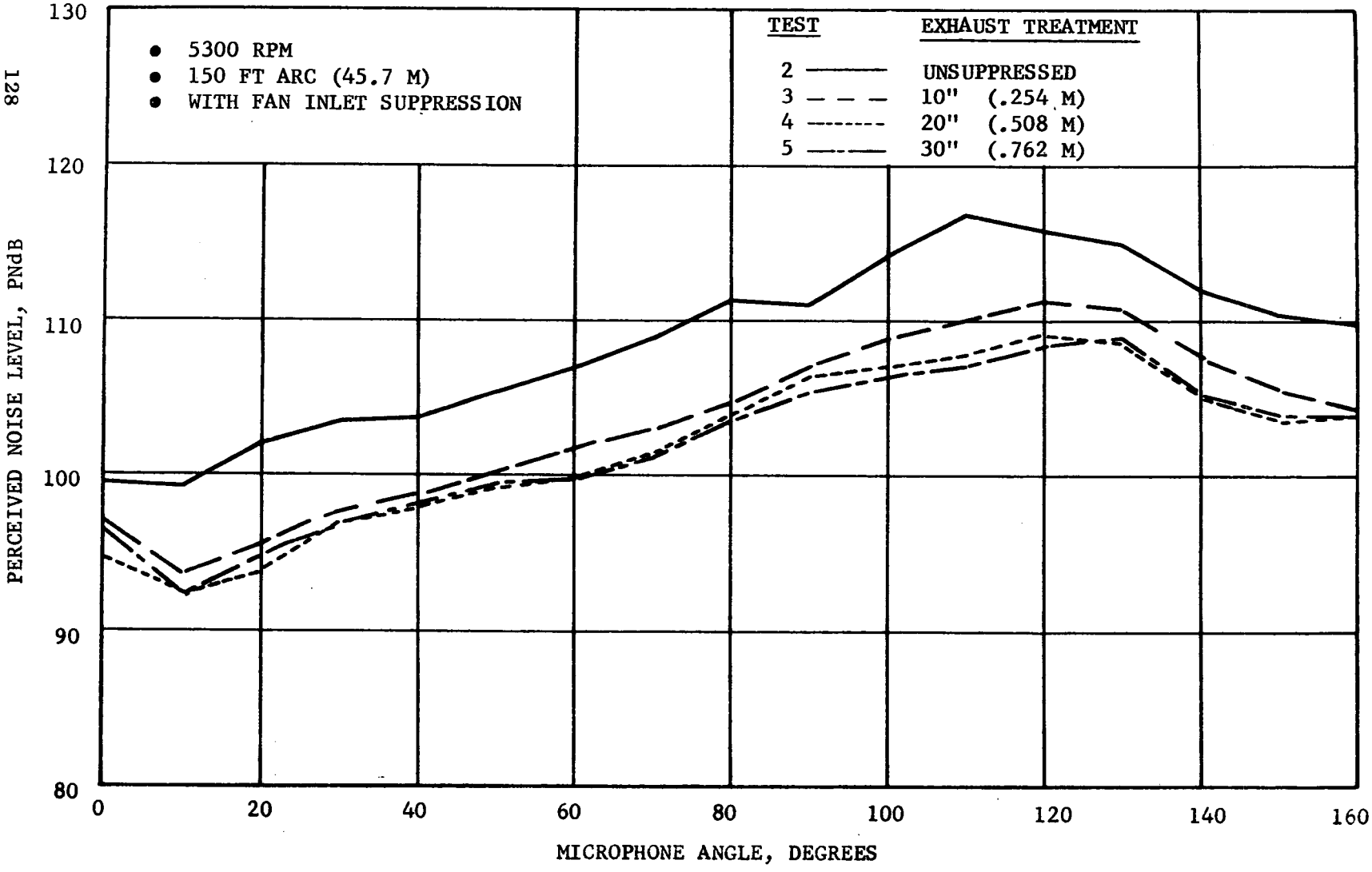

Figure 49. LF336/B Exhaust Radiated Perceived Noise Levels at 5300 RPM

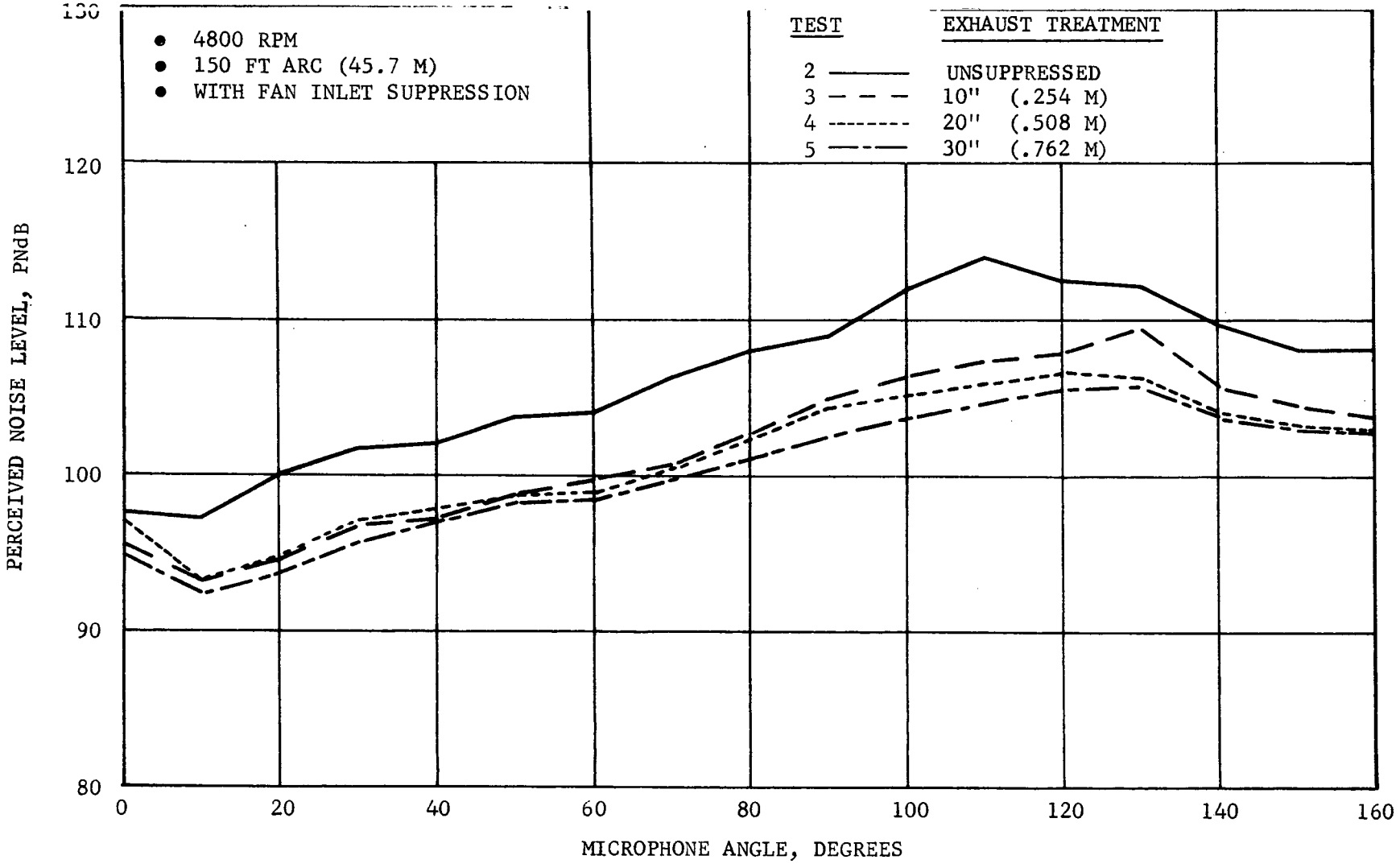

Figure 50. LF336/B Exhaust Radiated Perceived Noise Levels at 4800 RPM

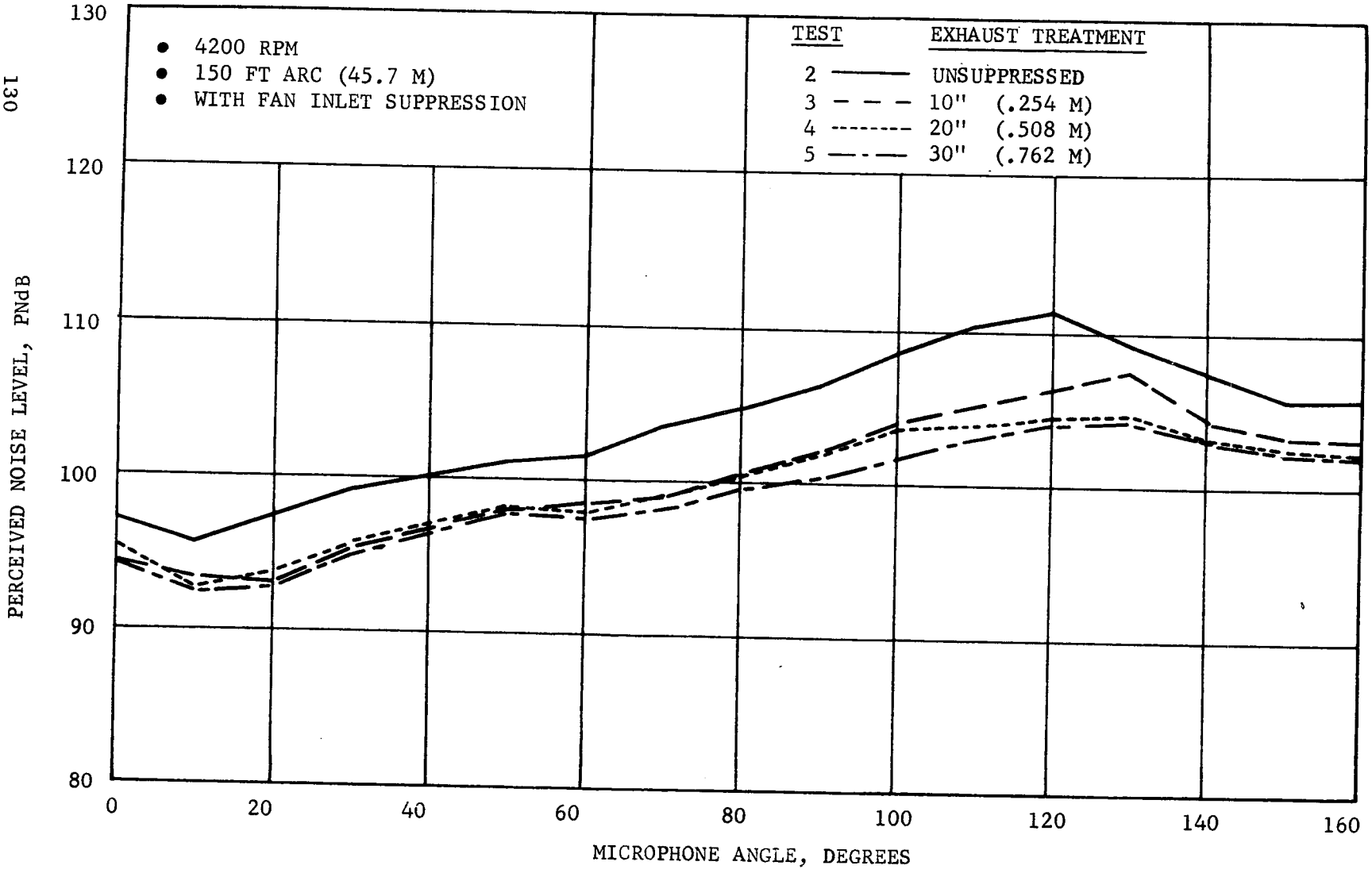

Figure 51. LF336/B Exhaust Radiated Perceived Noise Levels at 4200 RPM

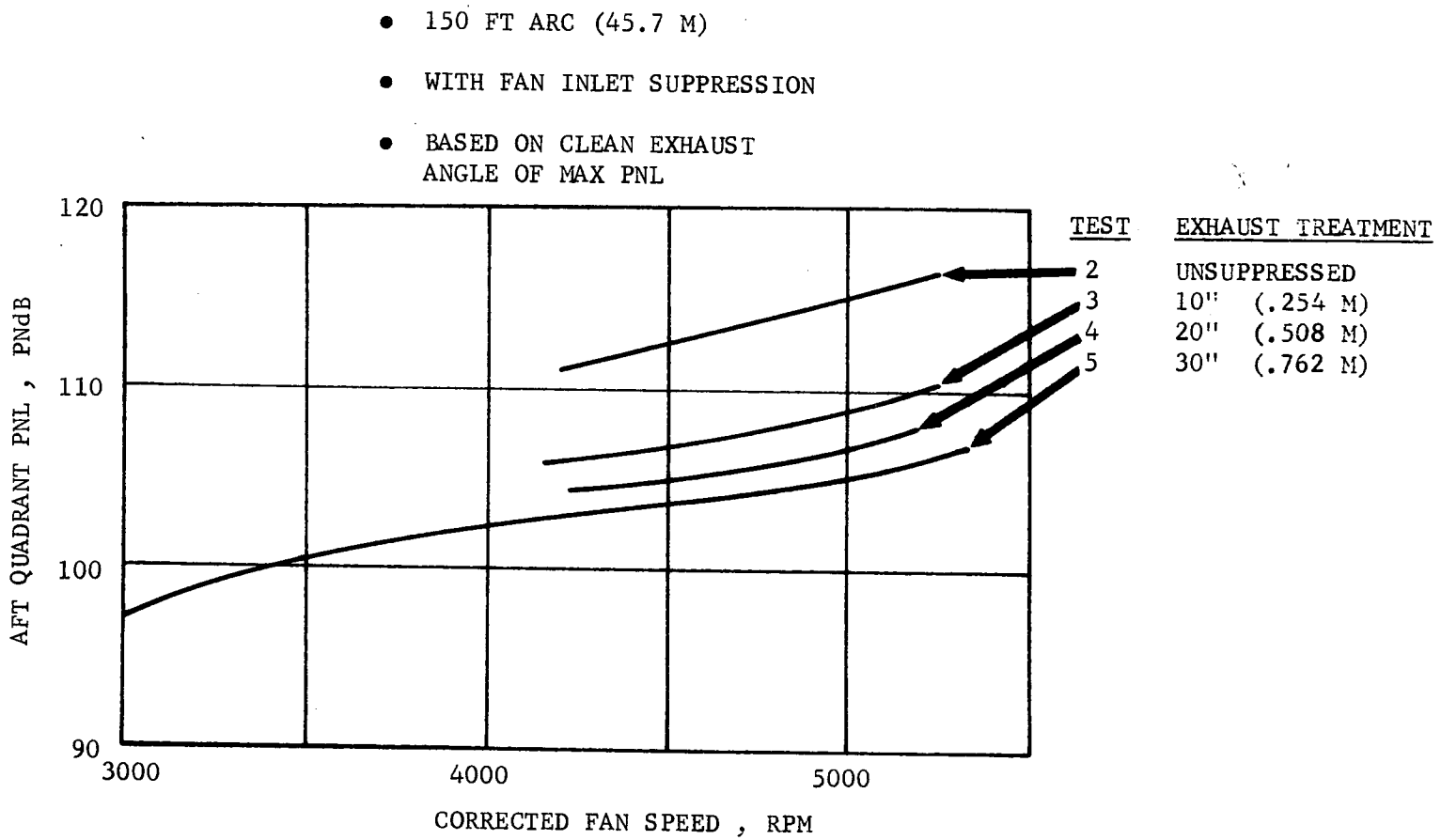

Figure 52. Aft Quadrant Perceived Noise Levels as a Function of Fan Speed

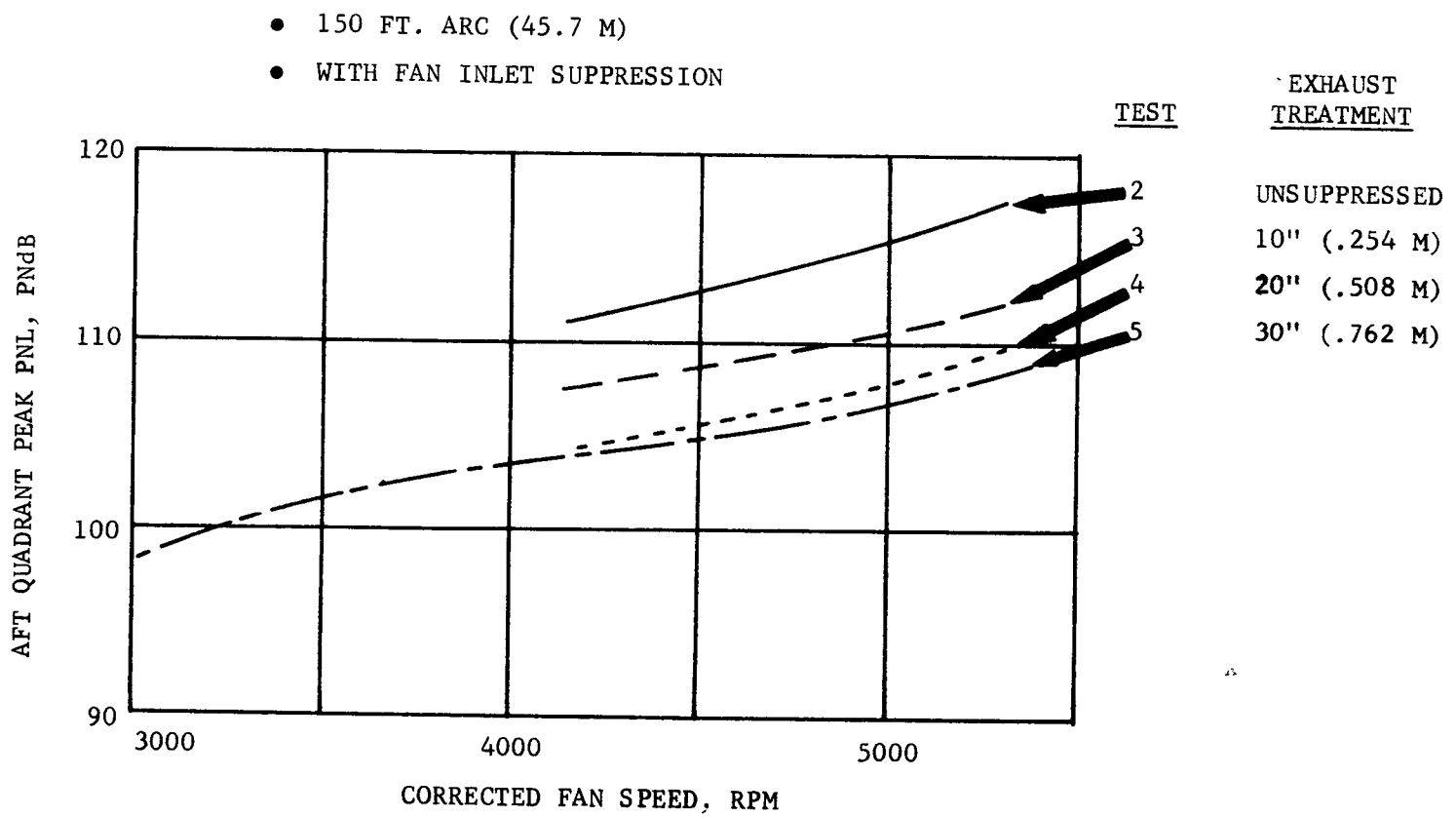

Figure 53. Peak-to-Peak PNL as a Function of Fan Speed

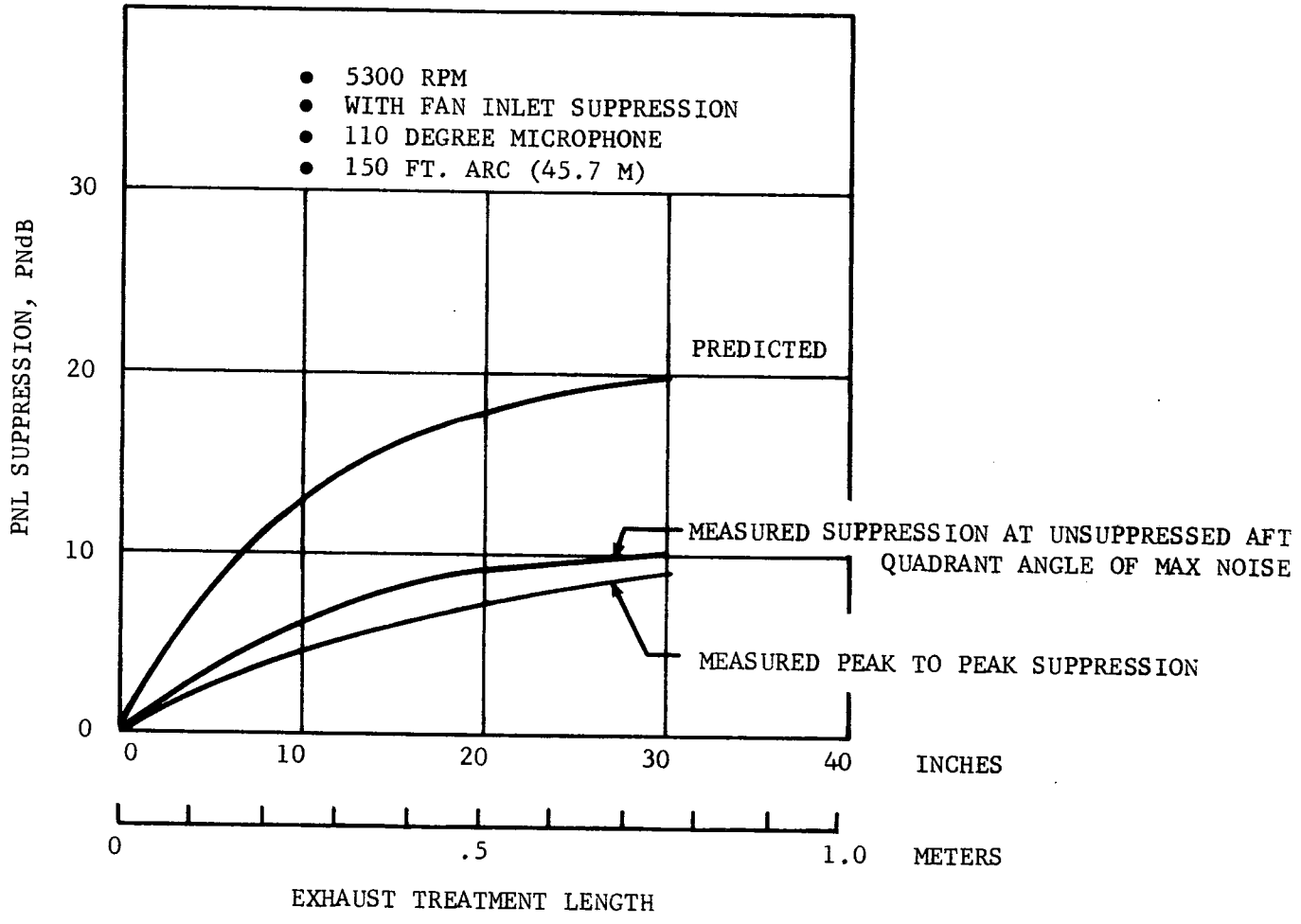

Figure 54. Comparison of Measured and Predicted PNL Suppression at the 110 Degree Microphone

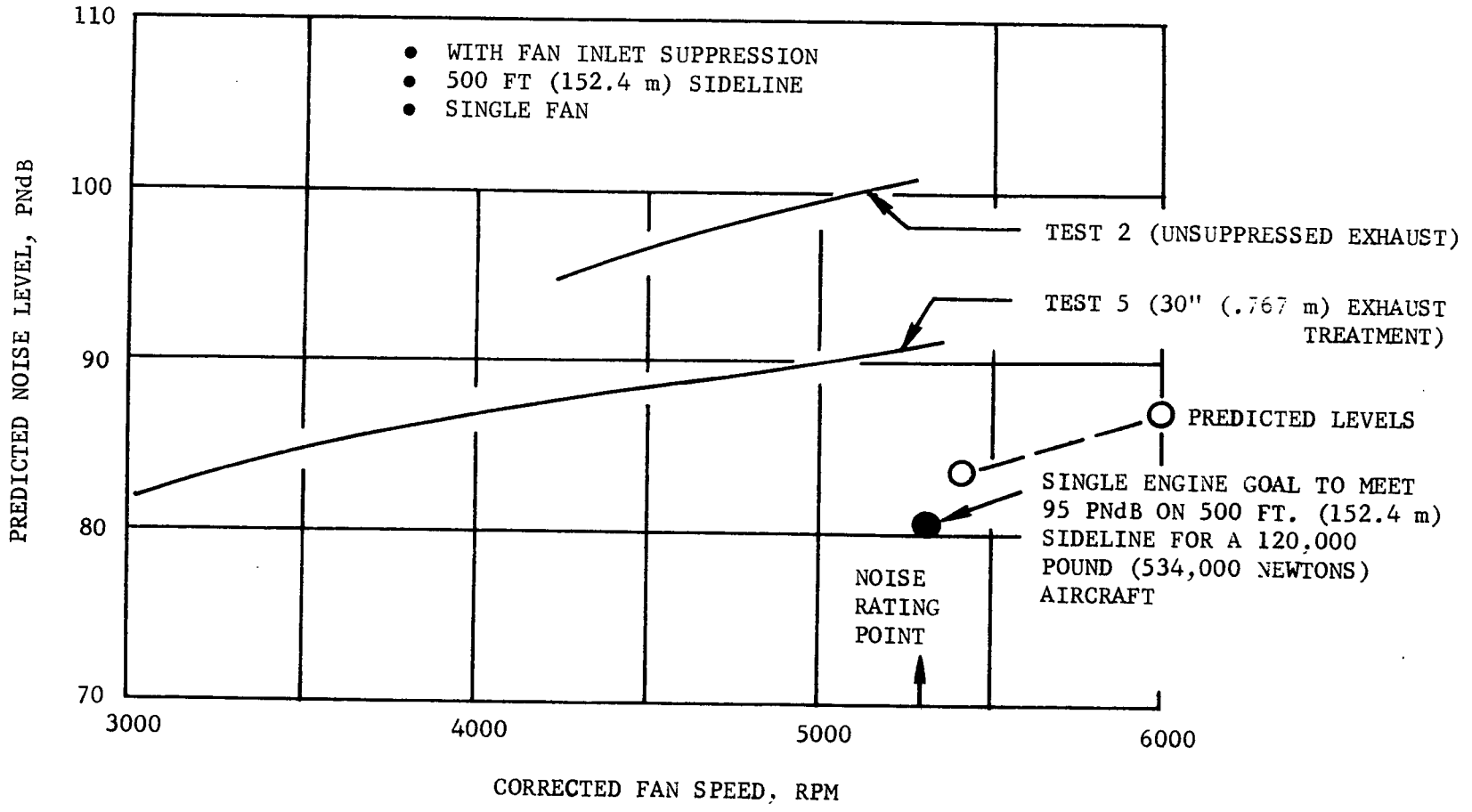

Figure 55. Perceived Noise Levels on a 500 Foot (152.4 m) Sideline

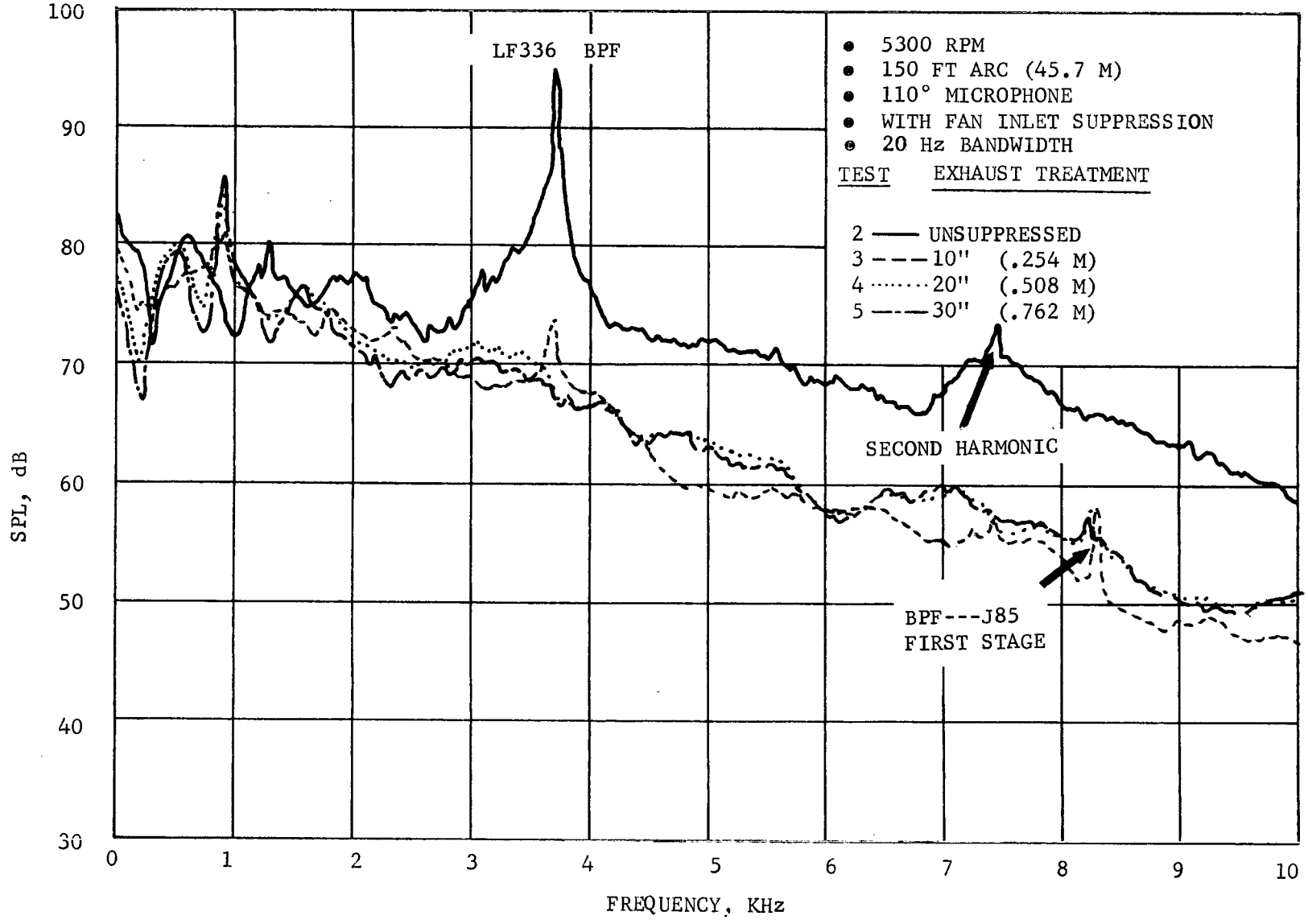

Figure 56. LF336/B Narrowband Spectrum at 110 Degree Microphone and 5300 RPM

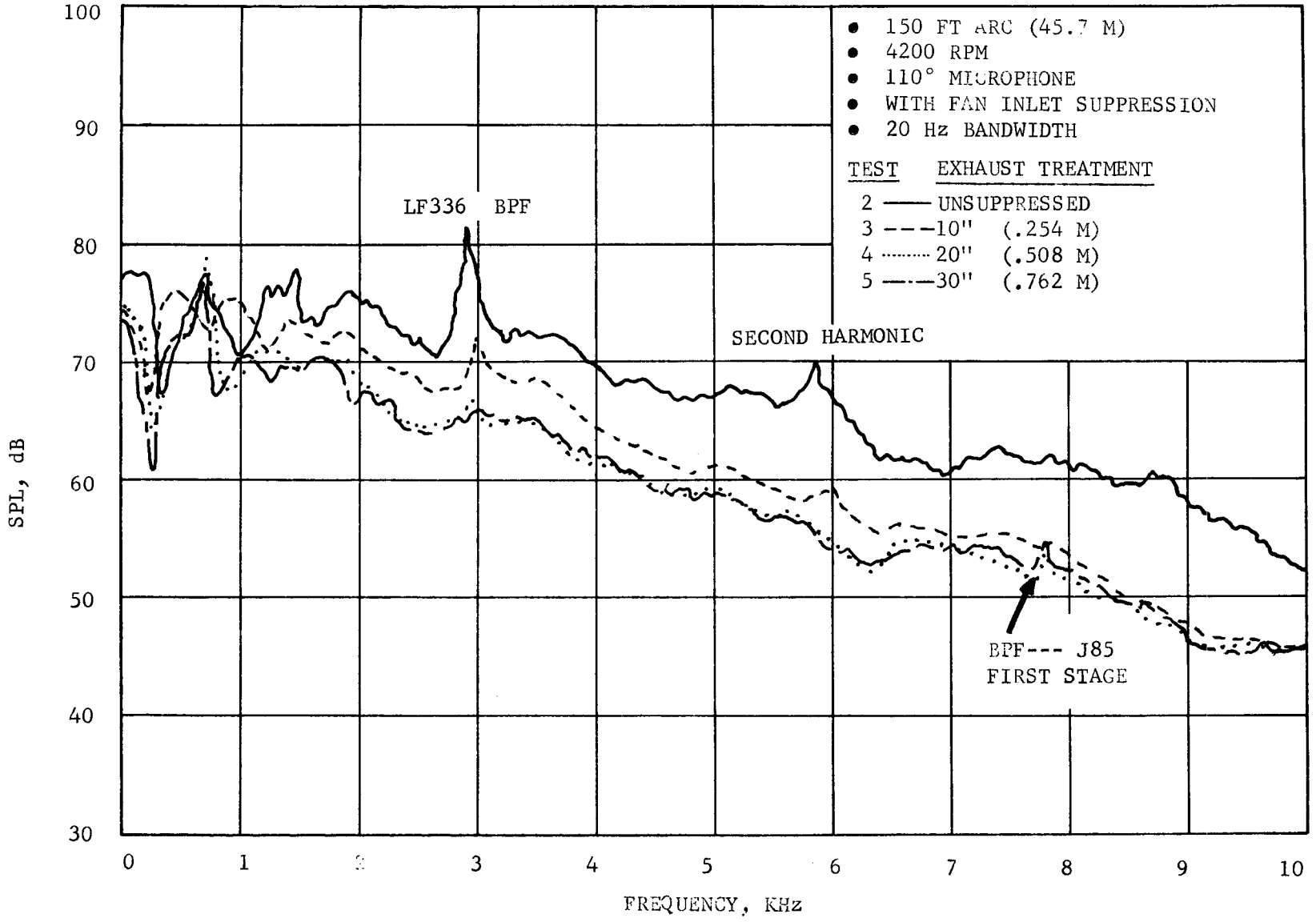

Figure 57. LF336/B Narrowband Spectrum at 110 Degree Microphone and 4200 RPM

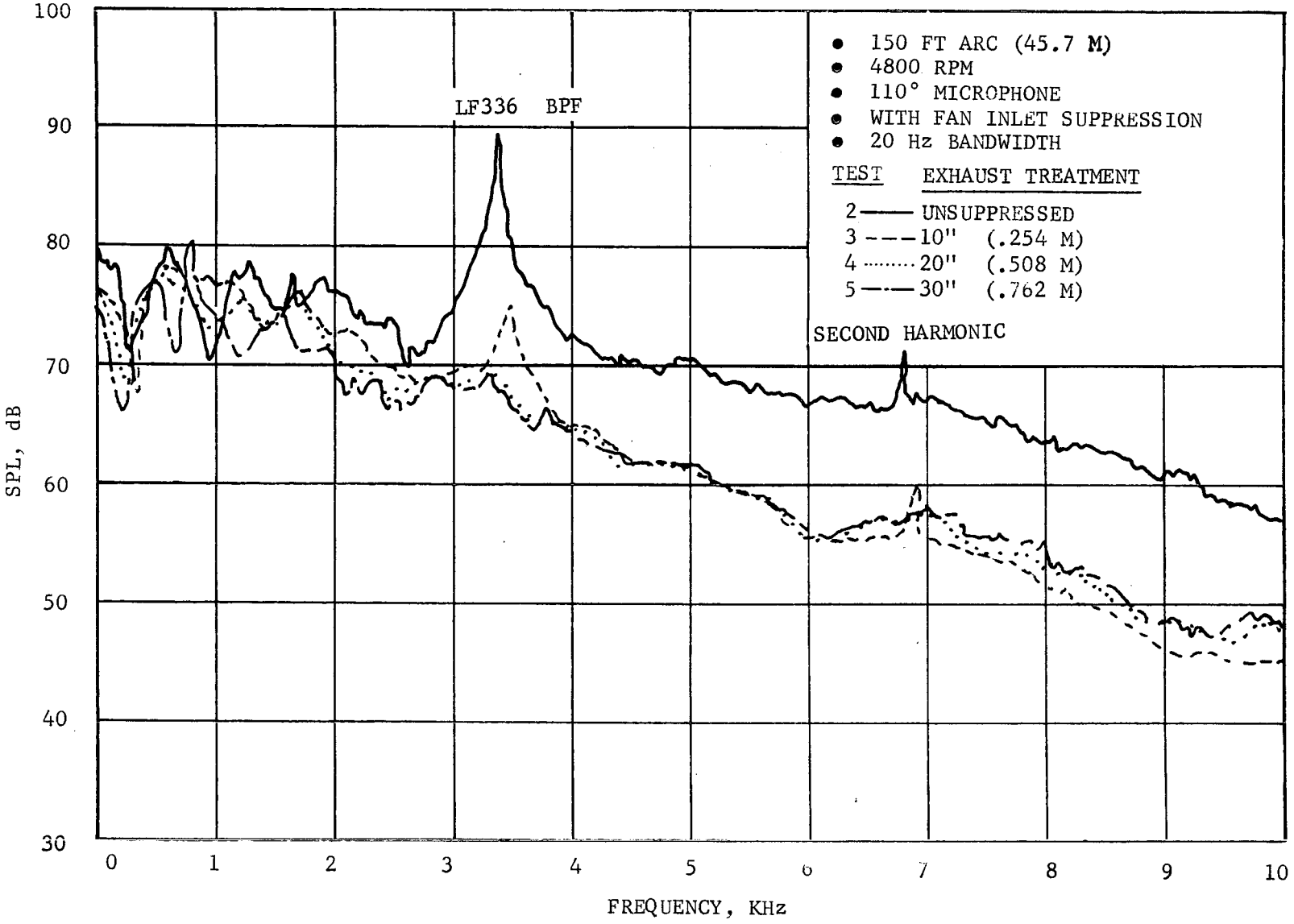

Figure 58. LF336/B Narrowband Spectrum at 110 Degree Microphone and 4800 RPM

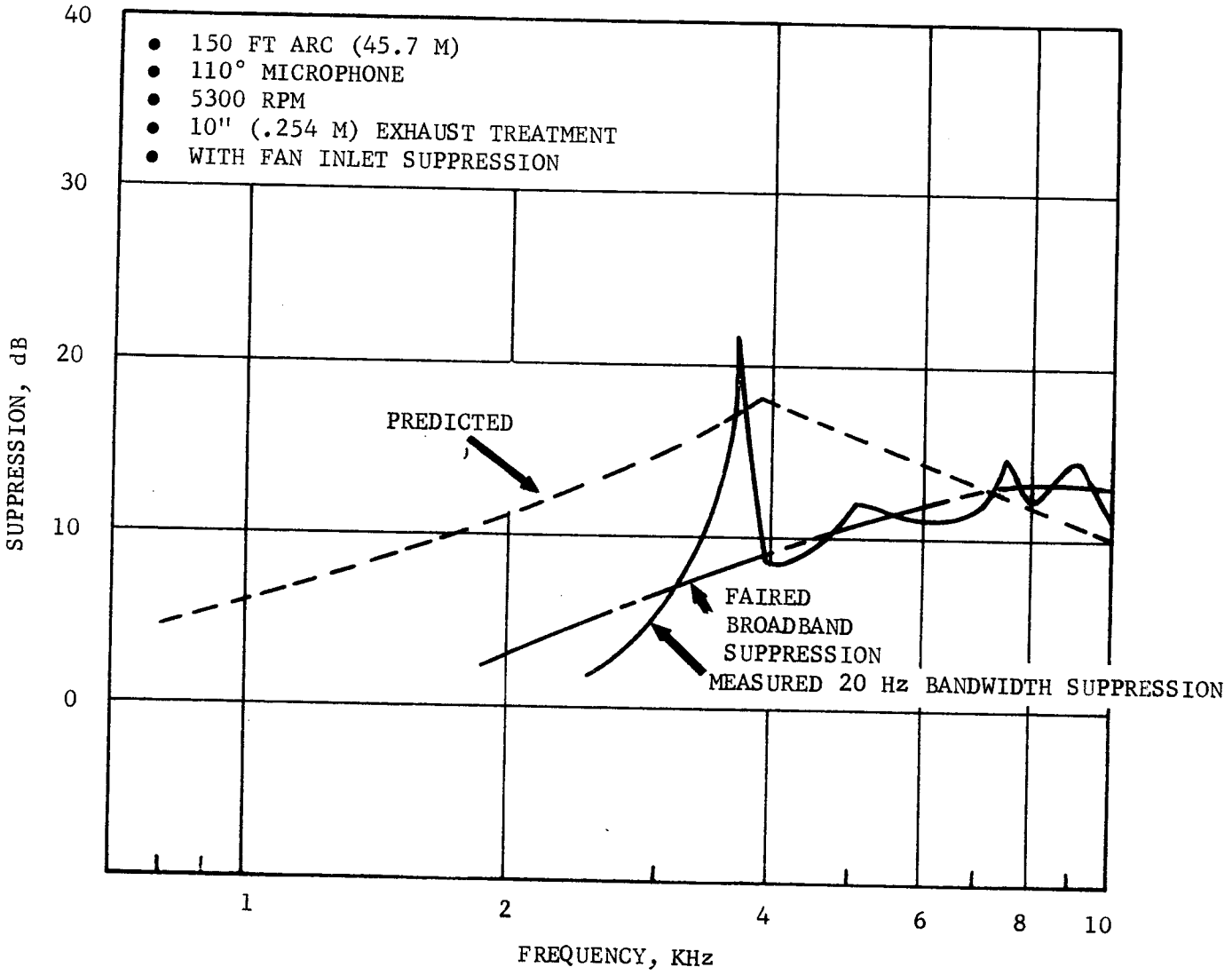

Figure 59. LF336/B Suppression Levels at 5300 RPM at the 110 Degree Microphone with 10 inches (25.4 cm) Exhaust Suppression

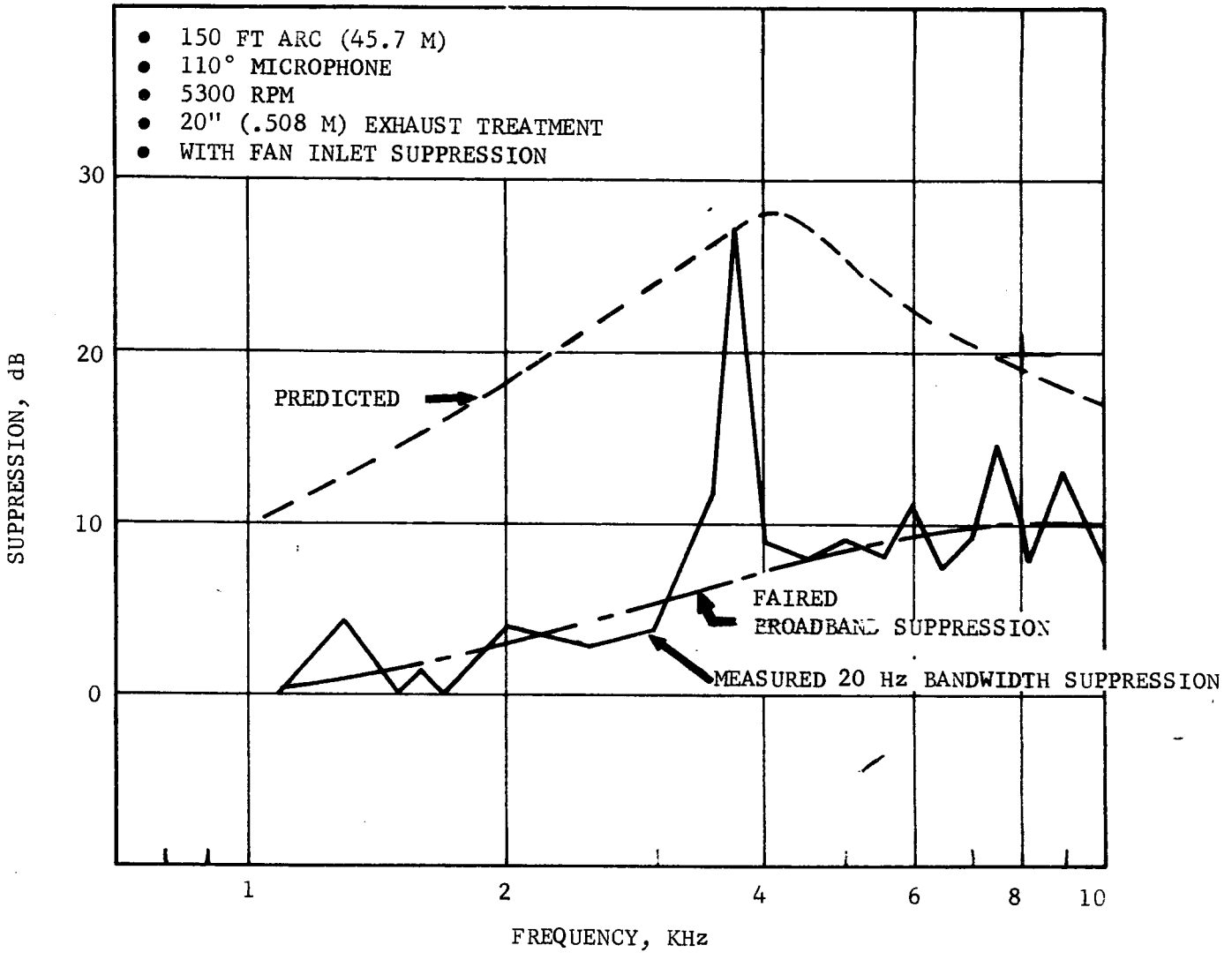

Figure 60. LF336/B Suppression Levels at 5300 RPM at the 110 Degree Microphone with 20 inches (50.8 cm) Exhaust Suppression

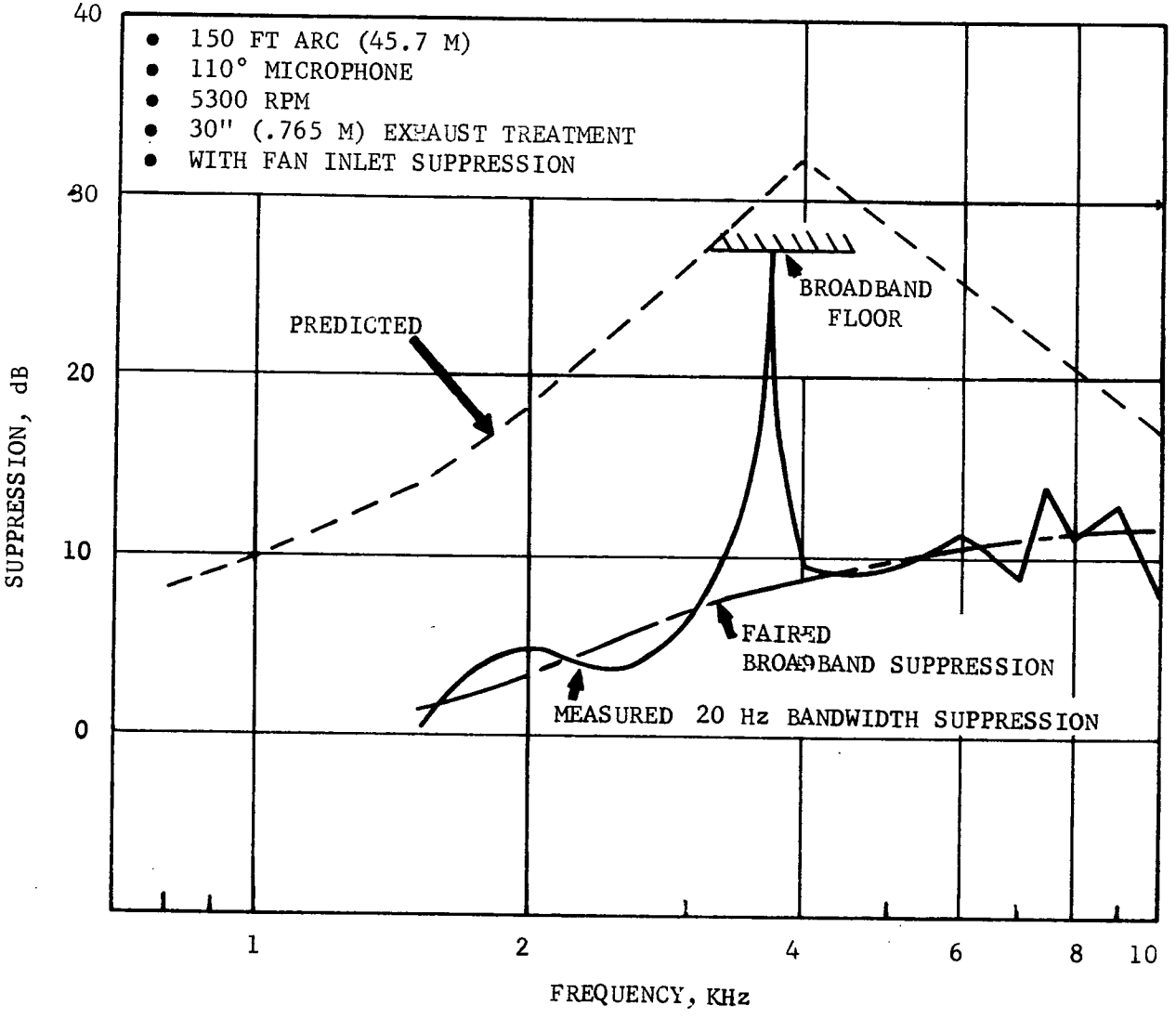

Figure 61. LF336/B Suppression Levels at 5300 RPM at the 110 Degree Microphone with 30 inches (76.2 cm) Exhaust Suppression

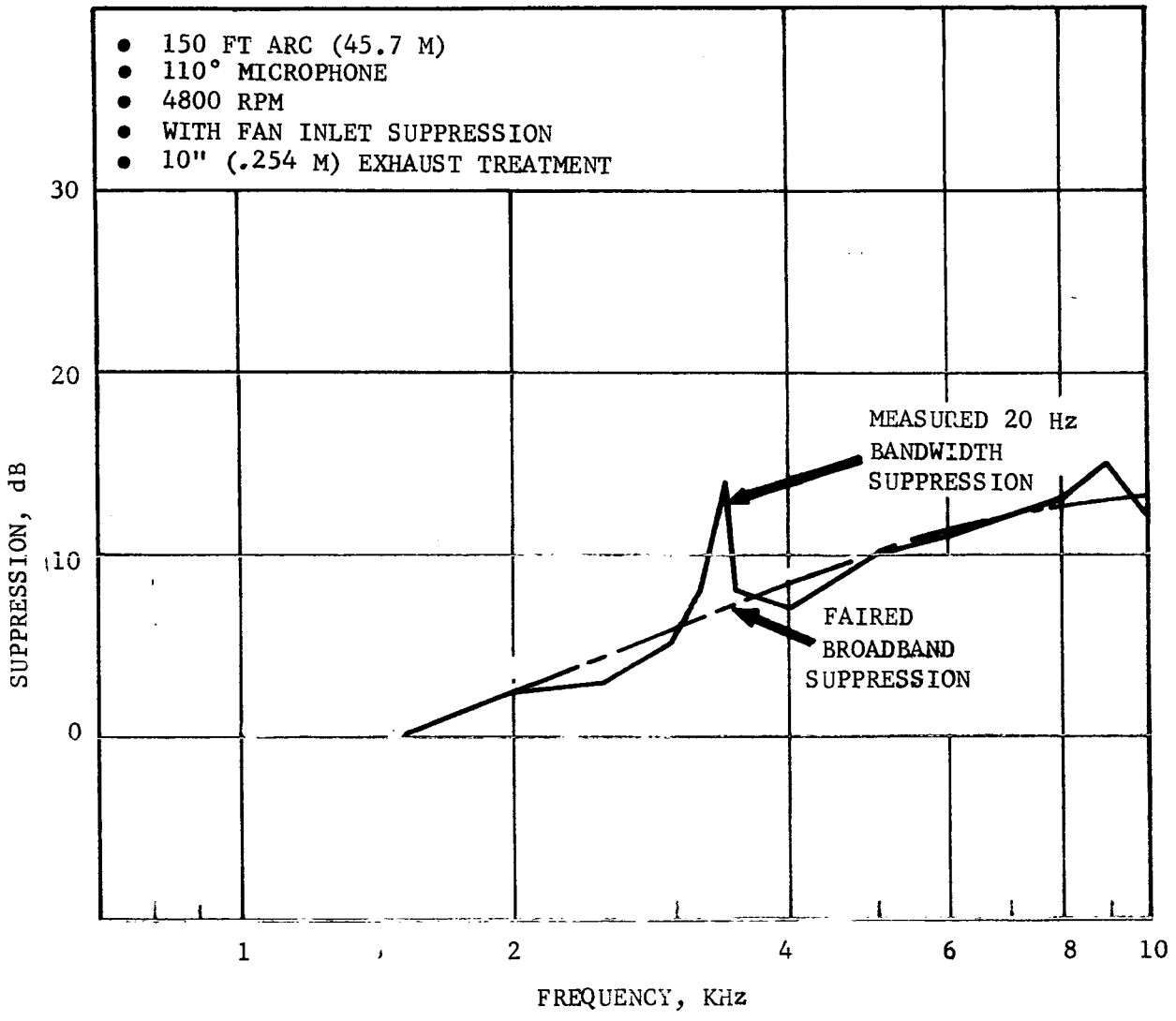

Figure 62. LF336/B Suppression Levels at 4800 RPM at the 110 Degree Microphone with 10 inches (25.4 cm) Exhaust Suppression

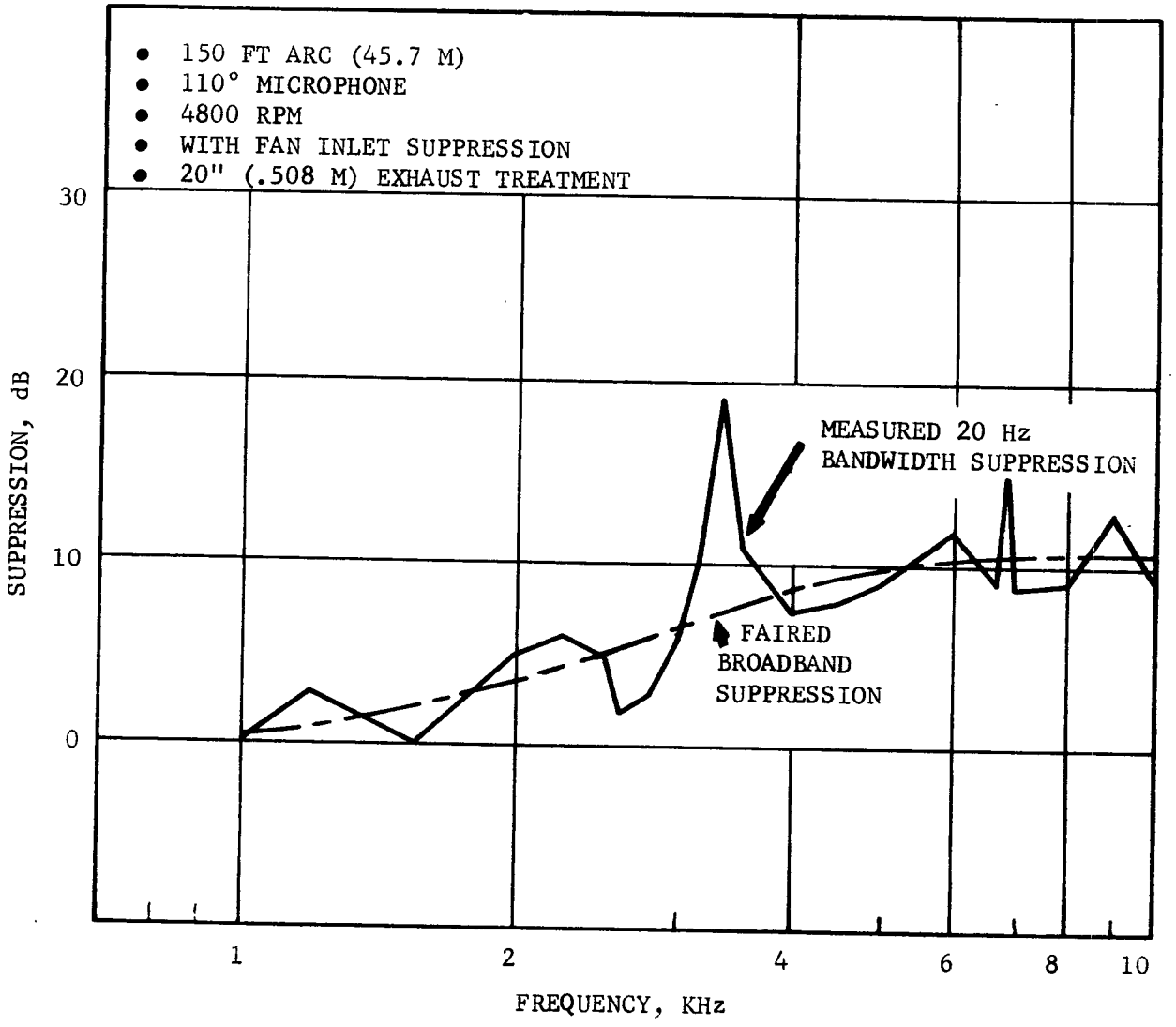

Figure 63. LF336/B Suppression Levels at 4800 RPM at the 110 Degree Microphone with 20 inches (50.8 cm) Exhaust Suppression

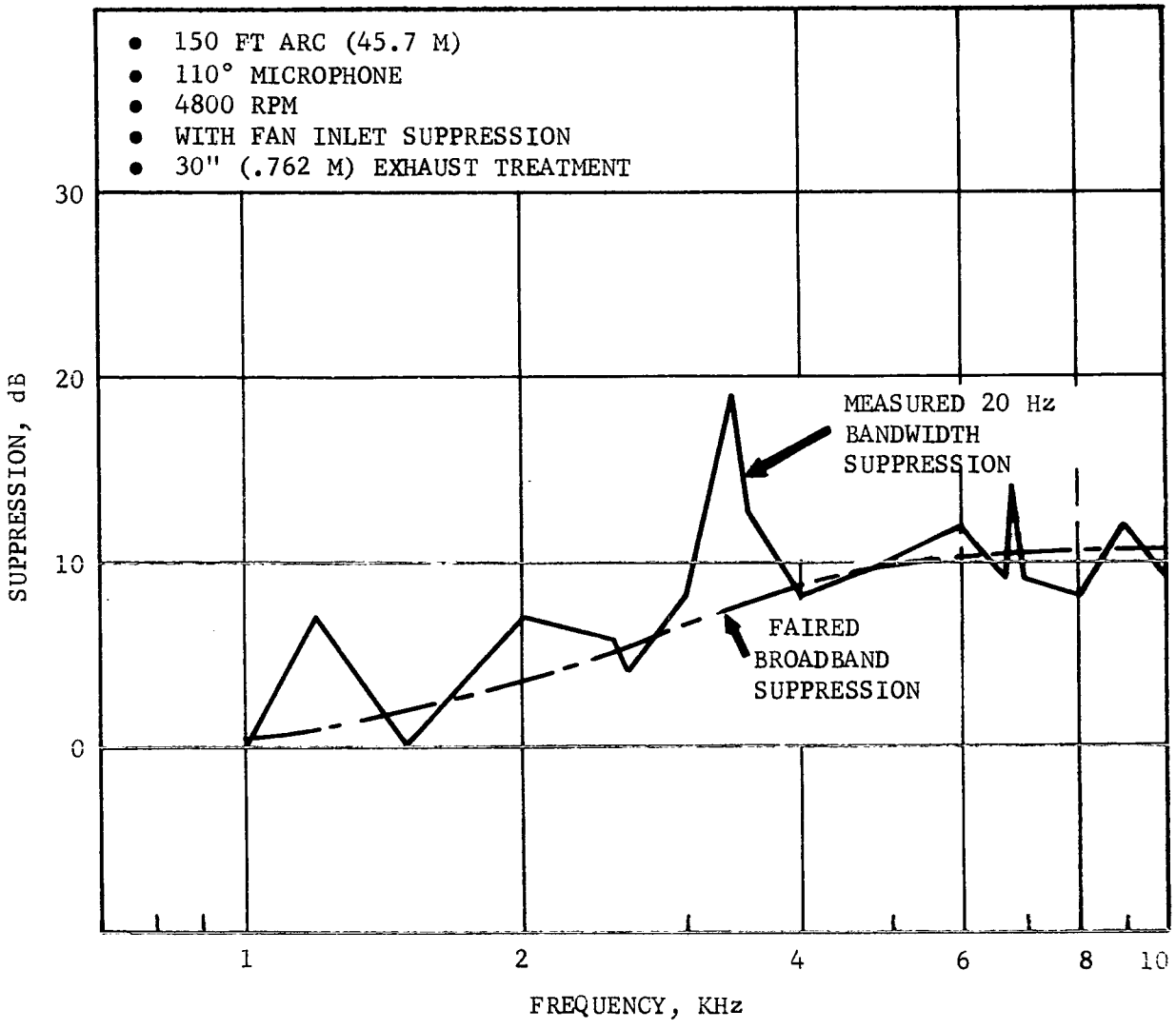

Figure 64. LF336/B Suppression Levels at 4800 RPM at the 110 Degree Microphone with 30 inches (76.2 cm) Exhaust Suppression

- 150 FT. ARC (45.7 M)
- 110° MICROPHONE
- WITH FAN INLET SUPPRESSION

TEST	EXHAUST TREATMENT
3	10" (.254 M)
4	20" (.508 M)
5	30" (.762 M)

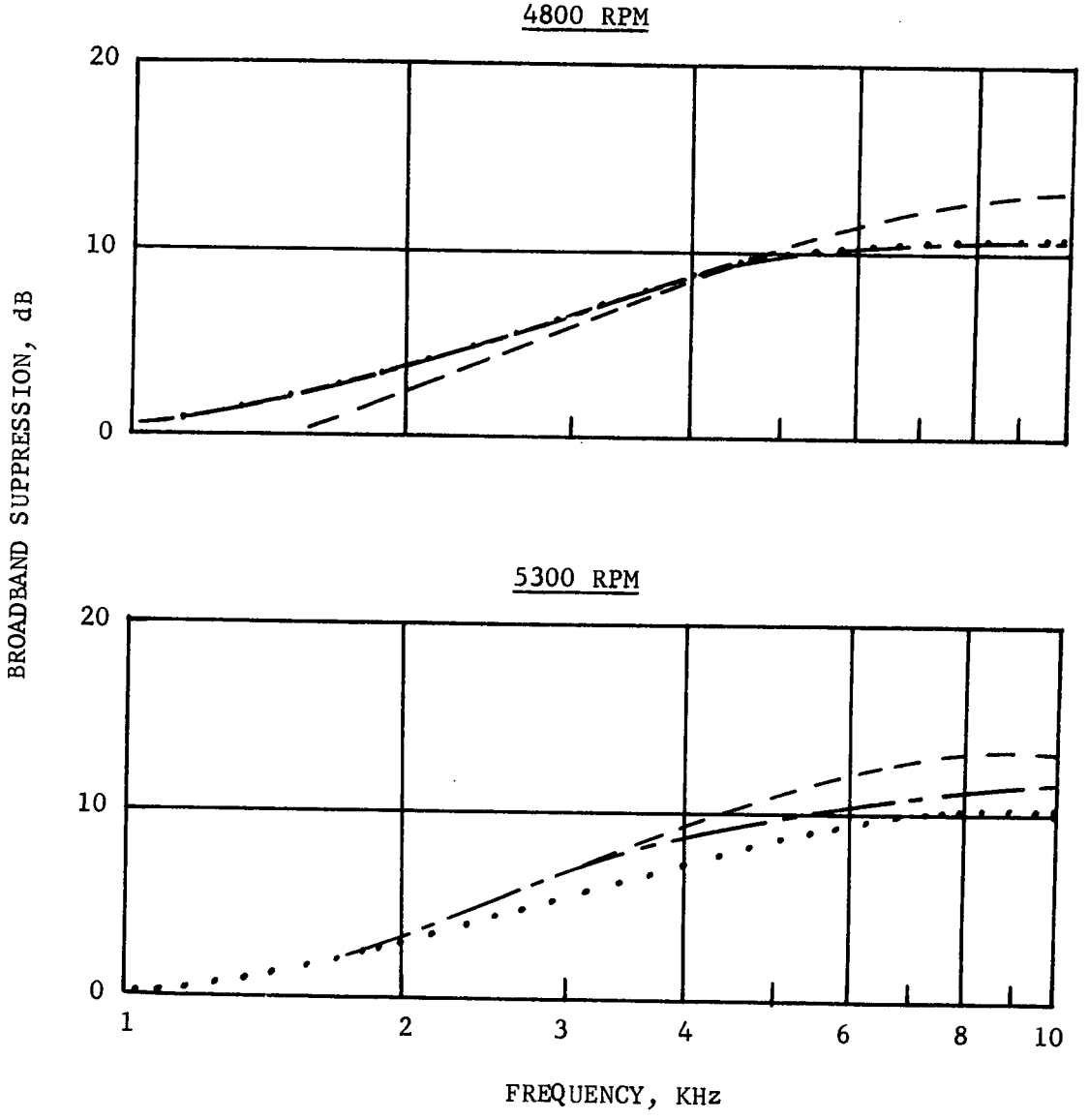

Figure 65. LF336/B Fan Broadband Suppression for Various Configurations

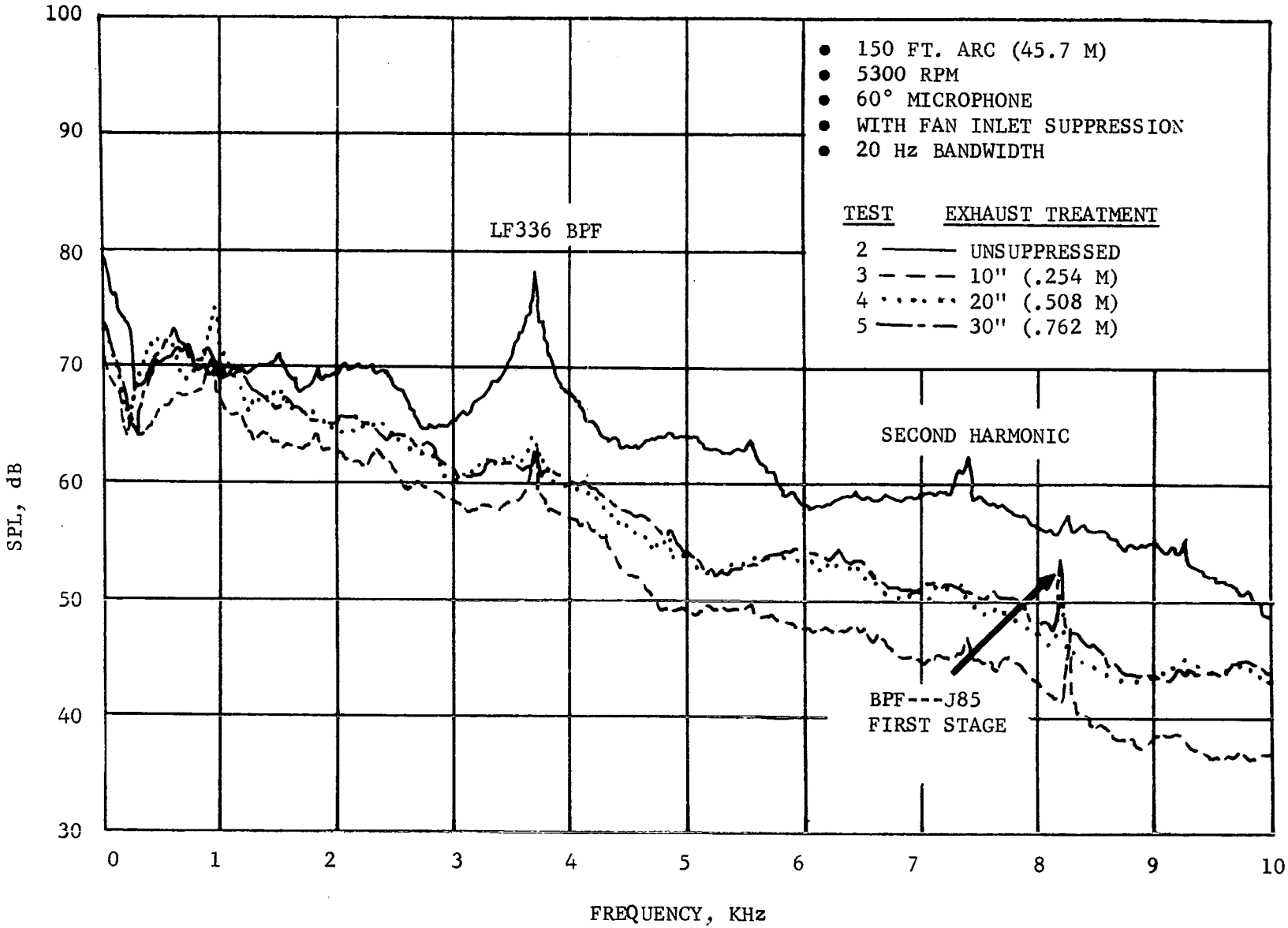

Figure 66. LF336/B Narrow Band Spectrum at 60 Degree Microphone and 5300 RPM

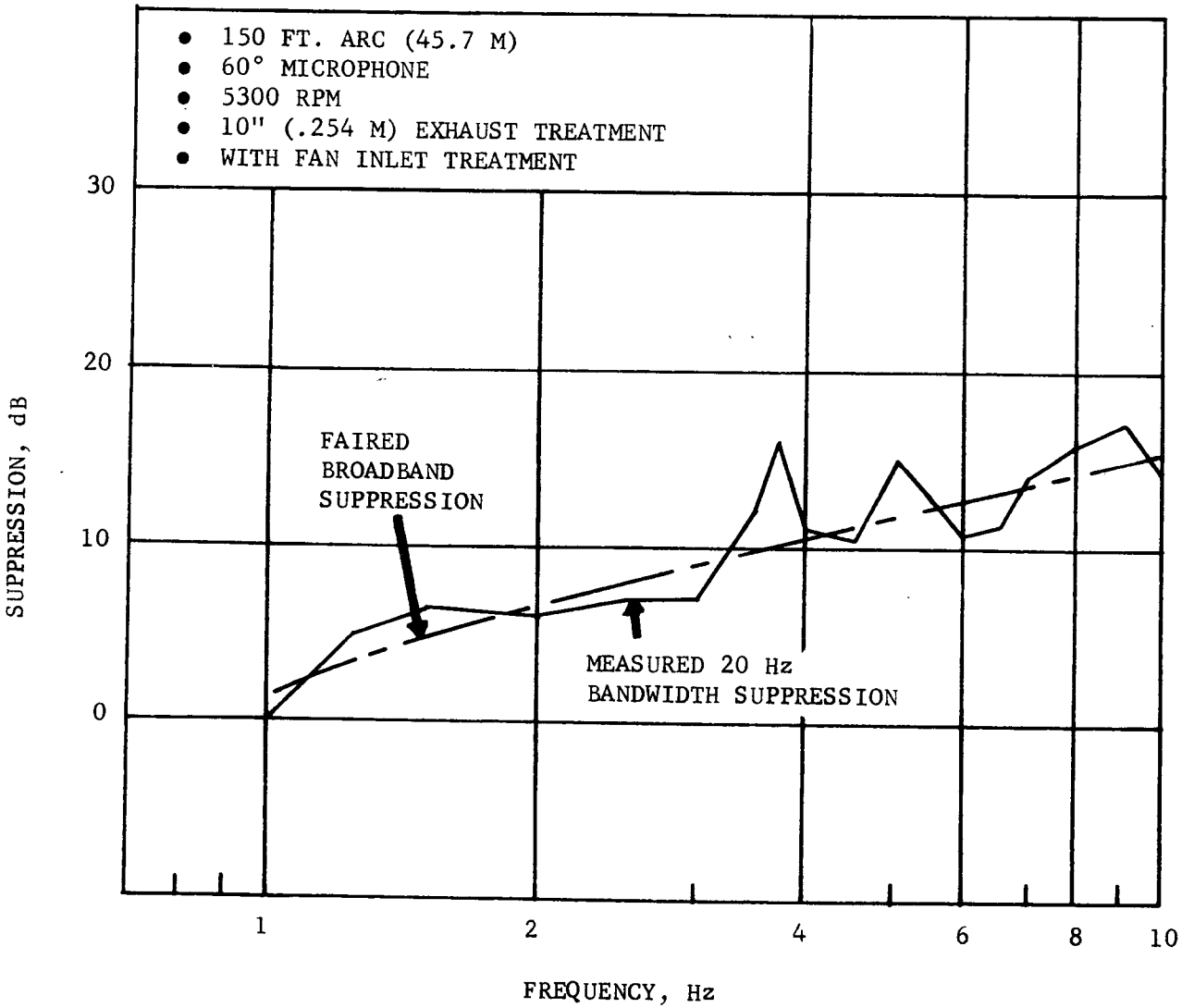

Figure 67. LF336/B Suppression Levels at 5300 RPM at the 60 Degree Microphone with 10 inches (25.4 cm) Exhaust Treatment

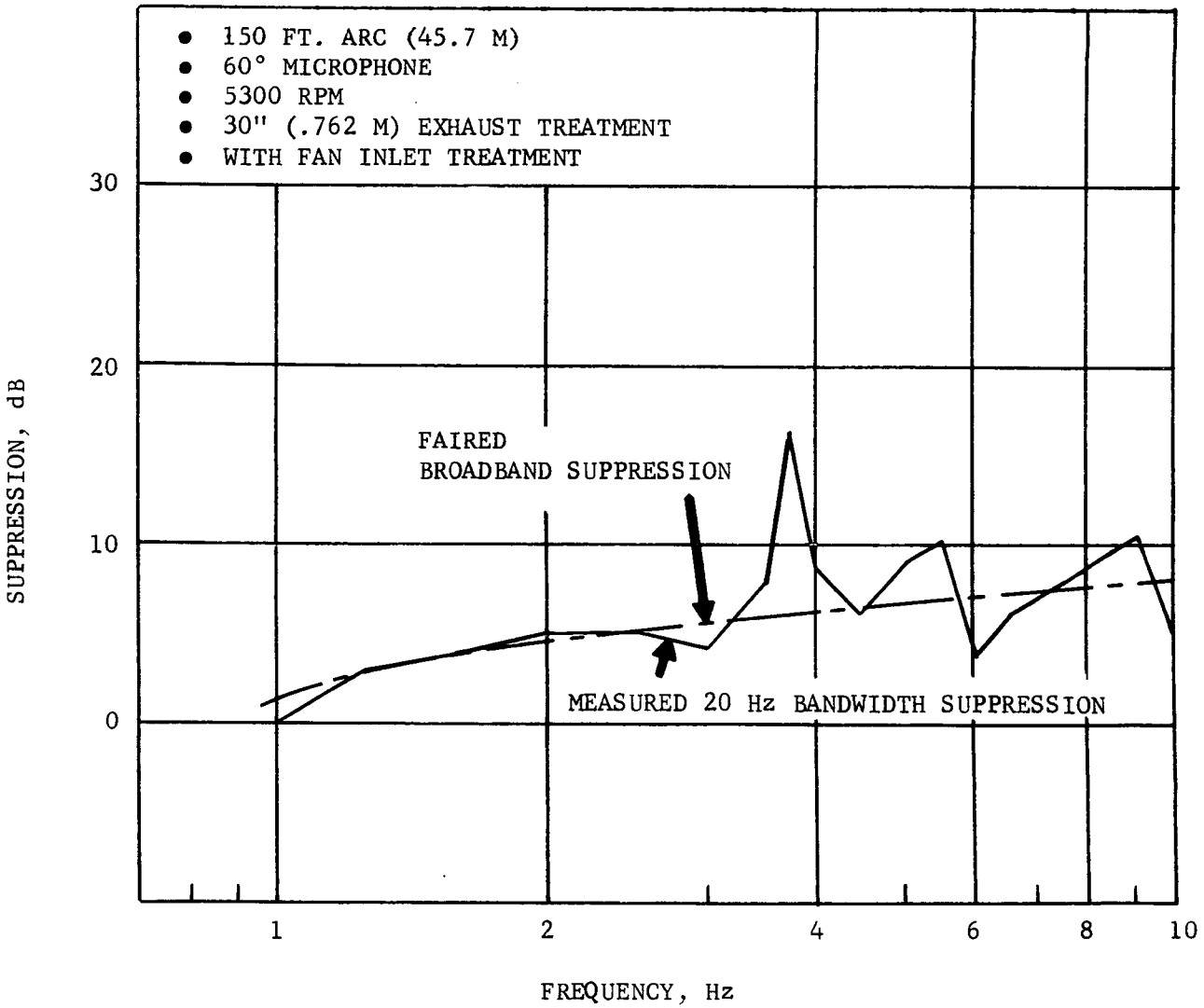

Figure 68. LF336/B Suppression Levels at 5300 RPM at the 60 Degree Microphone with 30 inches (76.2 cm) Exhaust Treatment

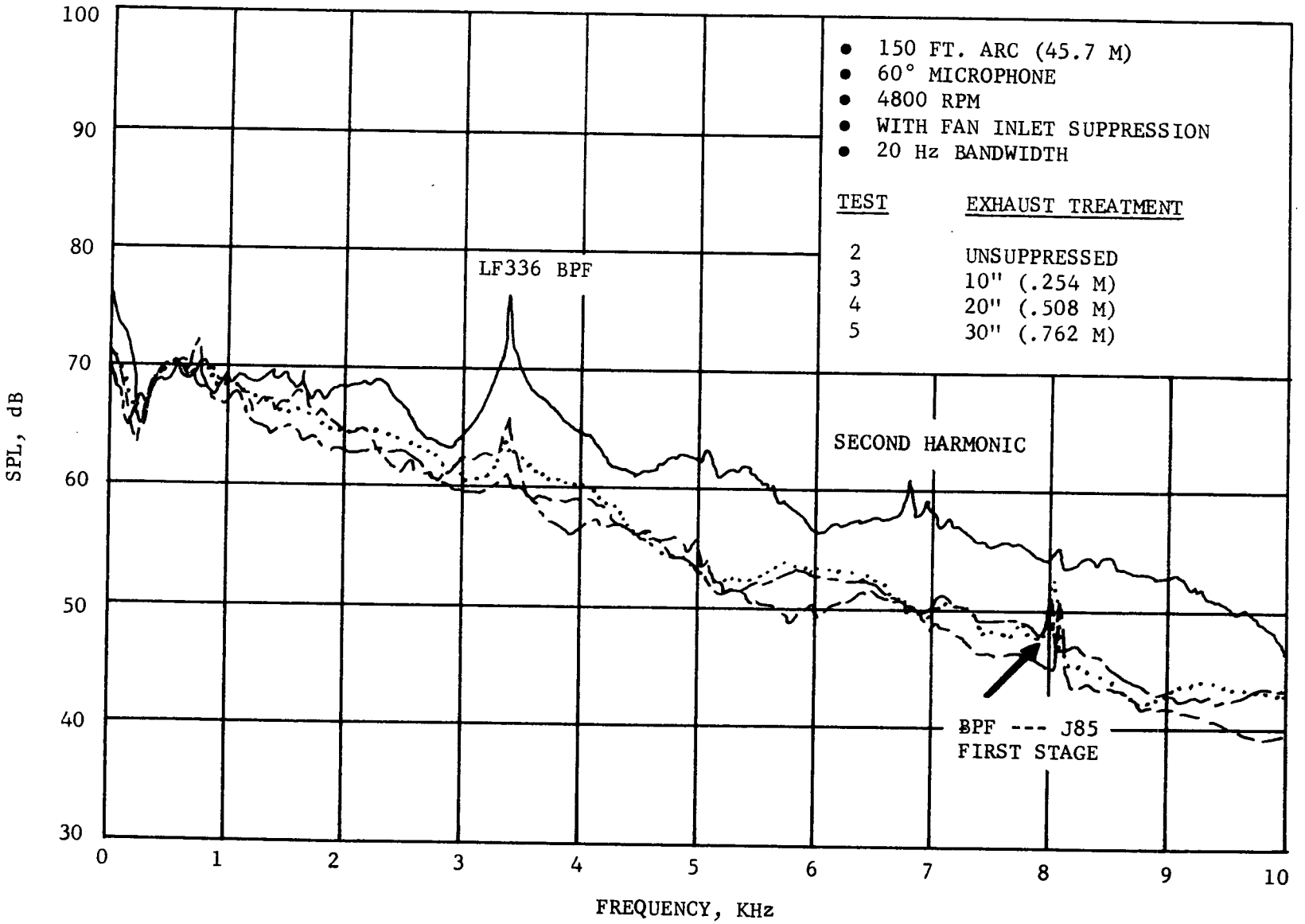

Figure 69. LF336/B Narrow Band Spectrum at 60 Degree Microphone and 4800 RPM

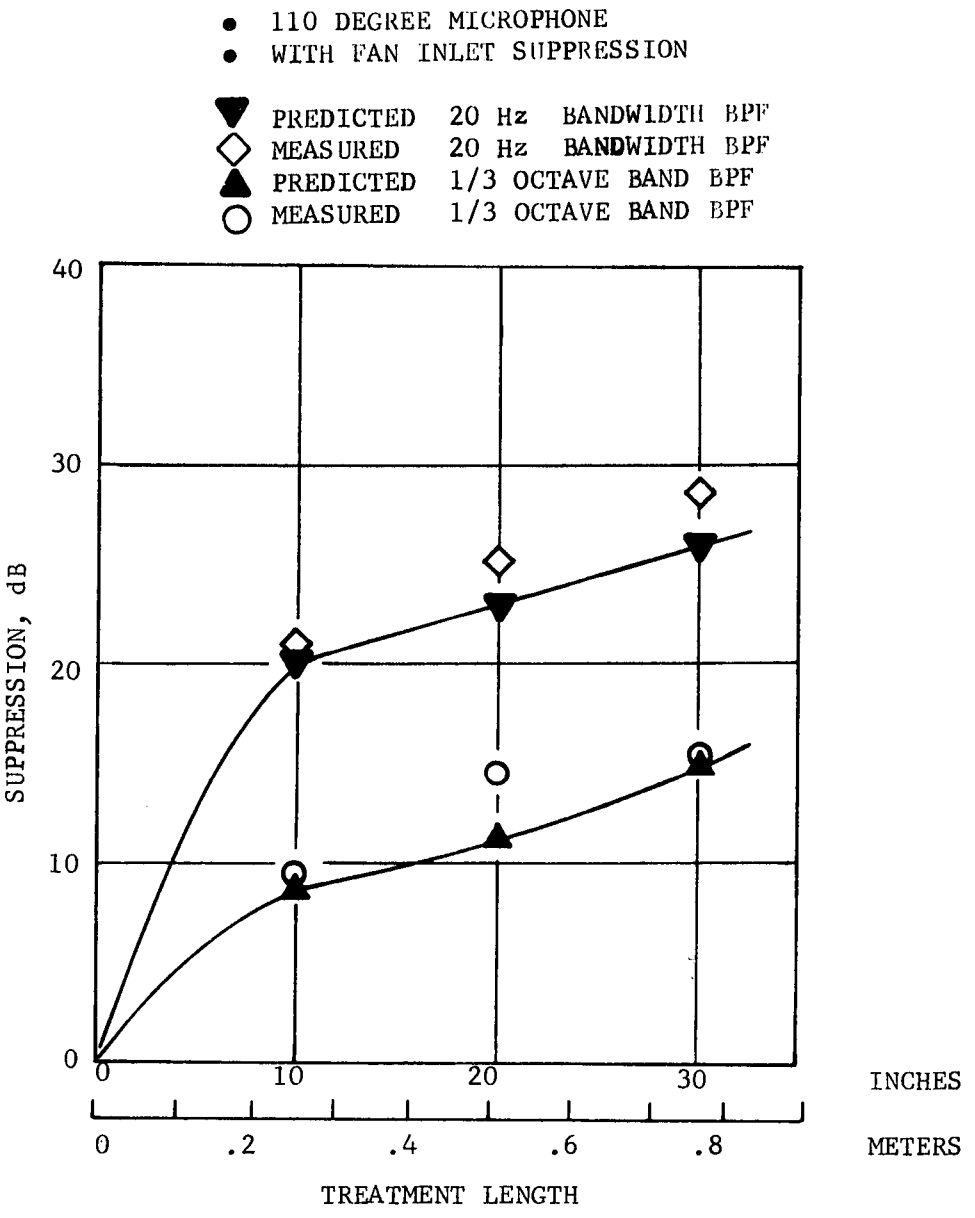

Figure 70. Comparison of Calculated and Measured Suppression Level at 5300 RPM

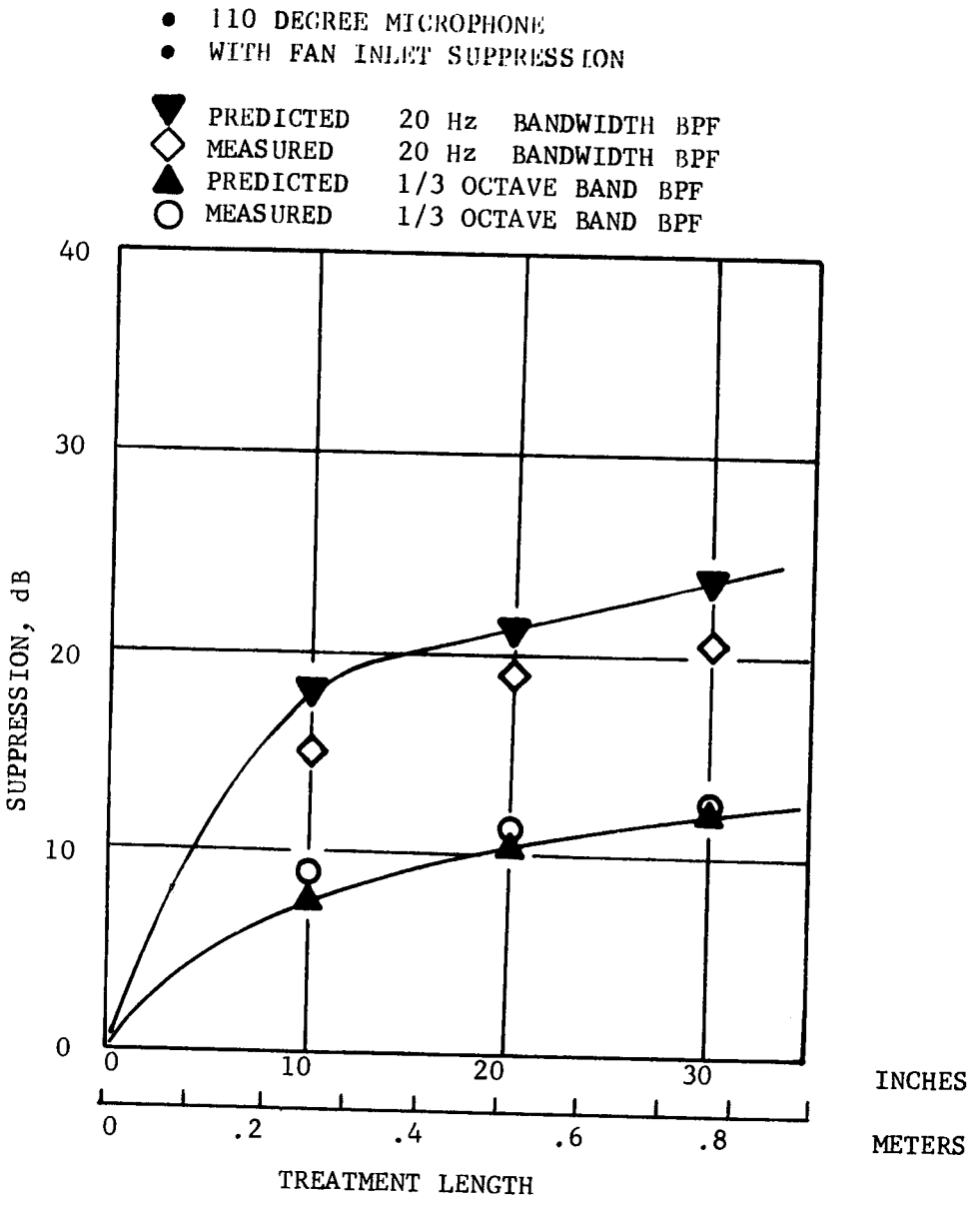

Figure 71. Comparison of Calculated and Measured Suppression Level at 4800 RPM

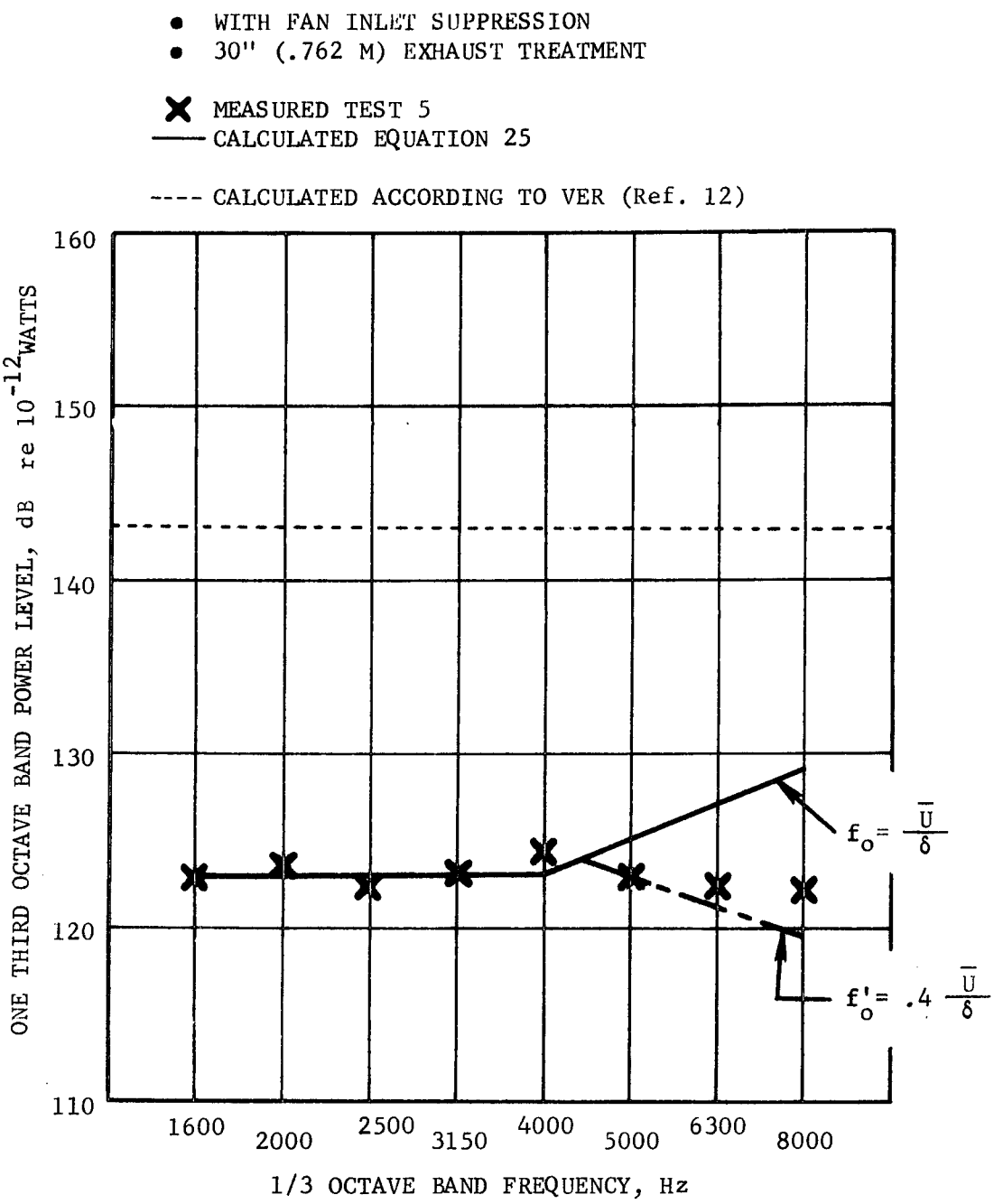

Figure 72. Comparison of Calculated and Measured Power Levels at 4800 RPM

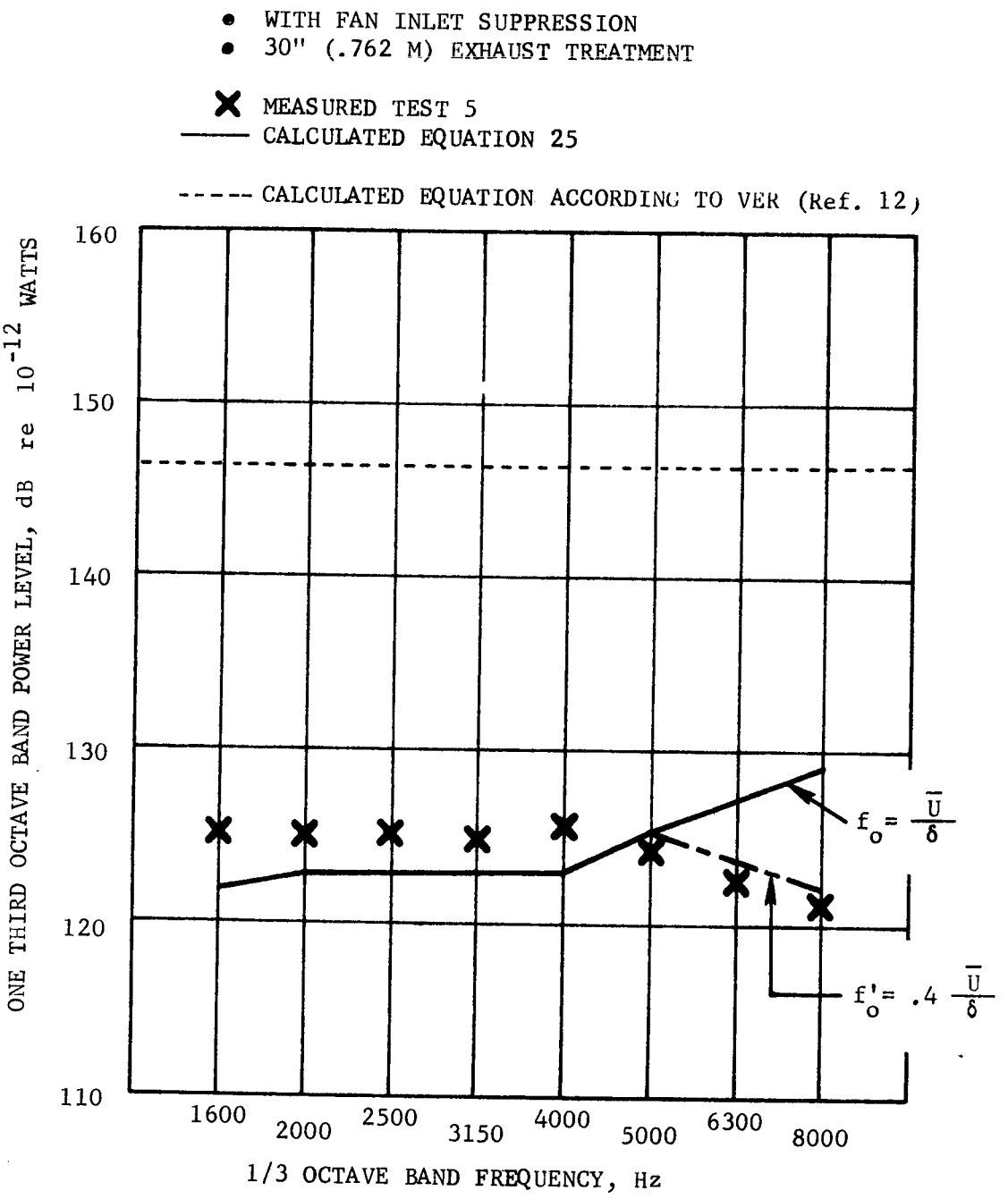

Figure 73. Comparison of Calculated and Measured Power Levels at 5300 RPM

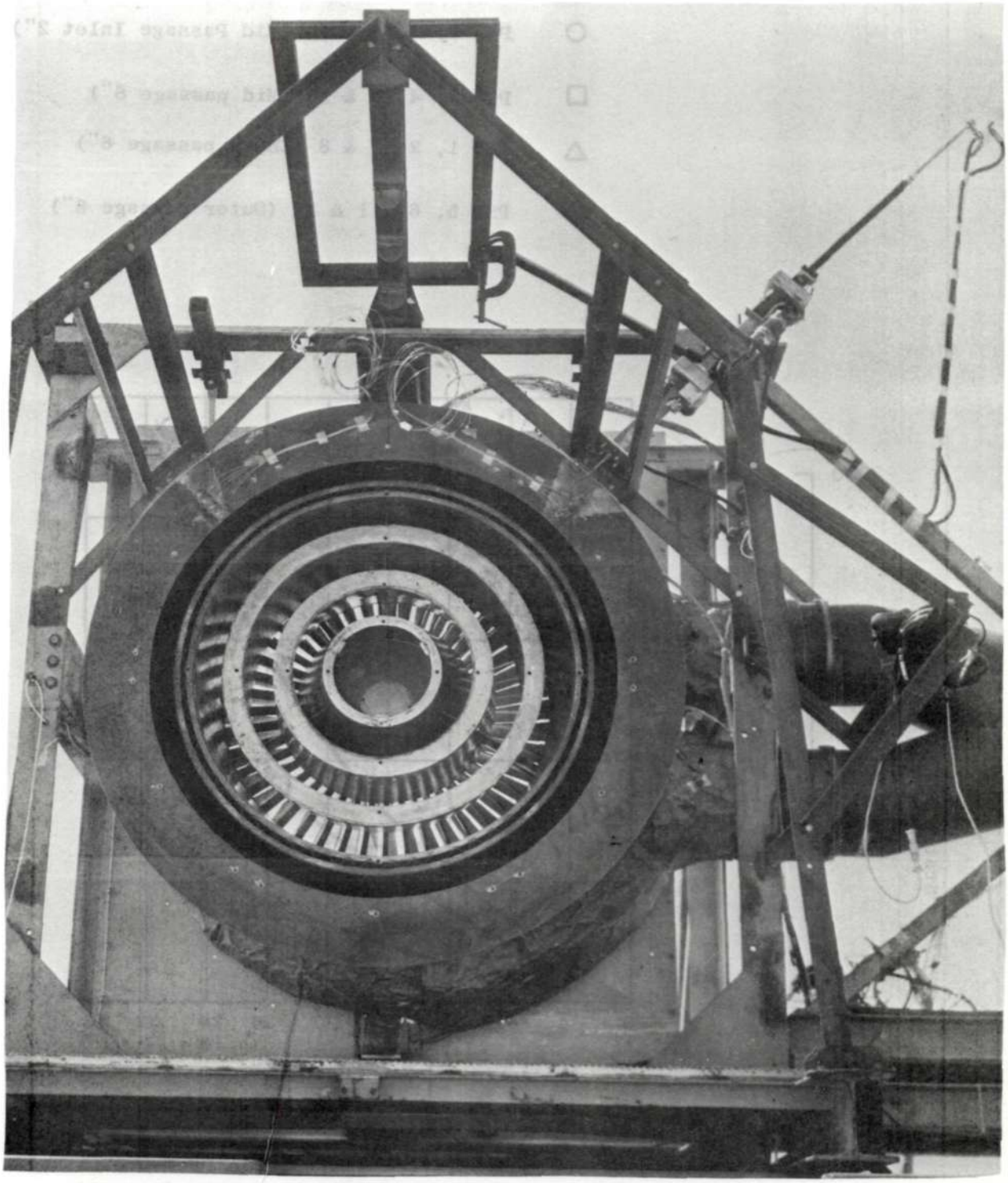

Figure 74. LF336/B Fan Exit with Exhaust Adapter

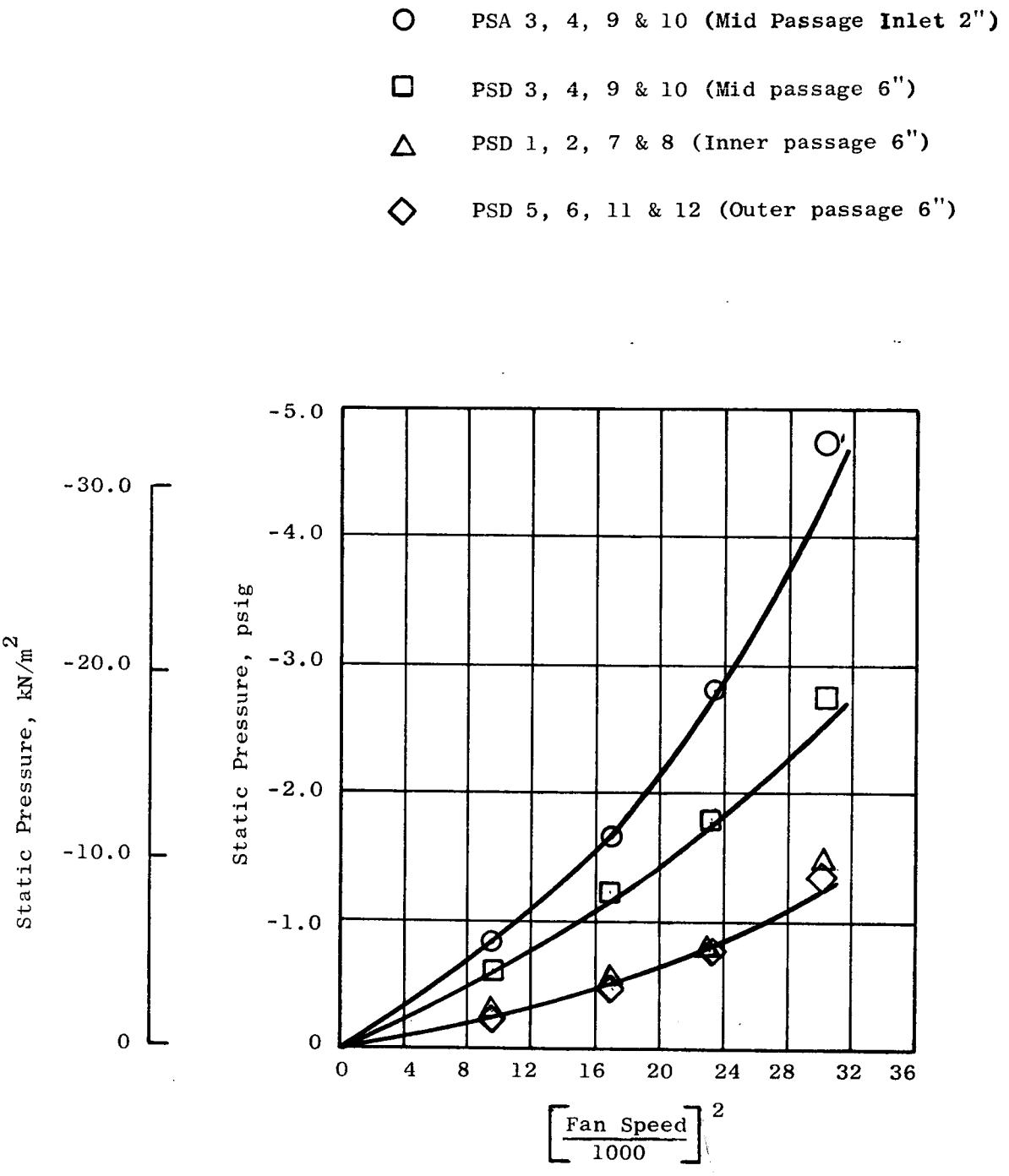

Figure 75. Transition Section Splitter Wall Static Pressure Distribution with the Exhaust Adapter Only (Run #1)

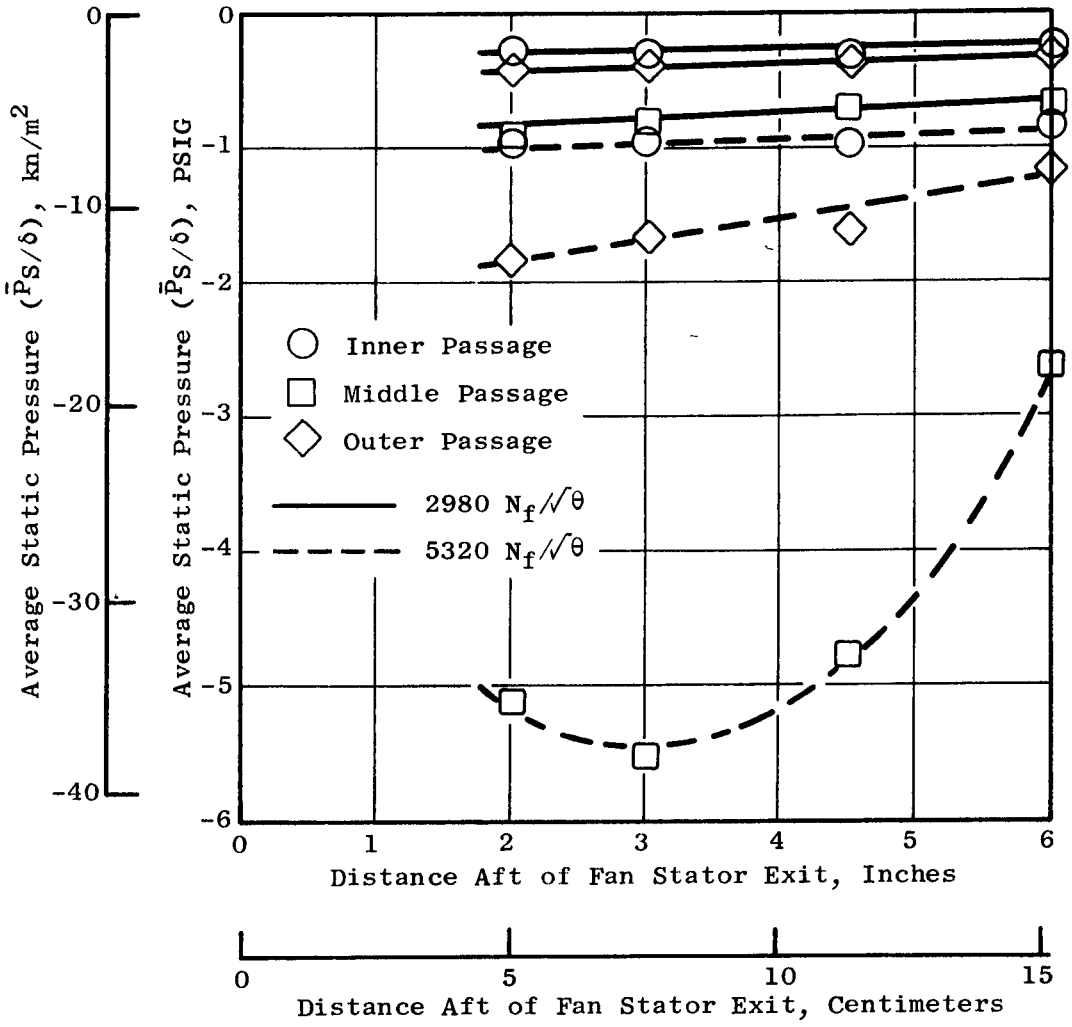

Figure 76. Average Adapter Section Wall Static Pressure Distribution for Adapter Only Configuration

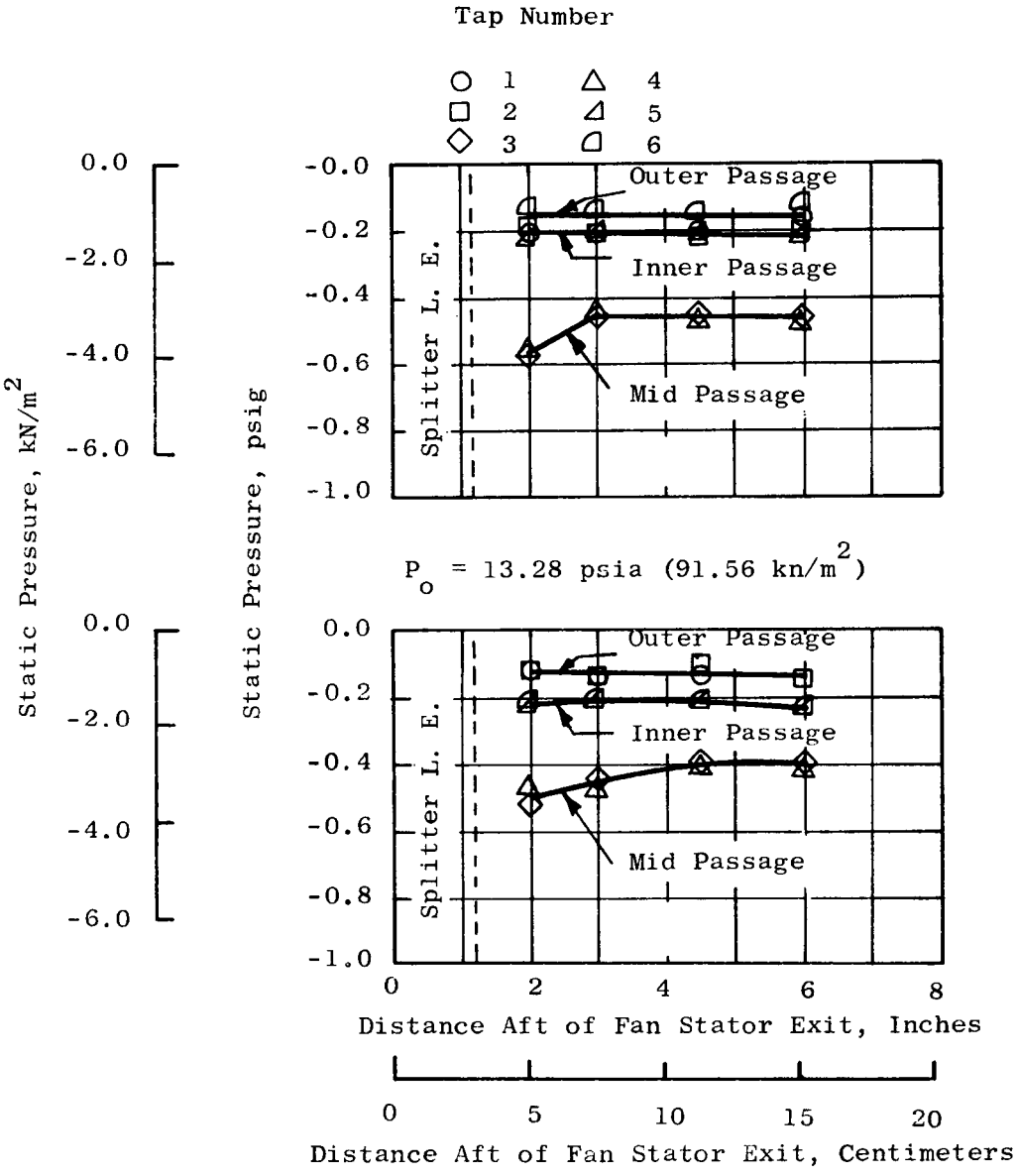

Figure 77. Transition Section Splitter Wall Static Pressure Distribution for Exhaust Adapter + 10" (25.4 cm) of Exhaust Suppression at 2870 Fan Speed

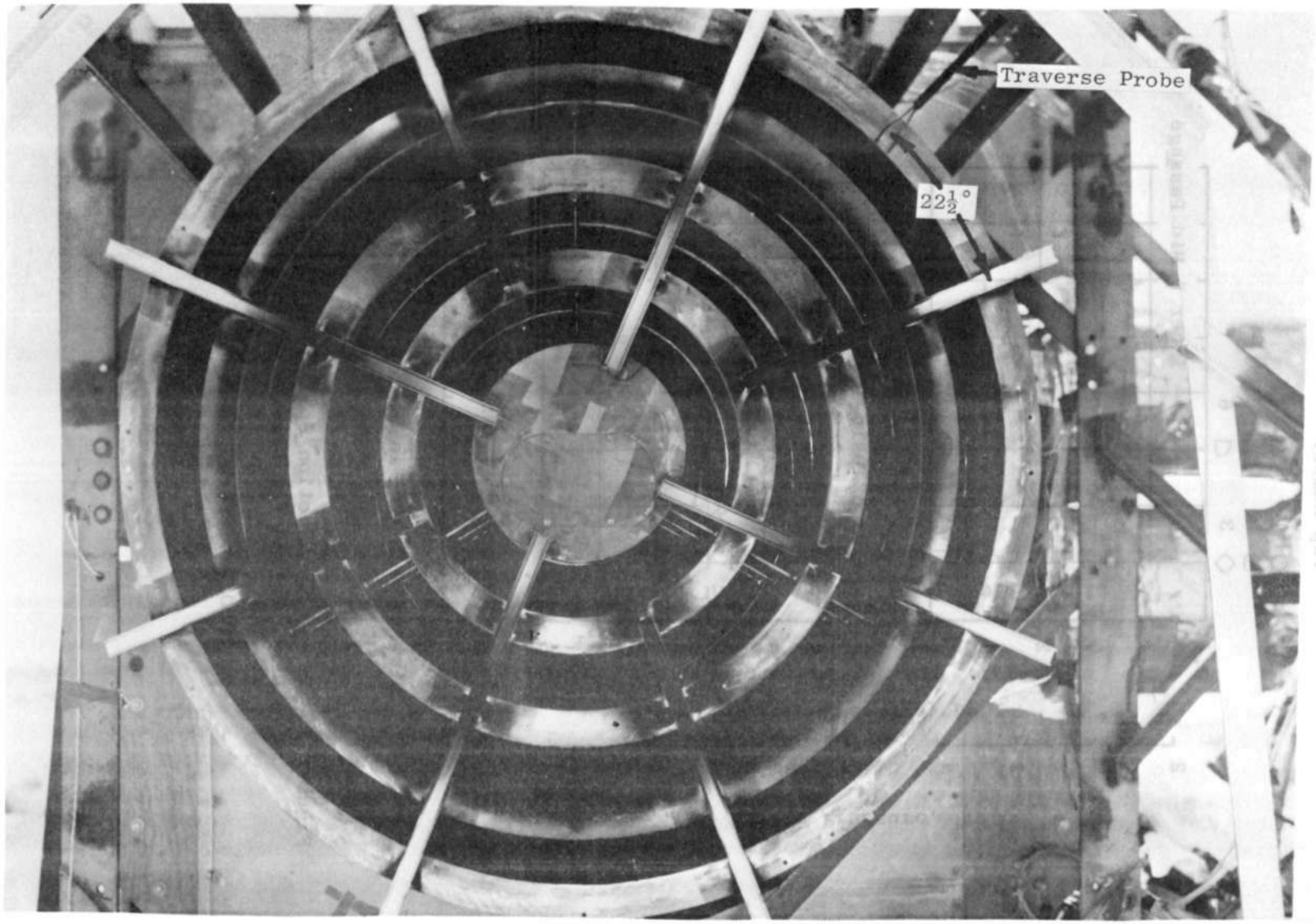

Figure 78. Radial U-Channel Blockage Attached to Fan Discharge

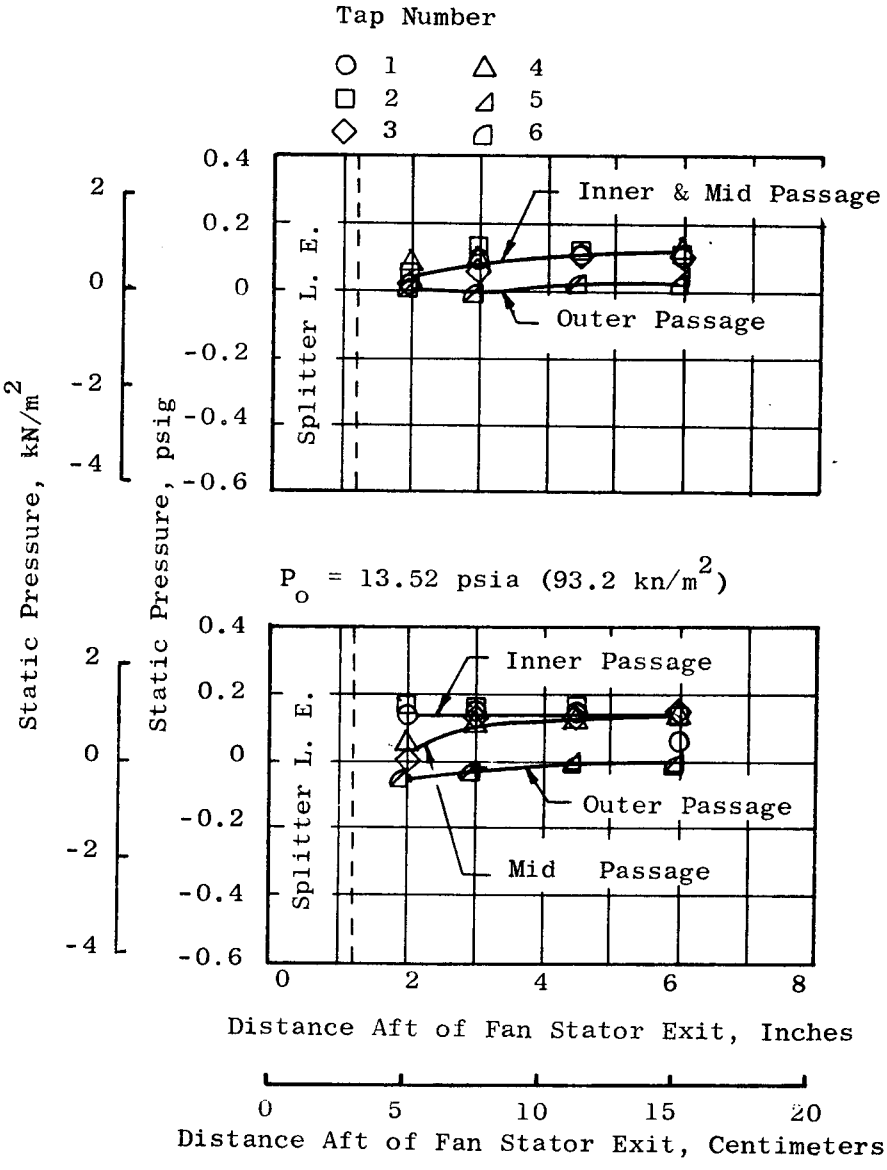

Figure 79. Transition Section Splitter Wall Static Pressure Distribution for Exhaust Adapter + 10" (25.4 cm) of Exhaust Suppression with U-Channeled Blockage at 2980 Fan Speed

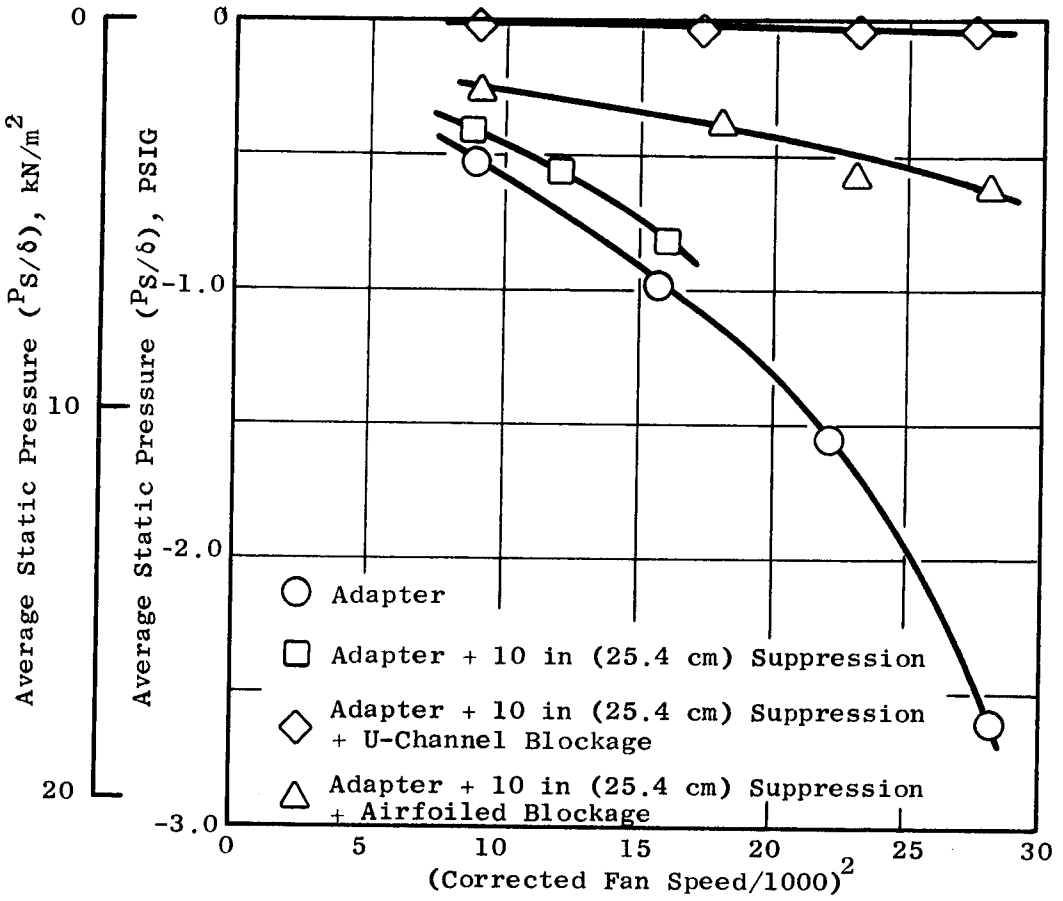

Figure 80. Average Static Pressure Distribution in Plane A of the Exhaust Adapter Section

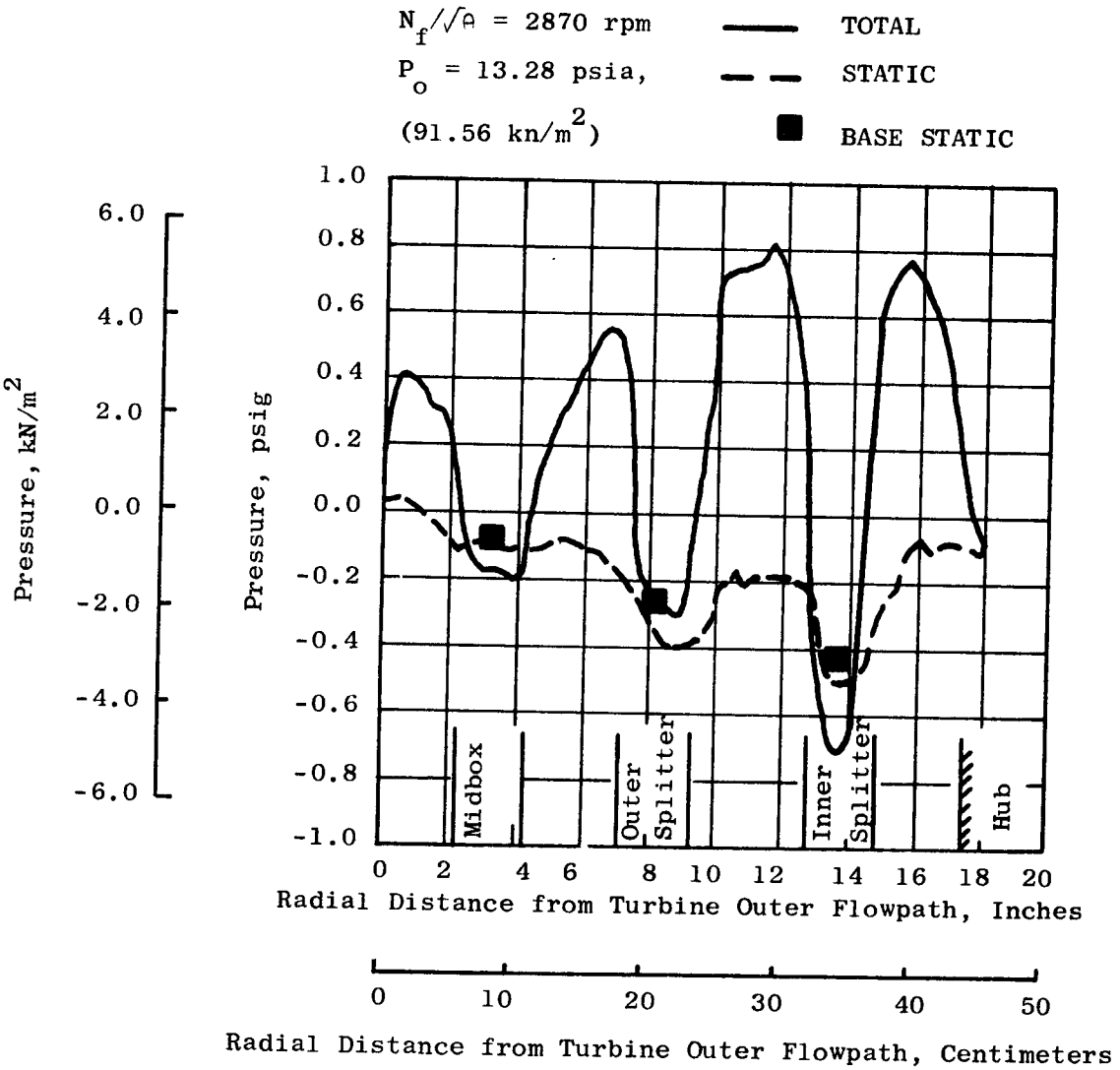

Figure 81. Total and Static Pressure Profile for Exhaust Adapter + 10" (25.4 cm) of Exhaust Suppression

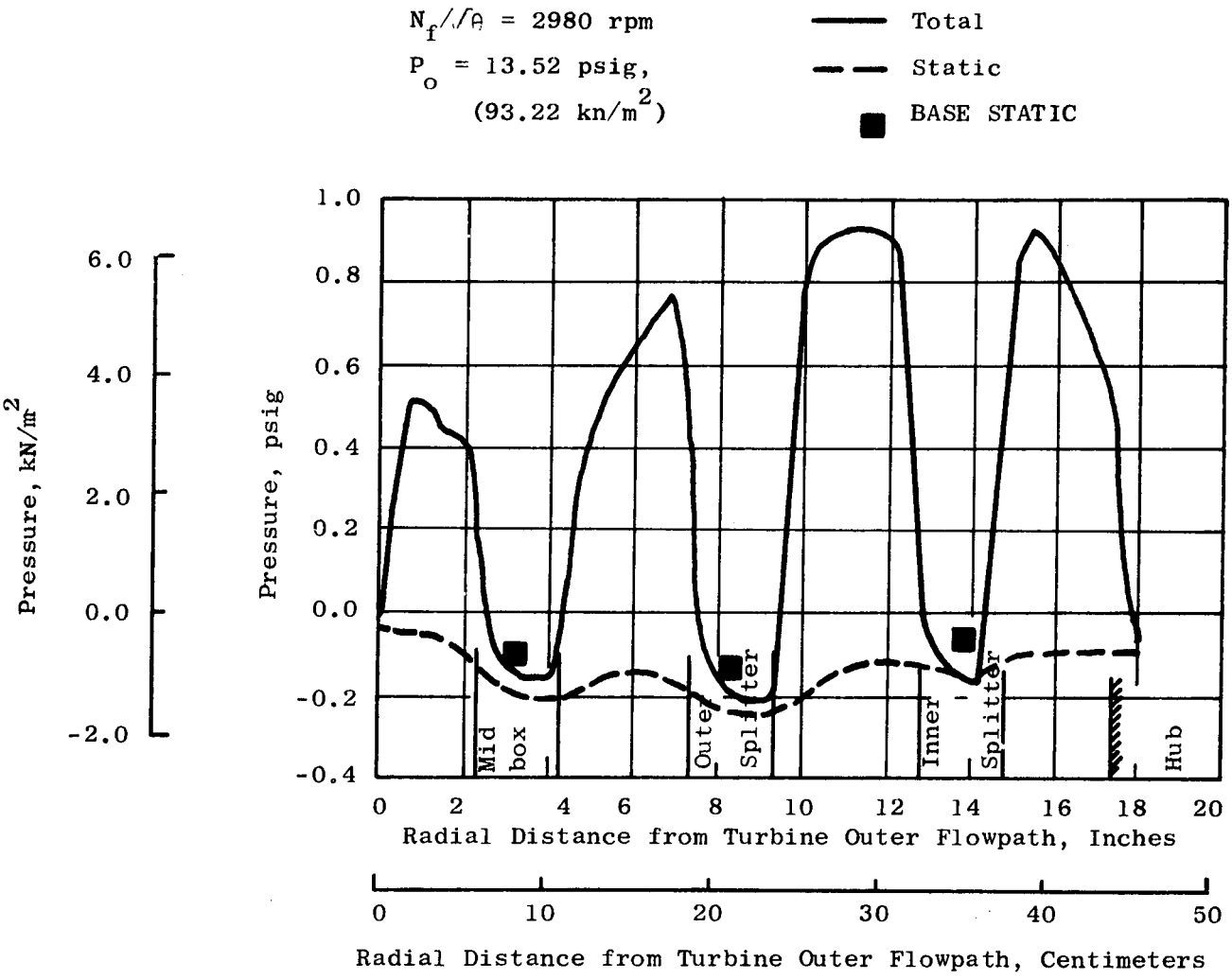

Figure 82. Total and Static Pressure Profile for Exhaust Adapter + 10" (25.4 cm) of Exhaust Suppression with U-Channeled Blockage

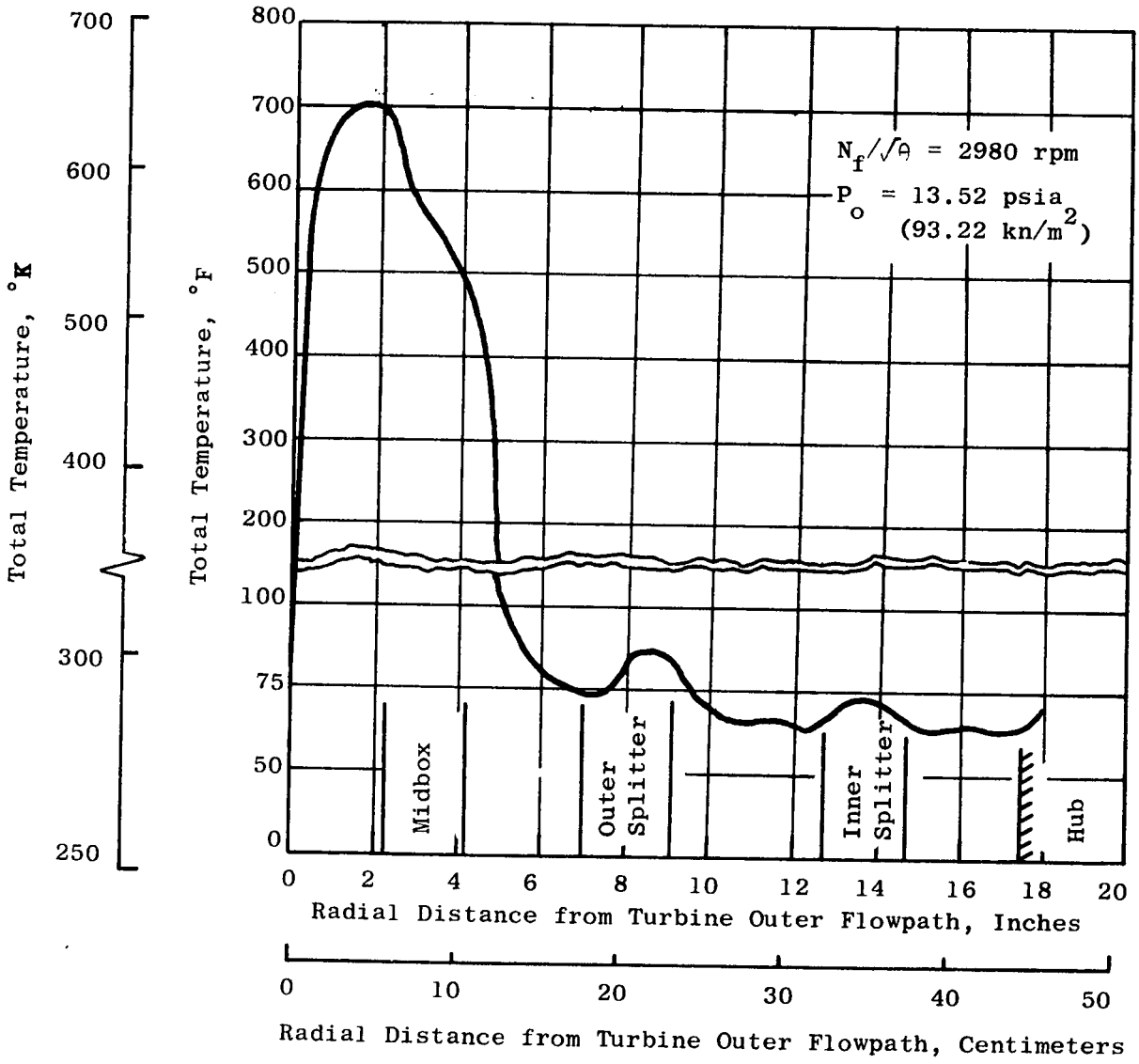

Figure 83. Total Temperature Profile with Added U-Channel Blockage

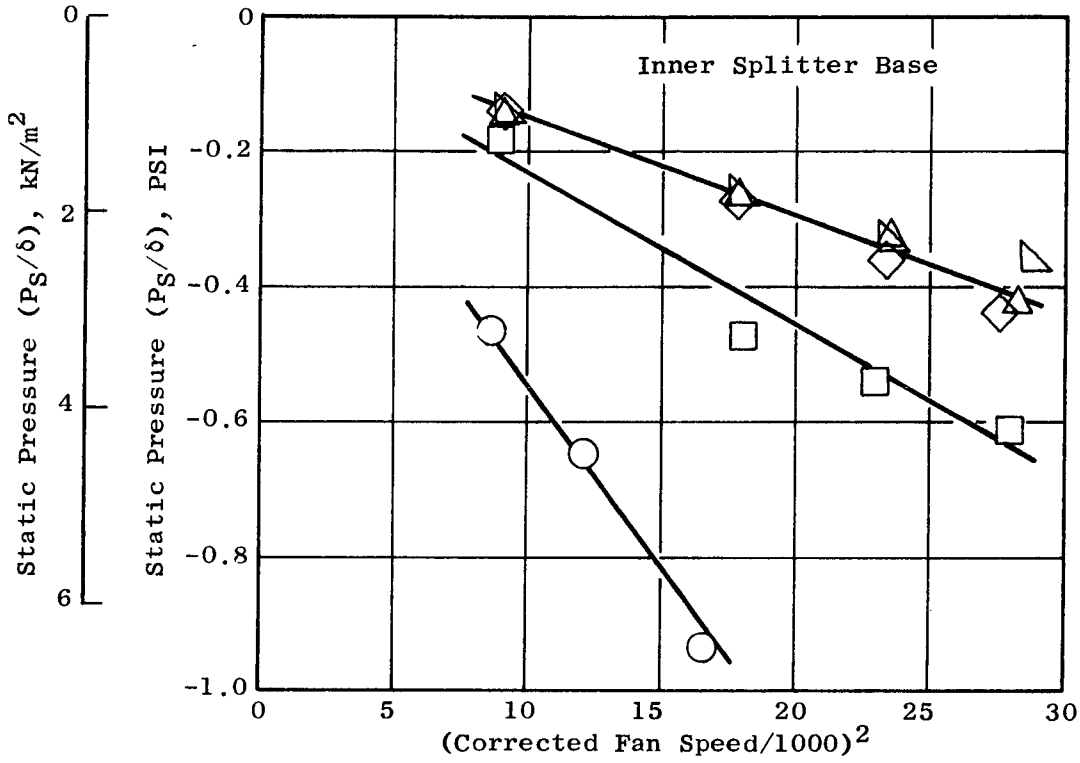

Figure 84. Inner Splitter Base Static Pressure Distribution

○ Adapter + 10" (25.4 cm) Sup

□ Adapter + 10" (25.4 cm) Sup + Airfoiled Blockage

◇ Adapter + 10" (25.4 cm) Sup + U-Channeled Blockage

△ Adapter + 20" (50.8 cm) Sup + U-Channeled Blockage

◺ Adapter + 30" (76.2 cm) Sup + U-Channeled Blockage

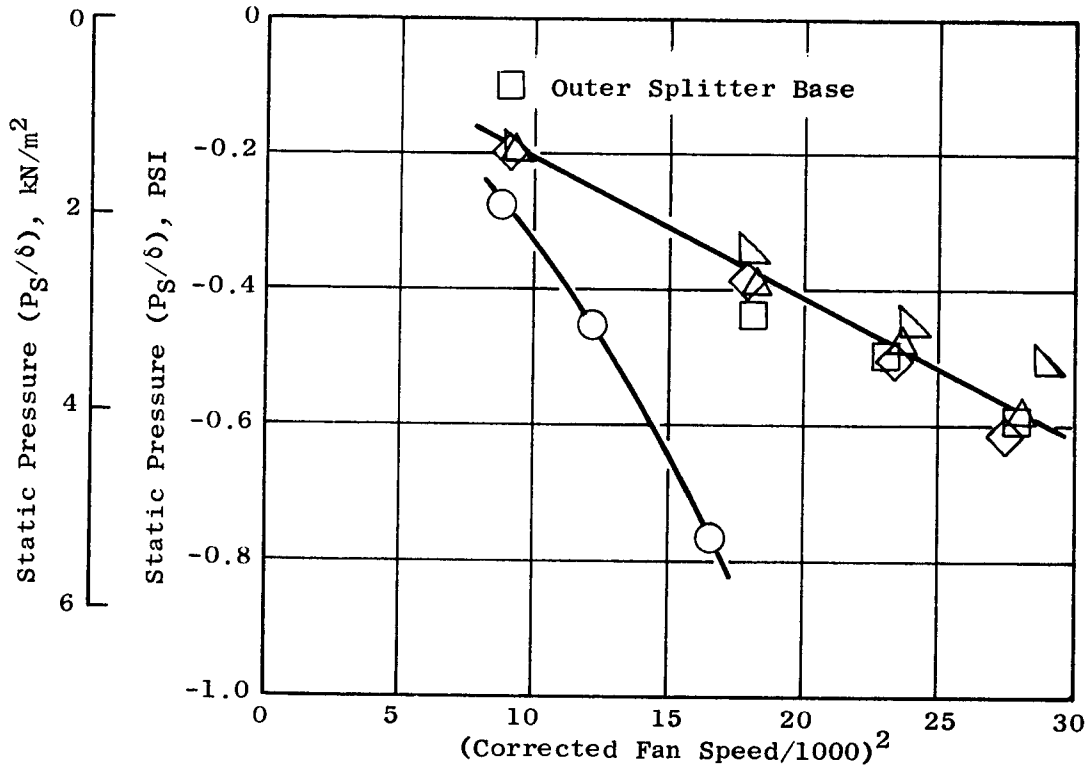

Figure 85. Outer Splitter Base Static Pressure Distribution

○ Adapter + 10" (25.4 cm) Sup

□ Adapter + 10" (25.4 cm) Sup + Airfoiled Blockage

◇ Adapter + 10" (25.4 cm) Sup + U-Channeled Blockage

△ Adapter + 20" (50.8 cm) Sup + U-Channeled Blockage

◺ Adapter + 30" (76.2 cm) Sup + U-Channeled Blockage

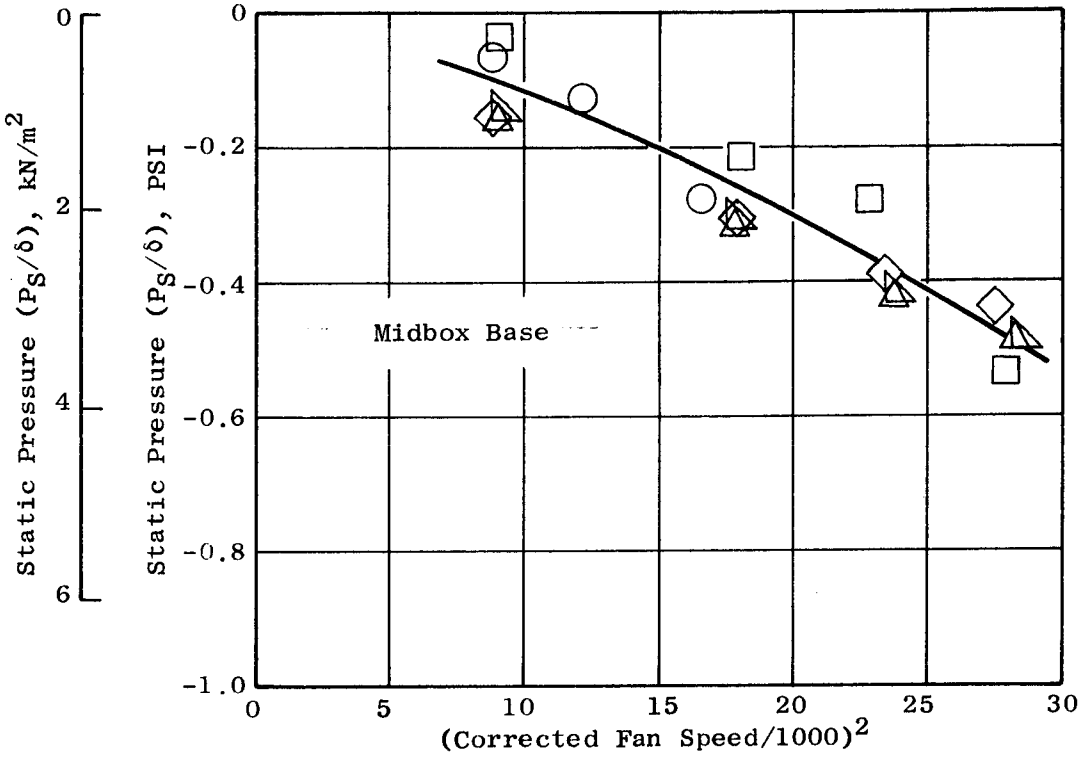

Figure 86. Midbox Base Static Pressure Distribution

○ Adapter + 10" (25.4 cm) Sup

□ Adapter + 10" (25.4 cm) Sup + Airfoiled Blockage

◇ Adapter + 10" (25.4 cm) Sup + U-Channeled Blockage

△ Adapter + 20" (50.8 cm) Sup + U-Channeled Blockage

◺ Adapter + 30" (76.2 cm) Sup + U-Channeled Blockage

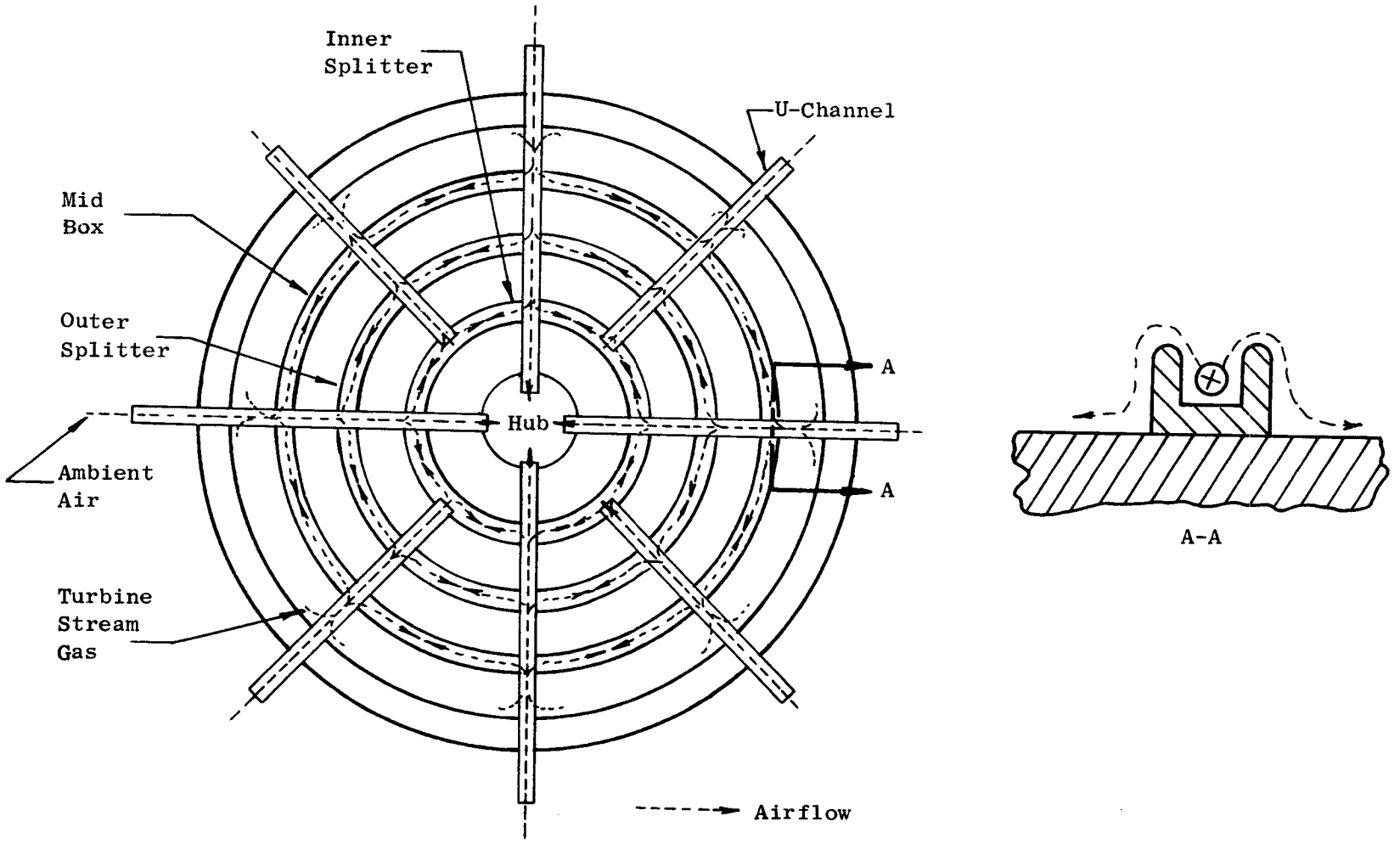

Figure 87. Base Venting Process Schematic

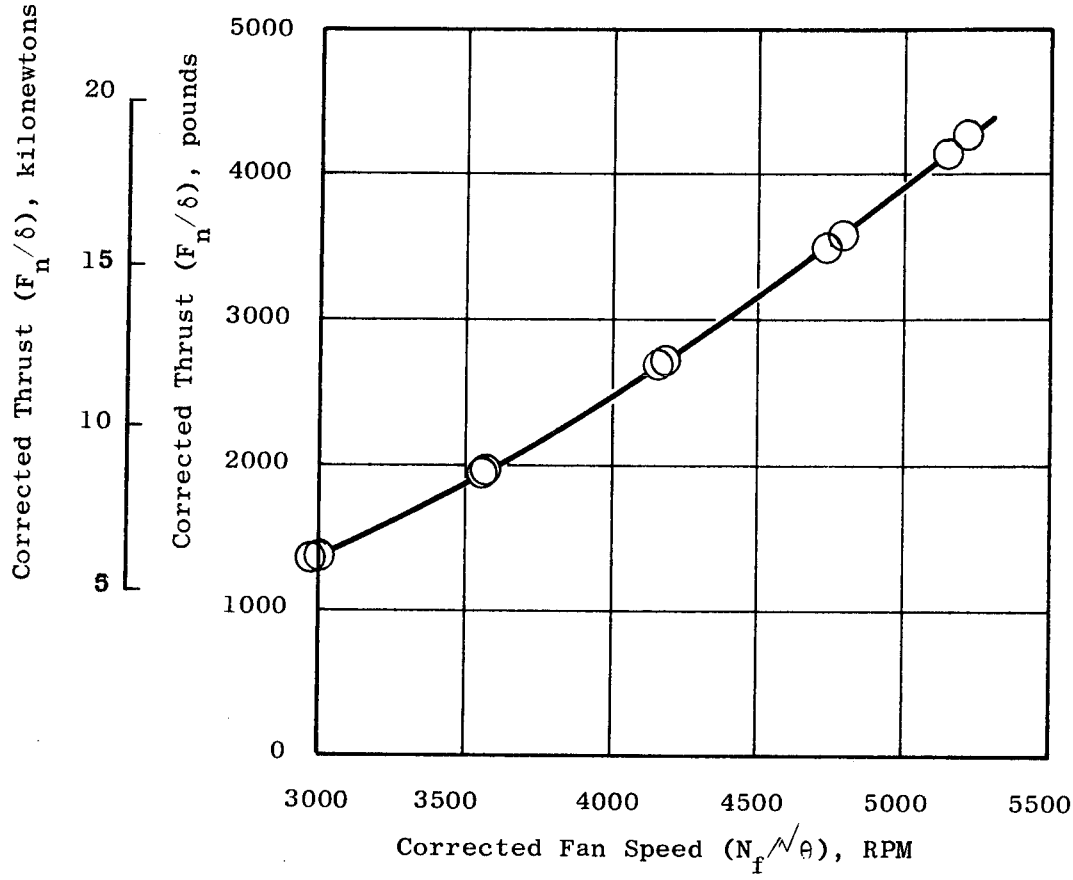

Figure 88. Thrust Variation with Fan Speed for Test 1, No Inlet or Exhaust Suppression

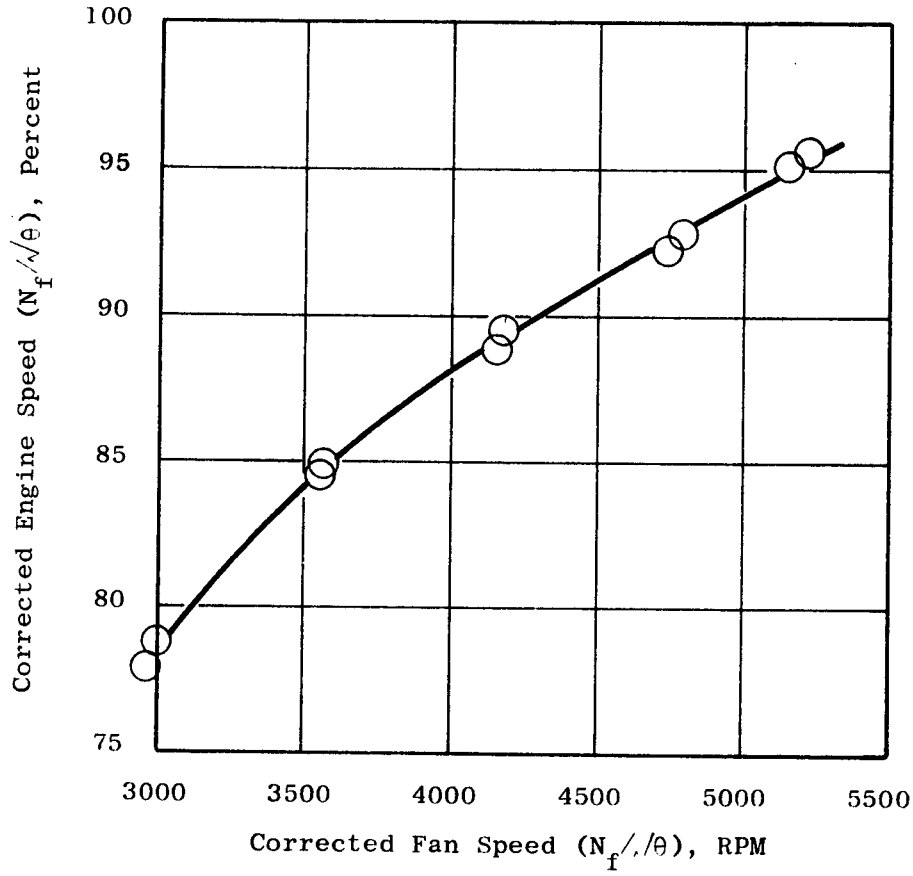

Figure 89. Engine Speed Variation with Fan Speed for Test 1, No Inlet or Exhaust Suppression

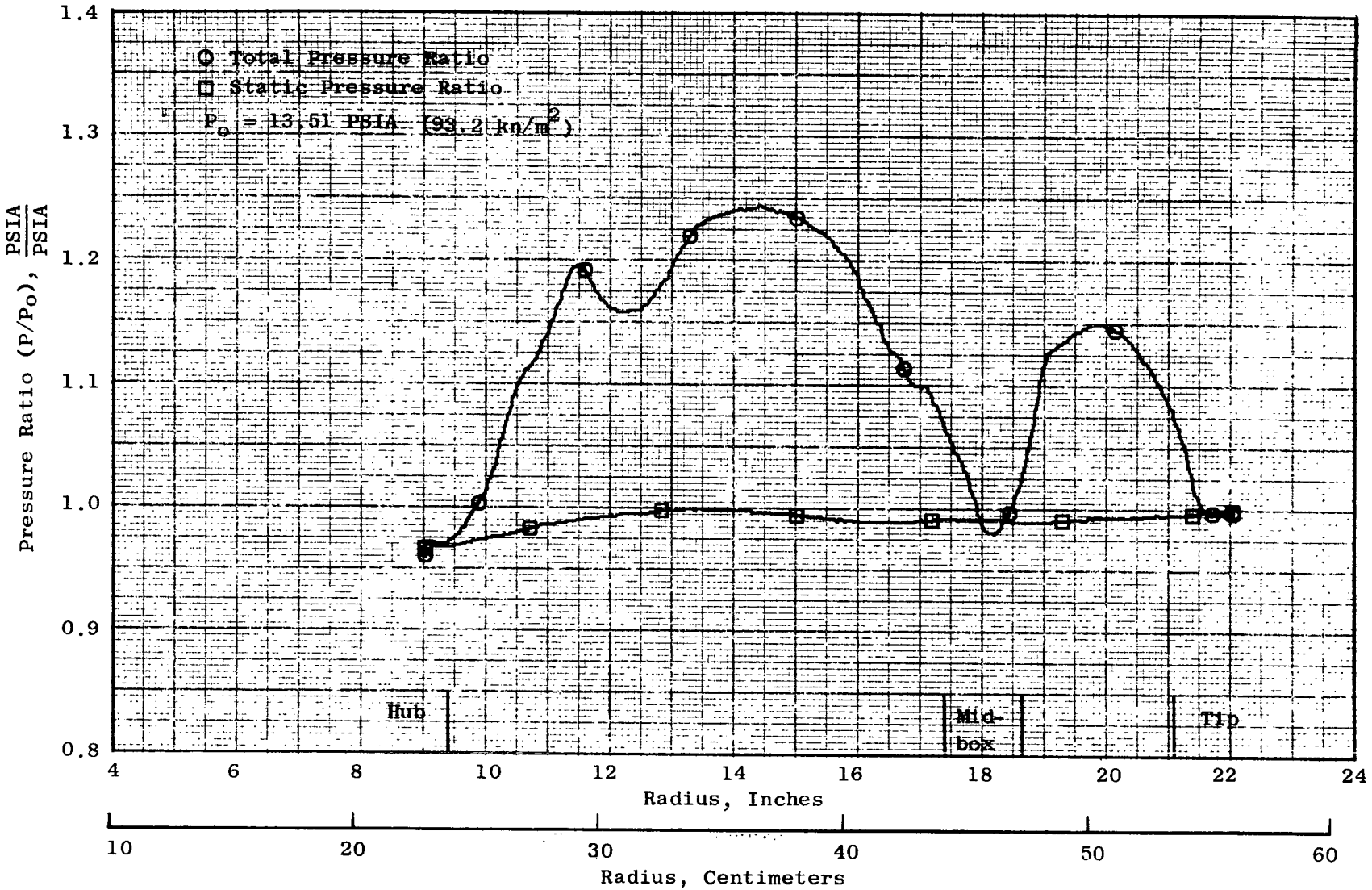

Figure 90. Exhaust Total and Static Pressure Profile for Test 1, No Inlet or Exhaust Suppression, $N_f/\sqrt{\theta}$ = 5180

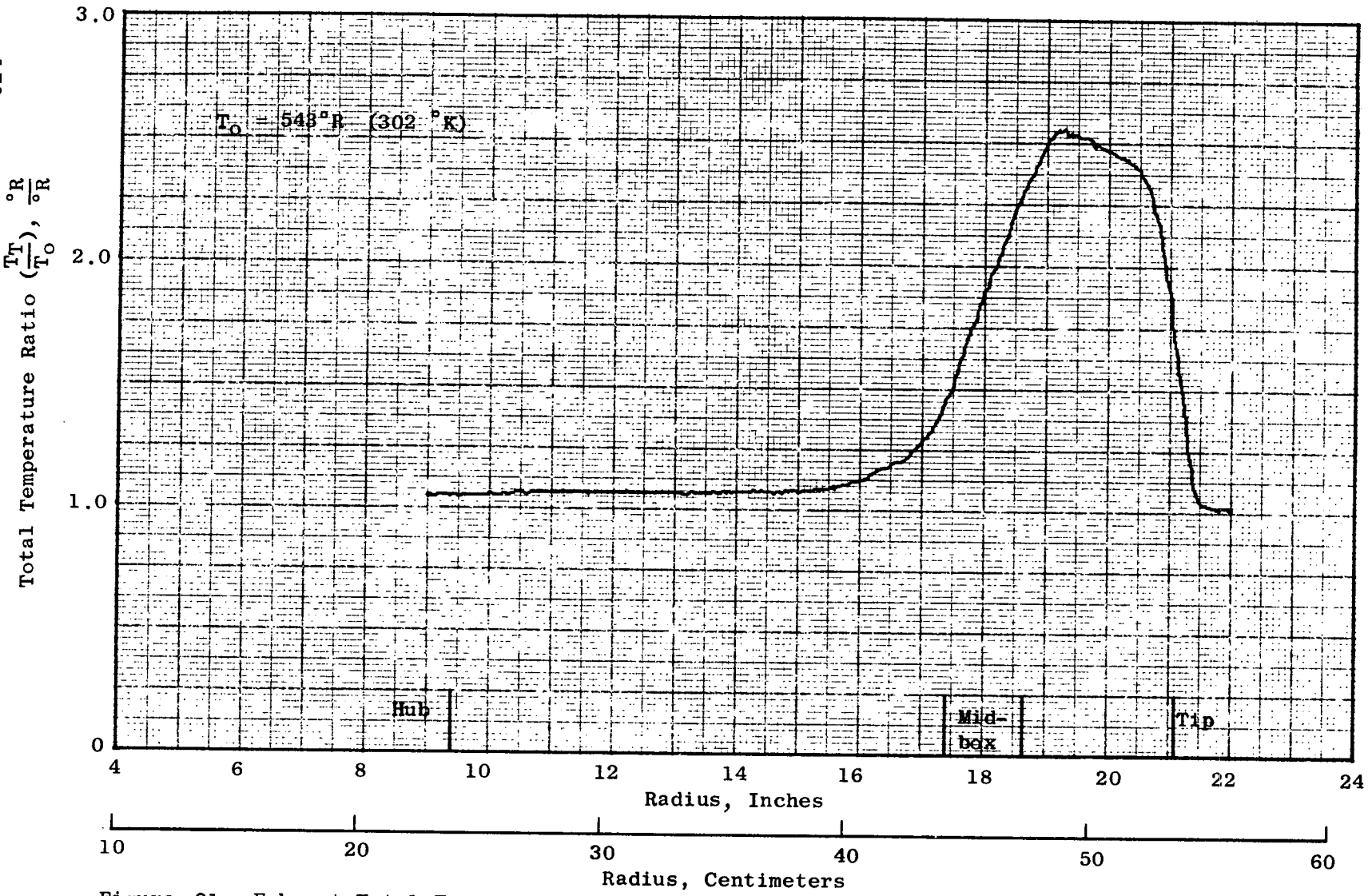

Figure 91. Exhaust Total Temperature Profile for Test 1, No Inlet or Exhaust Suppression, $N_f/\sqrt{\theta}$ = 5180

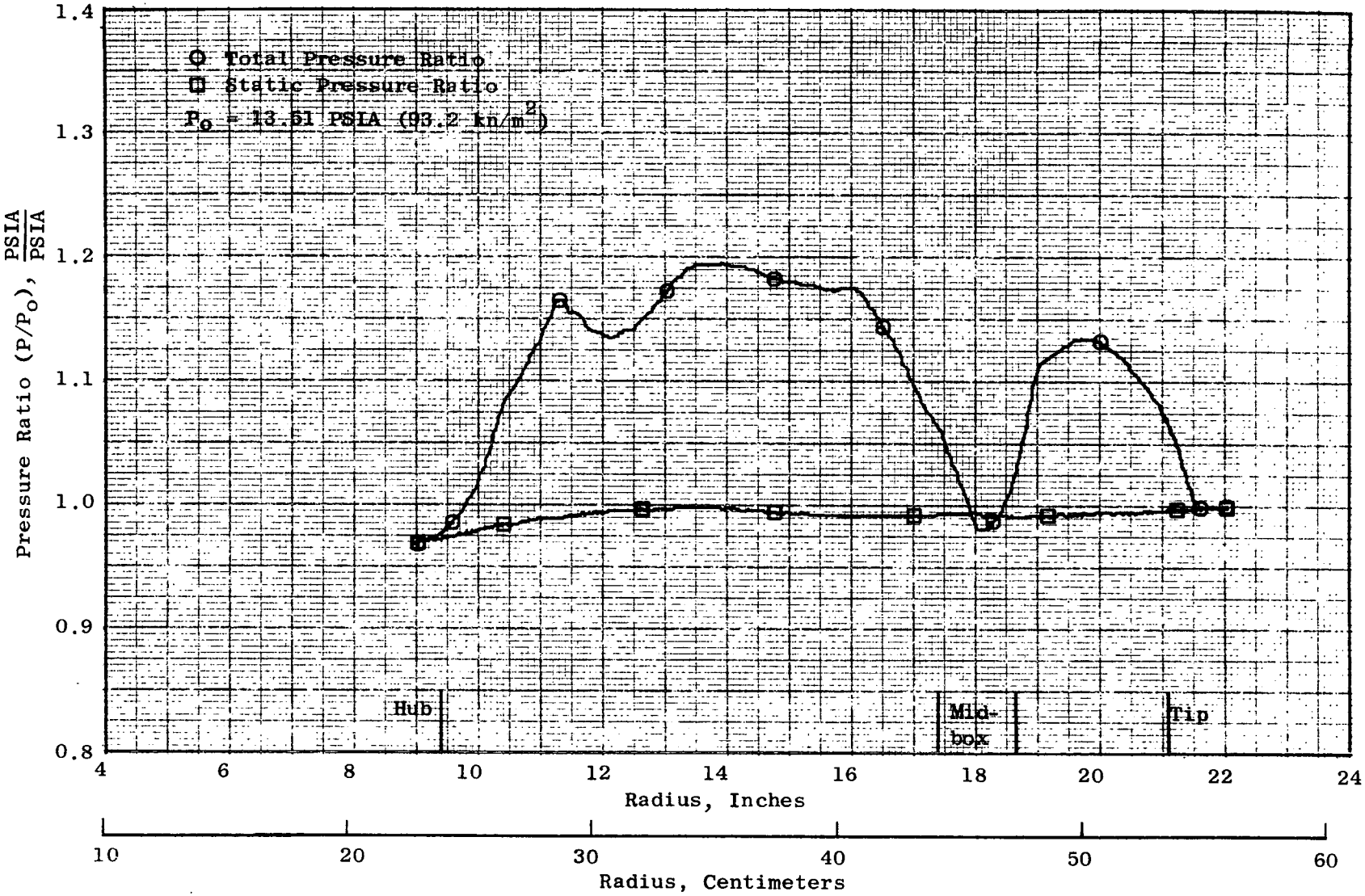

Figure 92. Exhaust Total and Static Pressure Profile for Test 1, No Inlet or Exhaust Suppression, N_f/θ = 4800

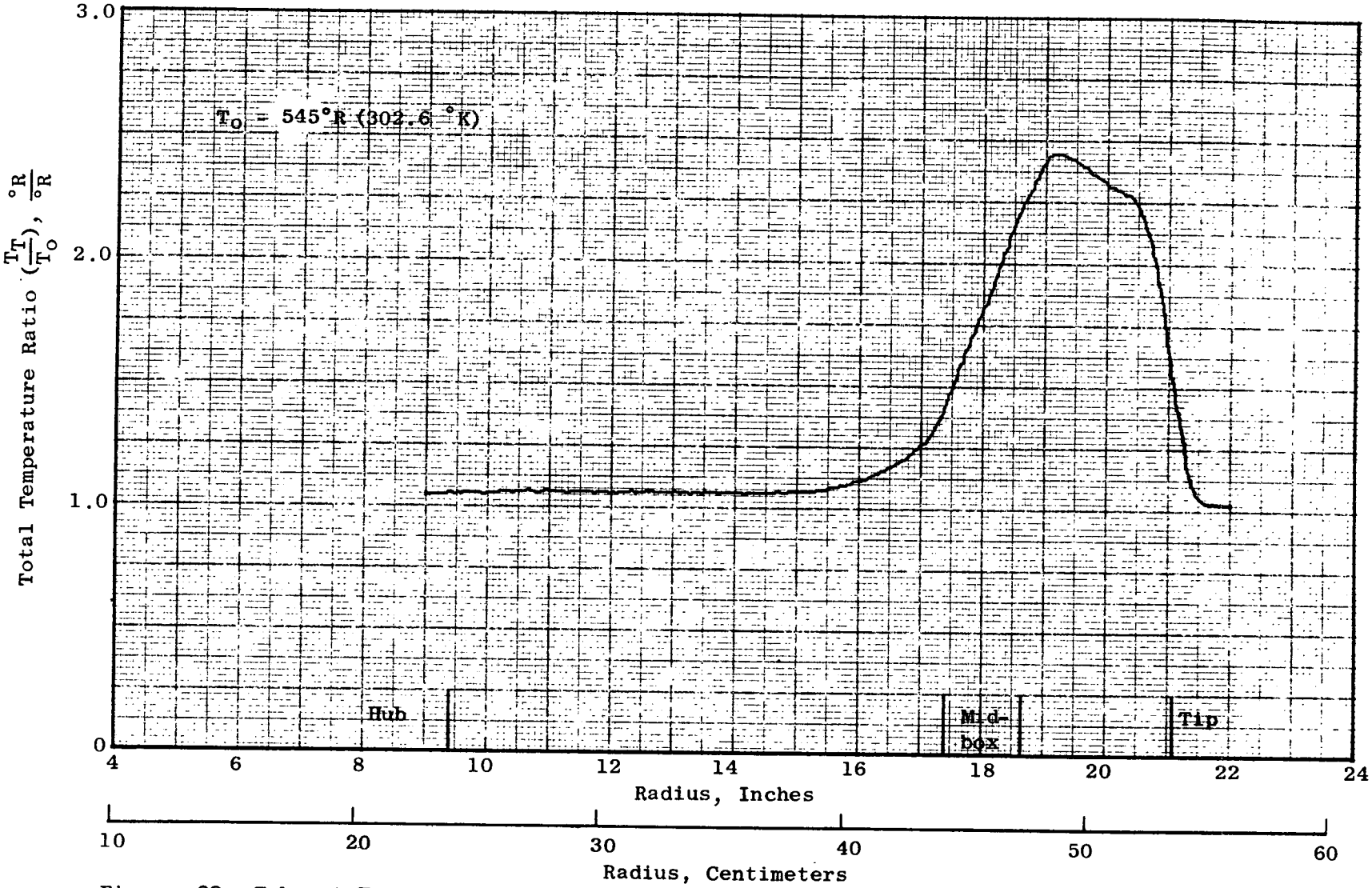

Figure 93. Exhaust Total Temperature Profile for Test 1, No Inlet or Exhaust Suppression, N_f/θ = 4800

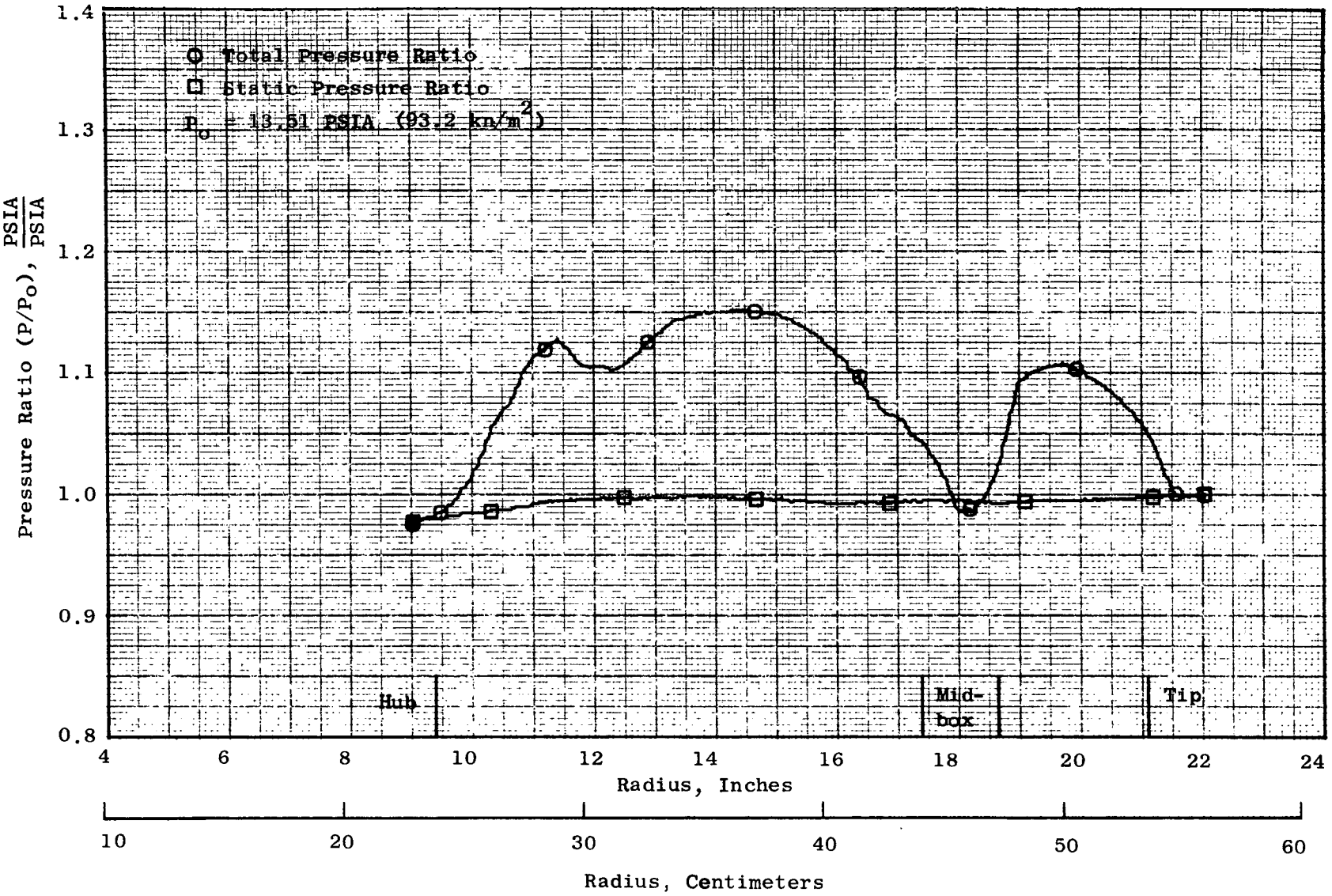

Figure 94. Exhaust Total and Static Pressure Profile for Test 1, No Inlet or Exhaust Suppression, $N_f/\sqrt{\theta}$ = 4190

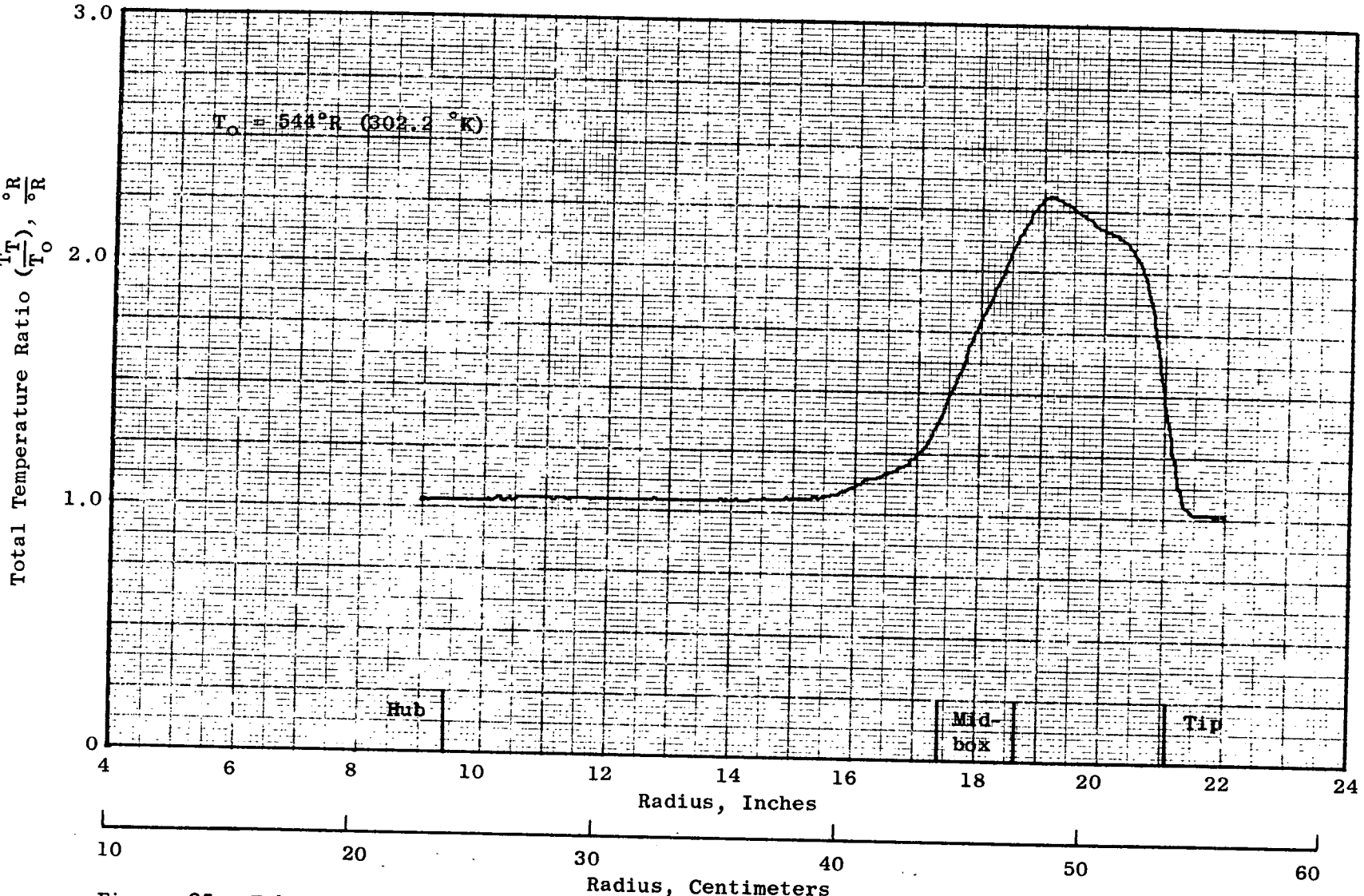

Figure 95. Exhaust Total Temperature Profile for Test 1, No Inlet or Exhaust Suppression, N_f/θ = 4190

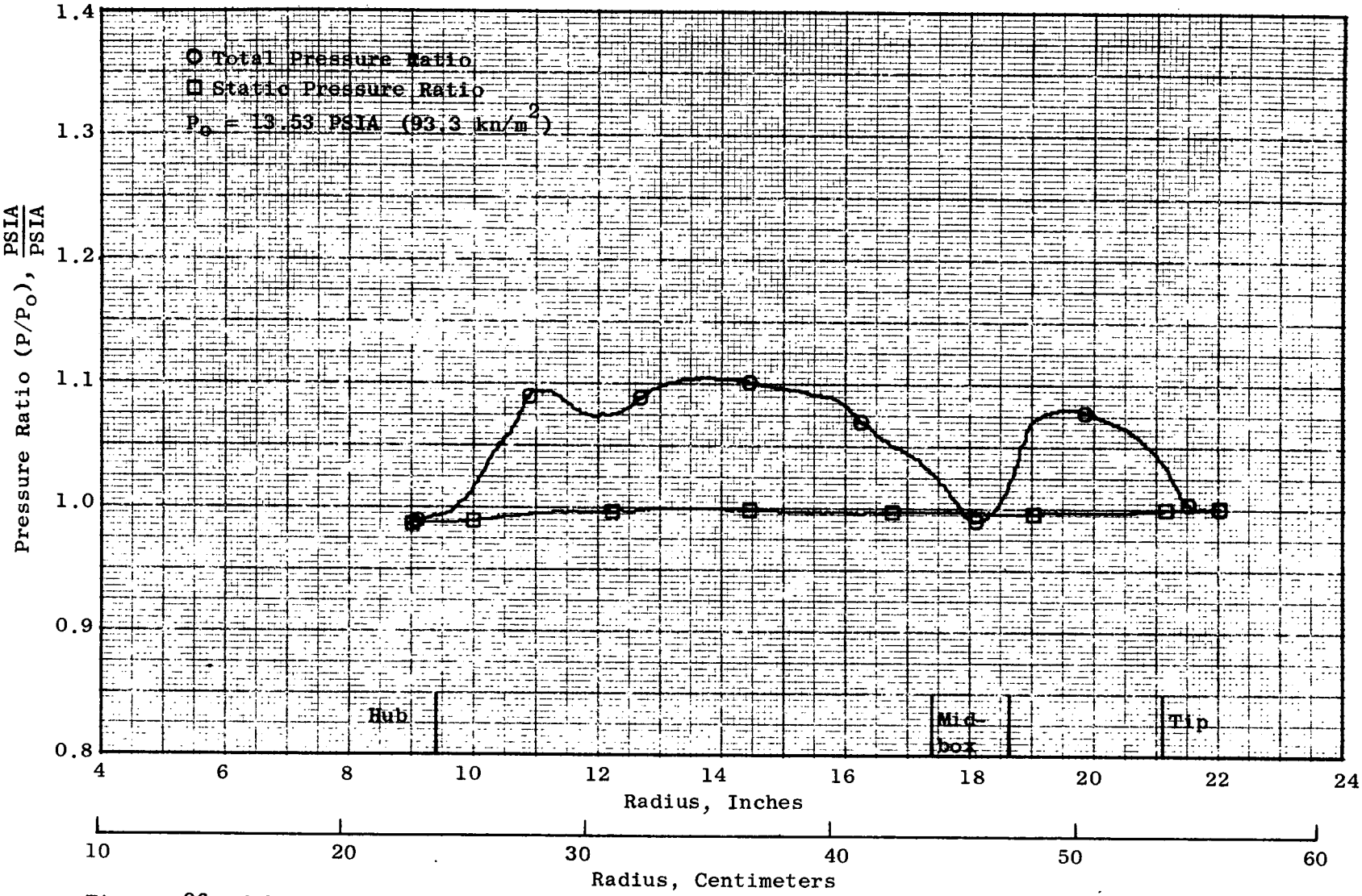

Figure 96. Exhaust Total and Static Pressure Profile for Test 1, No Inlet or Exhaust Suppression, $N_f/\sqrt{\theta}$ = 3575

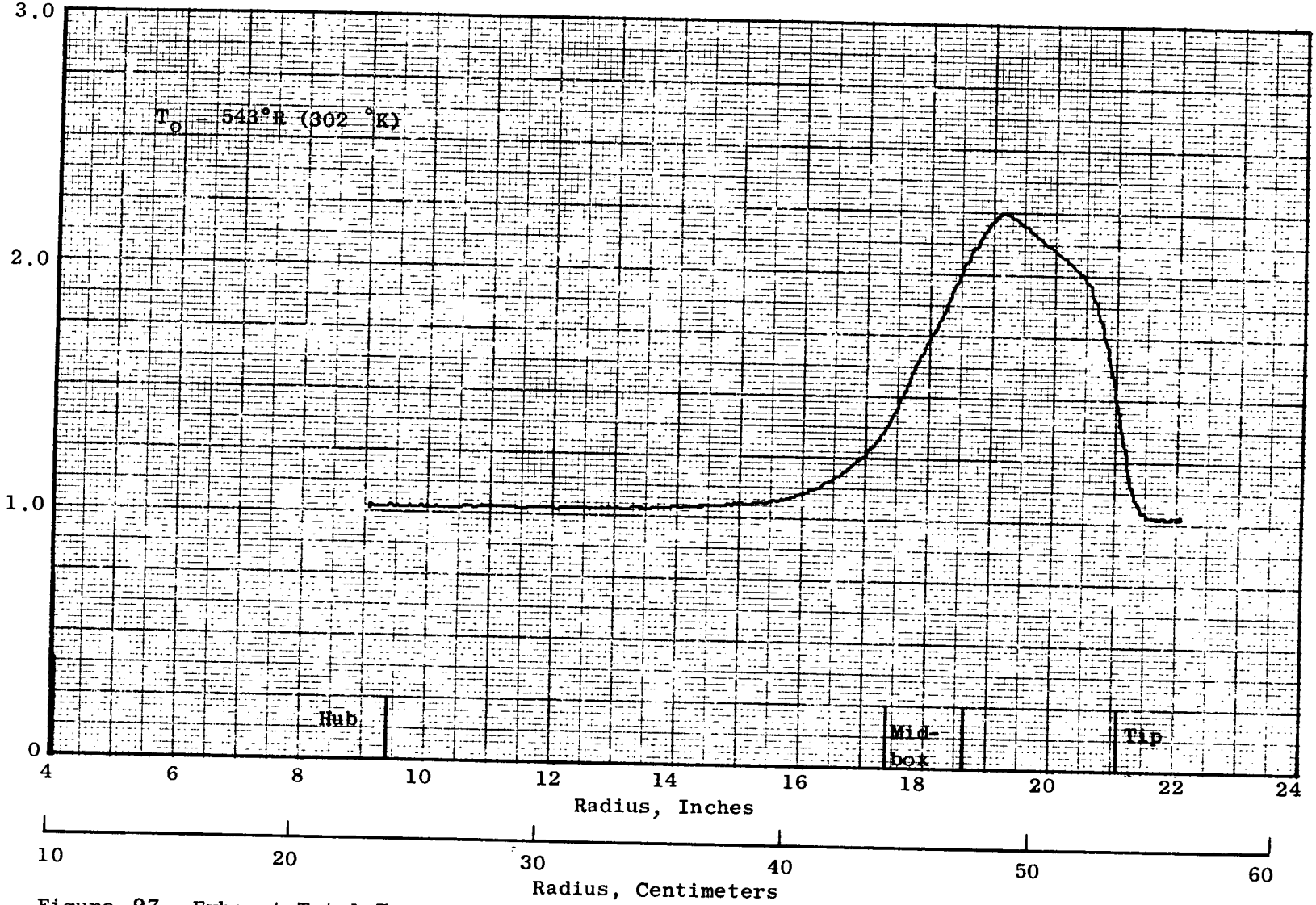

Figure 97. Exhaust Total Temperature Profile for Test 1, No Inlet or Exhaust Suppression, $N_f/\sqrt{\theta}$ = 3575

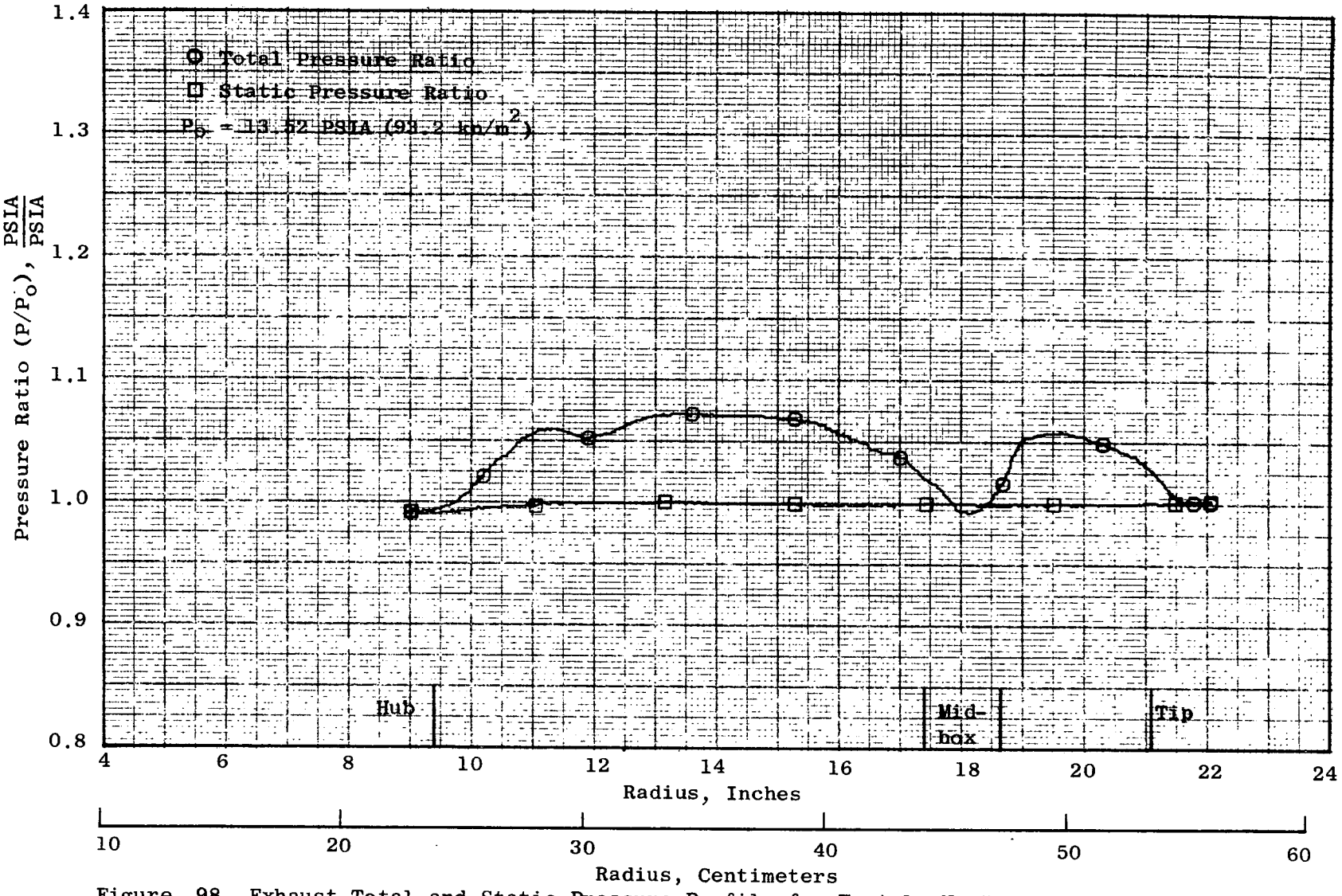

Figure 98. Exhaust Total and Static Pressure Profile for Test 1, No Inlet or Exhaust Suppression, $N_f/\sqrt{\theta}$ =3000

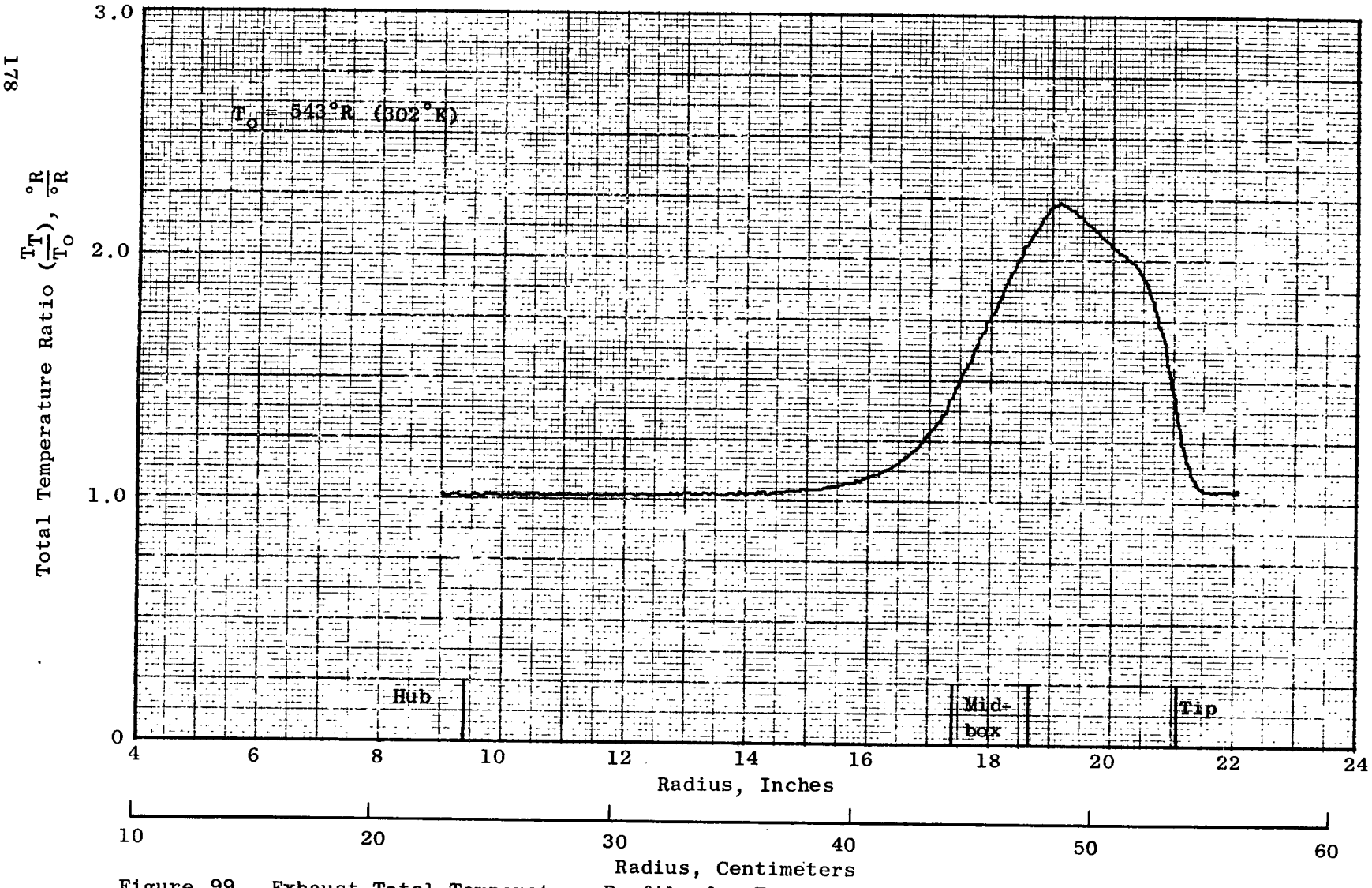

Figure 99. Exhaust Total Temperature Profile for Test 1, No Inlet or Exhaust Suppression $N_f/\sqrt{\theta}$ = 3000

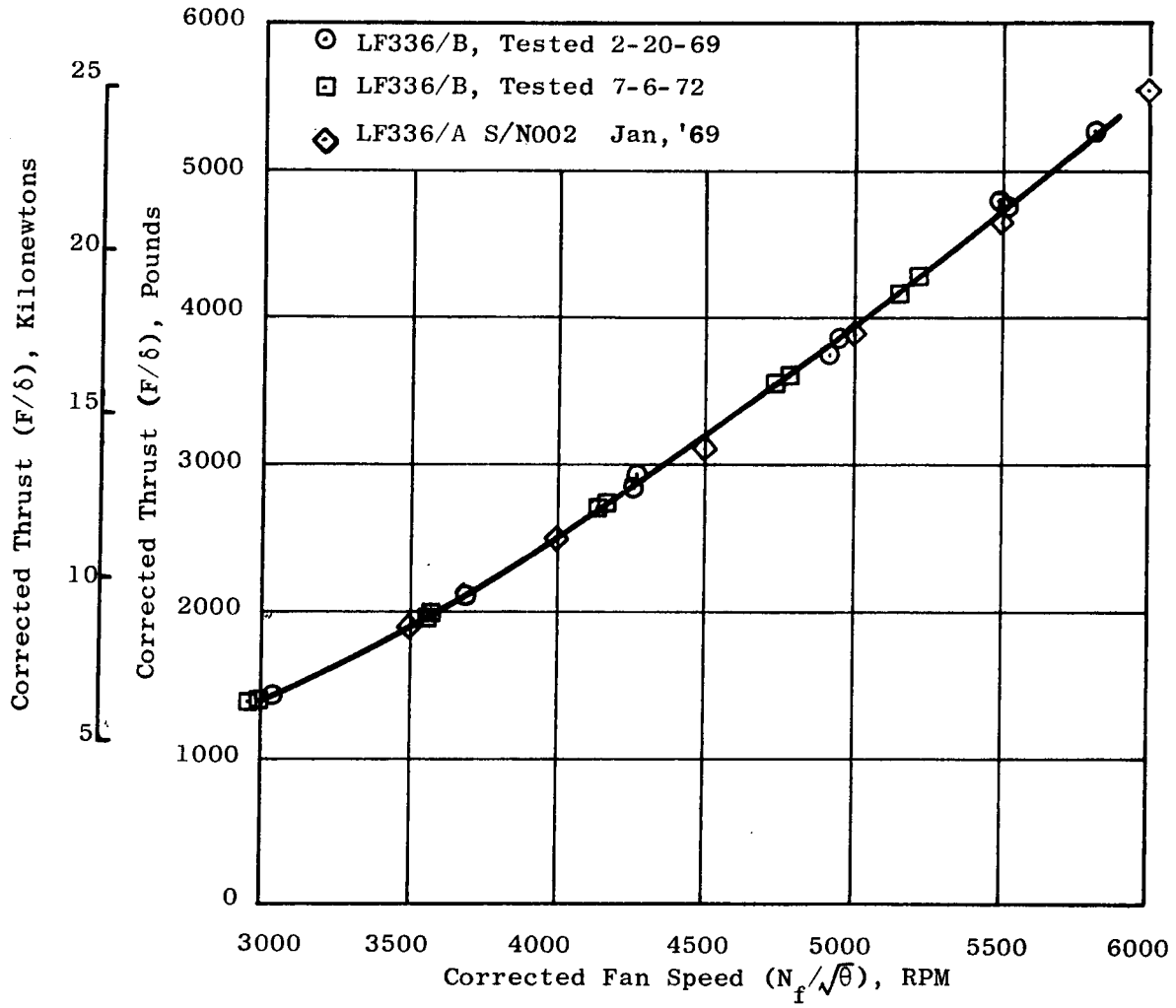

Figure 100. Thrust Comparison of LF336/A and LF336/B Lift Fans

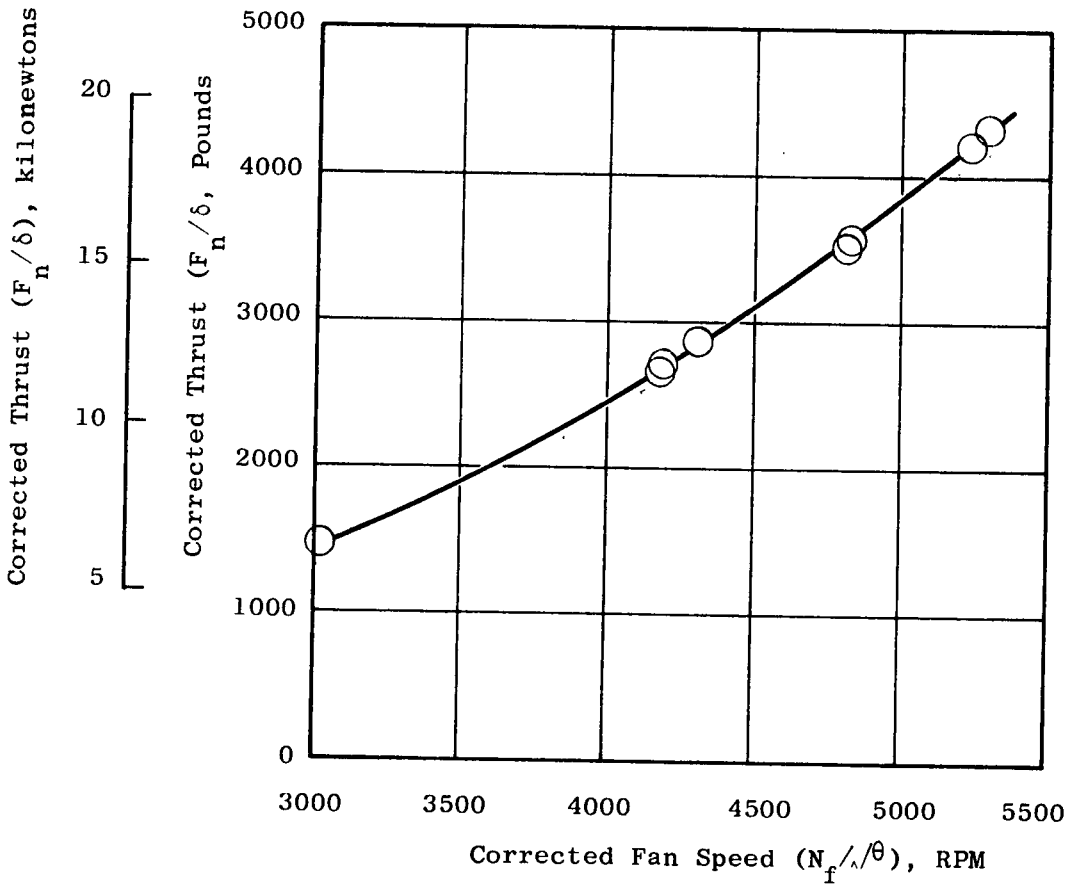

Figure 101. Thrust Variation with Fan Speed for Test 2, Inlet Box and No Exhaust Suppression

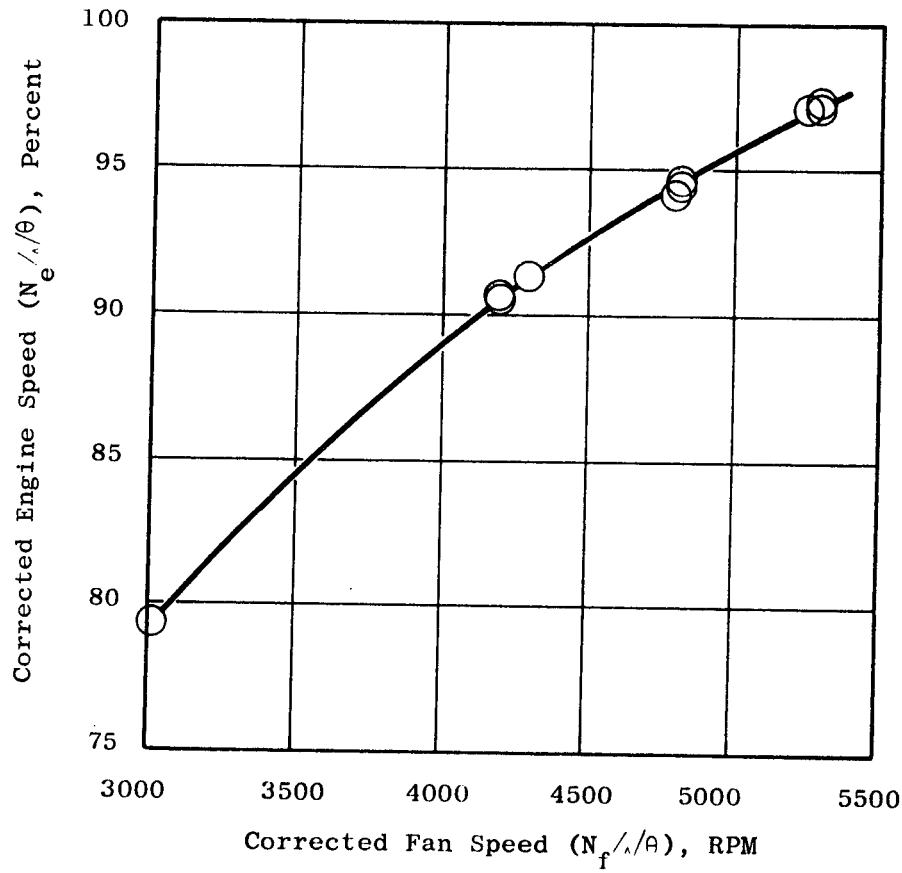

Figure 102. Engine Speed Variation with Fan Speed for Test 2, Inlet Box and No Exhaust Suppression

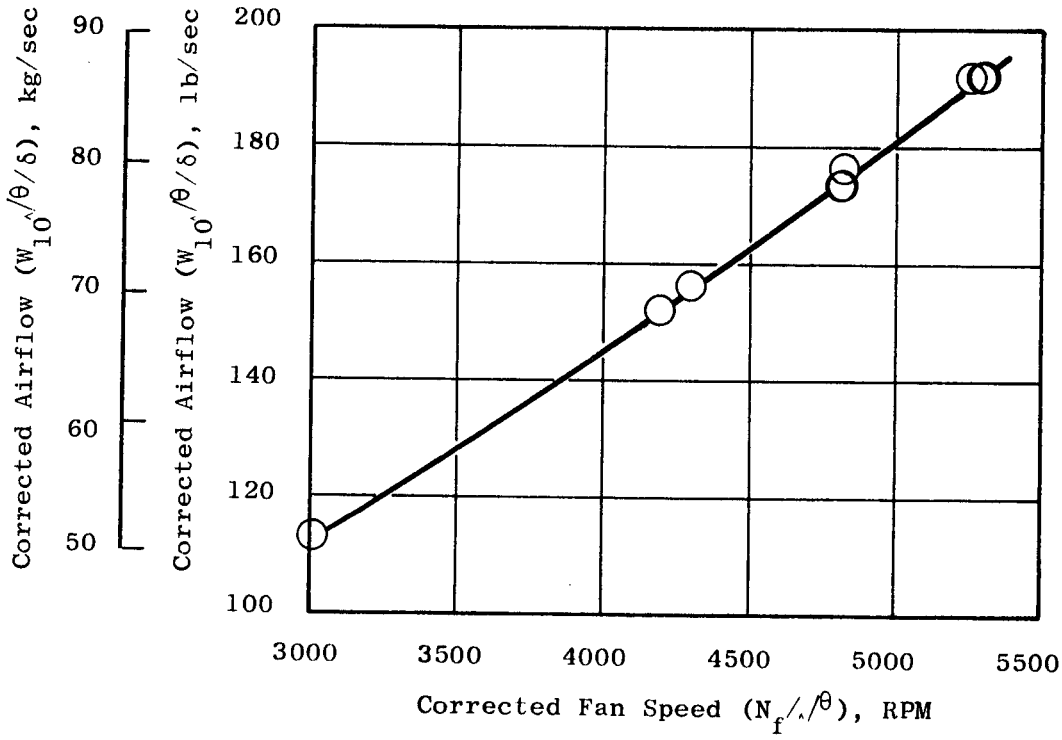

Figure 103. Airflow Variation with Fan Speed for Test 2, Inlet Box and No Exhaust Suppression

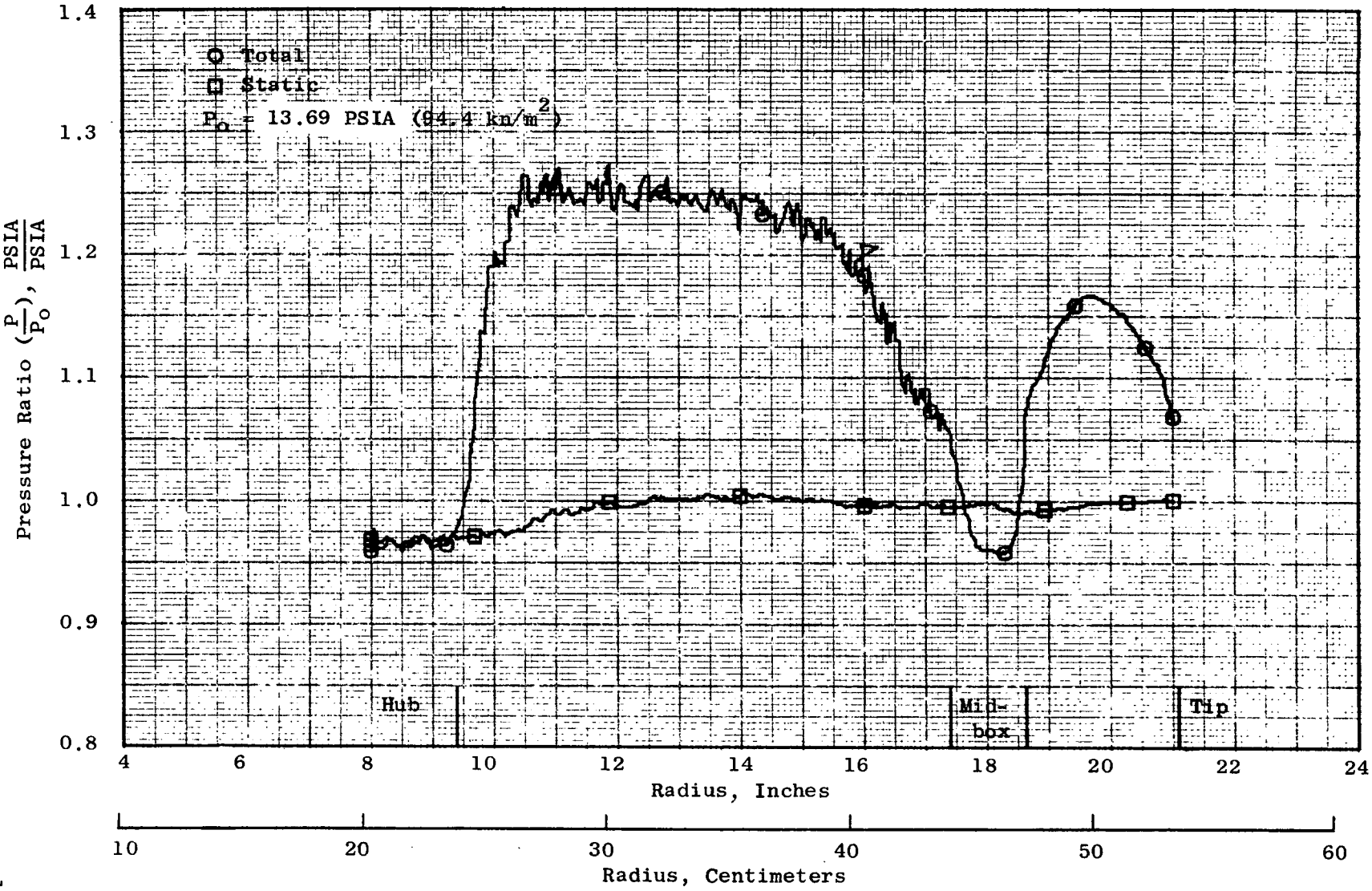

Figure 104. Exhaust Total and Static Pressure Profile for Test 2, Inlet Box and No Exhaust Suppression, $N_f/\sqrt{\theta}$ =5290

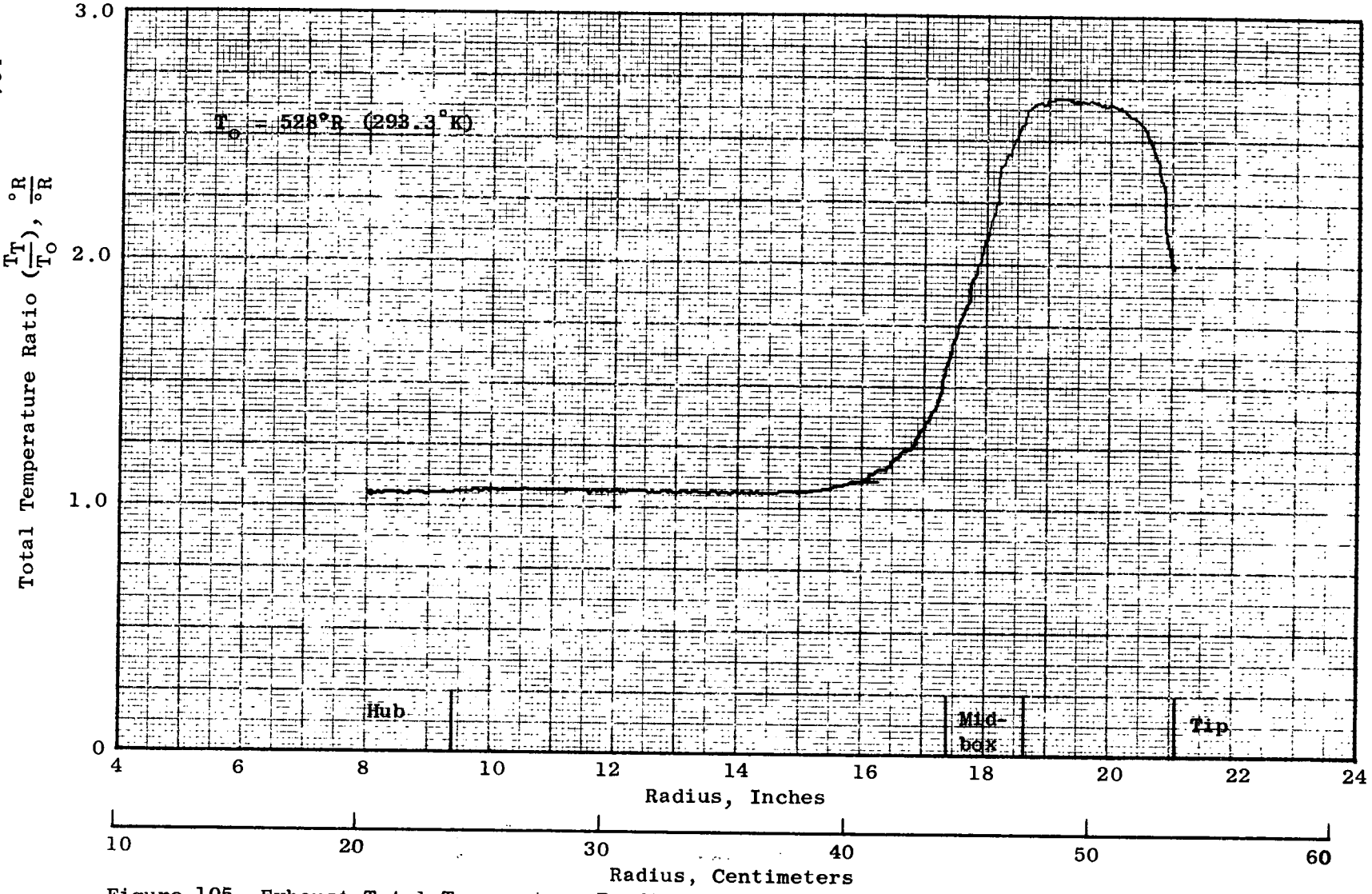

Figure 105. Exhaust Total Temperature Profile for Test 2, Inlet Box and No Exhaust Suppression, $N_f/\sqrt{\theta}$ = 5290

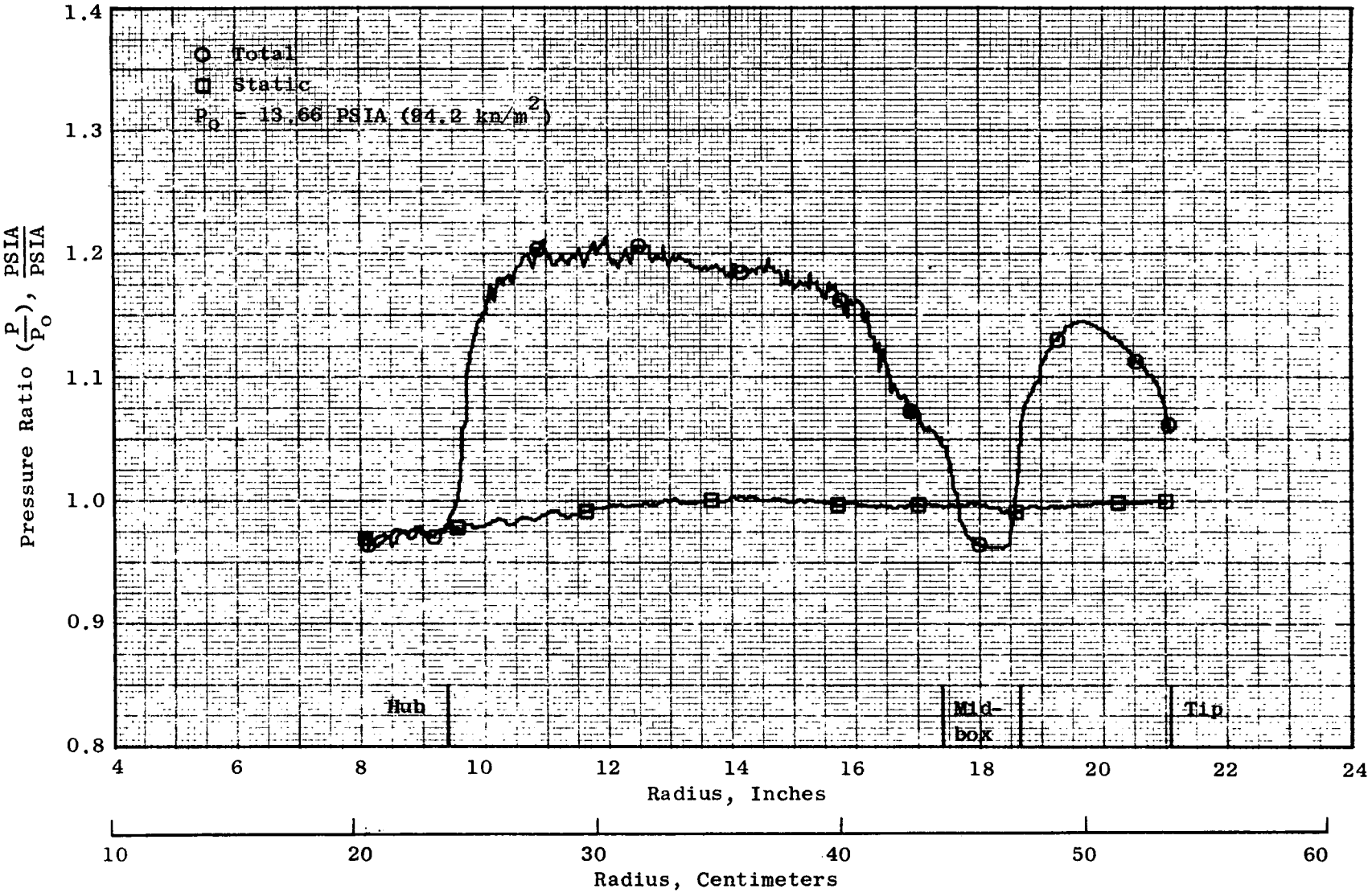

Figure 106. Exhaust Total and Static Pressure Profile for Test 2, Inlet Box and No Exhaust Suppression, $N_f/\sqrt{\theta}$ = 4820

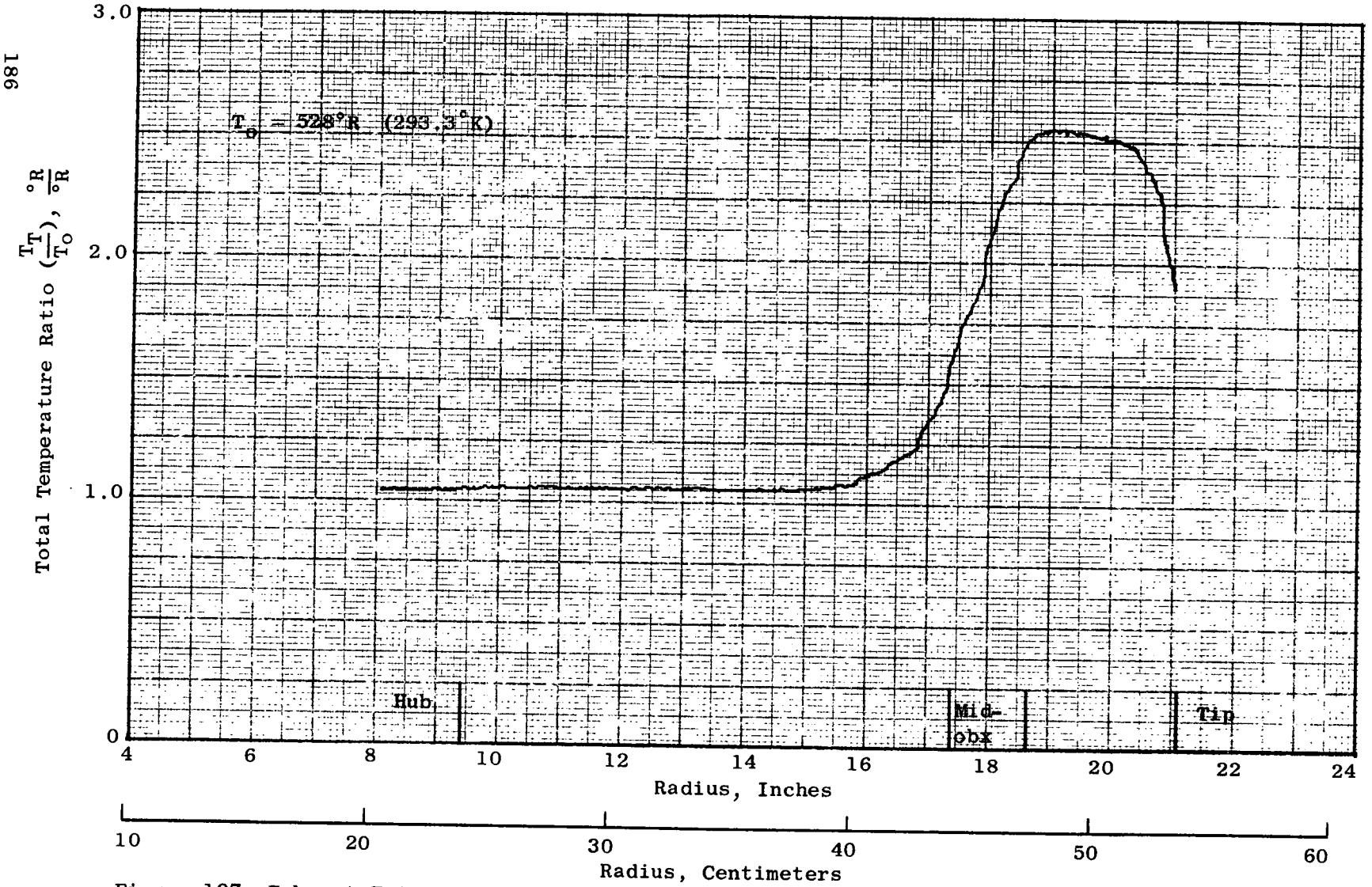

Figure 107. Exhaust Total Temperature Profile for Test 2, Inlet Box and No Exhaust Suppression, $N_f/\sqrt{\theta}$ = 4820

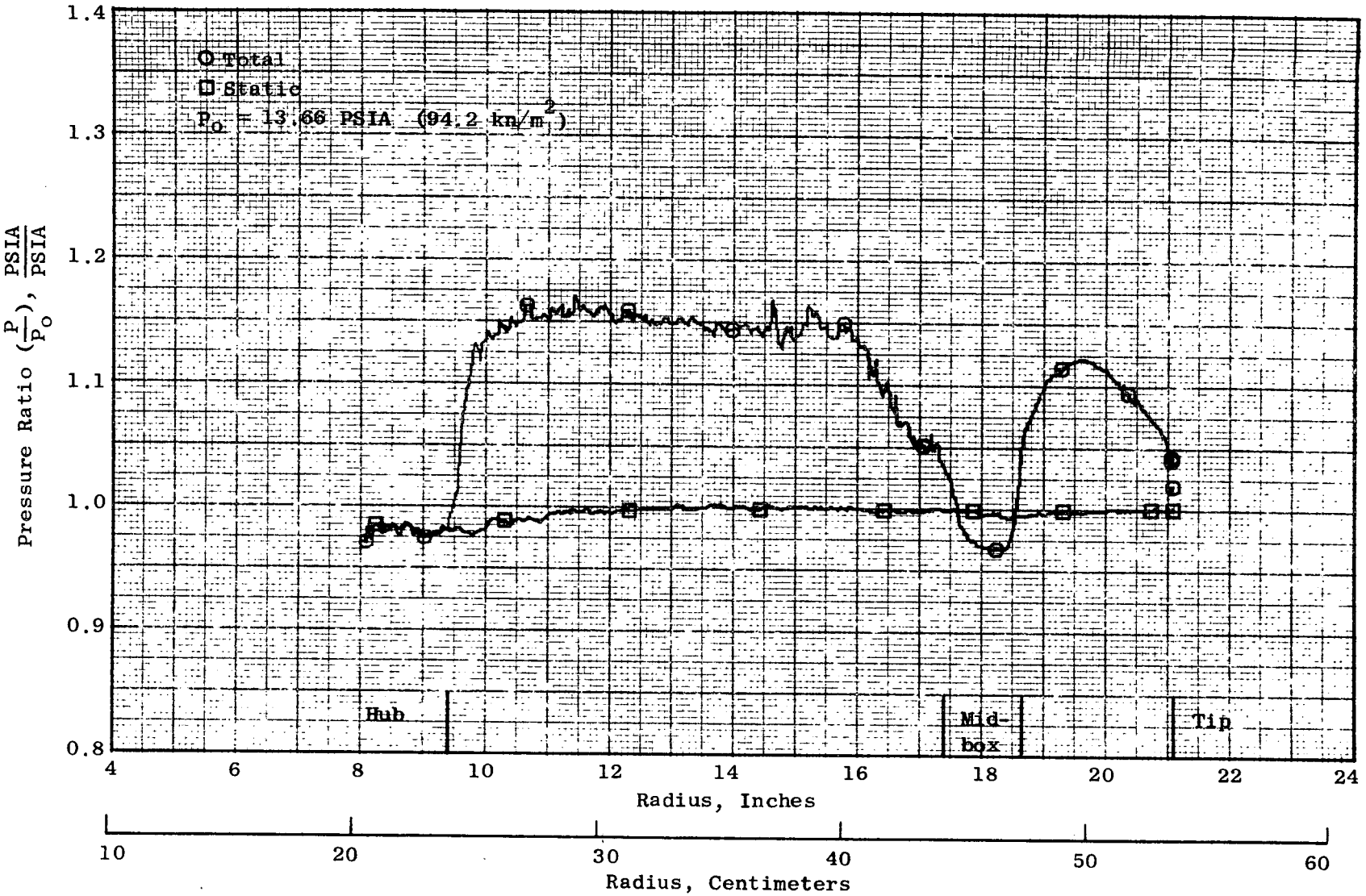

Figure 108. Exhaust Total and Static Pressure Profile for Test 2, Inlet Box and No Exhaust Suppression, $N_f/\sqrt{\theta}$ = 4300

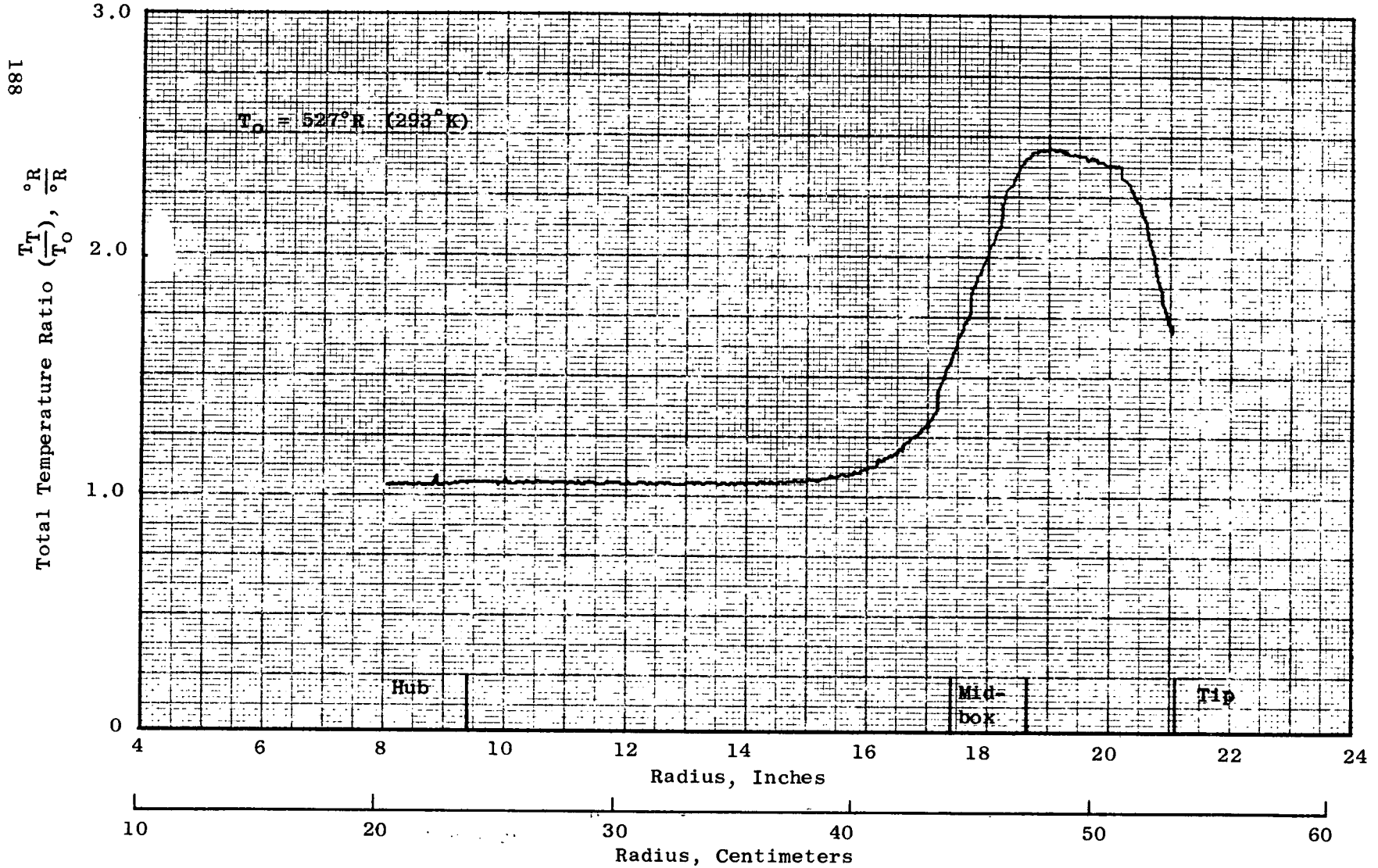

Figure 109. Exhaust Total Temperature Profile for Test 2, Inlet Box and No Exhaust Suppression, $N_f/\sqrt{\theta}$ =4300

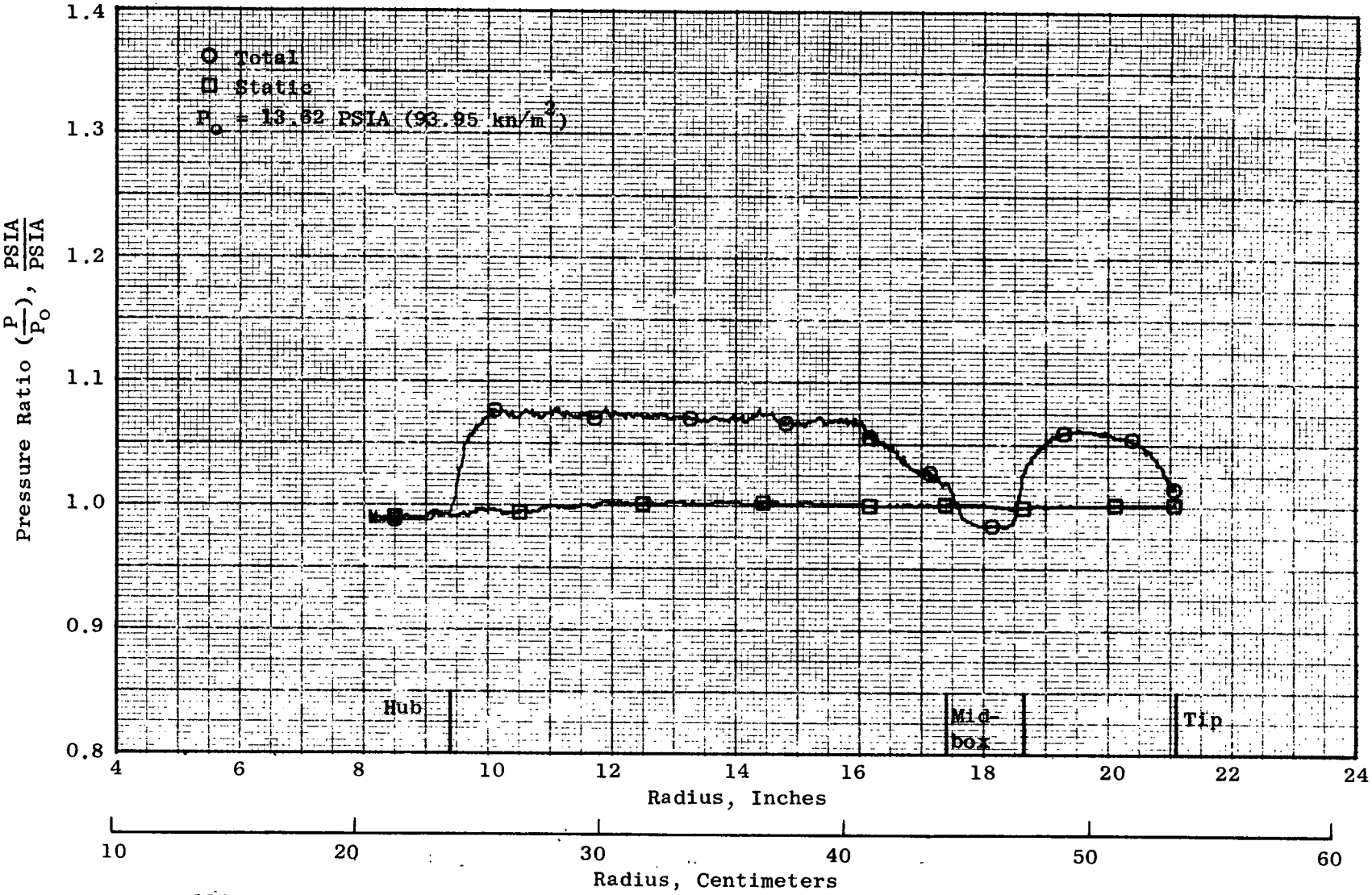

Figure 110. Exhaust Total and Static Pressure Profile for Test 2, Inlet Box and No Exhaust Suppression, $N_f/\sqrt{\theta}$ = 3052

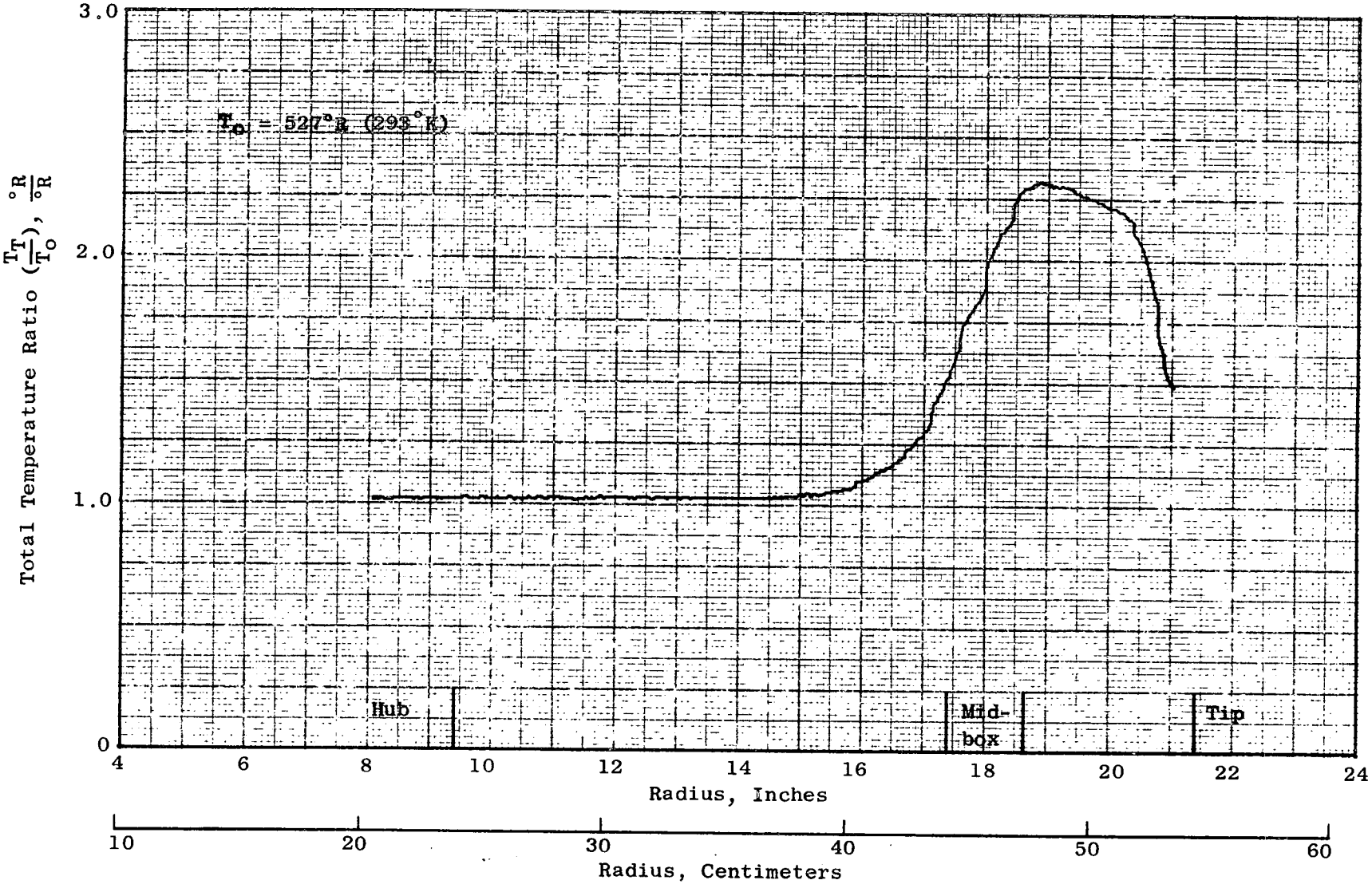

Figure 111. Exhaust Total Temperature Profile for Test 2, Inlet Box and No Exhaust Suppression, $N_f/\sqrt{\theta}$ = 3052

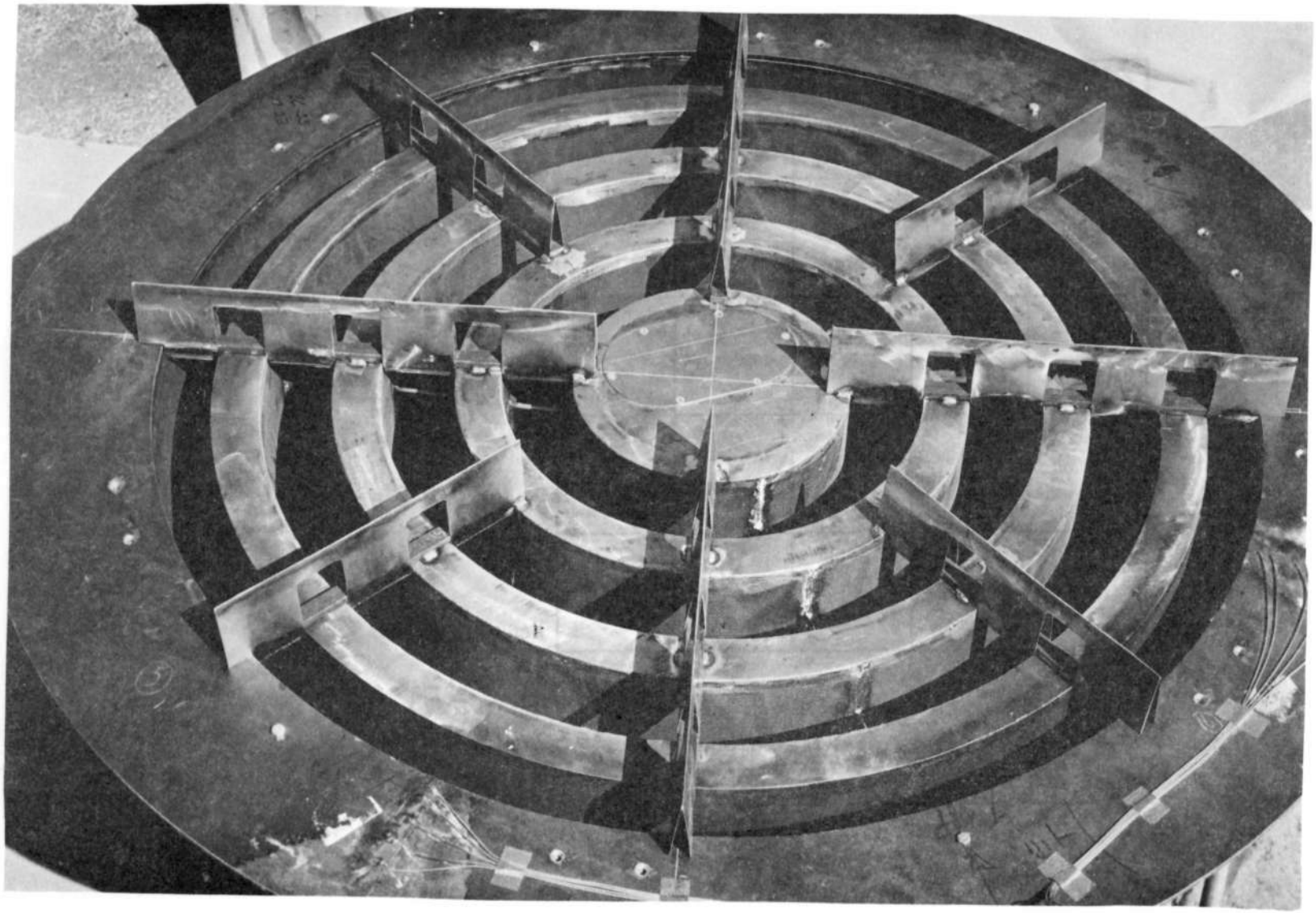

Figure 112. Faired U-Channel Blockage on 10 Inch (25.4 cm) Exhaust Section

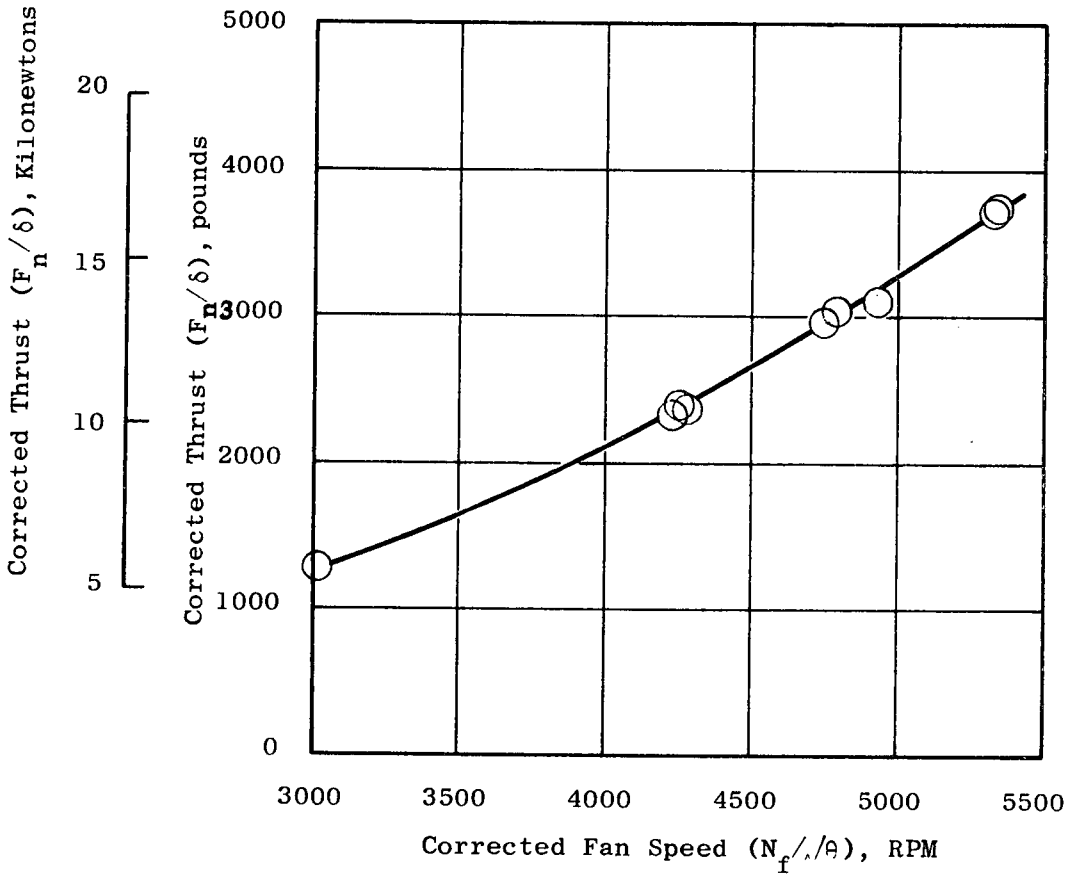

Figure 113. Thrust Variation with Fan Speed for Test 3, Inlet Box and 10 Inches (25.4 cm) of Exhaust Suppression with Airfoiled Blockage

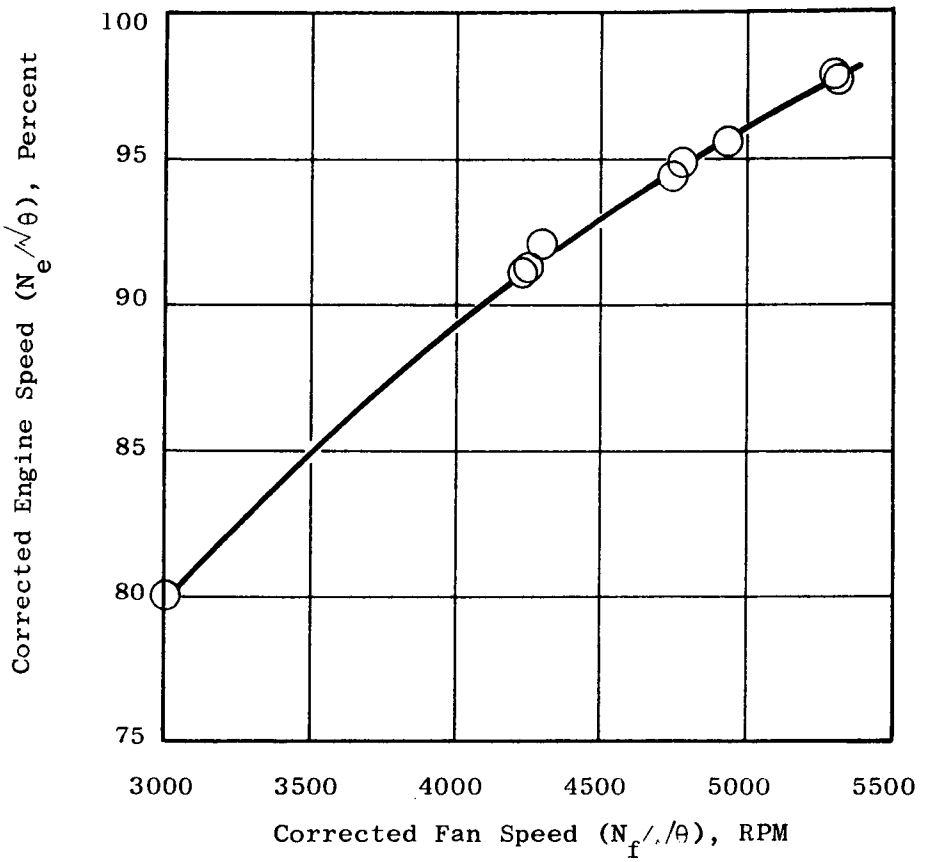

Figure 114. Engine Speed Variation with Fan Speed for Test 3, Inlet Box and 10 Inches (25.4 cm) of Exhaust Suppression with Airfoiled Blockage

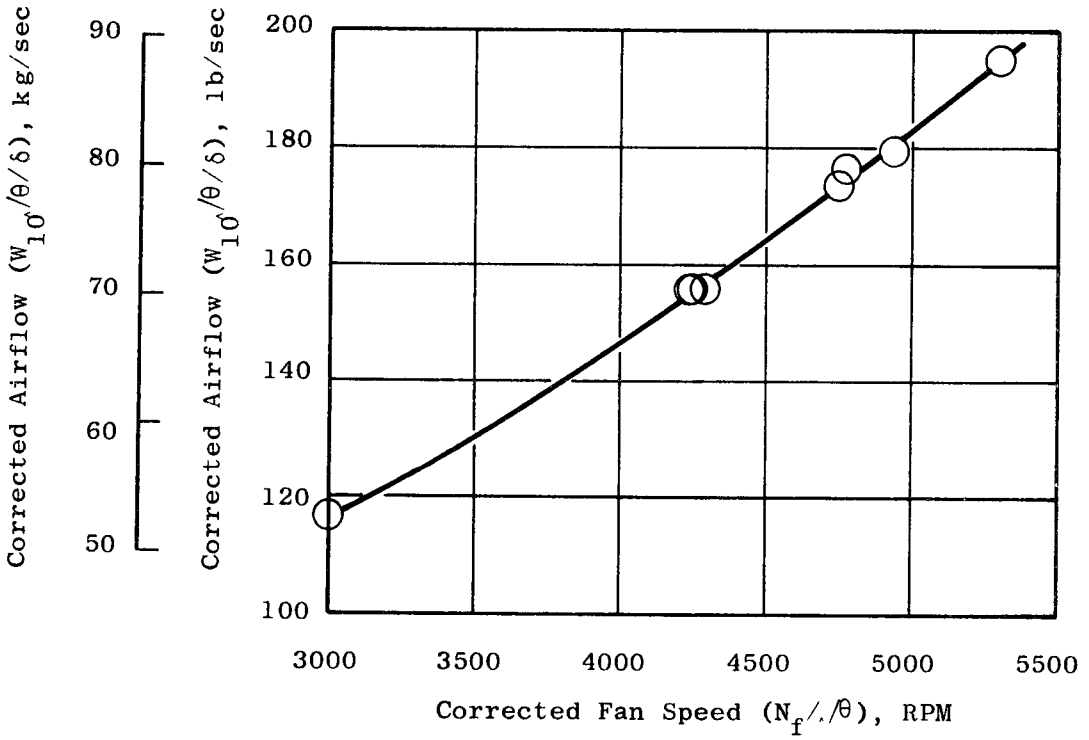

Figure 115. Airflow Variation with Fan Speed for Test 3, Inlet Box and 10 Inches (25.4 cm) of Exhaust Suppression with Airfoiled Blockage

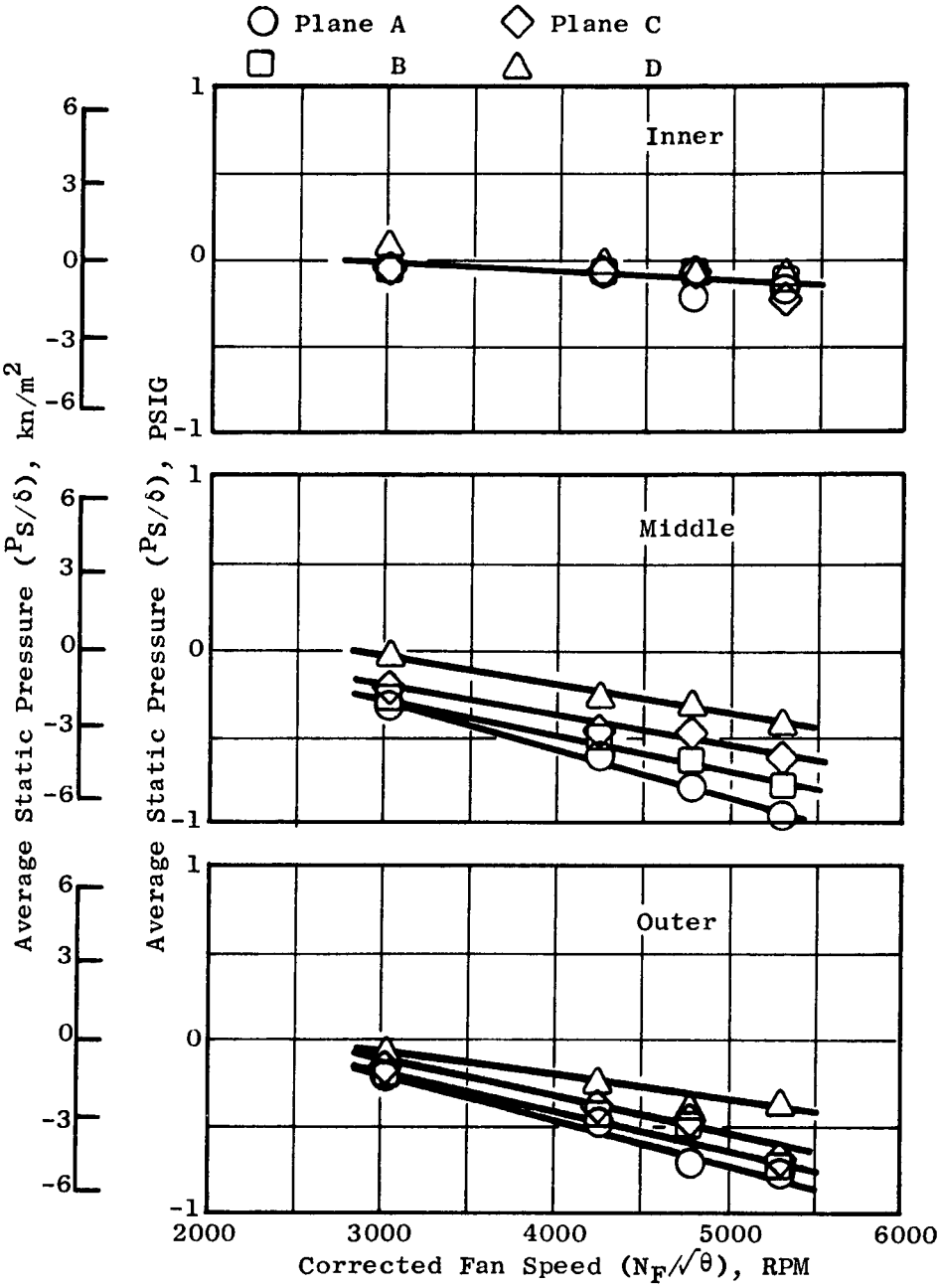

Figure 116. Adapter Section Average Wall Static Pressure Distribution for Test 3, Inlet Box and 10 Inches (25.4 cm) of Exhaust Suppression with Airfoiled Blockage

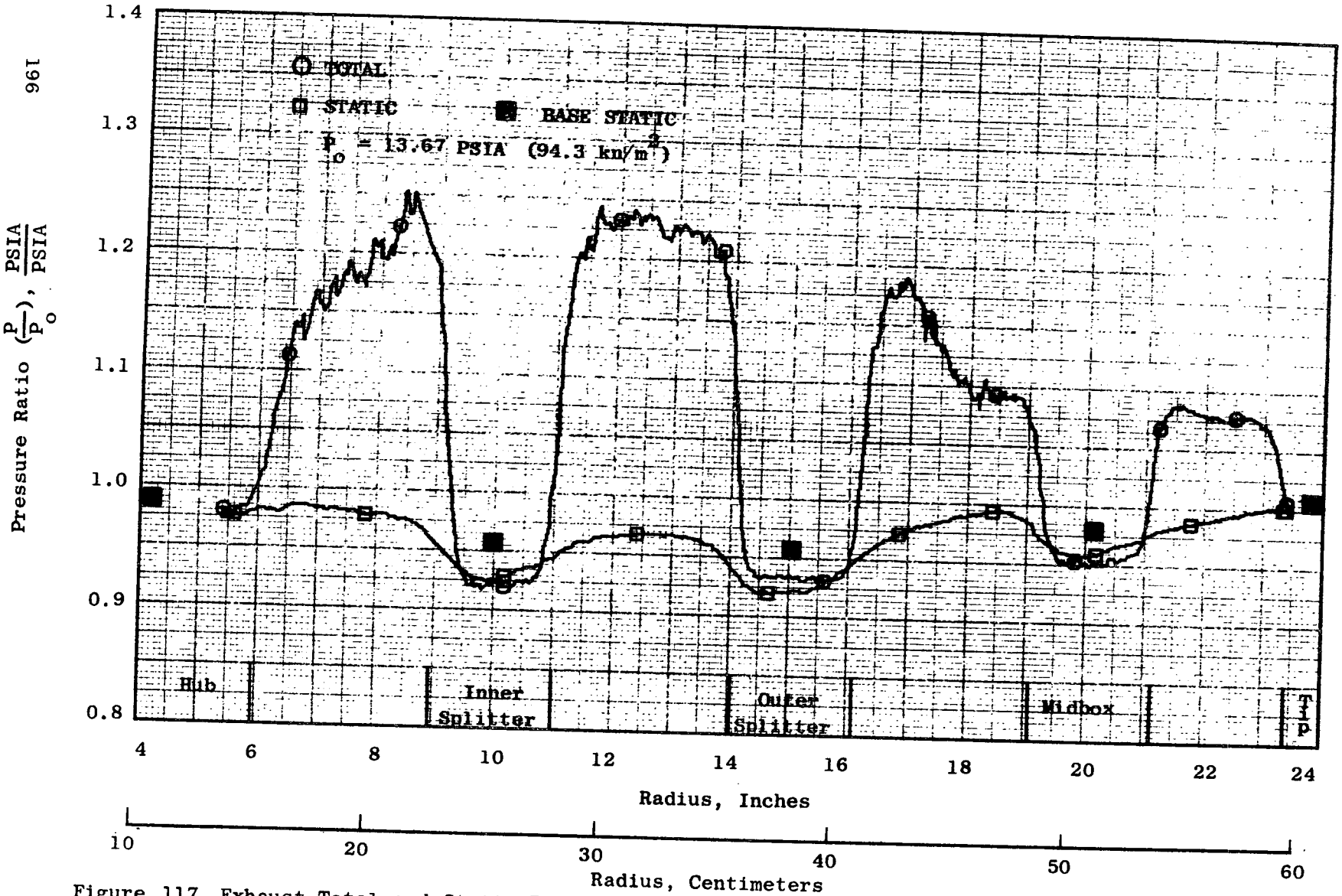

Figure 117. Exhaust Total and Static Pressure Profile for Test 3, Inlet Box and 10 Inches (25.4 cm) of Exhaust Suppression with Airfoiled Blockage, $N_f/\sqrt{\theta} = 5300$

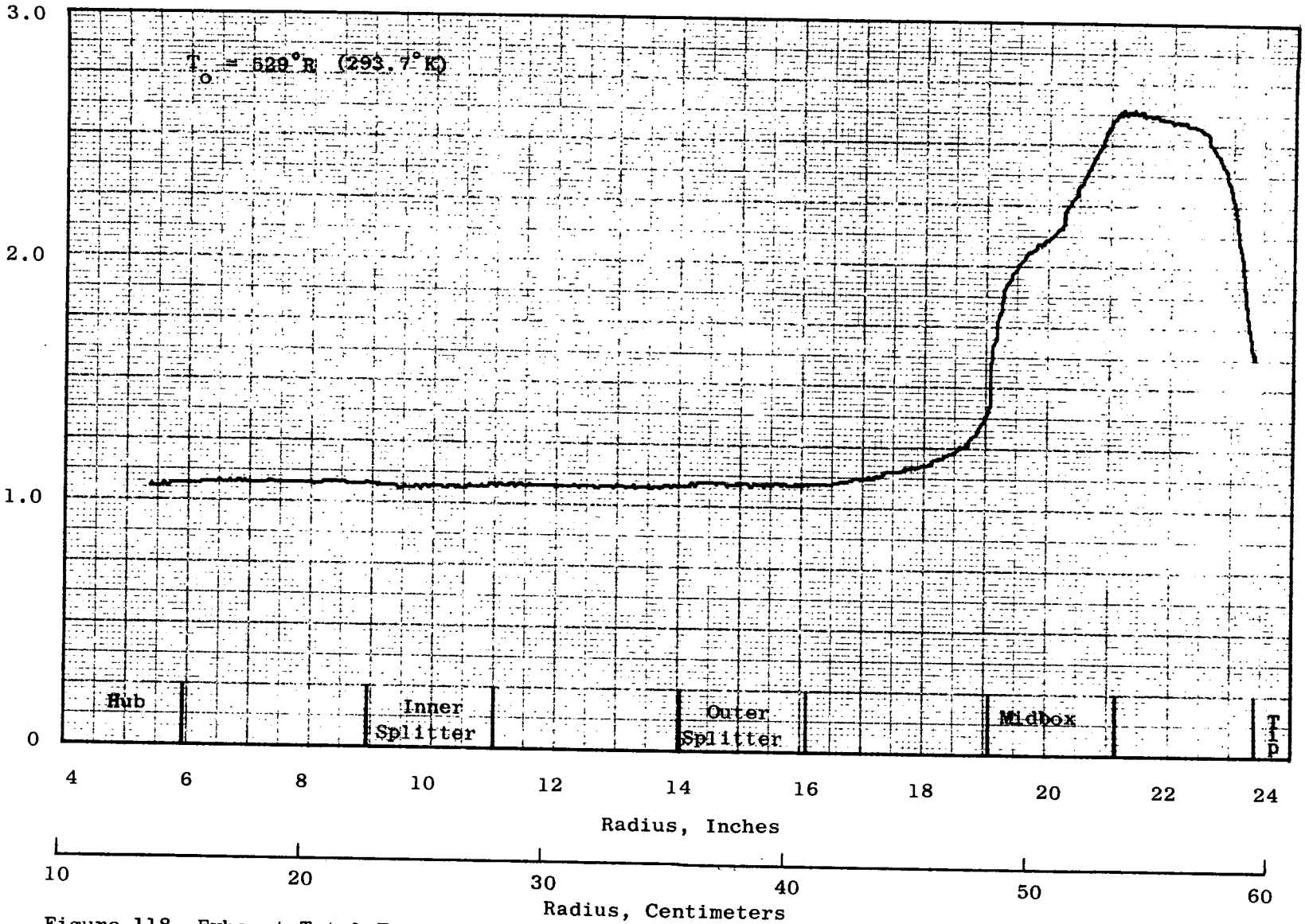

Figure 118. Exhaust Total Temperature Profile for Test 3, Inlet Box and 10 Inches (25.4 cm) of Exhaust Suppression with Airfoiled Blockage, N_f/θ = 5300

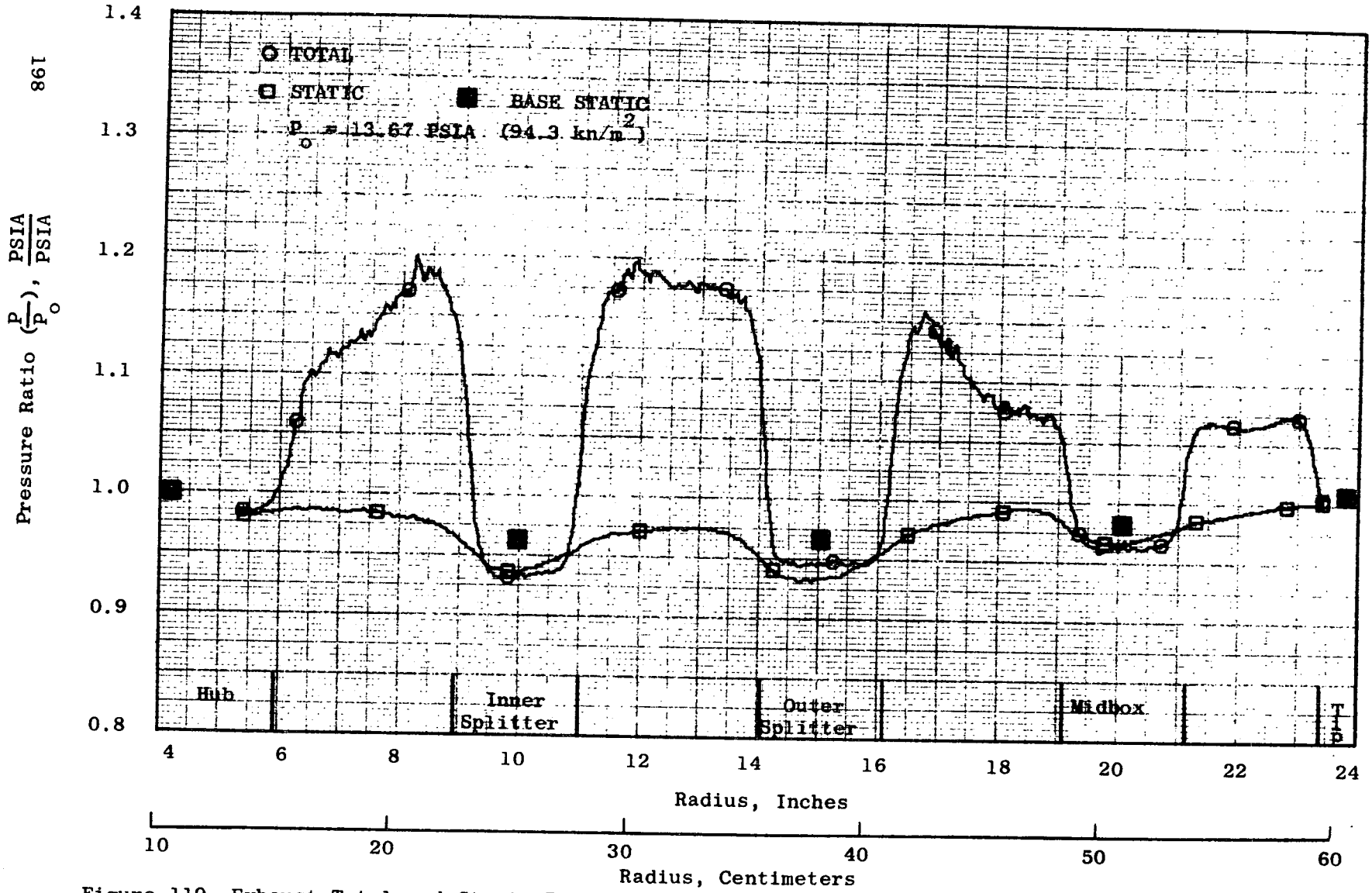

Figure 119. Exhaust Total and Static Pressure Profile for Test 3, Inlet Box and 10 Inches (25.4 cm) of Exhaust Suppression with Airfoiled Blockage, N_f/θ = 4790

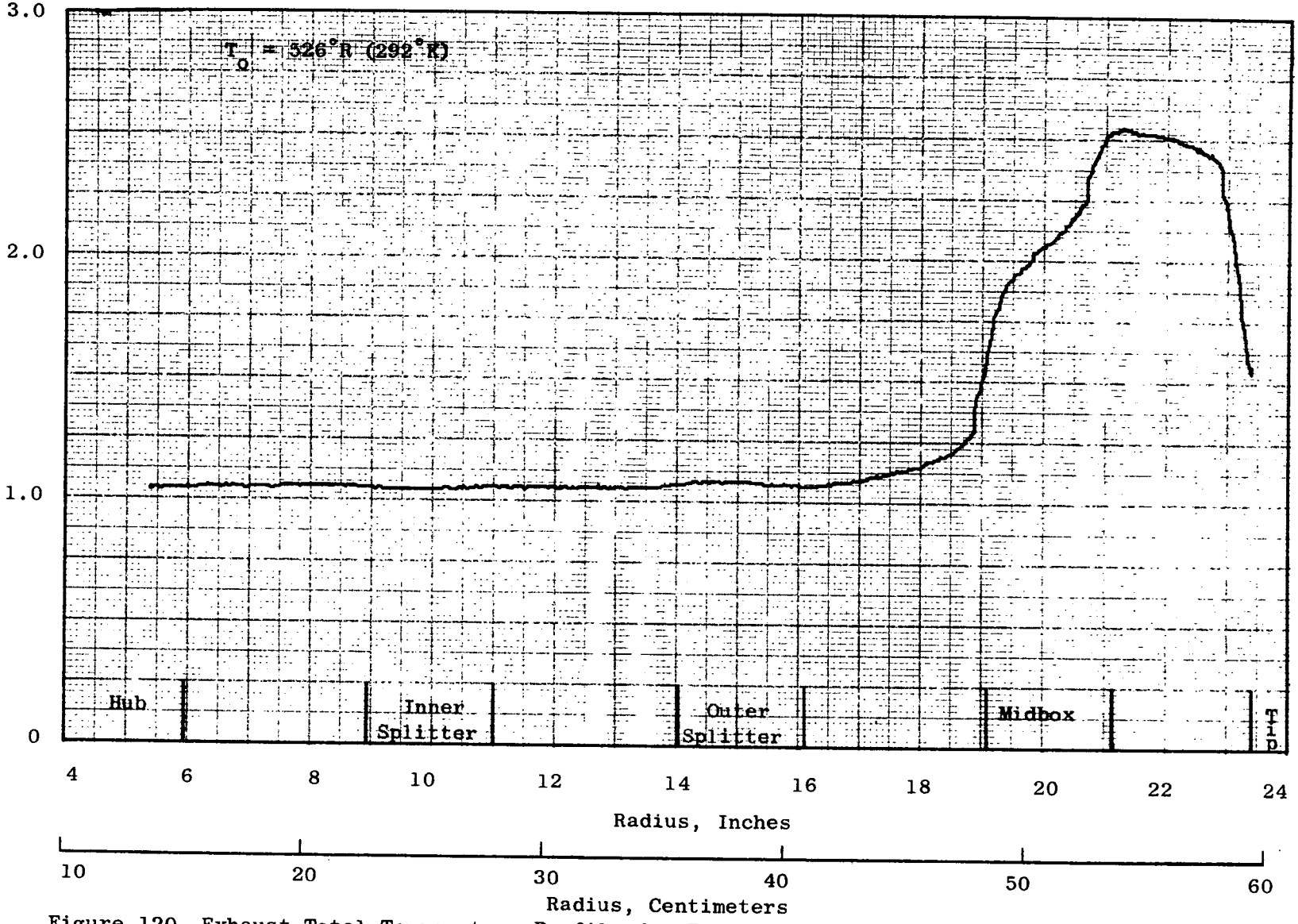

Figure 120. Exhaust Total Temperature Profile for Test 3, Inlet Box and 10 Inches (25.4 cm) of Exhaust Suppression with Airfoiled Blockage, $N_f/\sqrt{\theta}$ = 4790

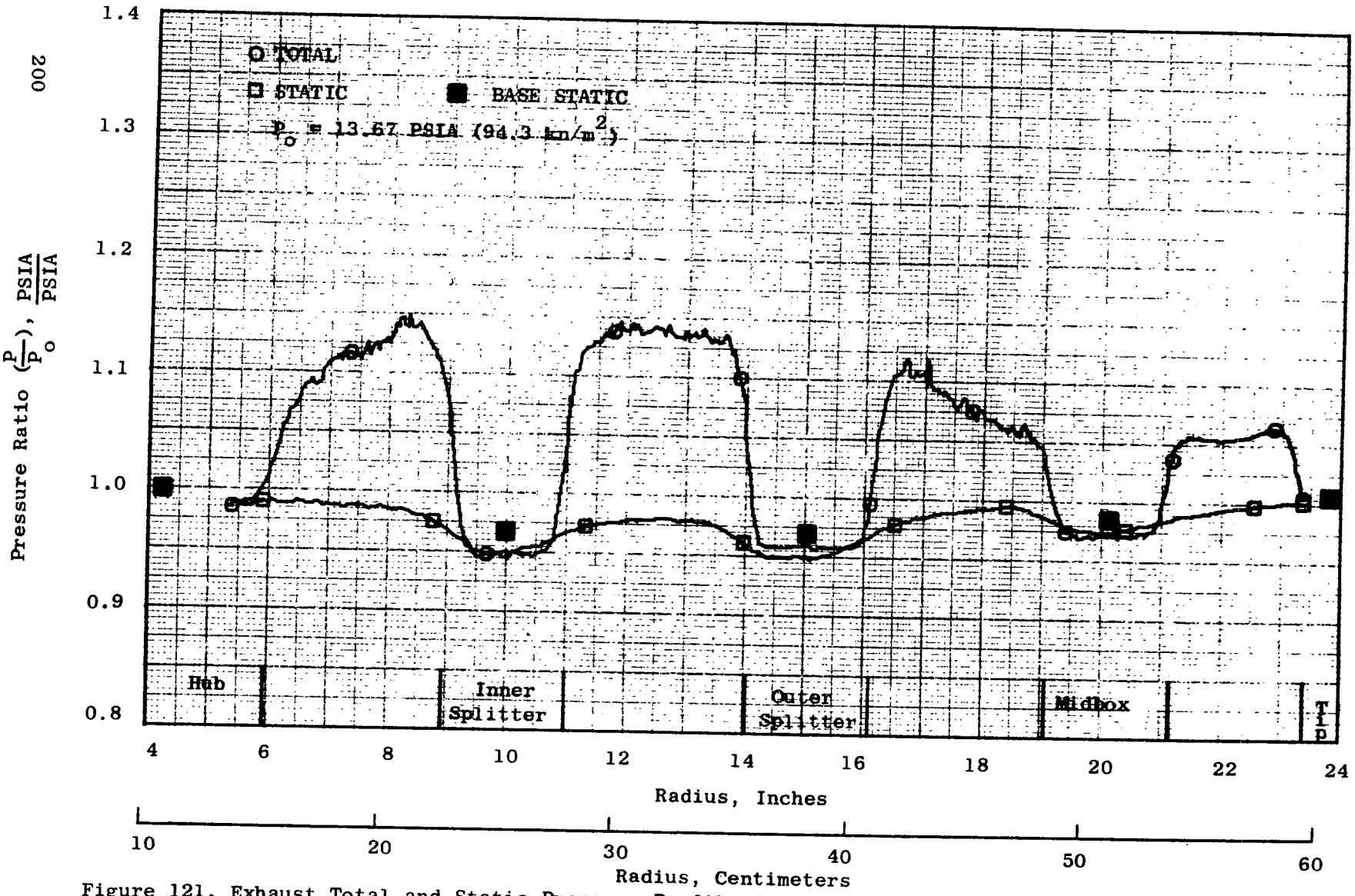

Figure 121. Exhaust Total and Static Pressure Profile for Test 3, Inlet Box and 10 Inches (25.4 cm) of Exhaust Suppression with Airfoiled Blockage, N_f/θ = 4250

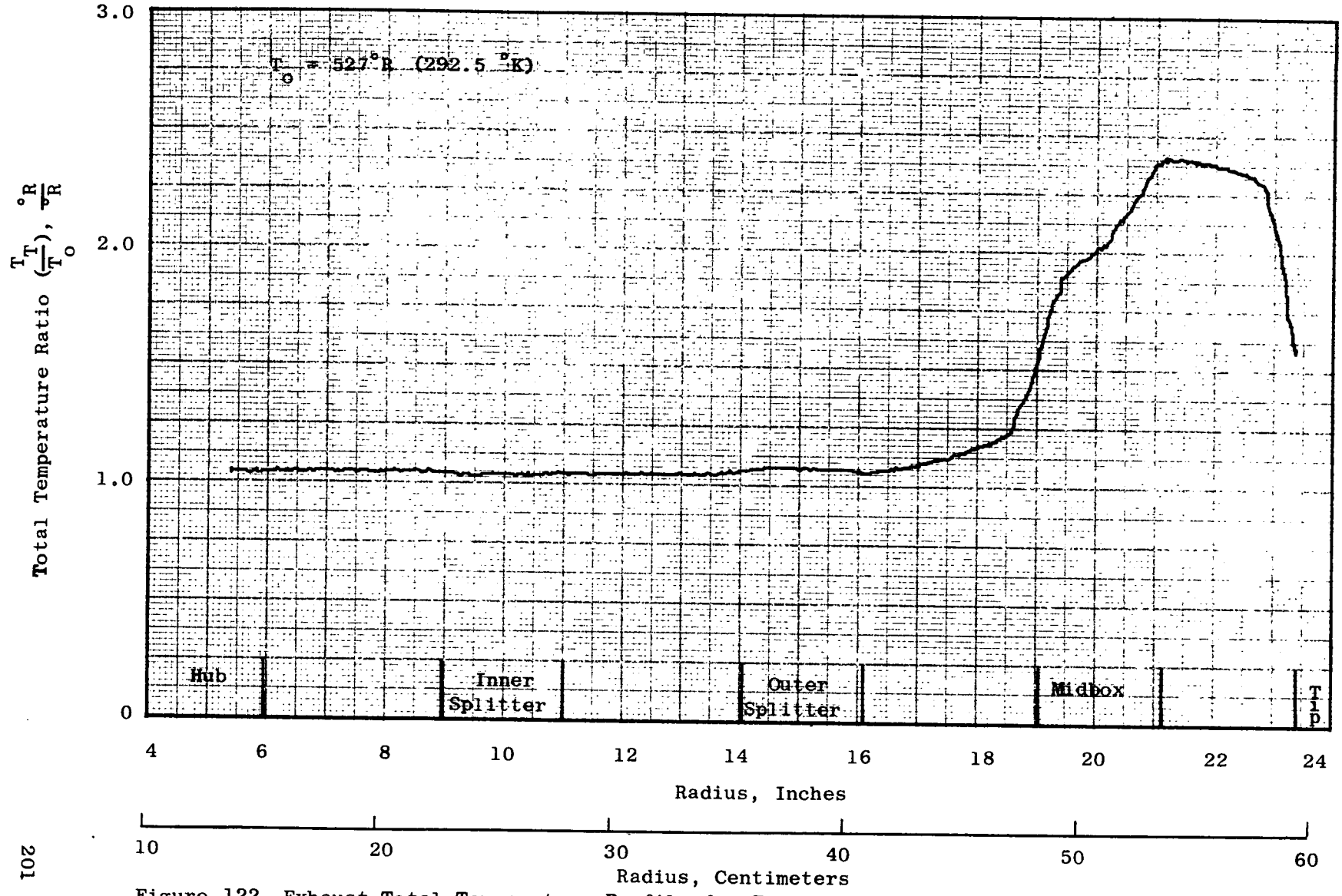

Figure 122. Exhaust Total Temperature Profile for Test 3, Inlet Box and 10 Inches (25.4 cm) of Exhaust Suppression with Airfoiled Blockage, $N_f\sqrt{\theta}$ = 4250

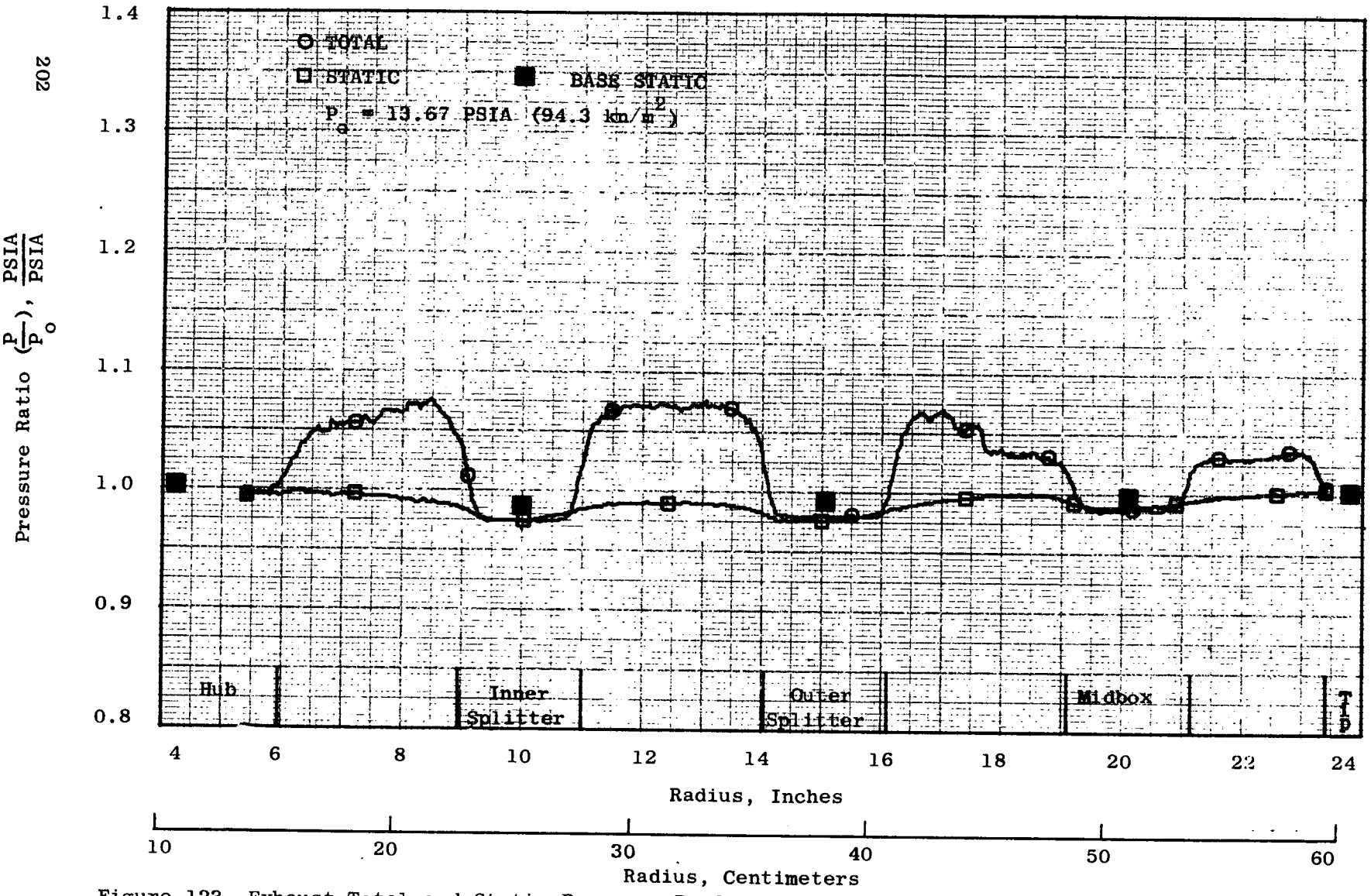

Figure 123. Exhaust Total and Static Pressure Profile for Test 3, Inlet Box and 10 Inches (25.4 cm) of Exhaust Suppression with Airfoiled Blockage, N_f/θ =3020

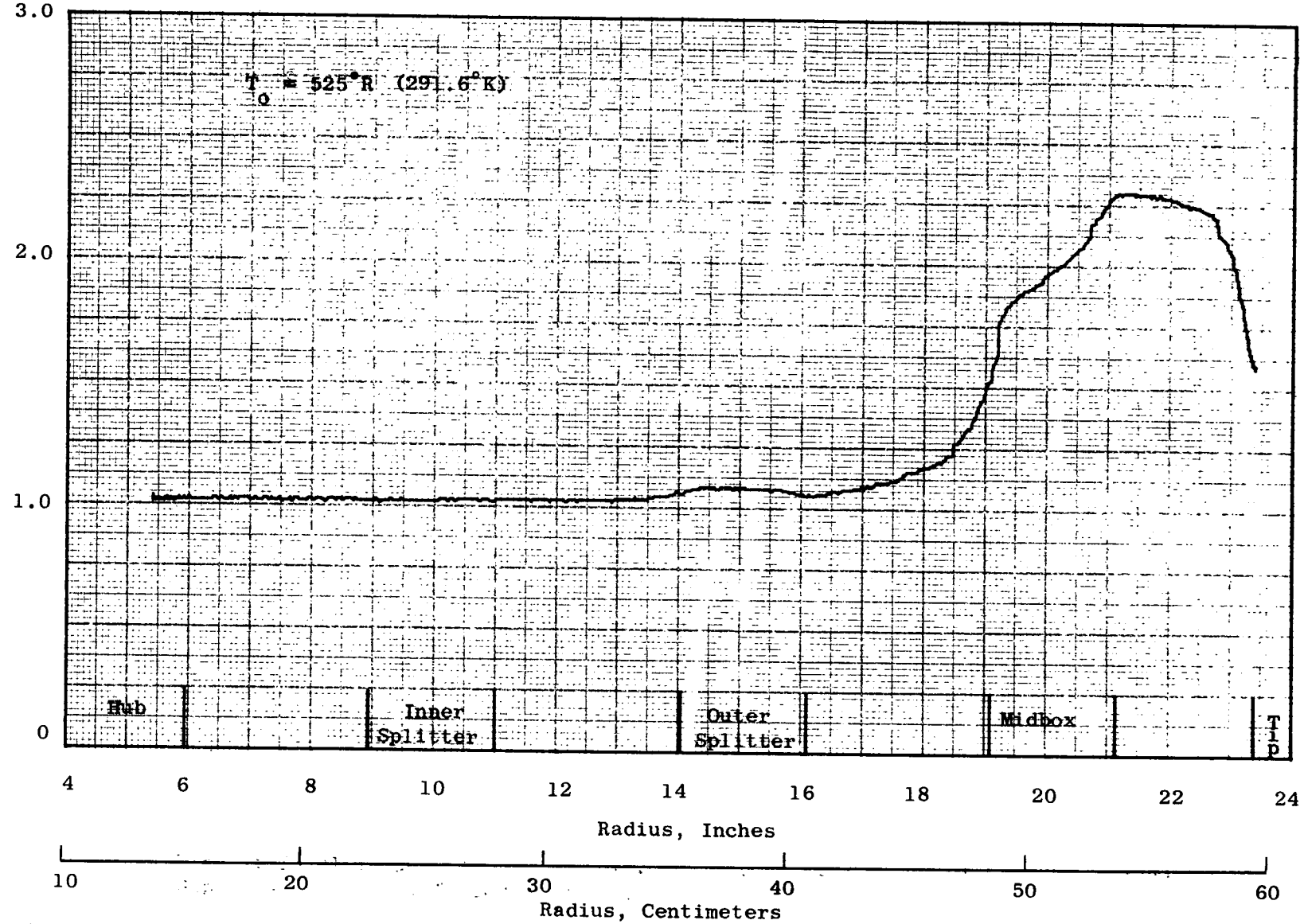

Figure 124. Exhaust Total Temperature Profile for Test 3, Inlet Box and 10 Inches (25.4 cm) of Exhaust Suppression with Airfoiled Blockage, $N_f/\sqrt{\theta}$ = 3020

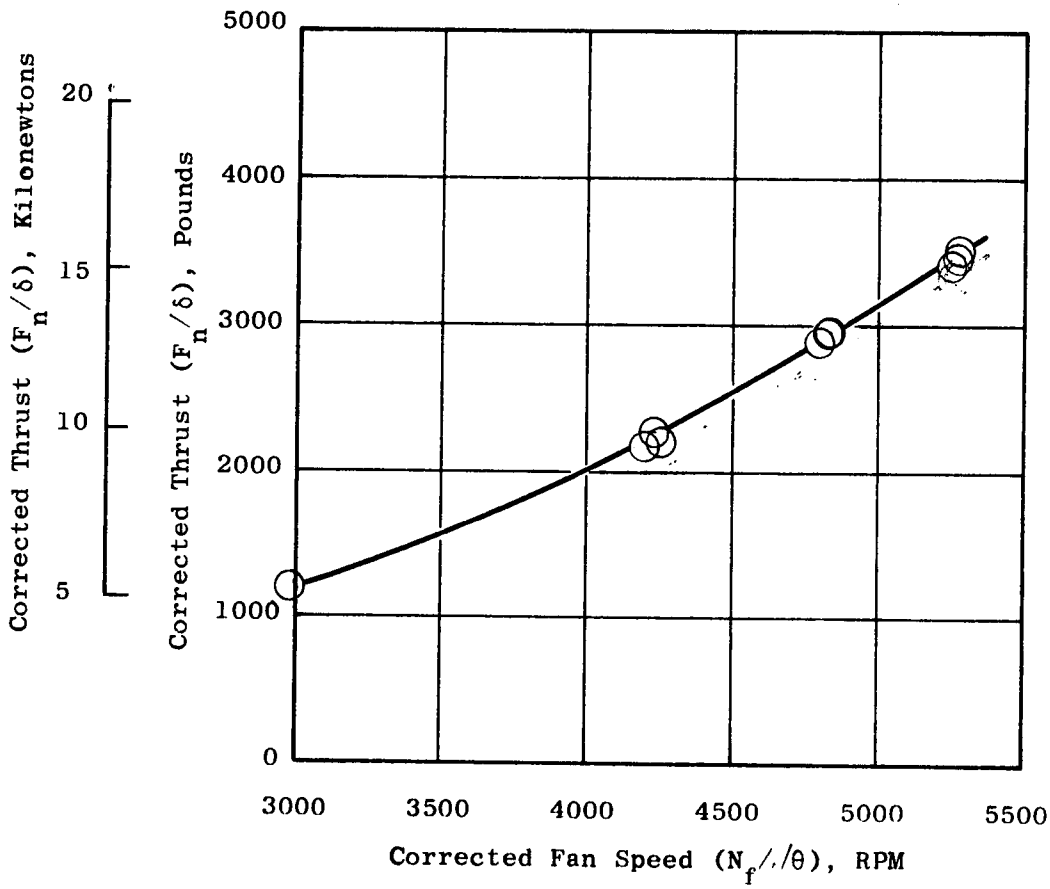

Figure 125. Thrust Variation with Fan Speed for Test 3, Inlet Box and 10 Inches (25.4 cm) of Exhaust Suppression with U-Channeled Blockage

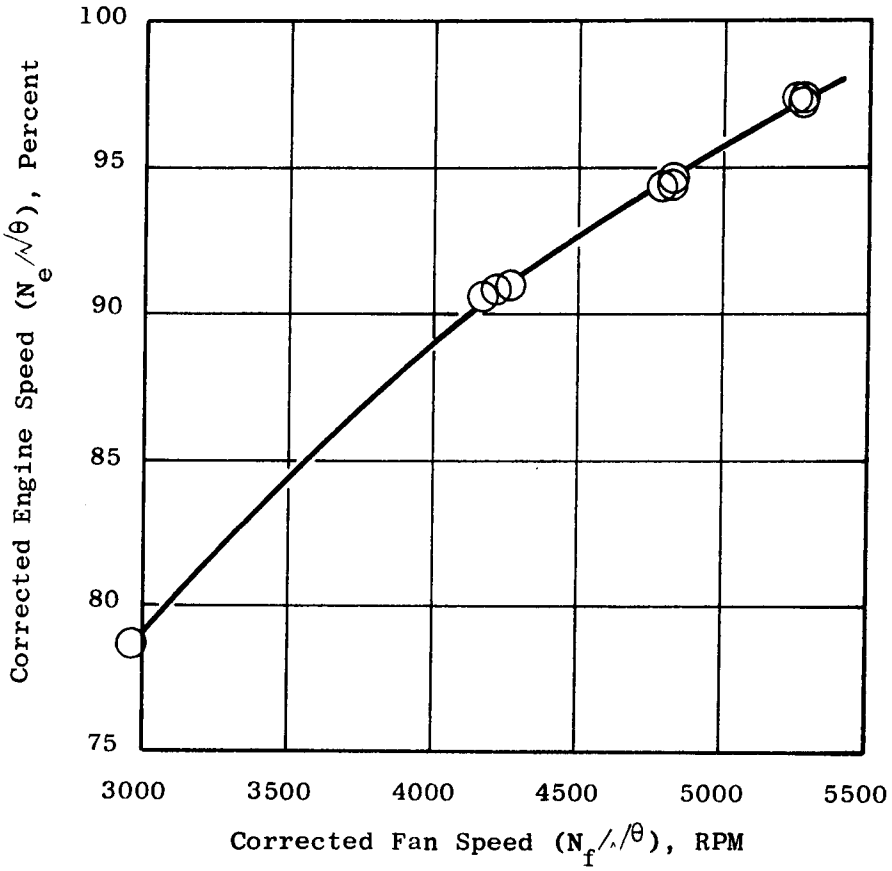

Figure 126, Engine Speed Variation with Fan Speed for Test 3, Inlet Box and 10 Inches (25.4 cm) of Exhaust Suppression with U-Channeled Blockage

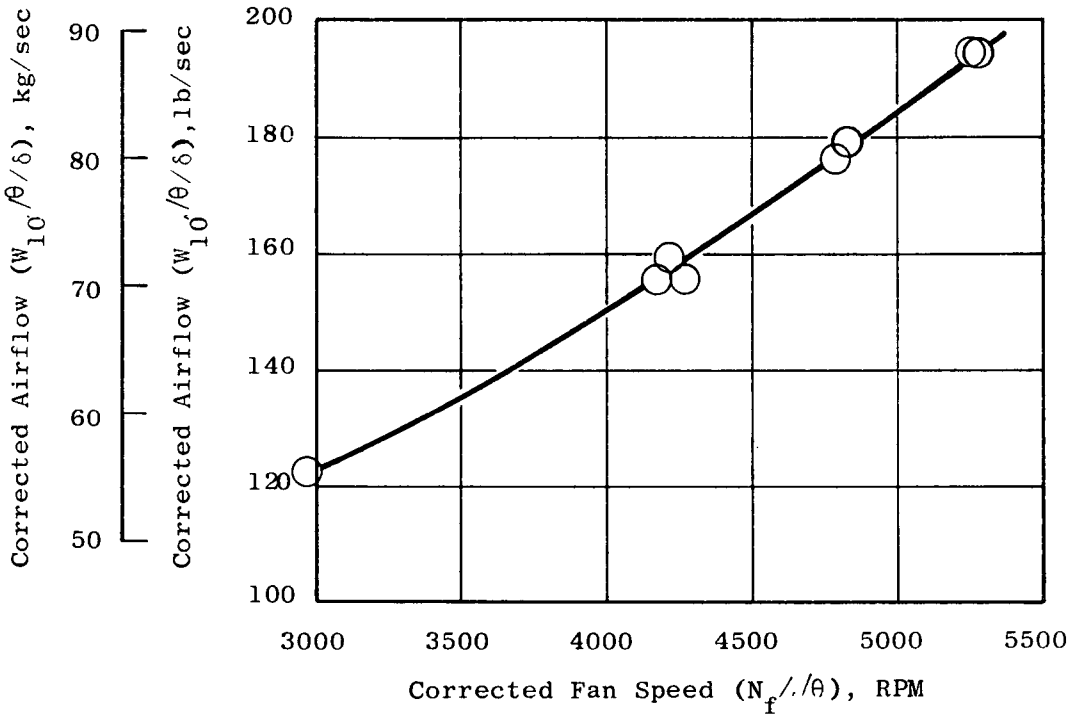

Figure 127. Airflow variation with Fan Speed for Test 3, Inlet Box and 10 Inches (25.4 cm) of Exhaust Suppression with U-Channeled Blockage

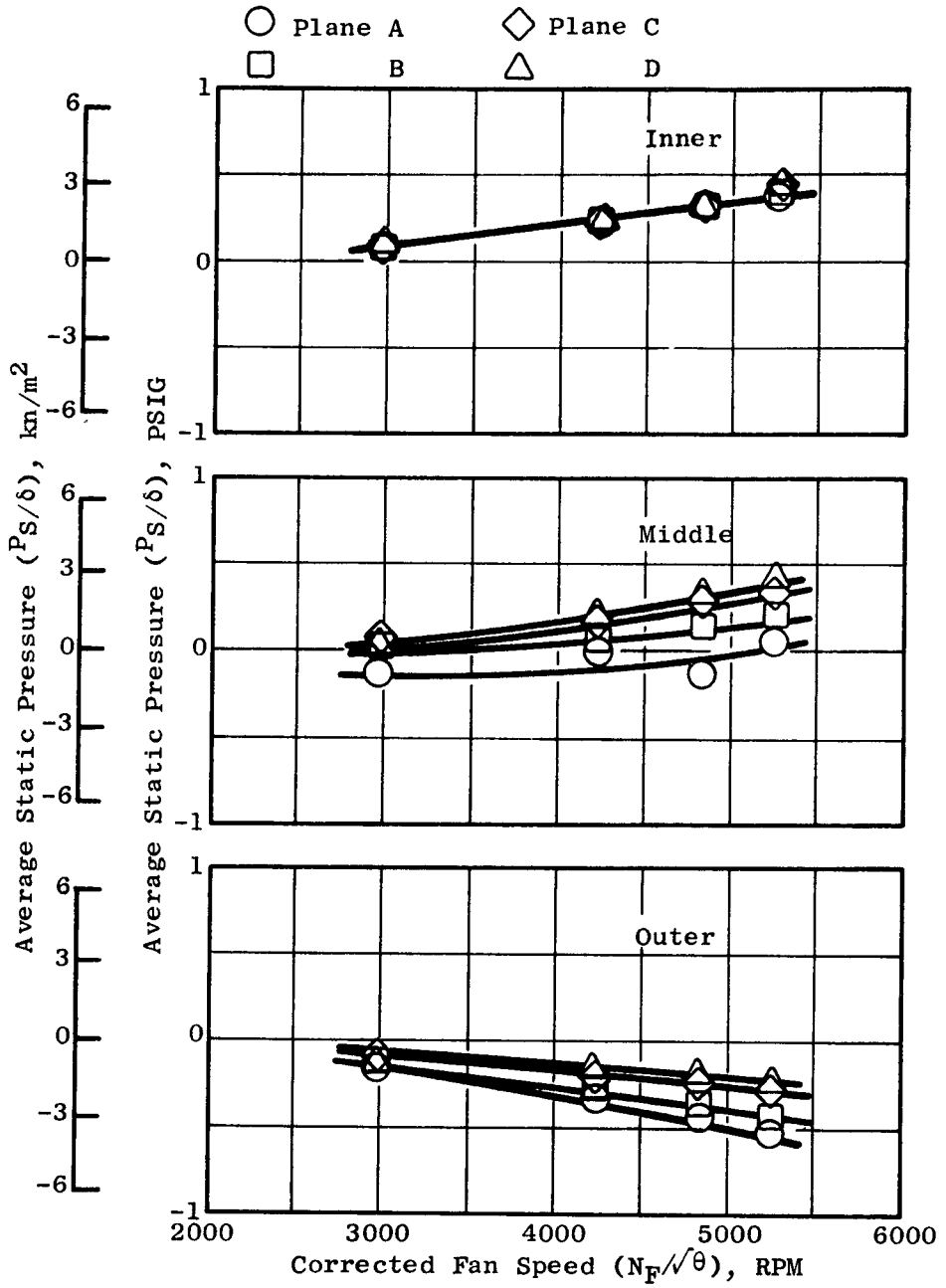

Figure 128. Adapter Section Average Wall Static Pressure Distribution for Test 3, Inlet Box and 10 Inches (25.4 cm) of Exhaust Suppression with U-Channeled Blockage

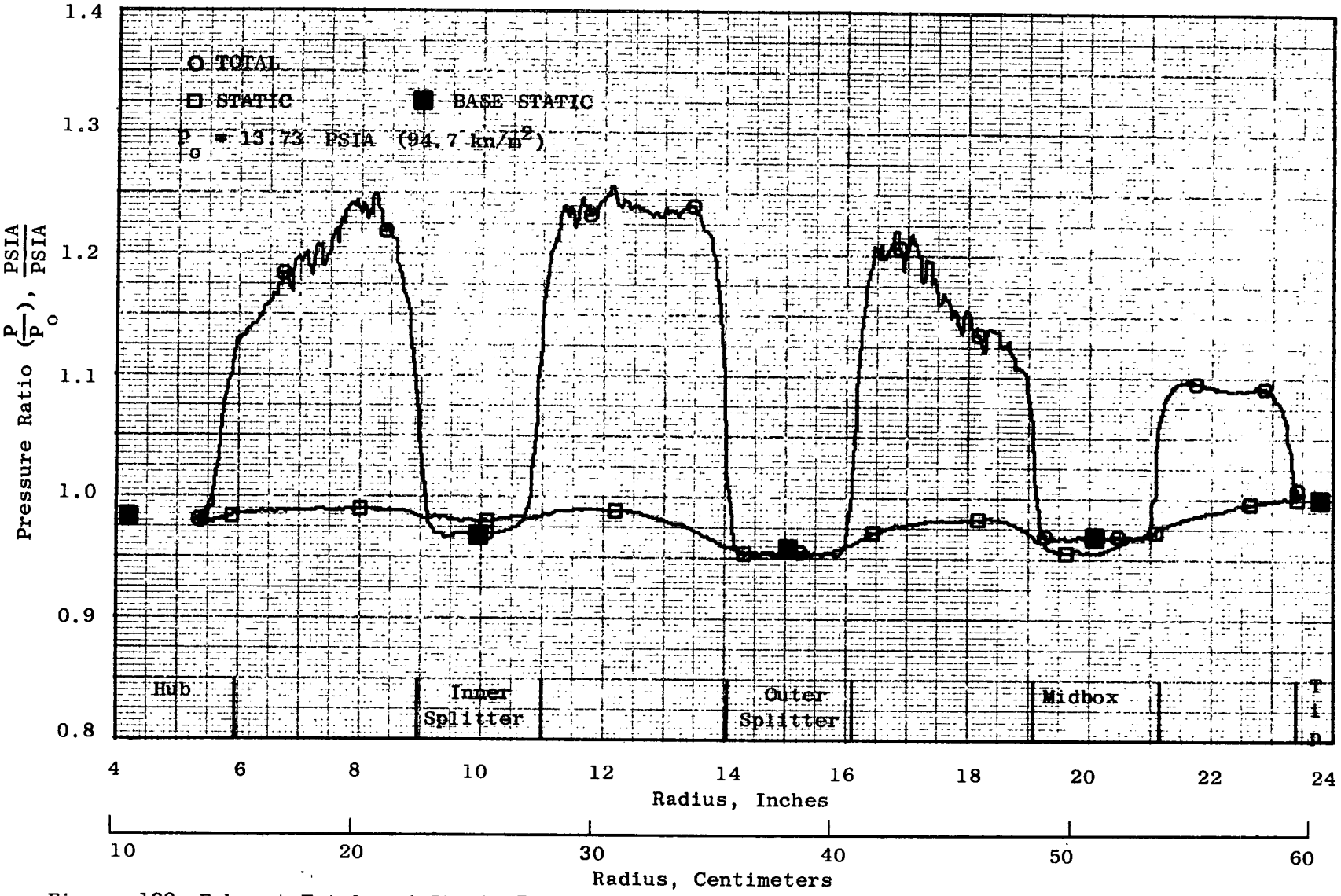

Figure 129. Exhaust Total and Static Pressure Profile for Test 3, Inlet Box and 10 Inches (25.4 cm) of Exhaust Suppression with U-Channeled Blockage, N_f/A = 5285

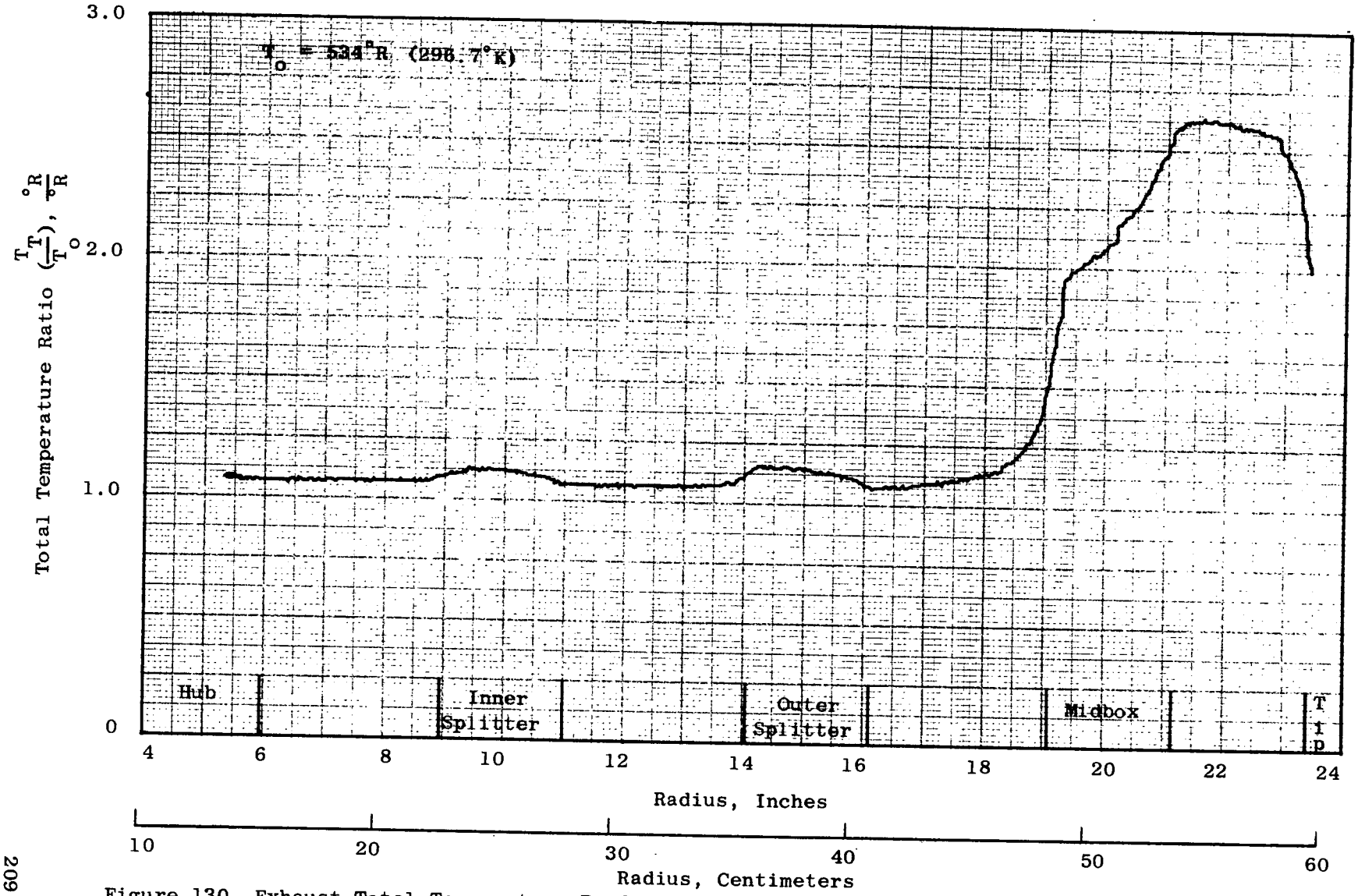

Figure 130. Exhaust Total Temperature Profile for Test 3, Inlet Box and 10 Inches (25.4 cm) of Exhaust Suppression with U-Channeled Blockage, $N_f/\sqrt{\theta}$ = 5285

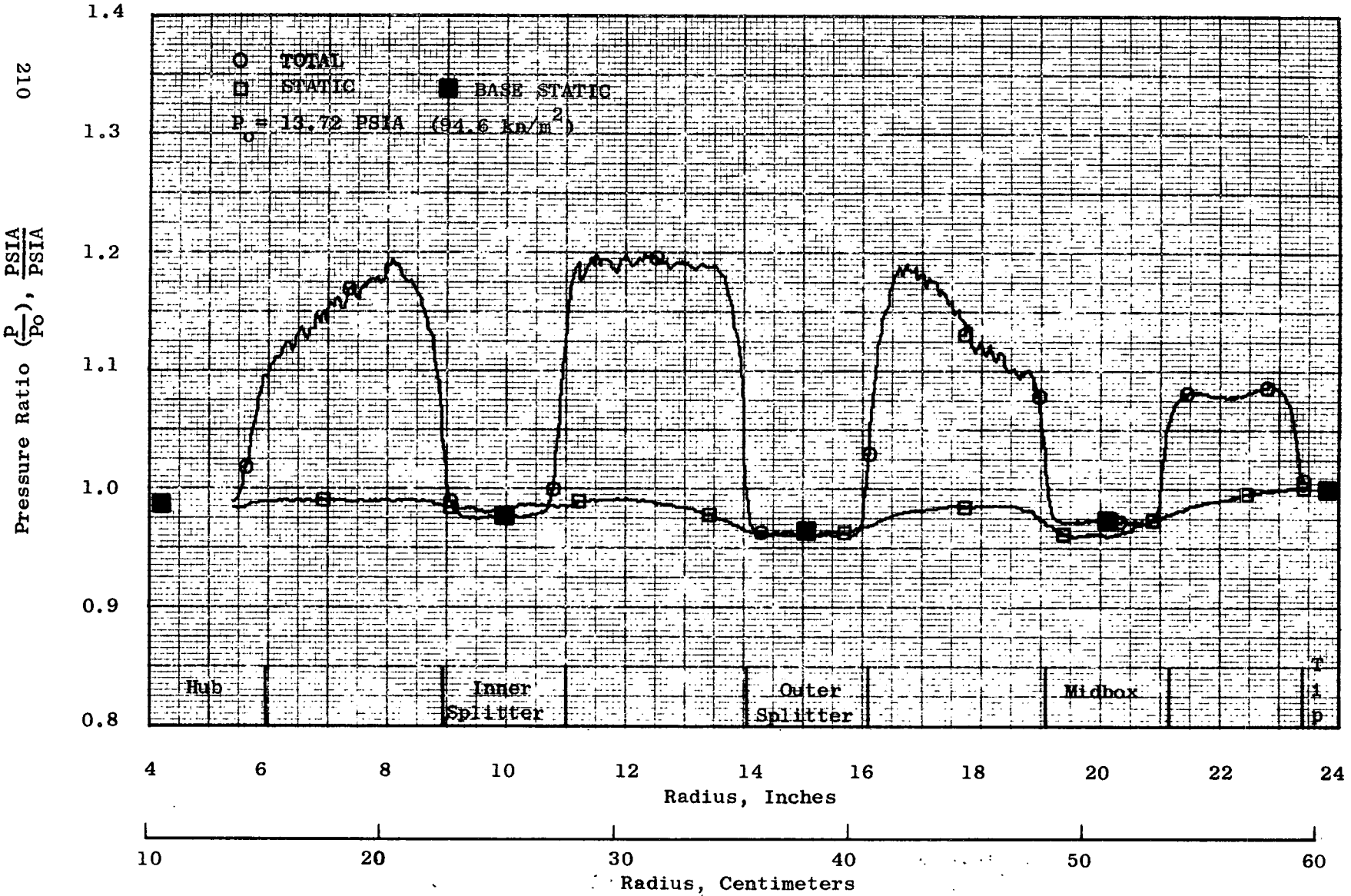

Figure 131. Exhaust Total and Static Pressure Profile for Test 3, Inlet Box and 10 Inches (25.4 cm) of Exhaust Suppression with U-Channeled Blockage, N_f/θ = 4830

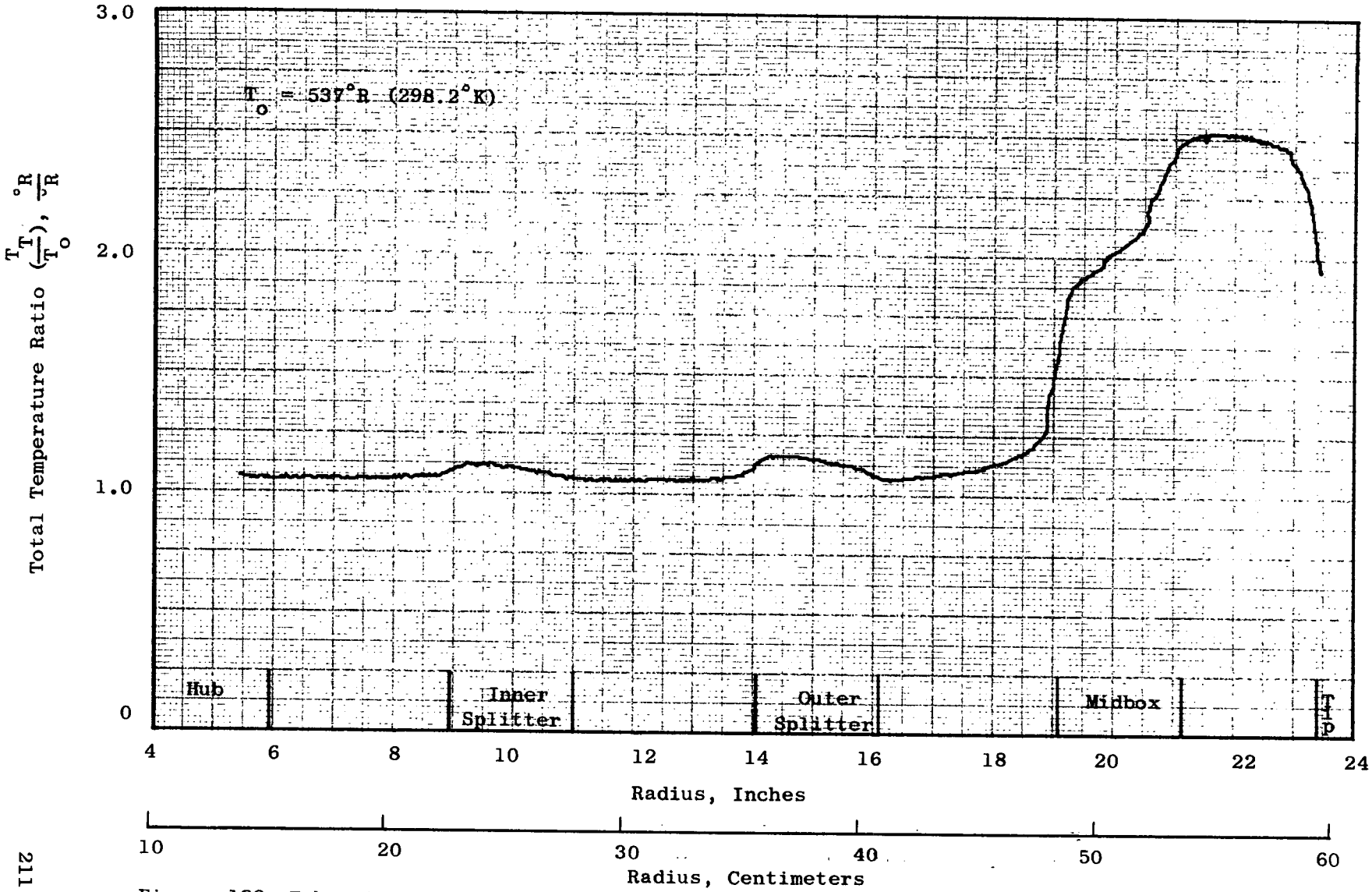

Figure 132. Exhaust Total Temperature Profile for Test 3, Inlet Box and 10 Inches (25.4 cm) of Exhaust Suppression with U-Channeled Blockage, N_f/θ = 4830

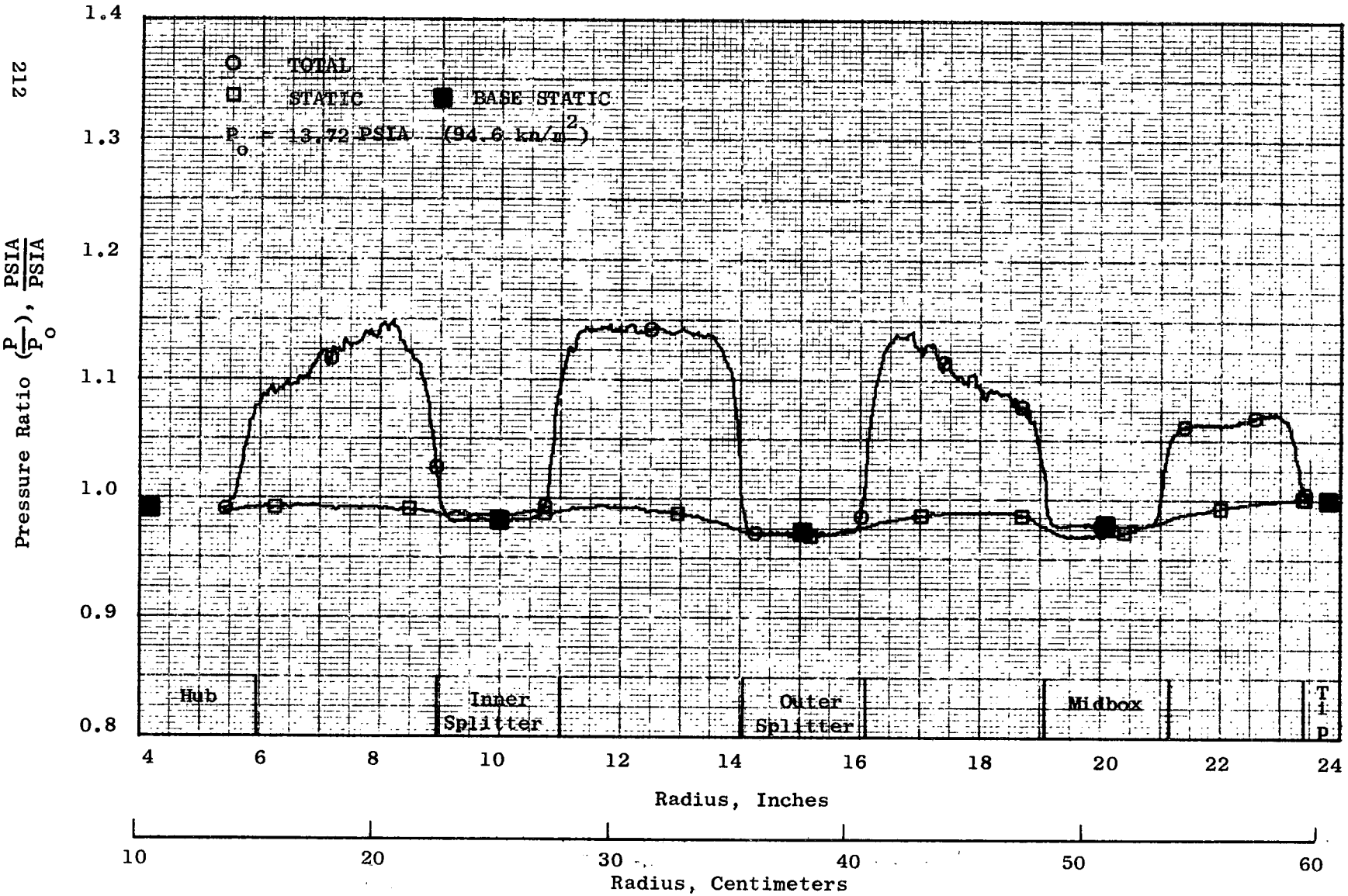

Figure 133. Exhaust Total and Static Pressure Profile for Test 3, Inlet Box and 10 Inches (25.4 cm) of Exhaust Suppression with U-Channeled Blockage $N_f/\lambda/\theta$ =4230

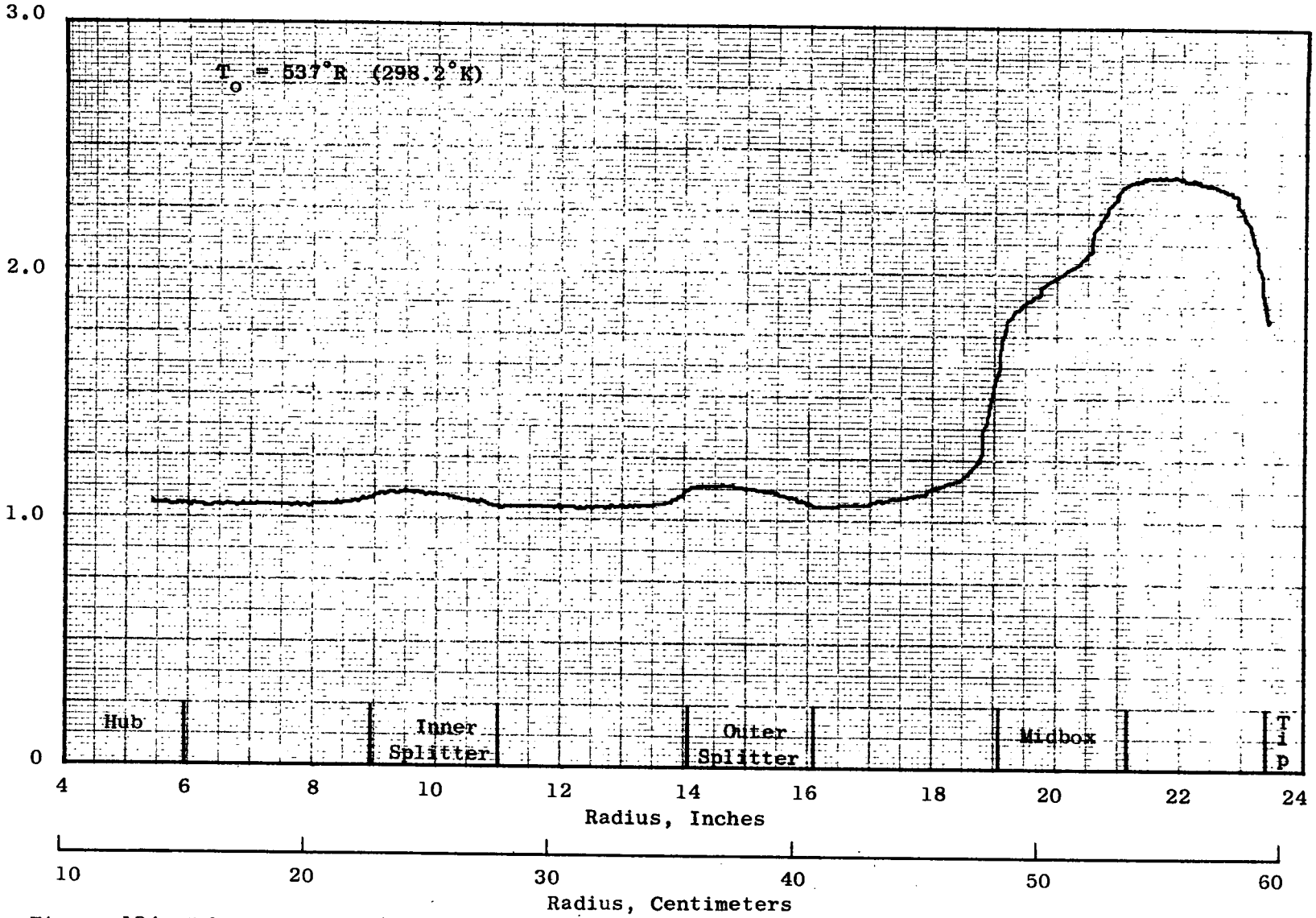

Figure 134. Exhaust Total Temperature Profile for Test 3, Inlet Box and 10 Inches (25.4 cm) of Exhaust Suppression with U-Channeled Blockage, N_f/θ = 4230

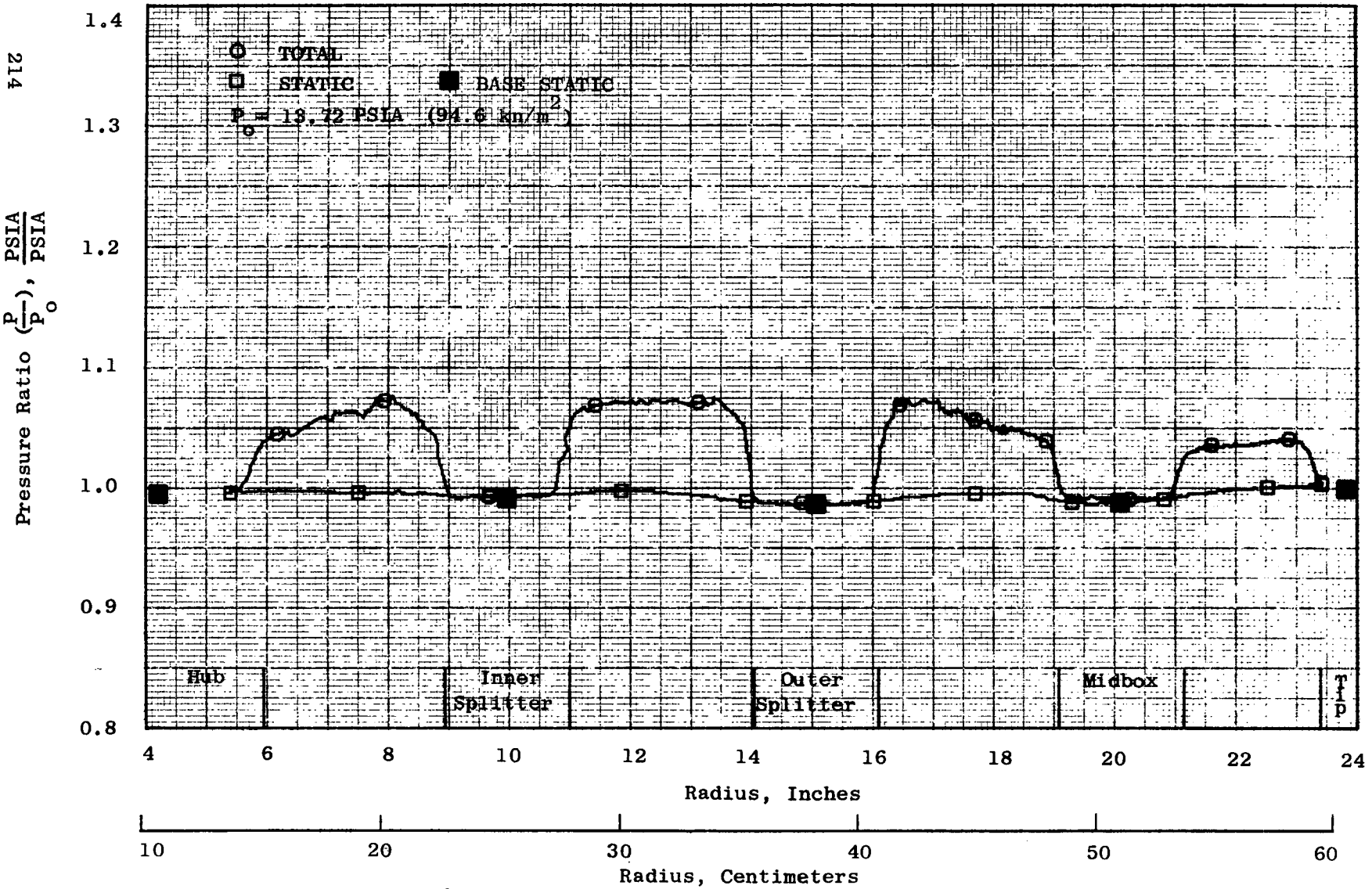

Figure 135. Exhaust Total and Static Pressure Profile for Test 3, Inlet Box and 10 Inches (25.4 cm) of Exhaust Suppression with U-Channeled Blockage, N_f/θ = 2980

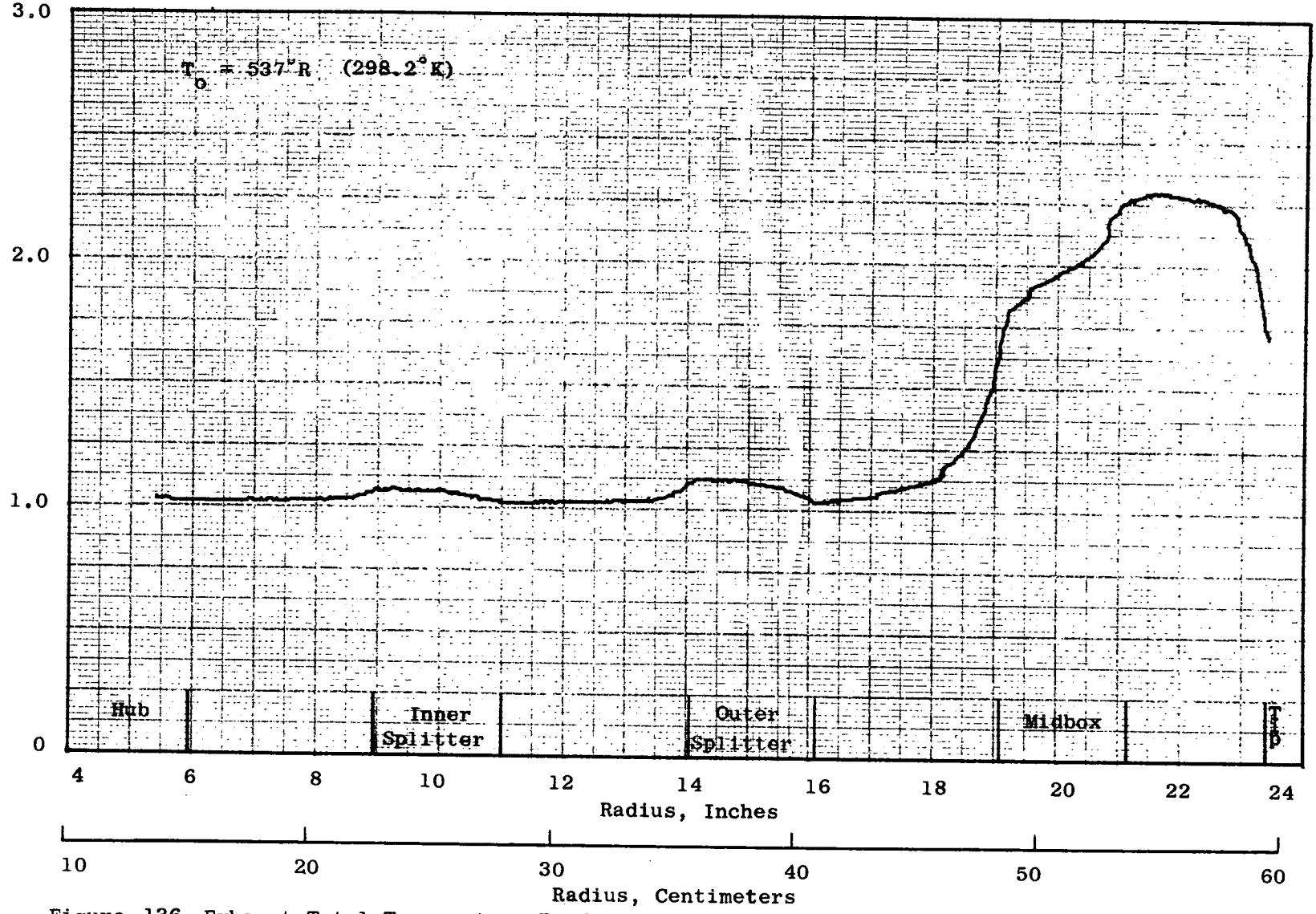

Figure 136. Exhaust Total Temperature Profile for Test 3, Inlet Box and 10 Inches (25.4 cm) of Exhaust Suppression with U-Channeled Blockage, N_f/θ = 2980

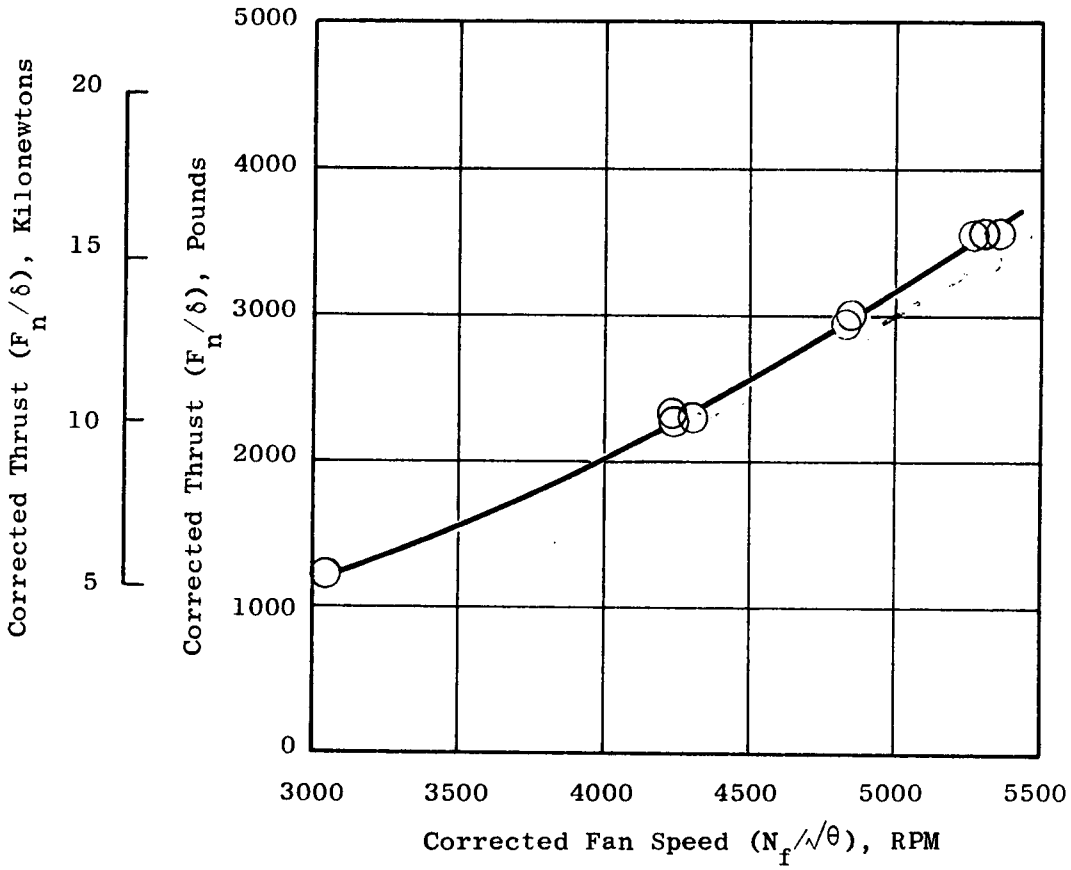

Figure 137. Thrust Variation with Fan Speed for Test 4, Inlet Box and 20 Inches (50.8 cm) of Exhaust Suppression with U-Channeled Blockage

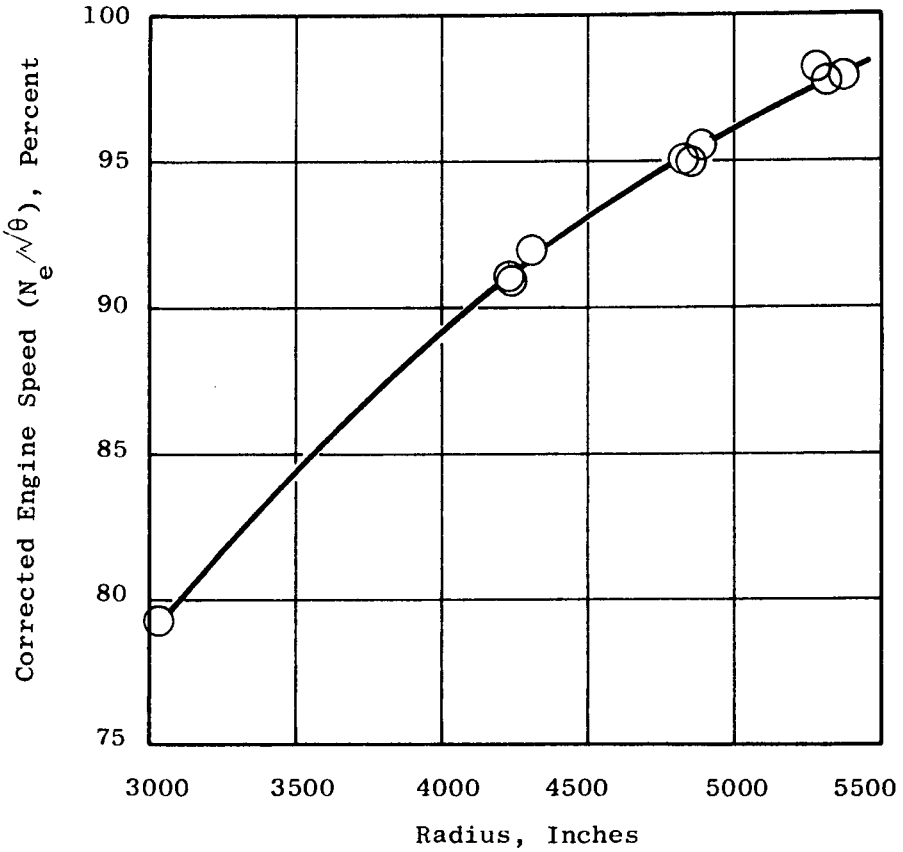

Figure 138. Engine Speed Variation with Fan Speed for Test 4, Inlet Box and 20 Inches (50.8 cm) of Exhaust Suppression with U-Channeled Blockage

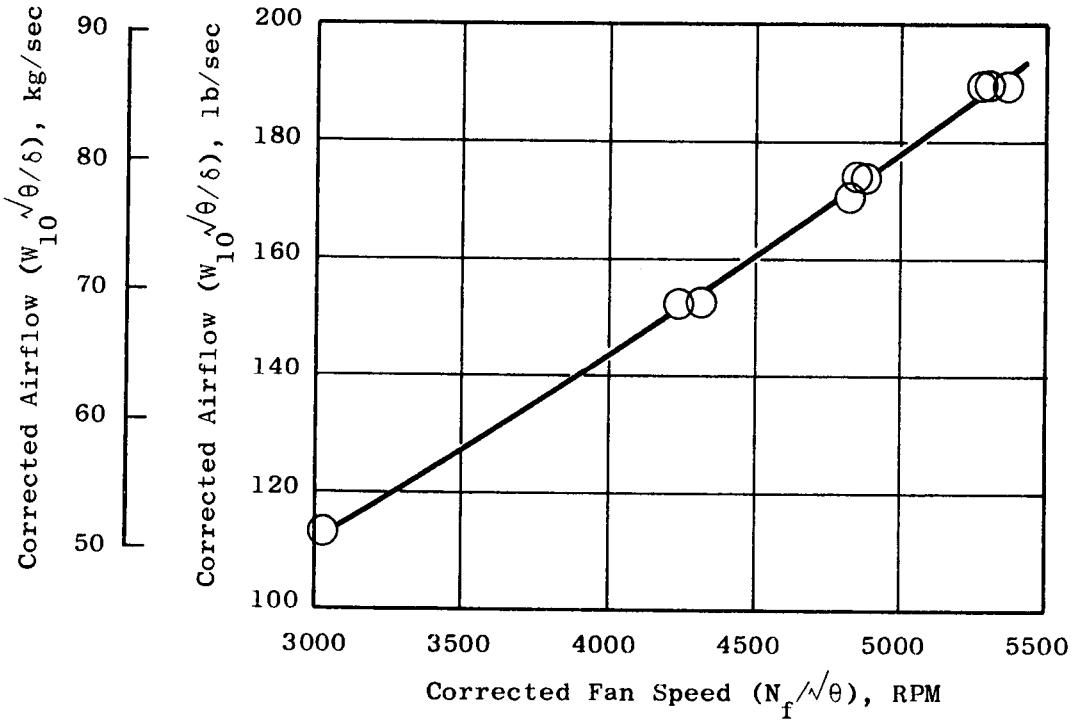

Figure 139. Airflow Variation with Fan Speed for Test 4, Inlet Box and 20 Inches (50.8 cm) of Exhaust Suppression with U-Channeled Blockage

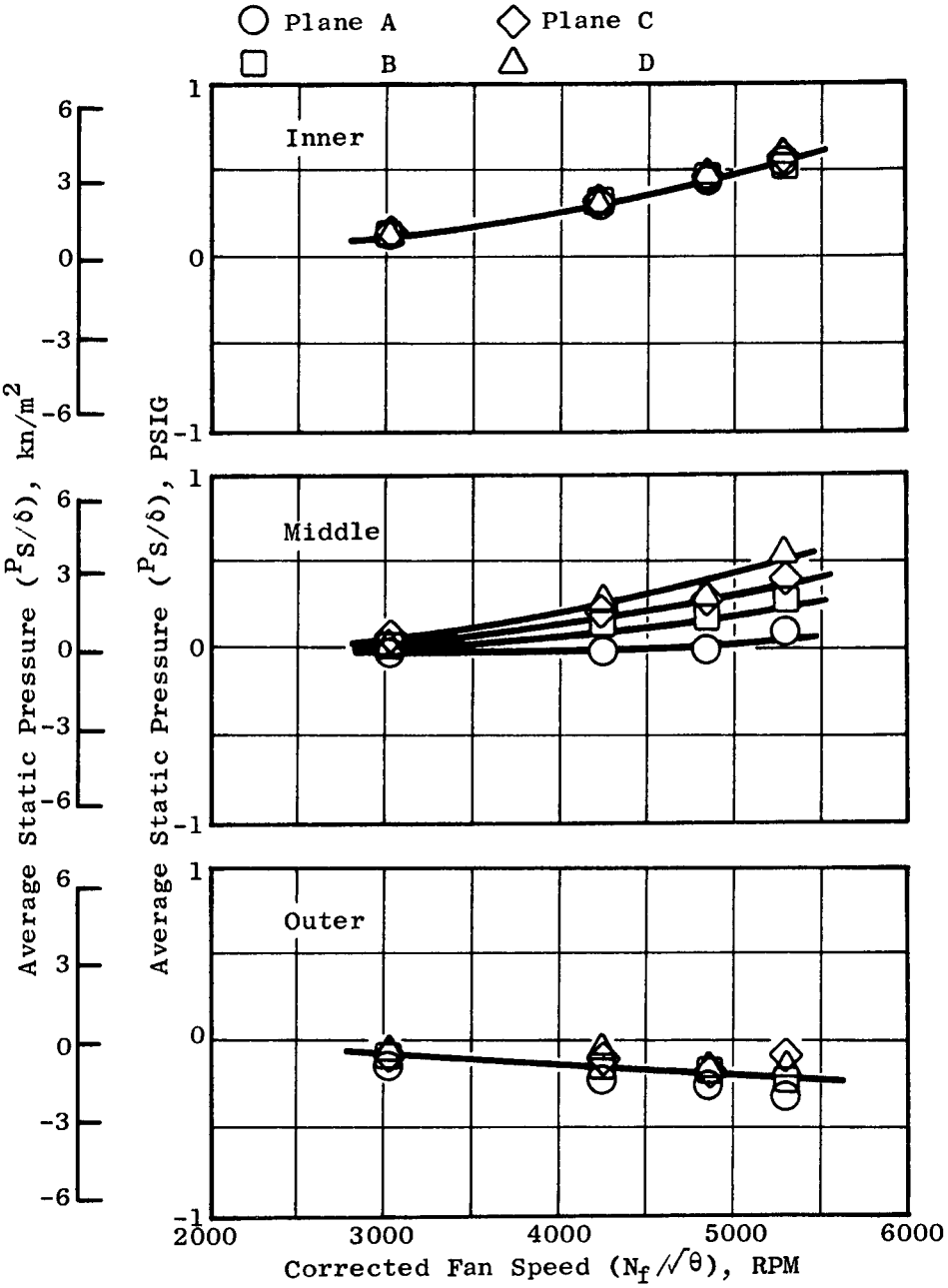

Figure 140. Adapter Section Average Wall Static Pressure Distribution for Test 4, Inlet Box and 20 Inches (50.8 cm) of Exhaust Suppression with U-Channeled Blockage

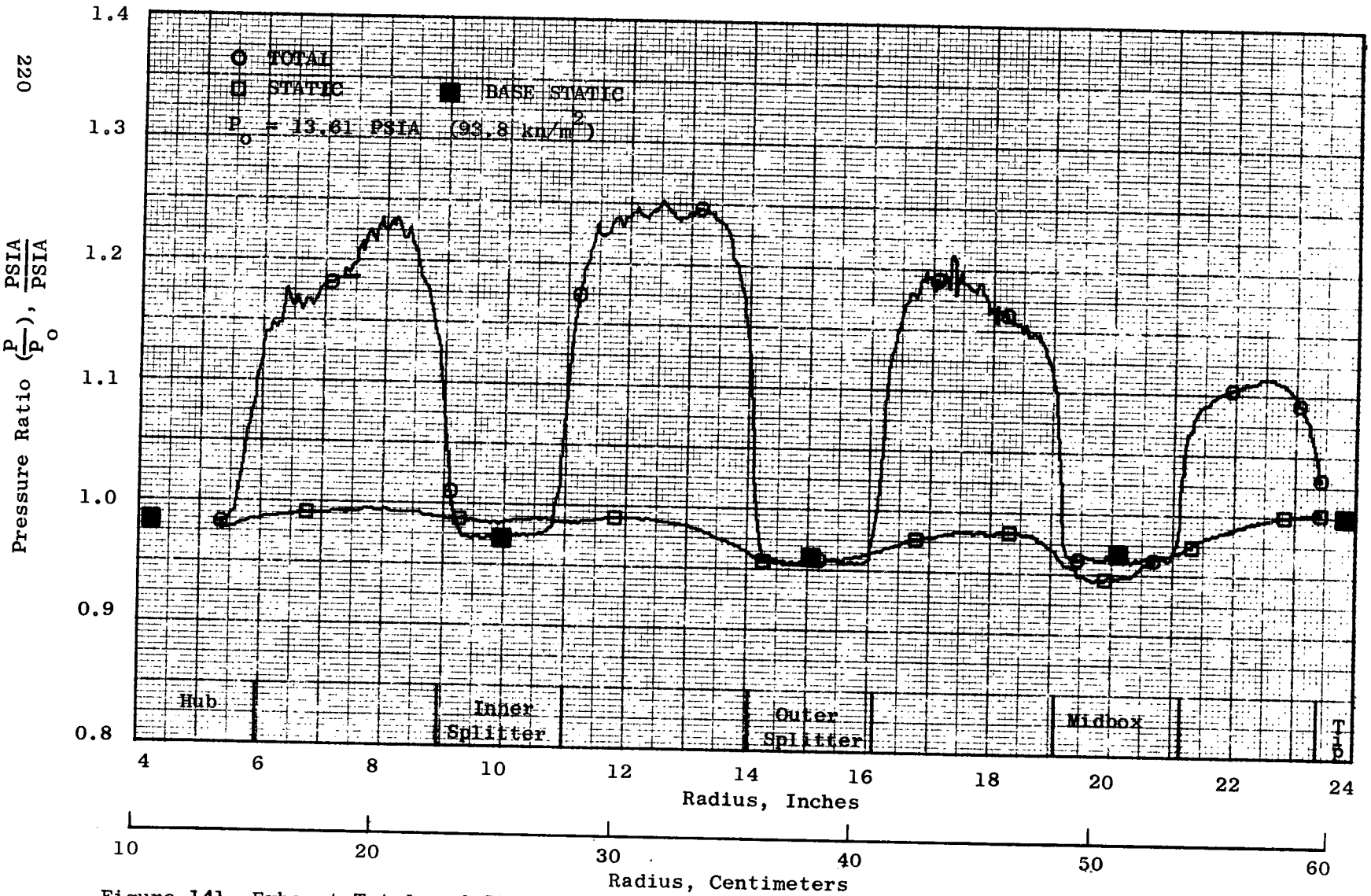

Figure 141. Exhaust Total and Static Pressure Profile for Test 4, Inlet Box and 20 Inches (50.8 cm) of Exhaust Suppression with U-Channeled Blockage, N_f/θ = 5300

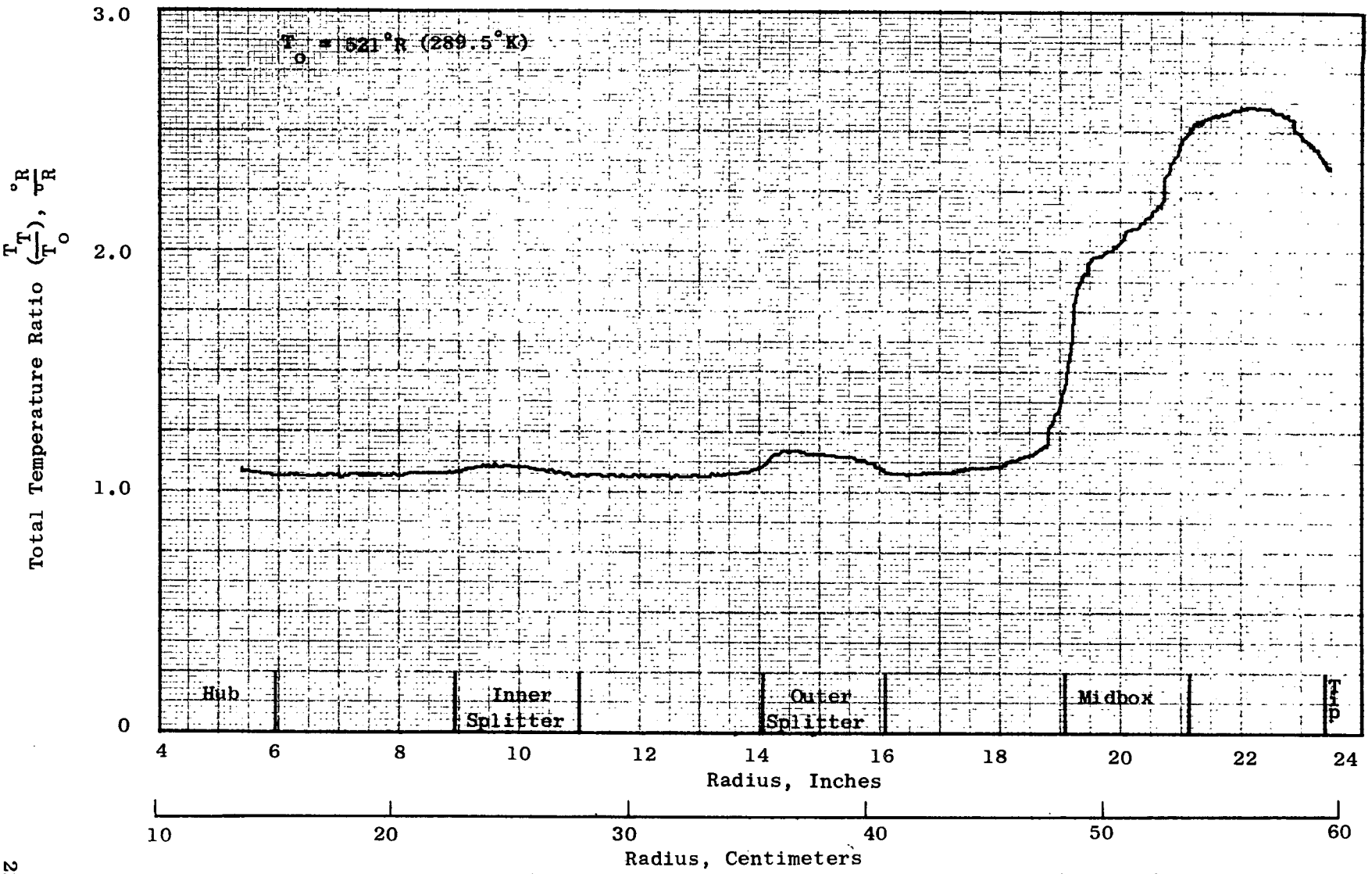

Figure 142. Exhaust Total Temperature Profile for Test 4, Inlet Box and 20 Inches (50.8 cm) of Exhaust Suppression with U-Channeled Blockage, $N_f/\sqrt{\theta}$ = 5300

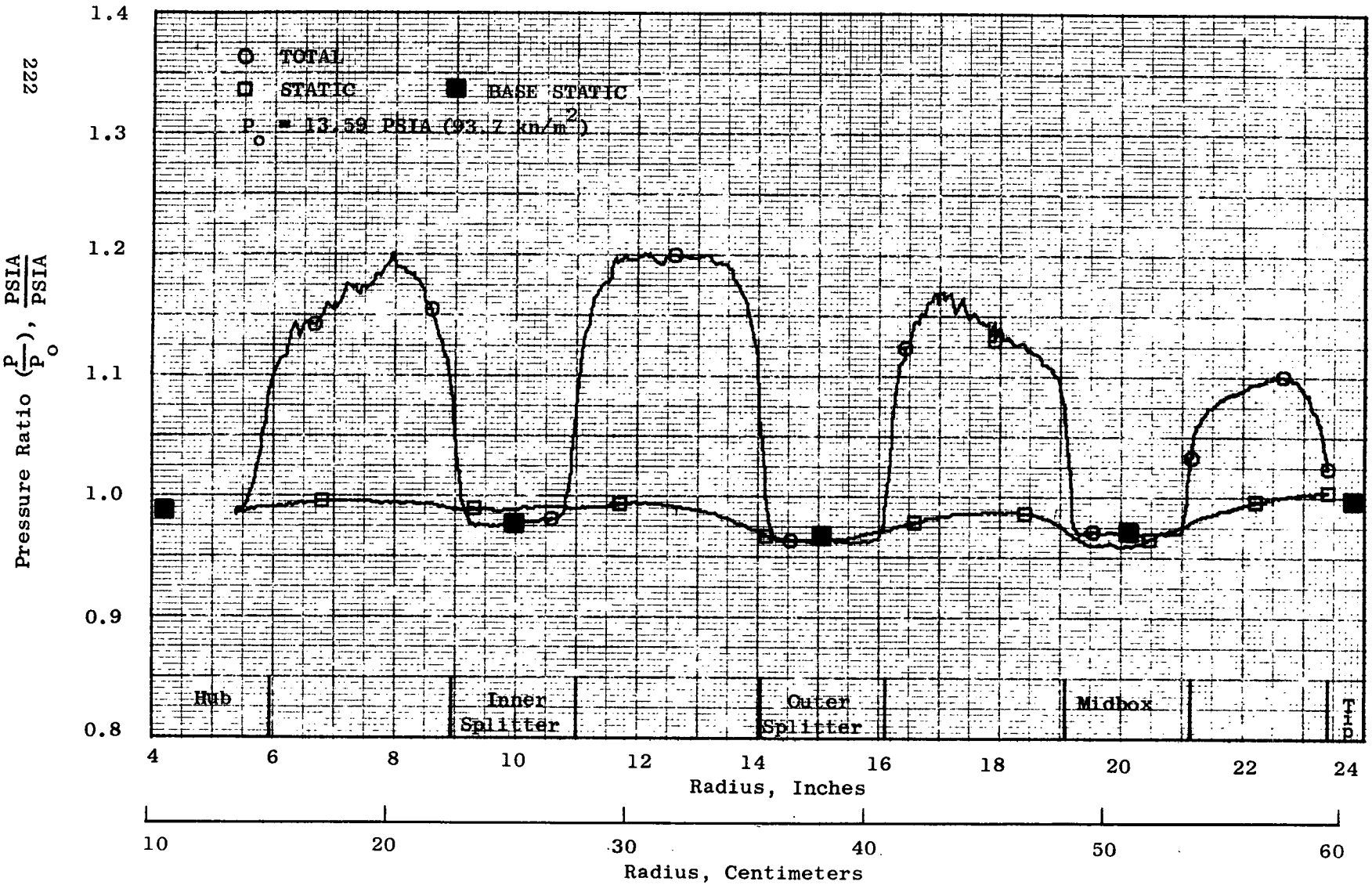

Figure 143. Exhaust Total and Static Pressure Profile for Test 4, Inlet Box and 20 Inches (50.8 cm) of Exhaust Suppression with U-Channeled Blockage, $N_f/\sqrt{\theta}$ = 4850

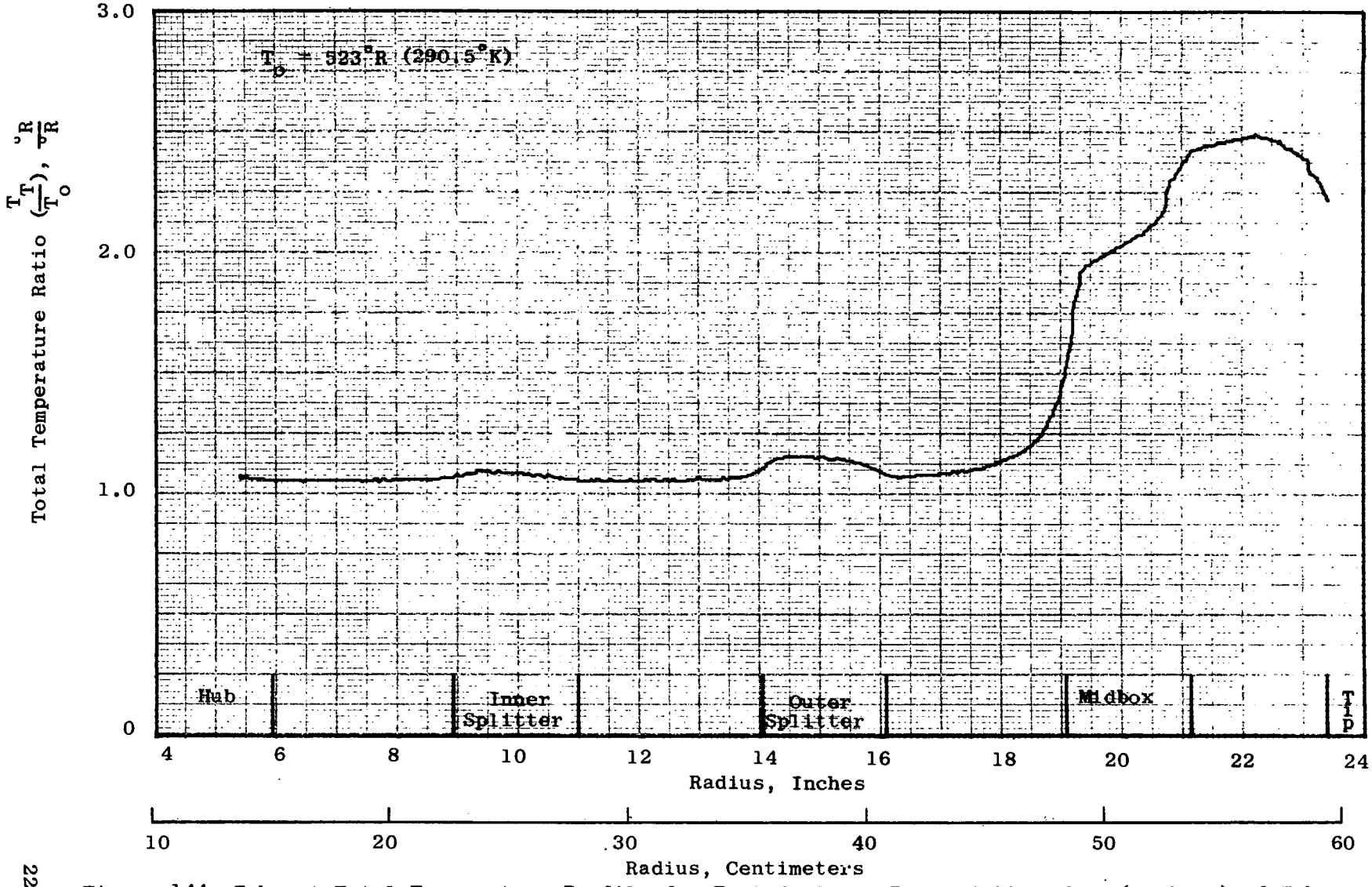

Figure 144. Exhaust Total Temperature Profile for Test 4, Inlet Box and 20 Inches (50.8 cm) of Exhaust Suppression with U-Channeled Blockage, N_f/θ = 4850

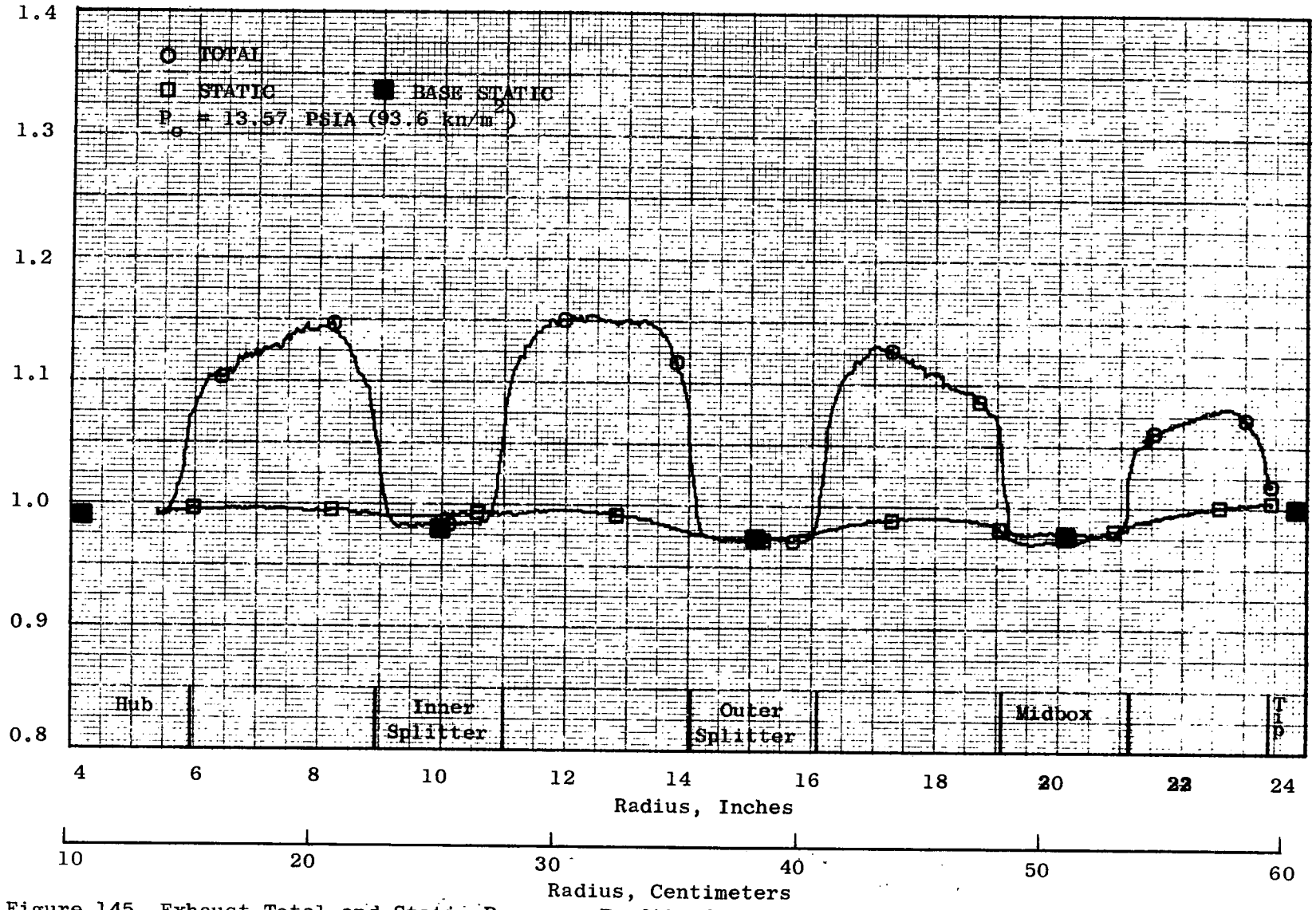

Figure 145. Exhaust Total and Static Pressure Profile for Test 4, Inlet Box and 20 Inches (50.8 cm) of Exhaust Suppression with U-Channeled Blockage, N_f/θ = 4260

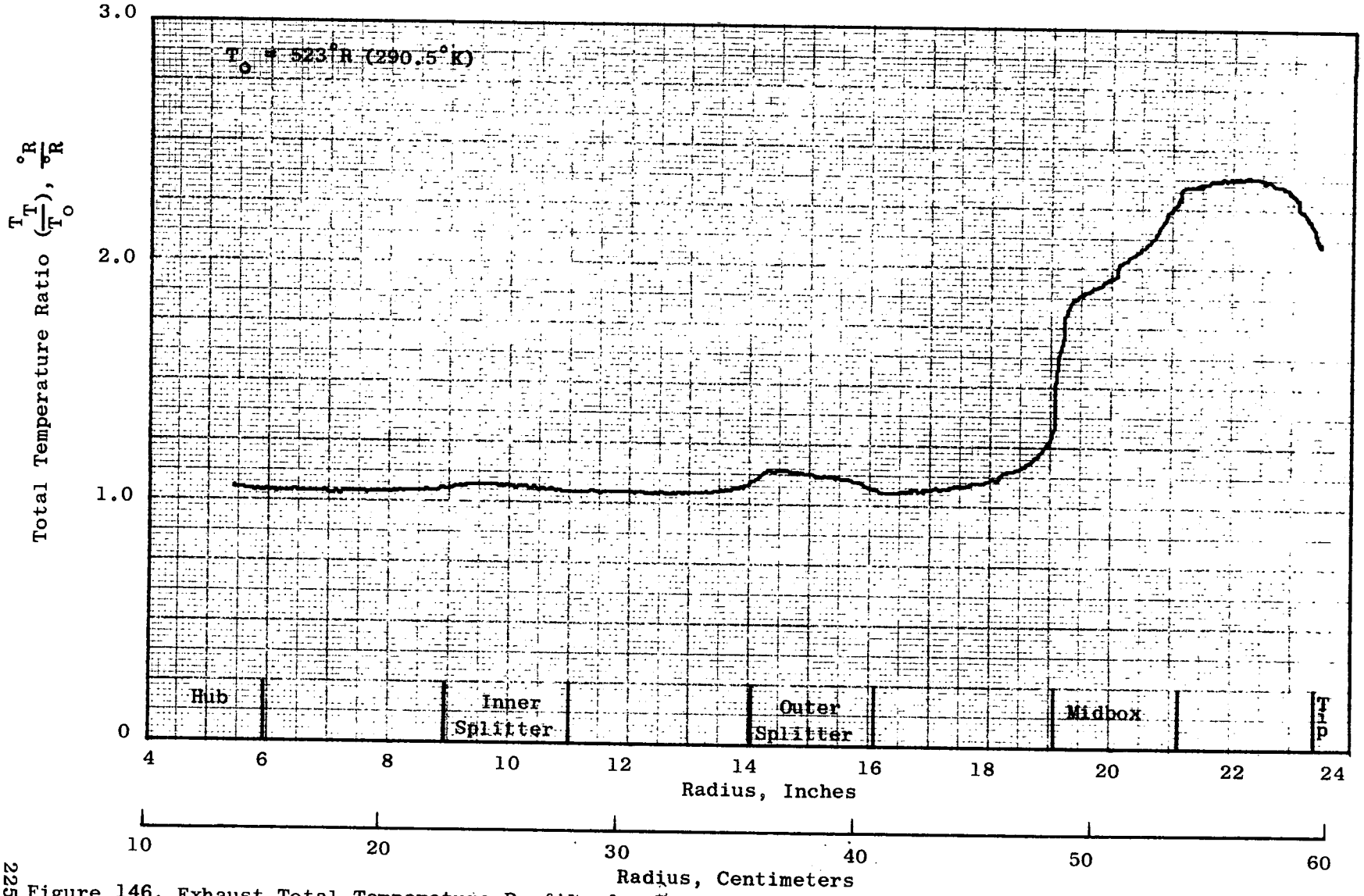

Figure 146. Exhaust Total Temperature Profile for Test 4, Inlet Box and 20 Inches (50.8 cm) of Exhaust Suppression with U-Channeled Blockage, N_f/θ = 4260

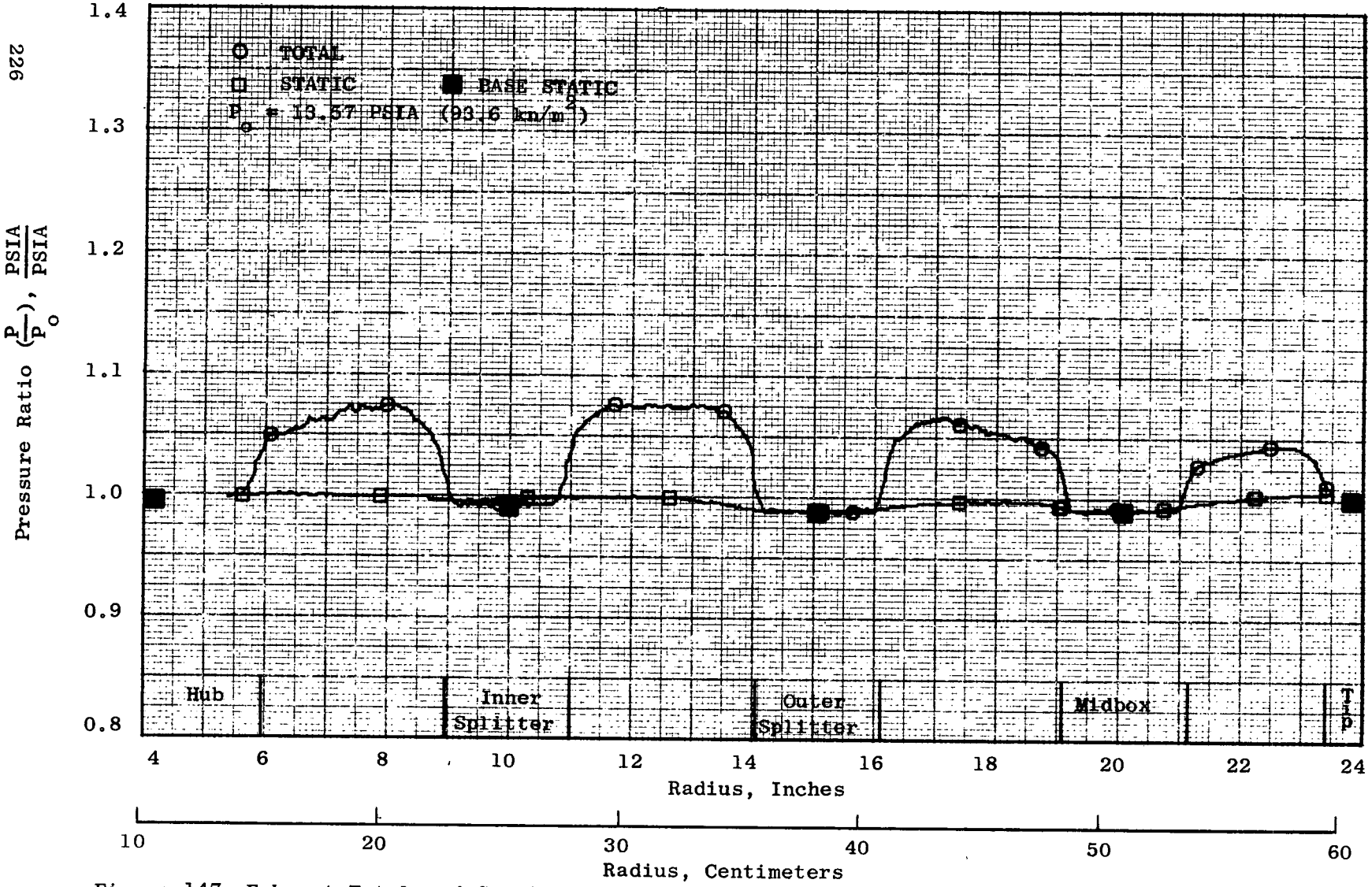

Figure 147. Exhaust Total and Static Pressure Profile for Test 4, Inlet Box and 20 Inches (50.8 cm) of Exhaust Suppression with U-Channeled Blockage, $N_f/\sqrt{\theta}$ = 3040

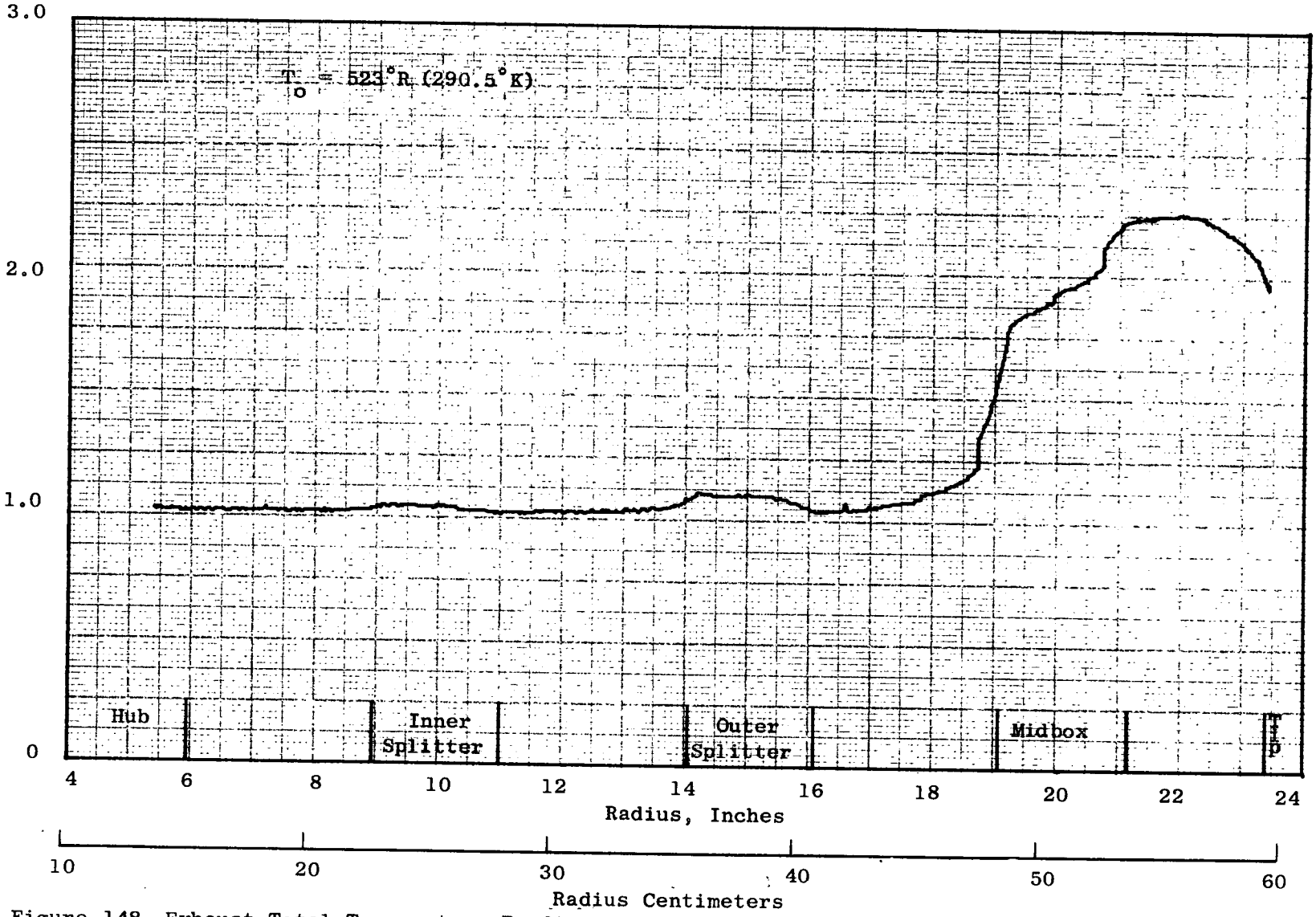

Figure 148. Exhaust Total Temperature Profile for Test 4, Inlet Box and 20 Inches (50.8 cm) of Exhaust Suppression with U-Channeled Blockage, $N_f/\sqrt{\theta}$ = 3040

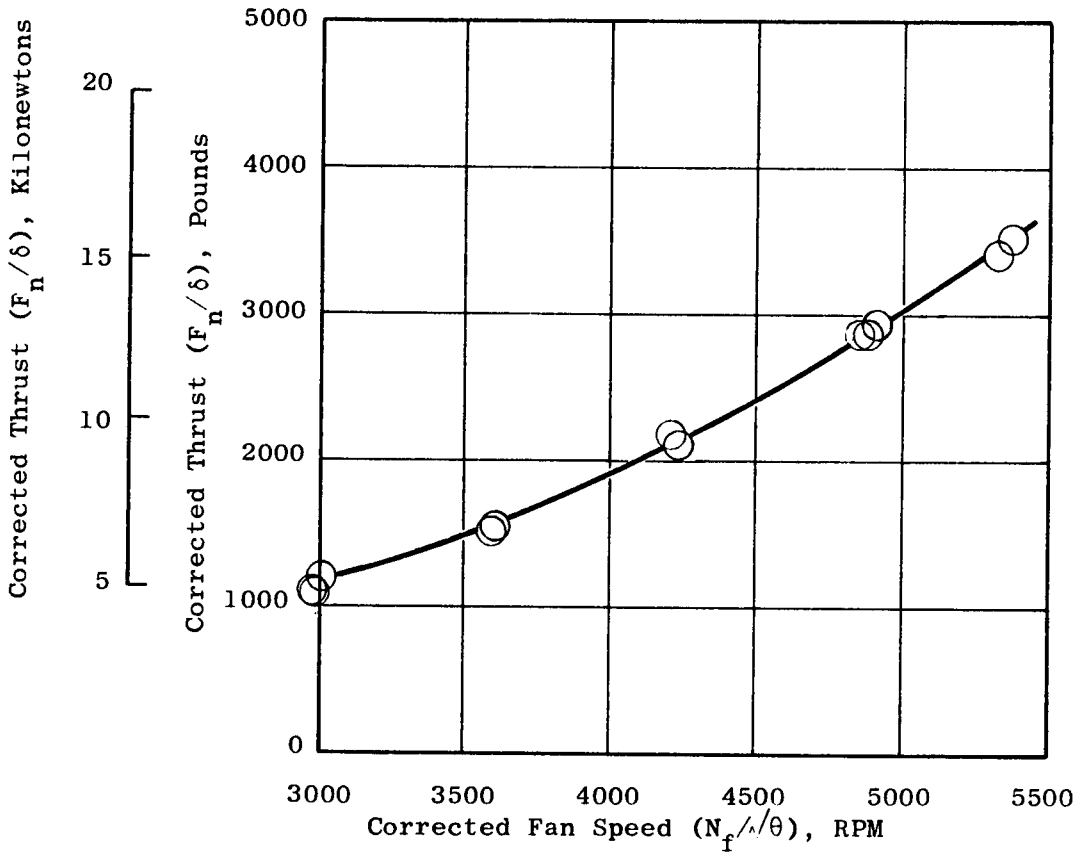

Figure 149. Thrust Variation with Fan Speed for Test 5, Inlet Box and 30 Inches (76.2 cm) of Exhaust Suppression with U-Channeled Blockage

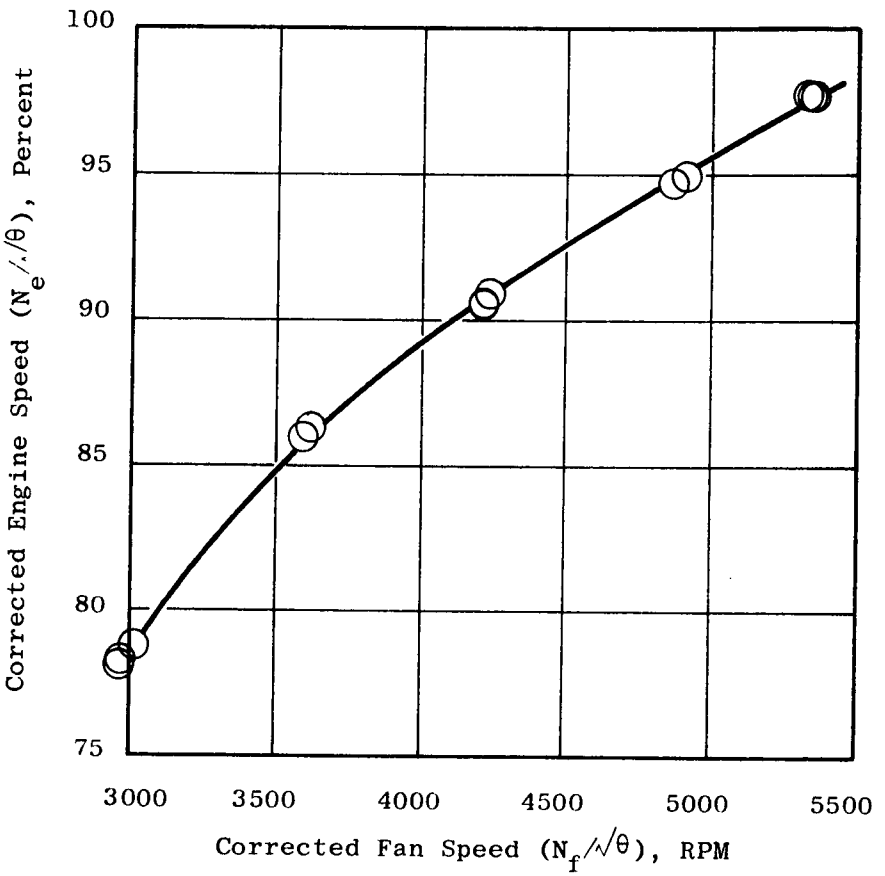

Figure 150. Engine Speed Variation with Fan Speed for Test 5, Inlet Box and 30 Inches (76.2 cm) of Exhaust Suppression with U-Channeled Blockage

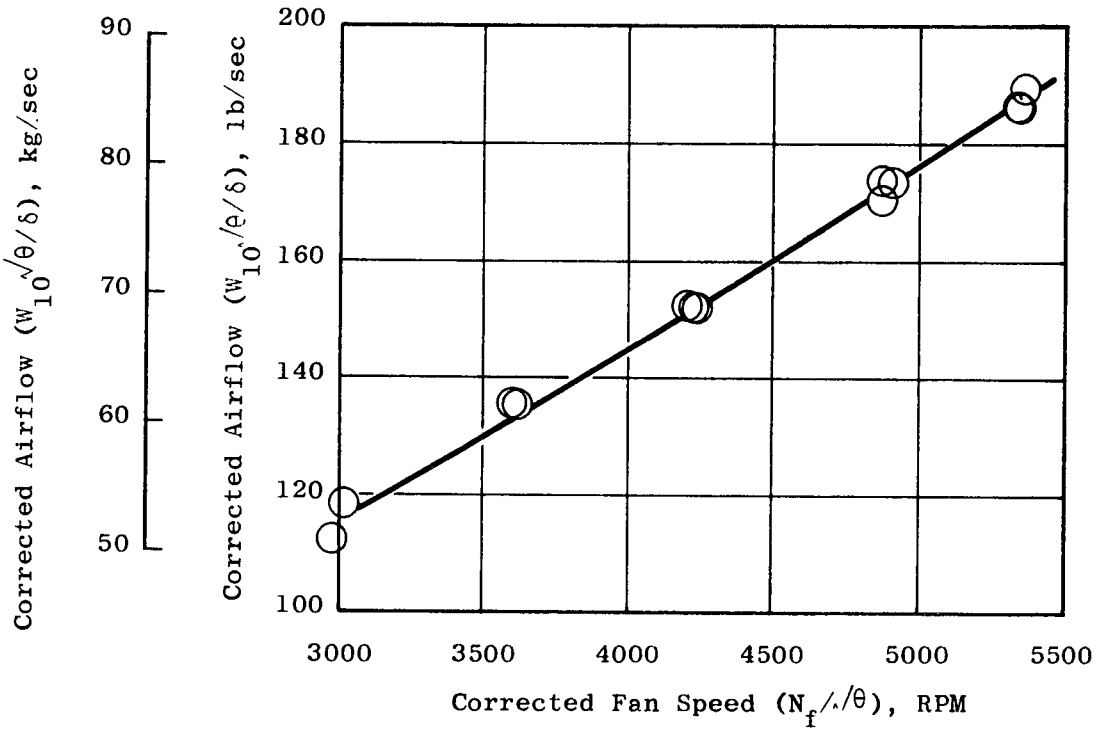

Figure 151. Airflow Variation with Fan Speed for Test 5, Inlet Box and 30 Inches (76.2 cm) of Exhaust Suppression with U-Channeled Blockage

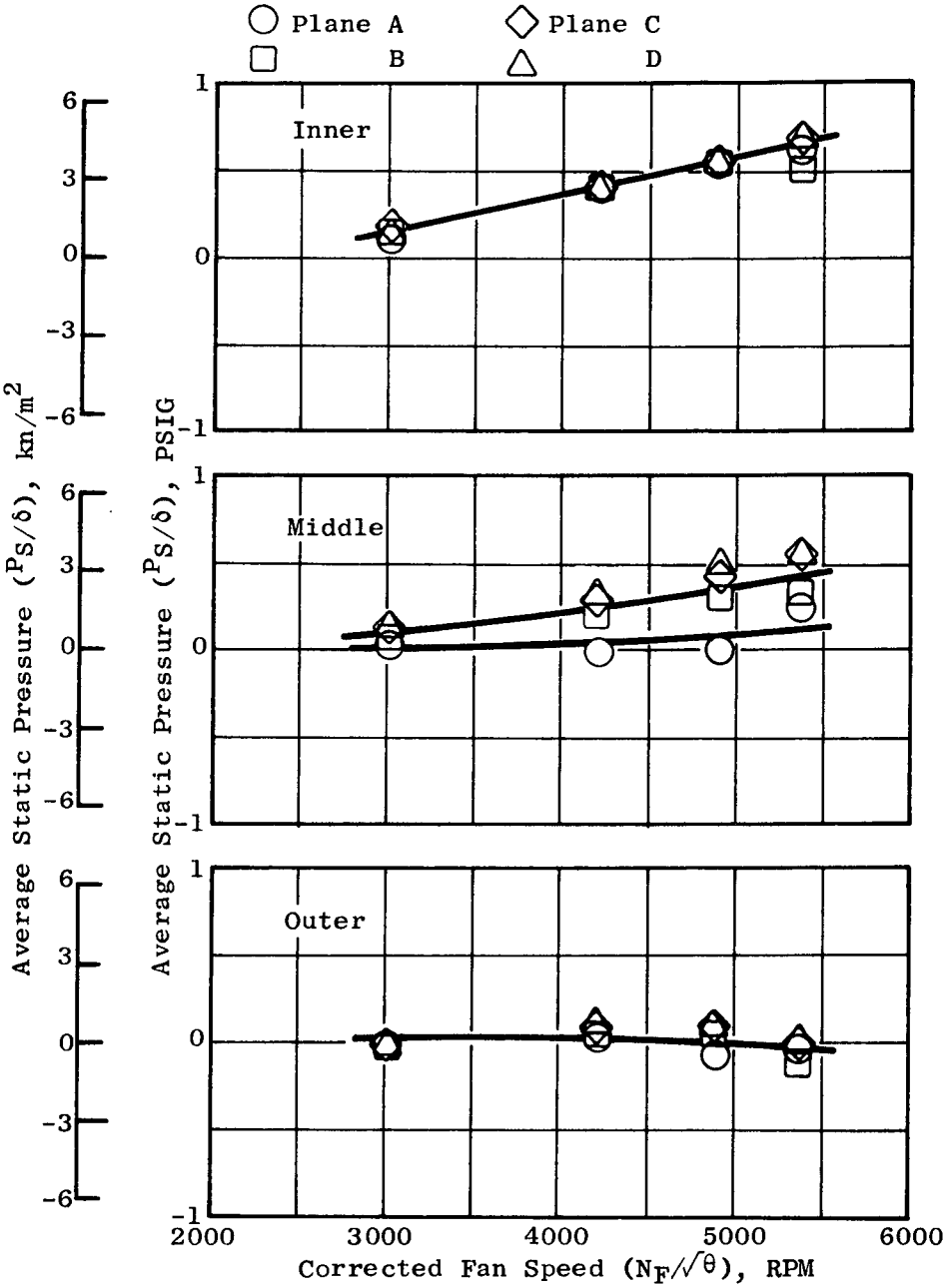

Figure 152. Adapter Section Average Wall Static Pressure Distribution for Test 5, Inlet Box and 30 Inches (76.2 cm) of Exhaust Suppression with U-Channeled Blockage

E

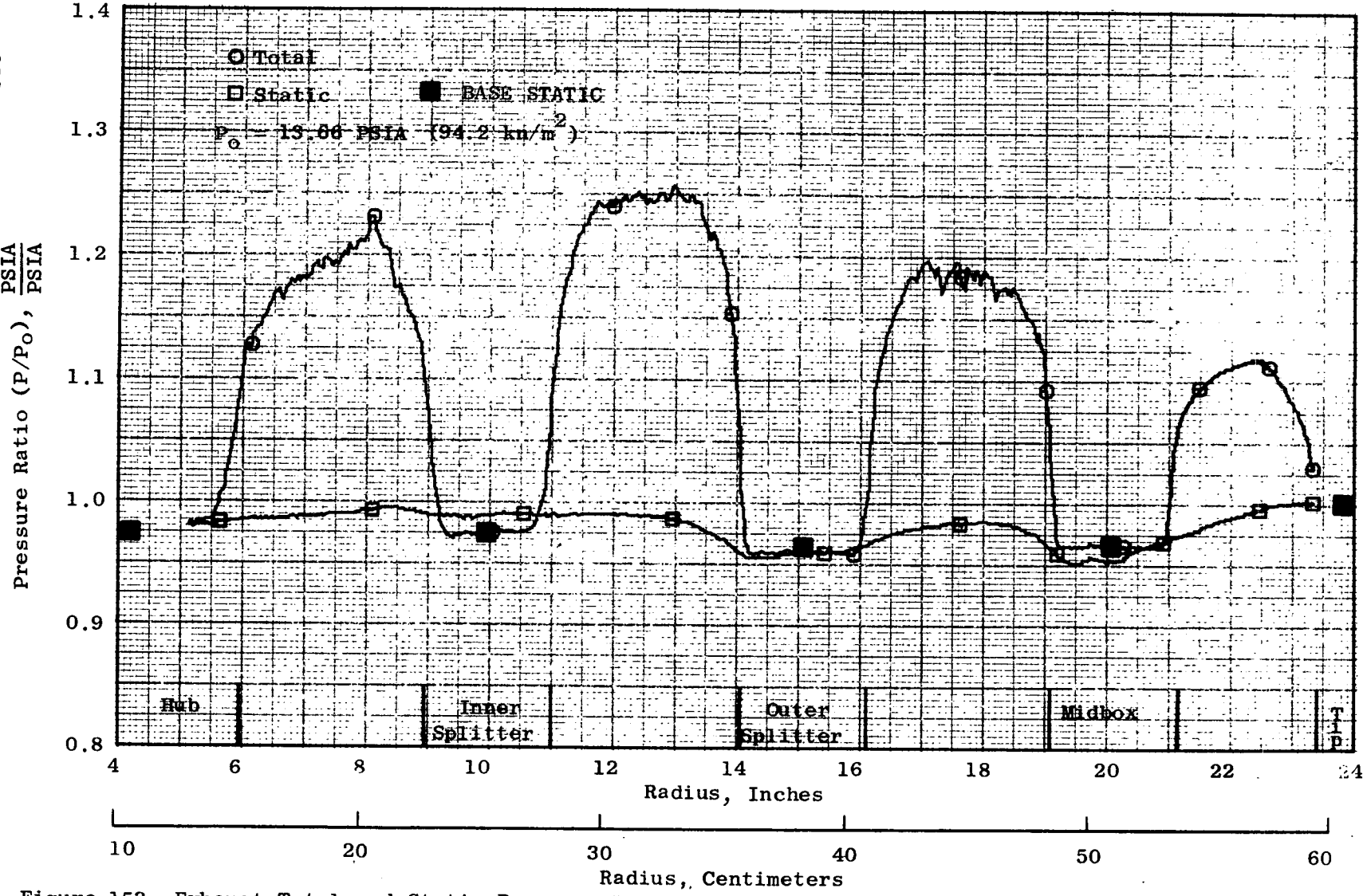

Figure 153. Exhaust Total and Static Pressure Profile for Test 5, Inlet Box and 30 Inches (76.2 cm) of Exhaust Suppression with U-Channeled Blockage, N_f/θ = 5350

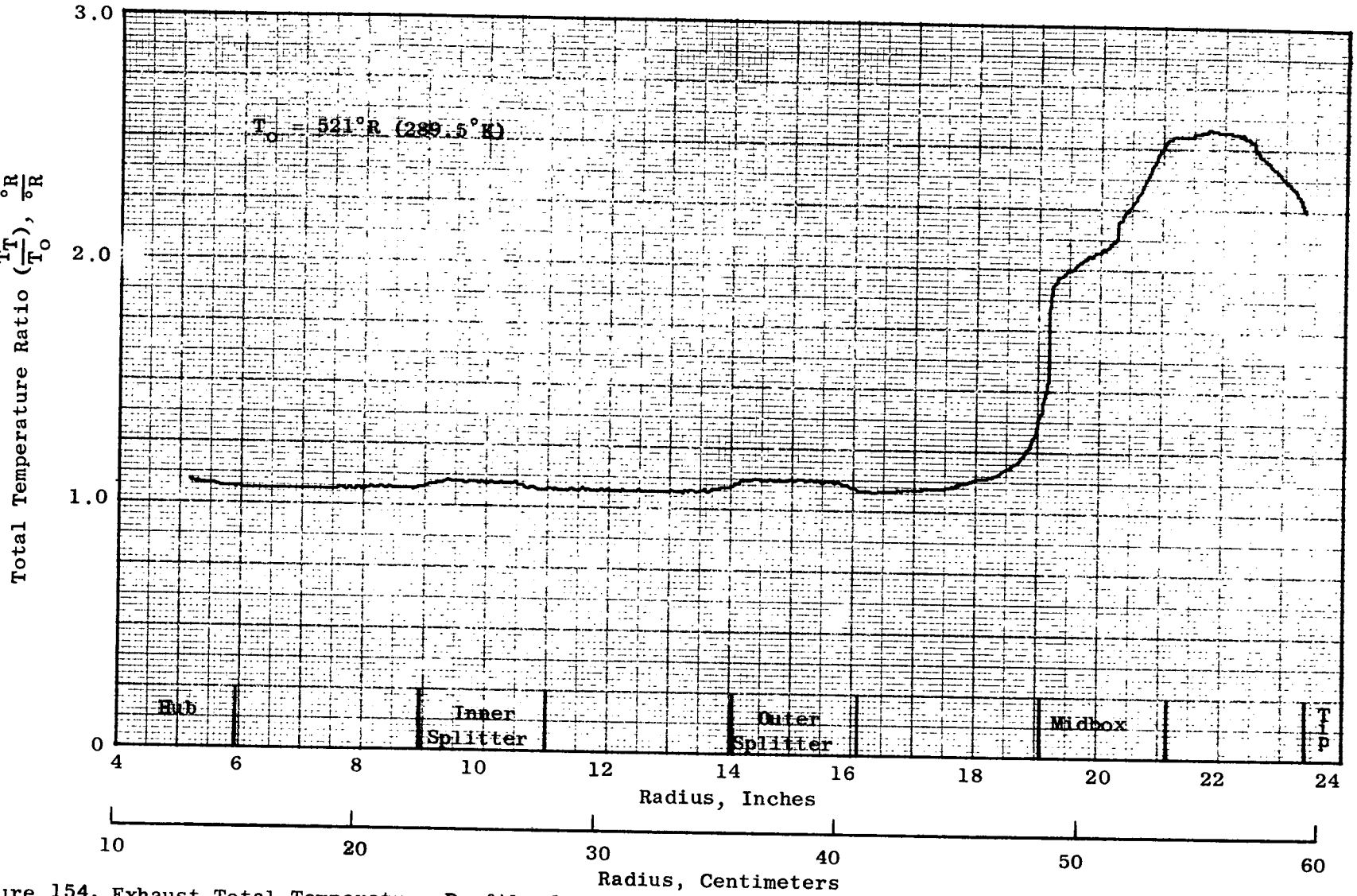

Figure 154. Exhaust Total Temperature Profile for Test 5, Inlet Box and 30 Inches (76.2 cm) of Exhaust Suppression with U-Channeled Blockage, N_f/θ =5350

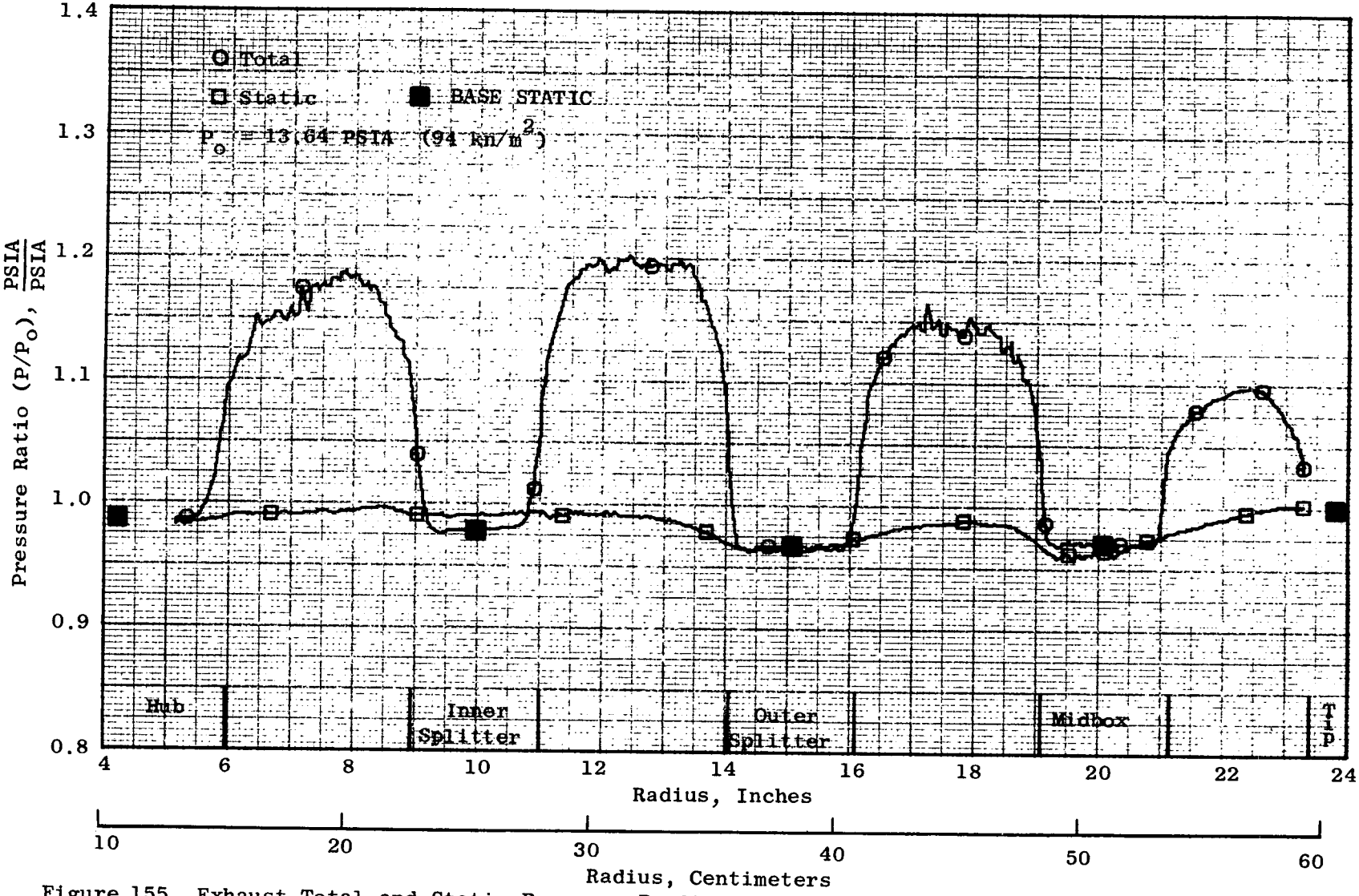

Figure 155. Exhaust Total and Static Pressure Profile for Test 5, Inlet Box and 30 Inches (76.2 cm) of Exhaust Suppression with U-Channeled Blockage, $N_f/\sqrt{\theta}$ = 4880

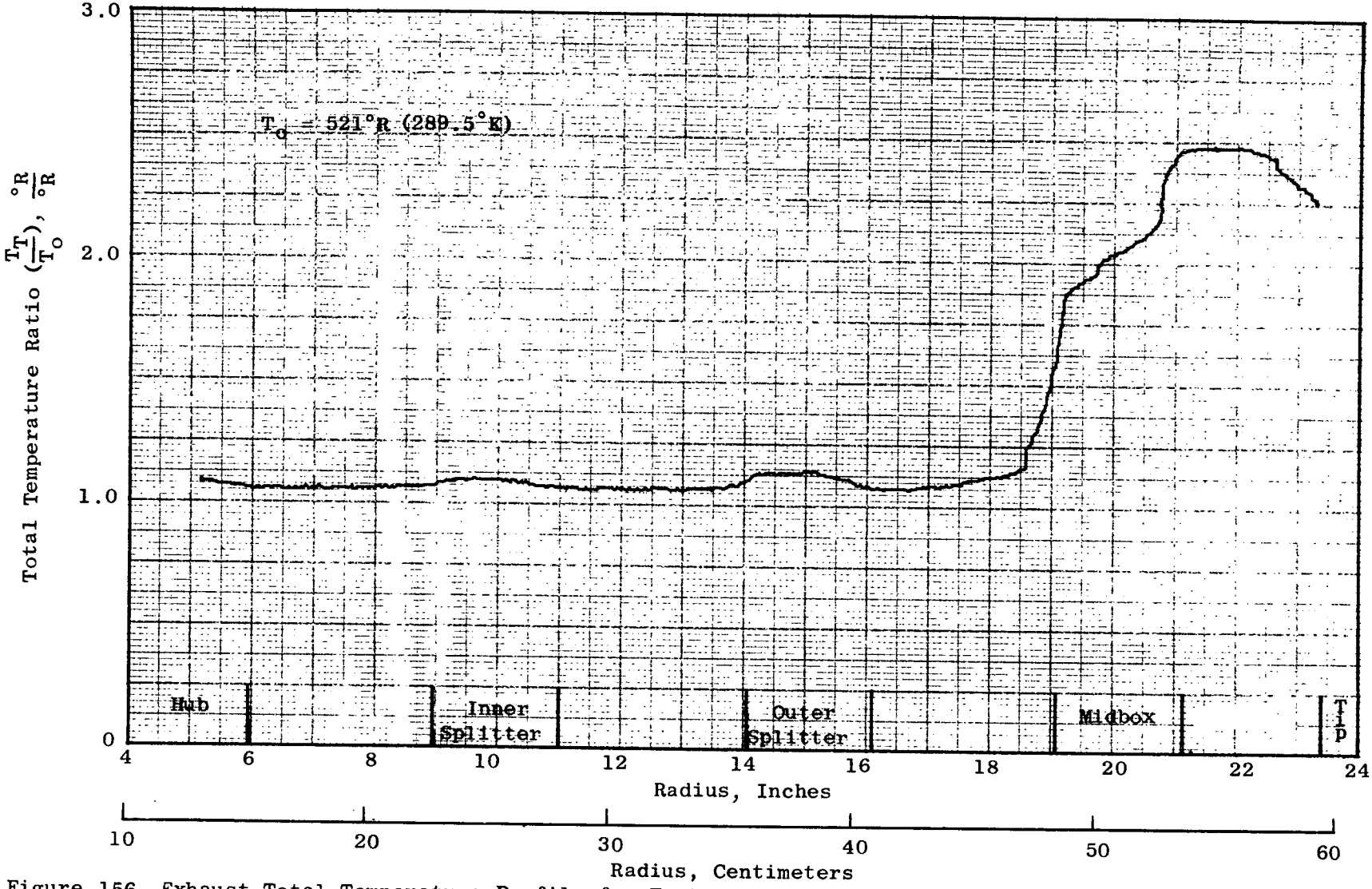

Figure 156. Exhaust Total Temperature Profile for Test 5, Inlet Box and 30 Inches (76.2 cm) of Exhaust Suppression with U-Channeled Blockage, N_f/θ =4880

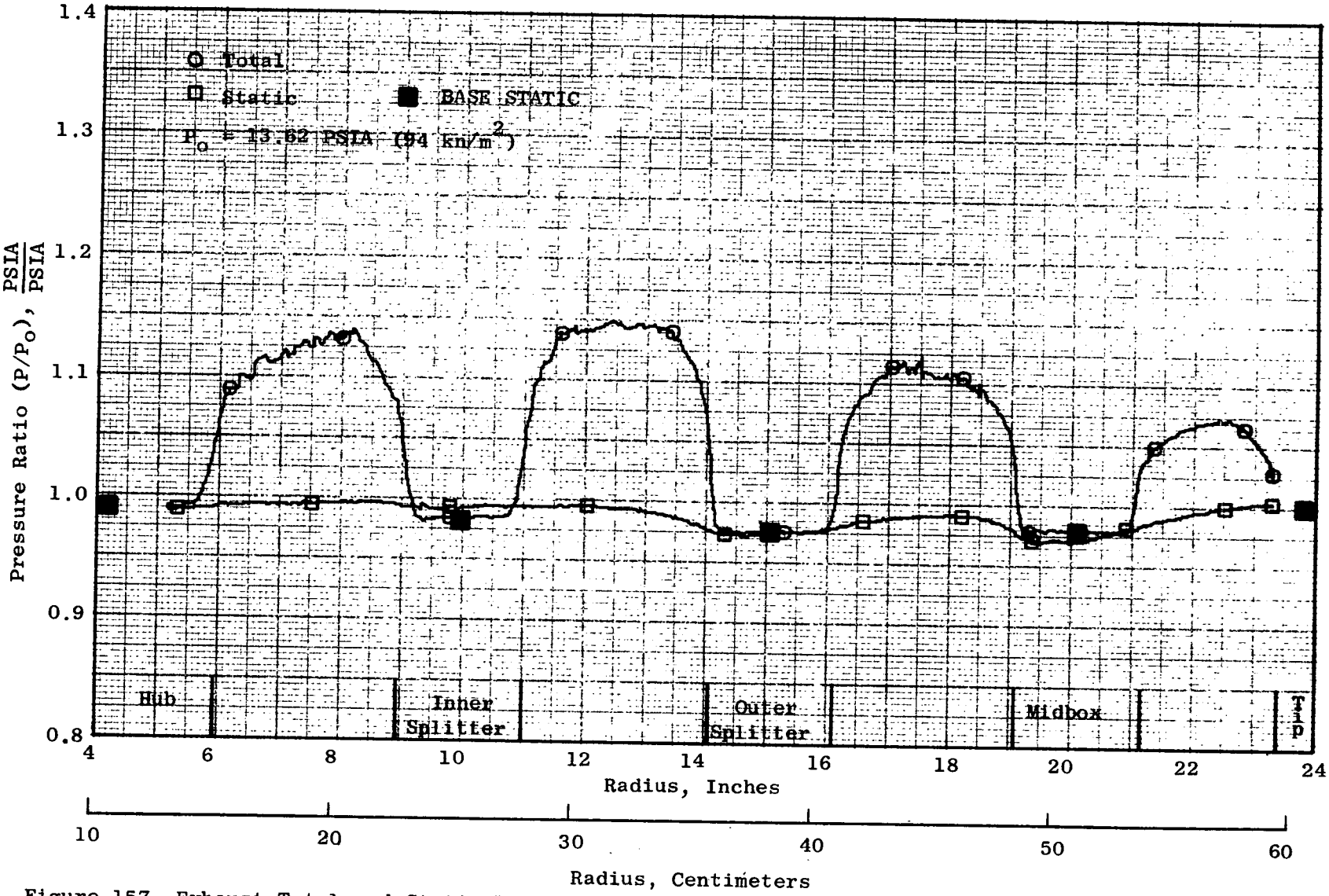

Figure 157. Exhaust Total and Static Pressure Profile for Test 5, Inlet Box and 30 Inches (76.2 cm) of Exhaust Suppression with U-Channeled Blockage, $N_f/\sqrt{\theta}$ = 4220

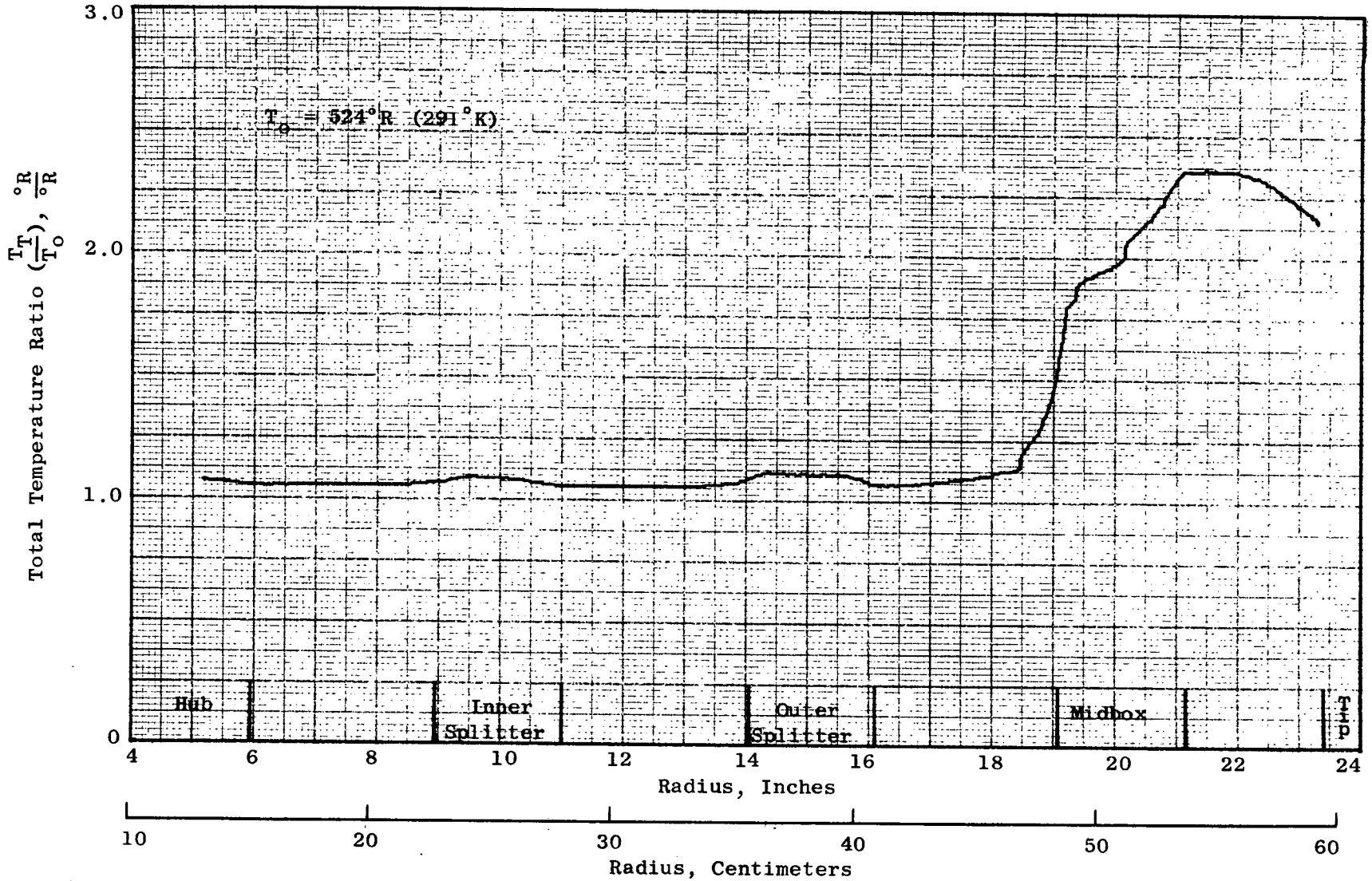

Figure 158. Exhaust Total Temperature Profile for Test 5, Inlet Box and 30 Inches (76.2 cm) of Exhaust Suppression with U-Channeled Blockage, $N_f/\sqrt{\theta}$ = 4220

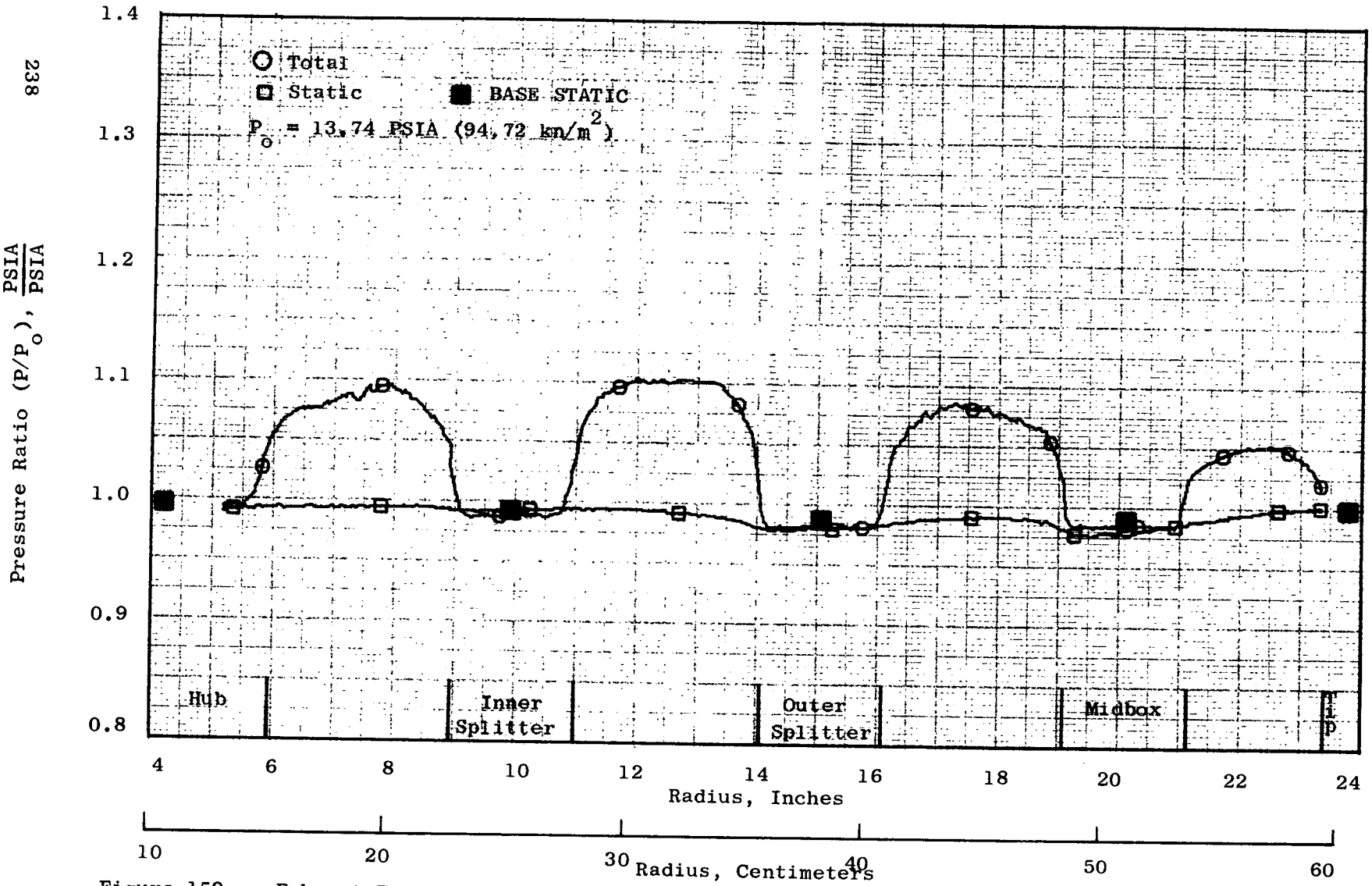

Figure 159. Exhaust Total and Static Pressure Profile for Test 5, Inlet Box and 30 Inches (76.2 cm) of Exhaust Suppression with U-Channeled Blockage, $N_f/\sqrt{\theta}$ = 3600

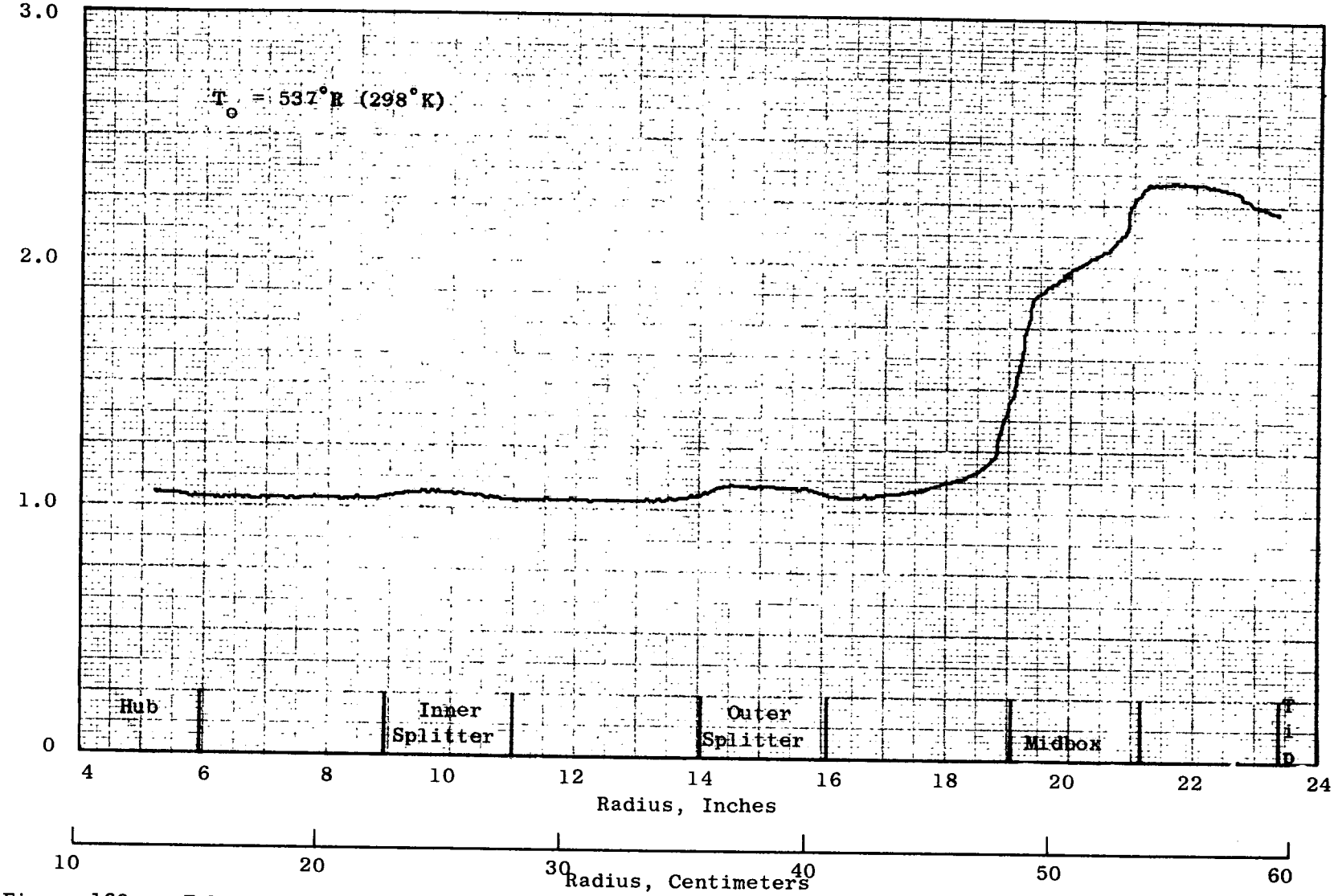

Figure 160. Exhaust Total Temperature Profile for Test 5, Inlet Box and 30 Inches (76.2 cm) of Exhaust Suppression with U-Channeled Blockage, $N_f/\sqrt{\theta}$ = 3600

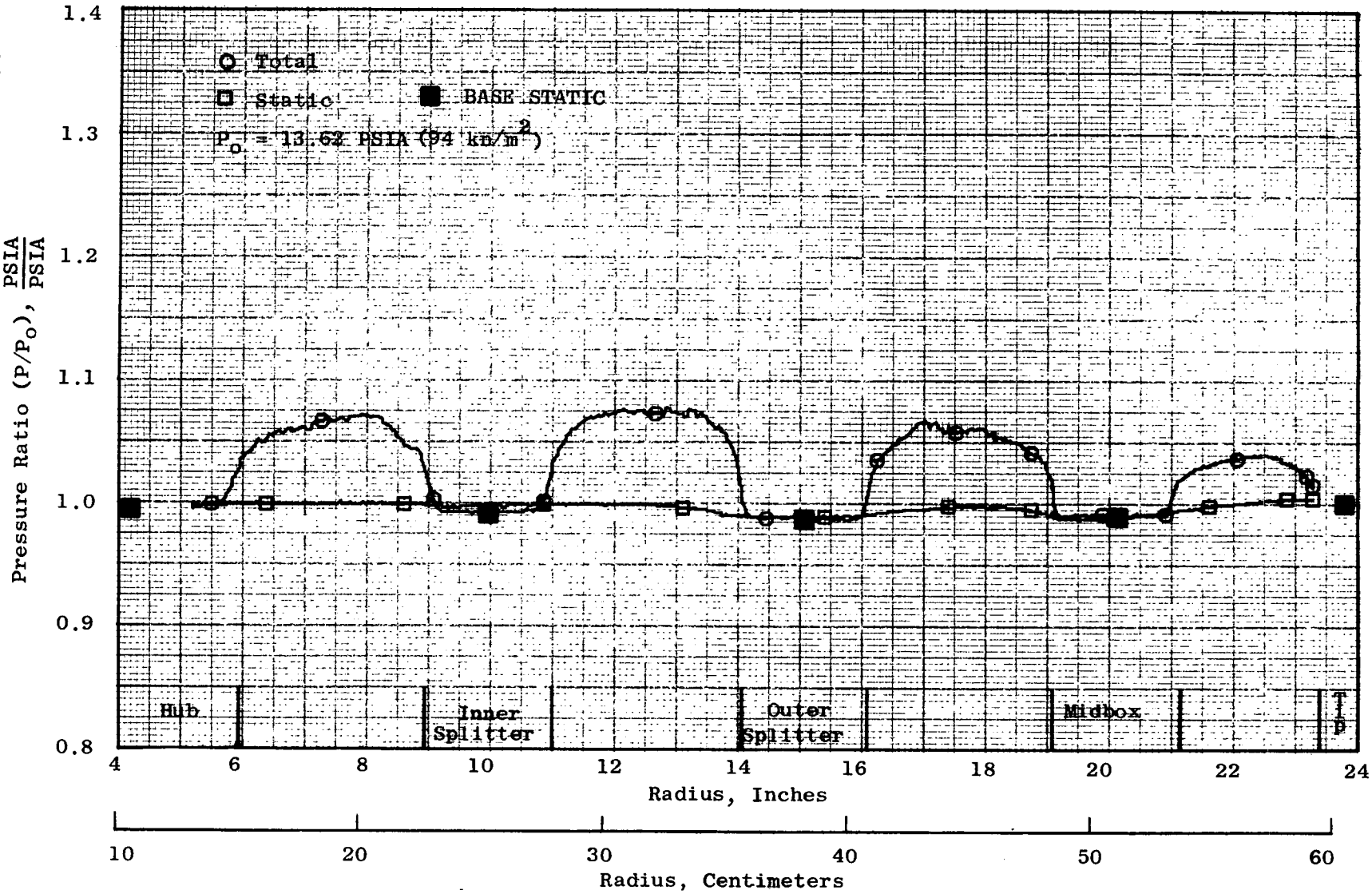

Figure 161. Exhaust Total and Static Pressure Profile for Test 5, Inlet Box and 30 Inches (76.2 cm) of Exhaust Suppression with U-Channeled Blockage, $N_f/\sqrt{\theta}$ = 3020

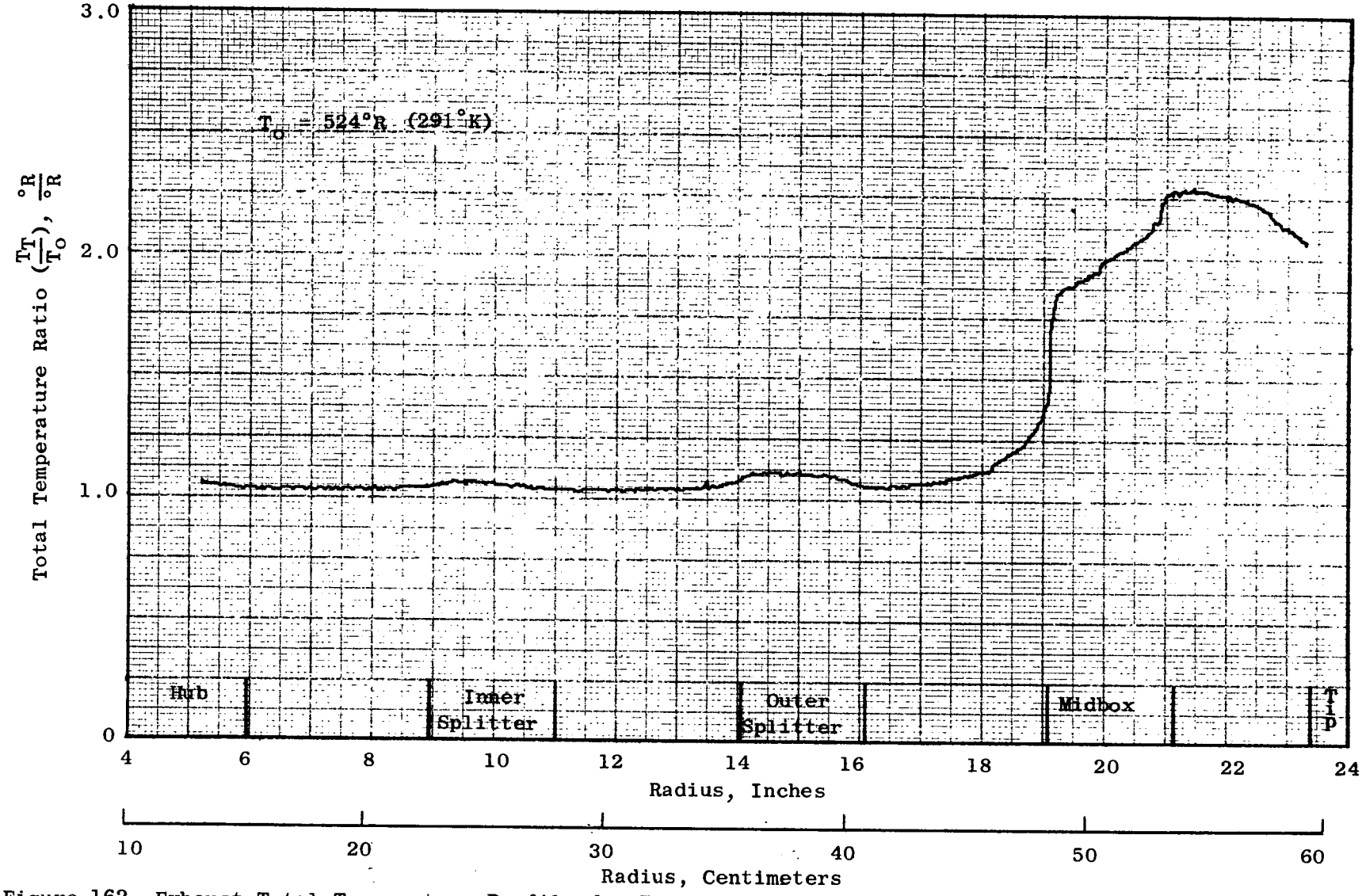

Figure 162. Exhaust Total Temperature Profile for Test 5, Inlet Box and 30 Inches (76.2 cm) of Exhaust Suppression with U-Channeled Blockage, $N_f/\sqrt{\theta}$ = 3020

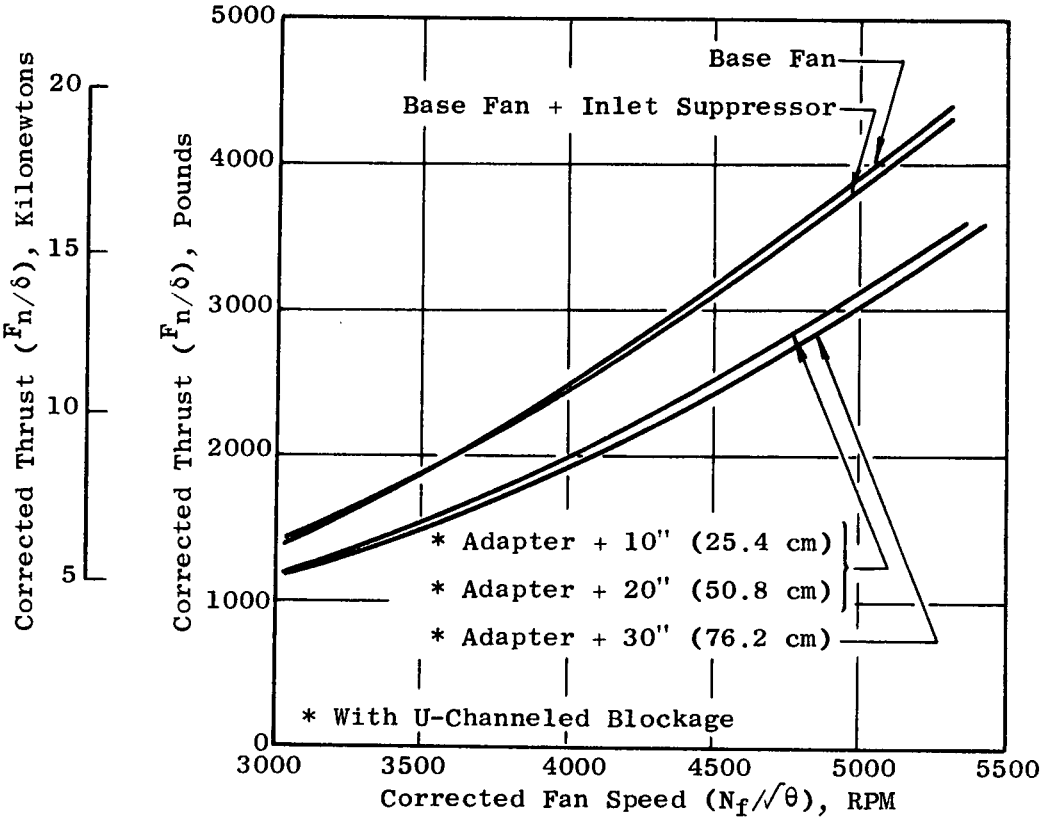

Figure 163. Thrust Comparison for Various Fan Configurations

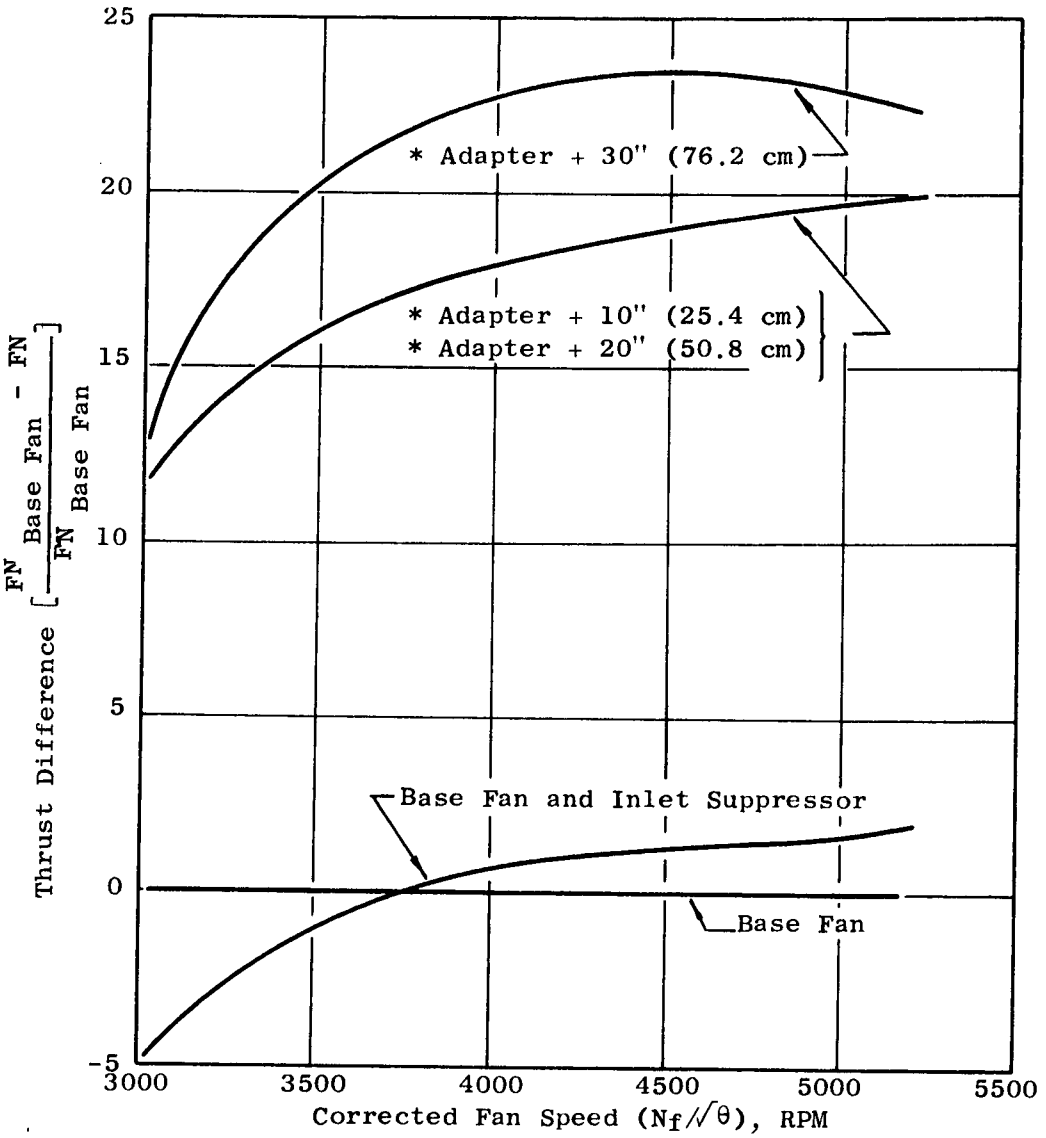

Figure 164. Thrust Differences for Various Fan Configurations

* With U-Channeled Blockage

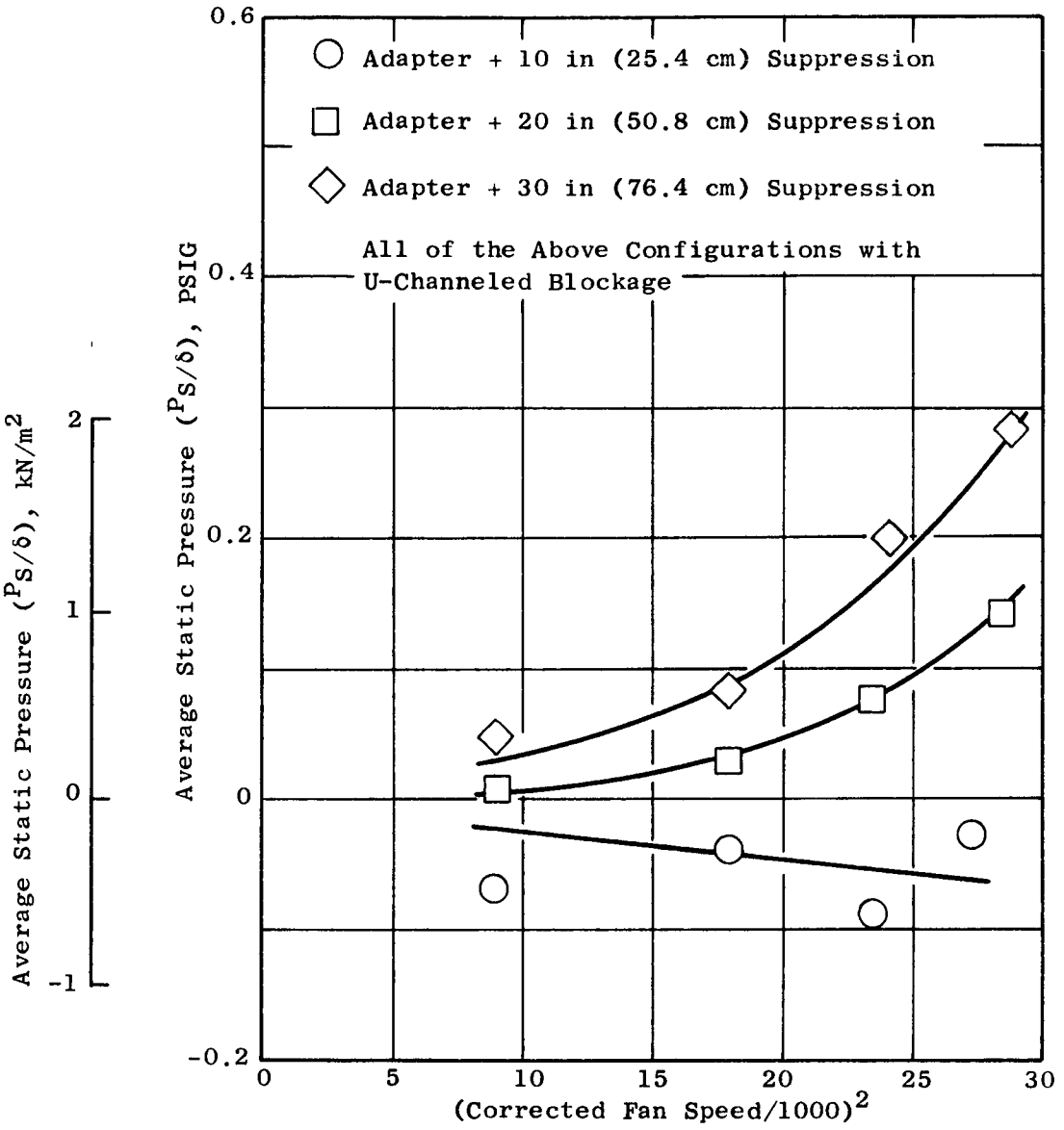

Figure 165. Average Static Pressure Distribution in Plane A of the Exhaust Adapter Section for Various Fan Configurations

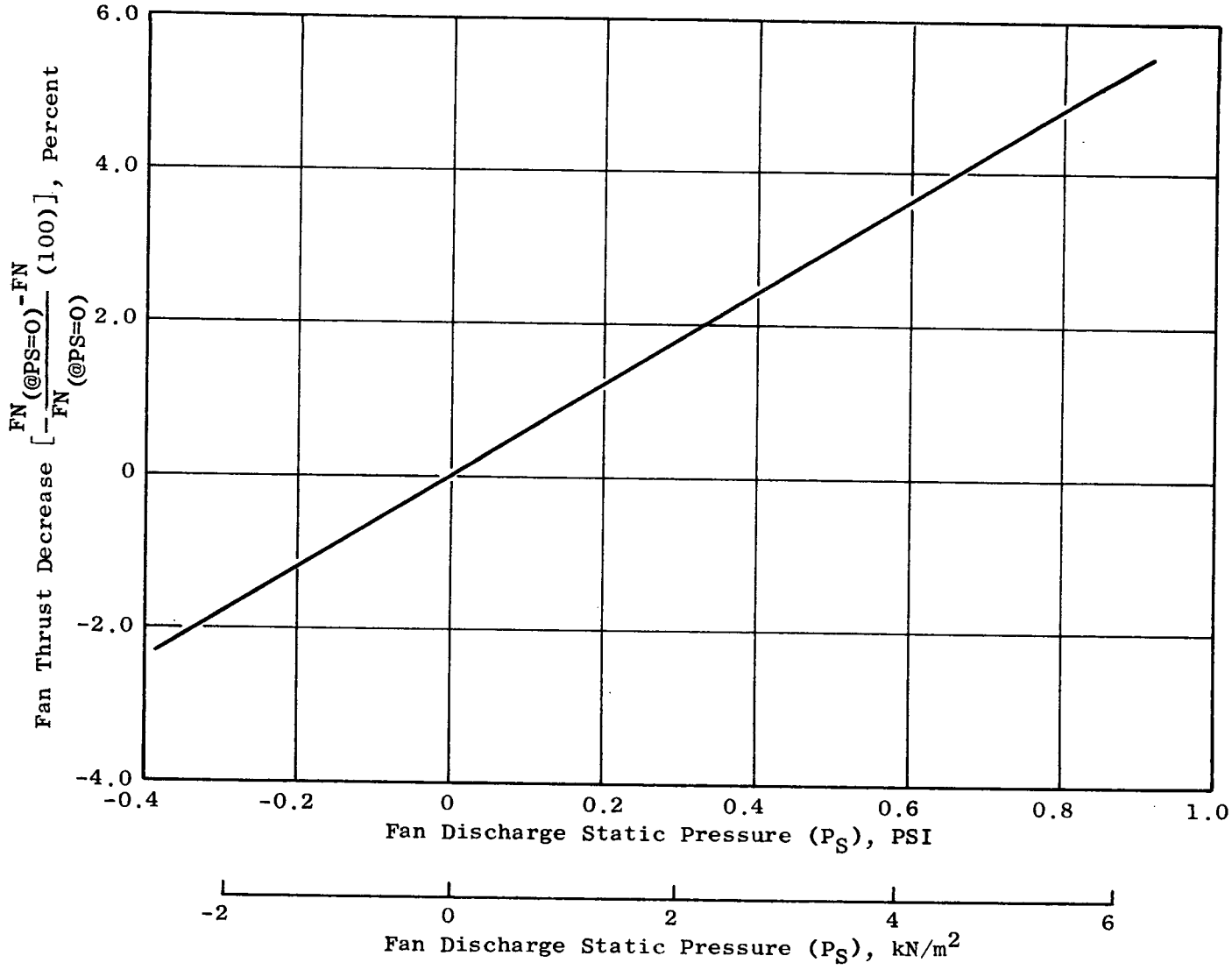

Figure 166. Fan Thrust Decrease Variation with Fan Discharge Static Pressure

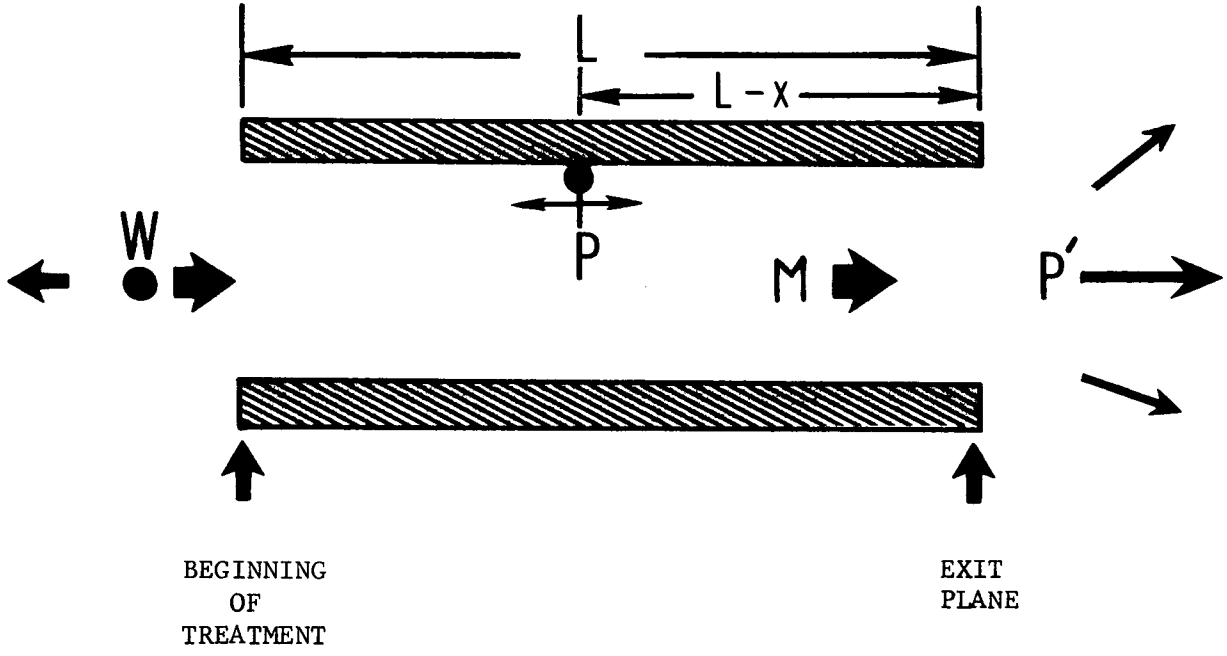

Figure 167. Relationship of Source Power and Flow Generated Power to Exhaust Radiated Power

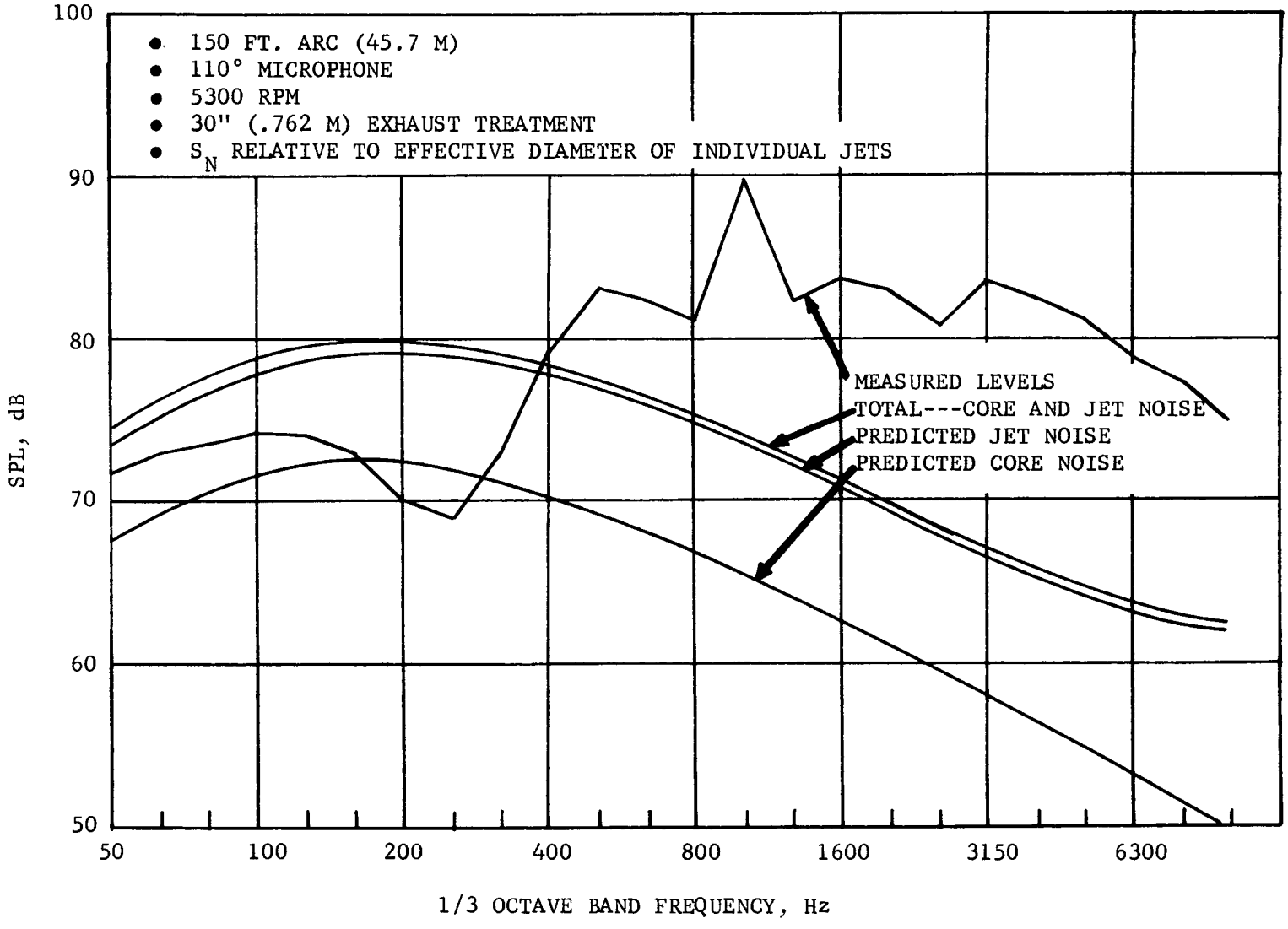

Figure 168. Comparison of Predicted Jet Noise Based on Effective Diameter of Exhaust Passages and Core Noise with Measured Noise at 5300 RPM

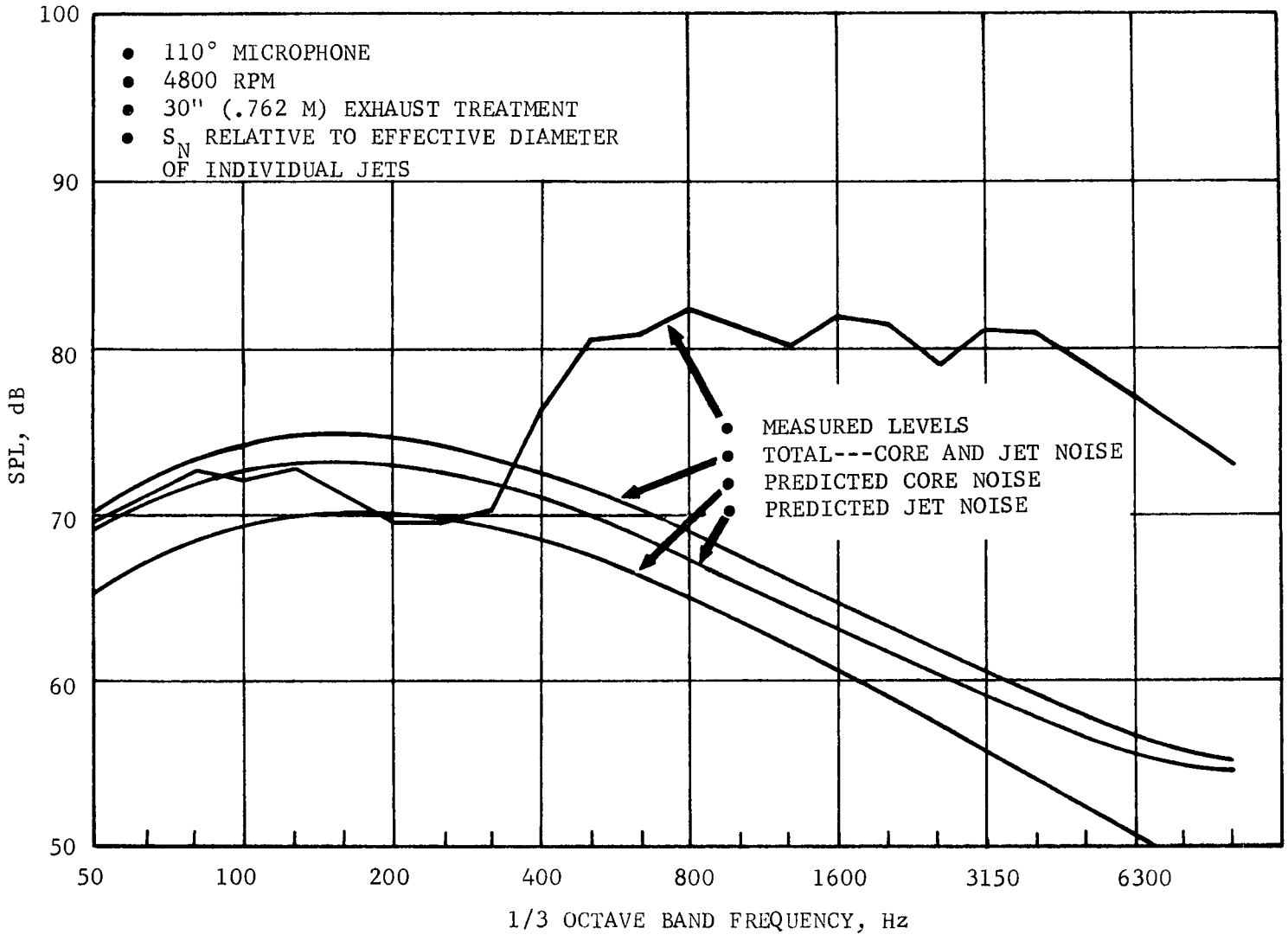

Figure 169. Comparison of Predicted Jet Noise Based on Effective Diameter of Exhaust Passages and Core Noise with Measured Noise at 4800 RPM

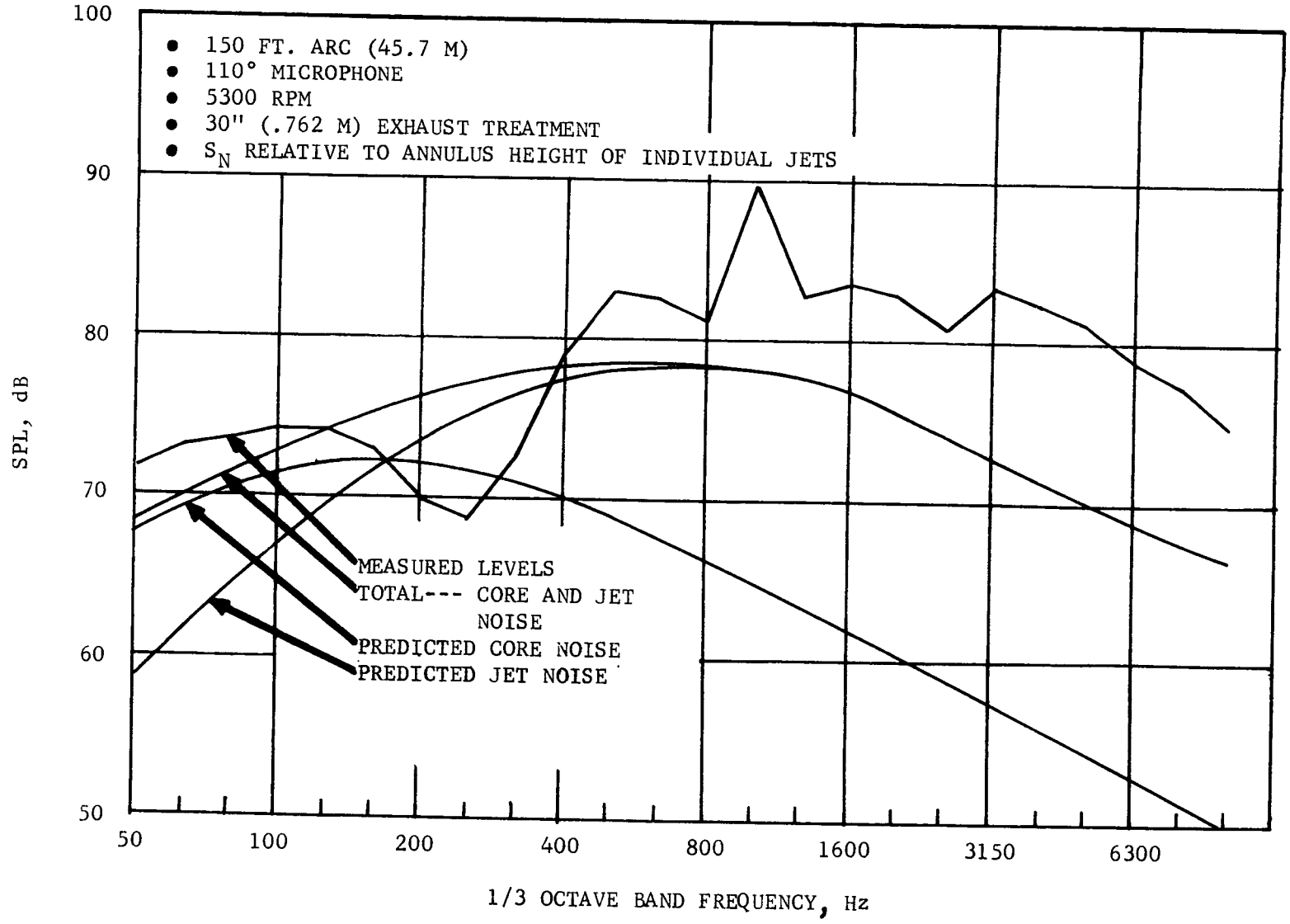

Figure 170. Comparison of Predicted Jet Noise Referenced to Annulus Height and Core Noise with Measured Noise at 5300 RPM

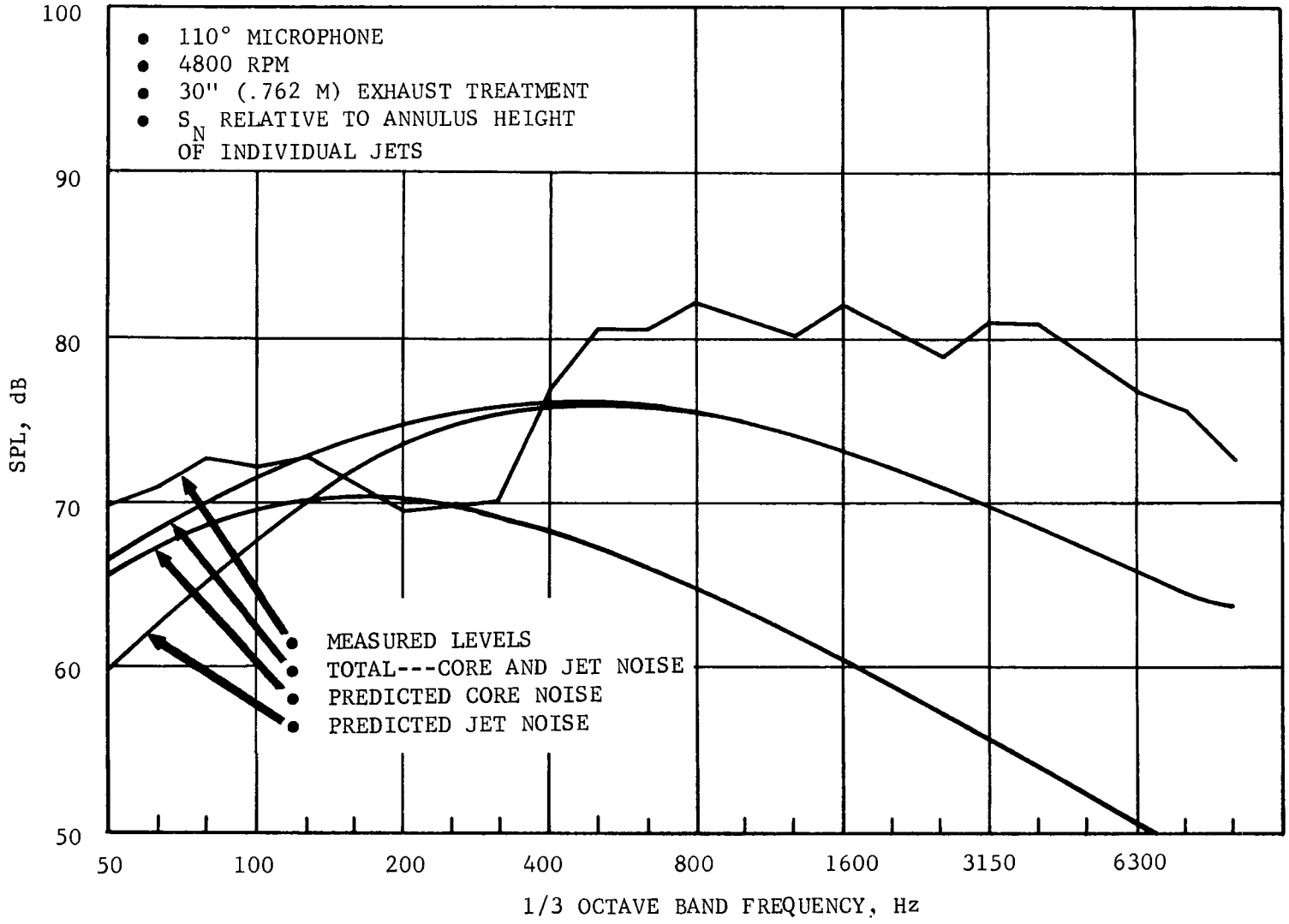

Figure 171. Comparison of Predicted Jet Noise Referenced to Annulus Height and Core Noise with Measured Noise at 4800 RPM

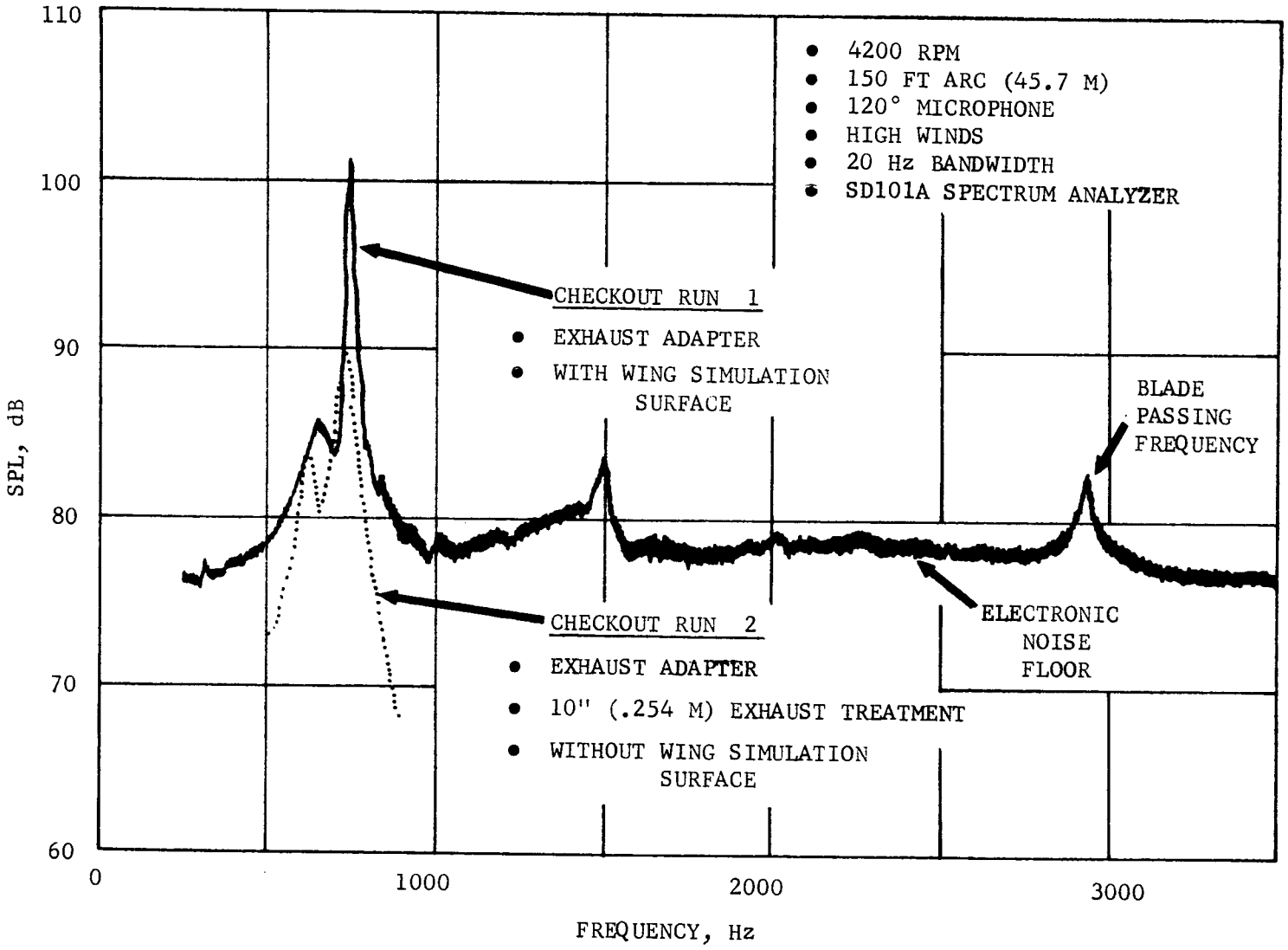

Figure 172. LF336/B Spectrum at 120 Degree Microphone and 4200 RPM for Checkout Runs 1 and 2

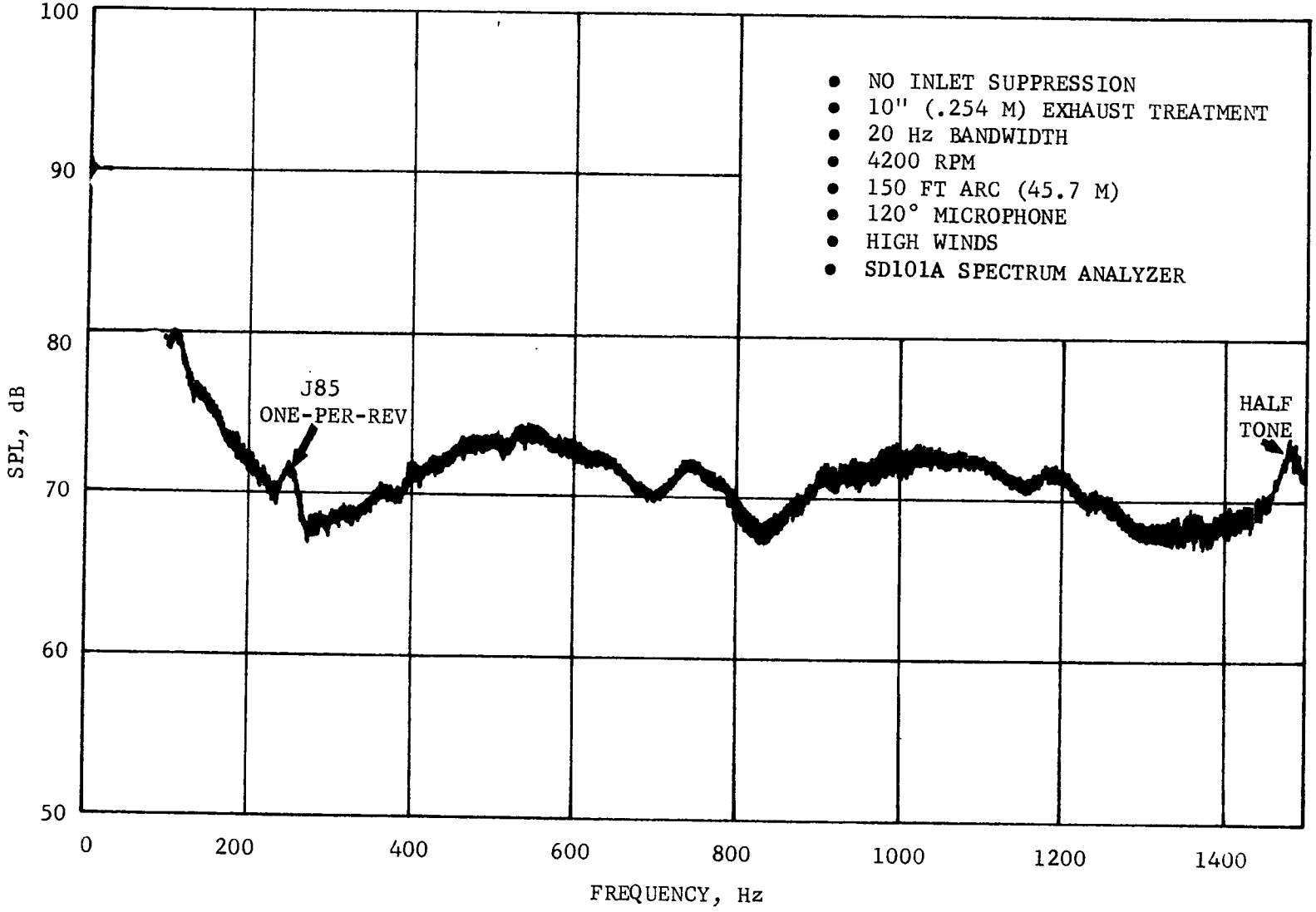

Figure 173. LF336/B Spectrum at 4200 RPM and 120 Degree Microphones for Checkout Run 3

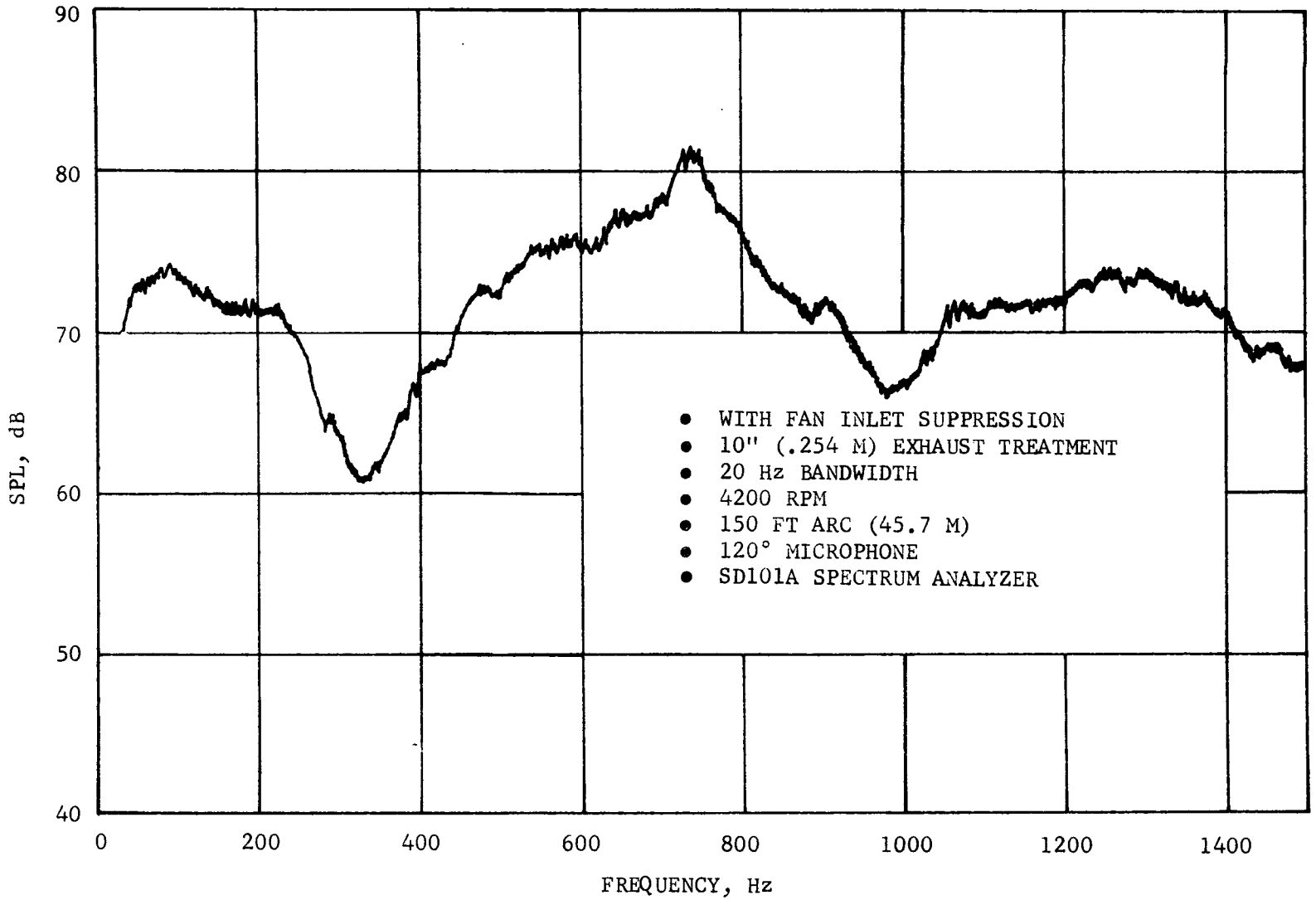

Figure 174. LF336/B Spectrum at 4200 RPM and 120 Degree Microphone with Faired Radial Tabs

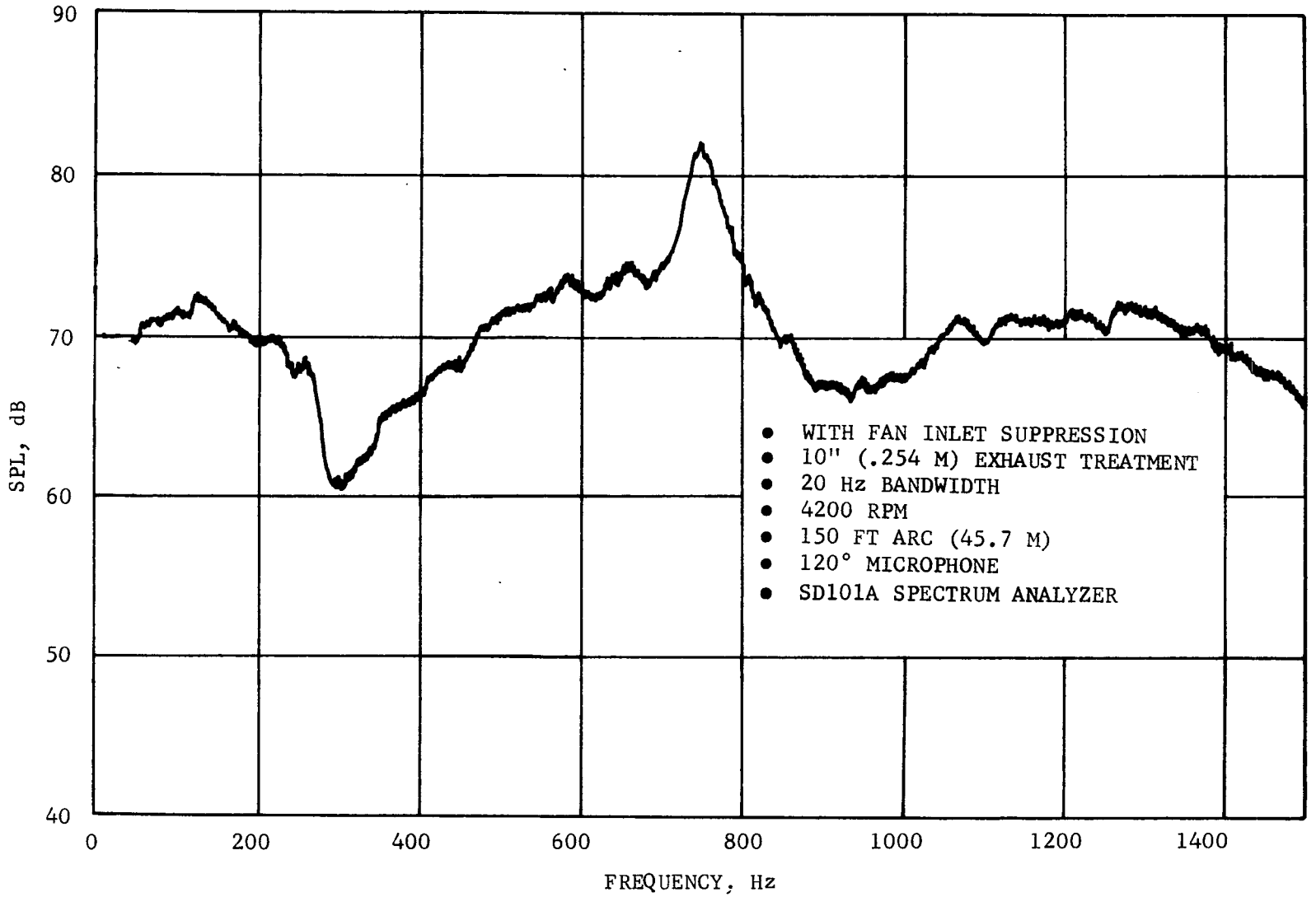

Figure 175. LF336/B Spectrum at 4200 RPM and 120 Degree Microphone from Test 3

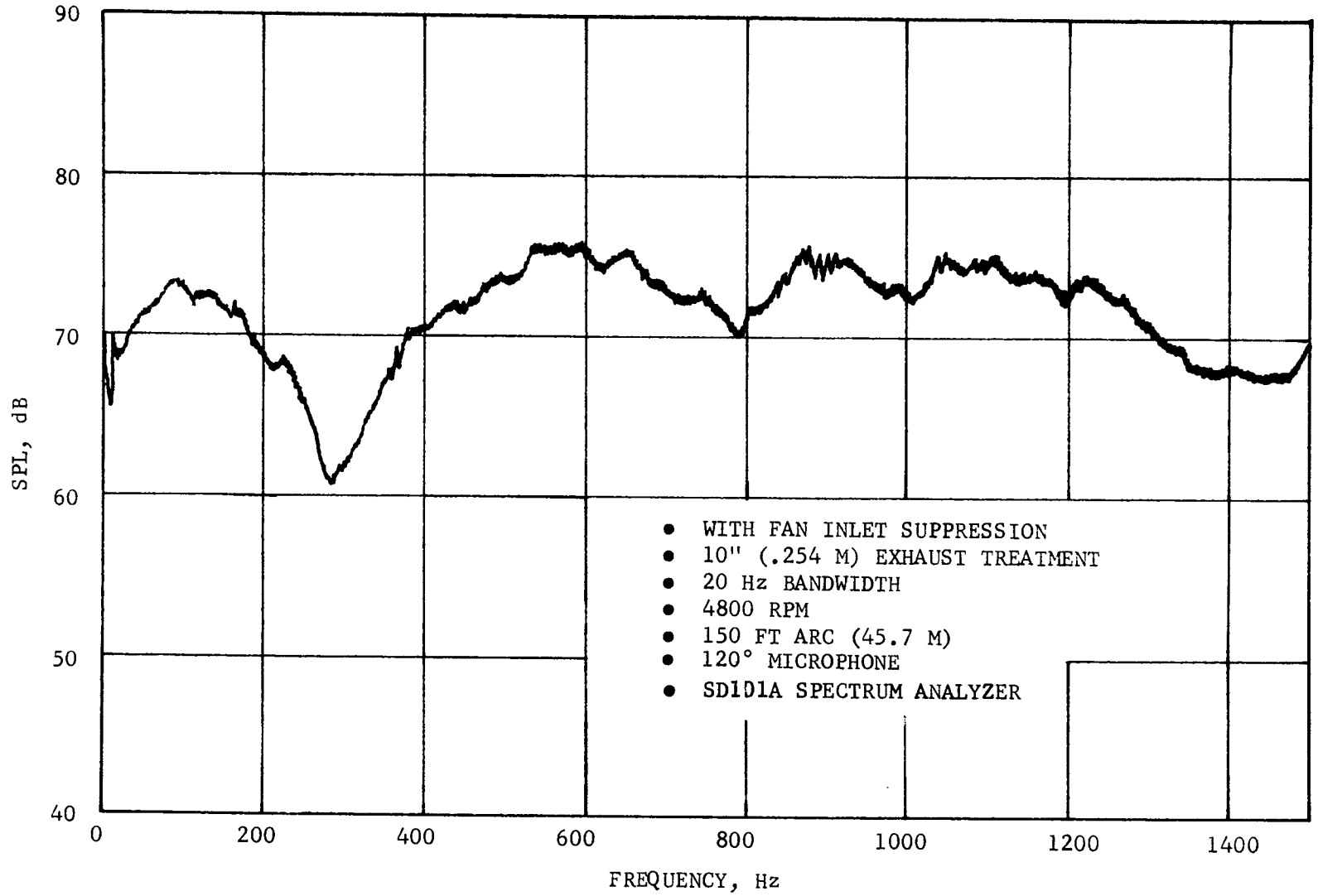

Figure 176. LF336/B Spectrum at 4800 RPM and 120 Degree Microphone from Test 3

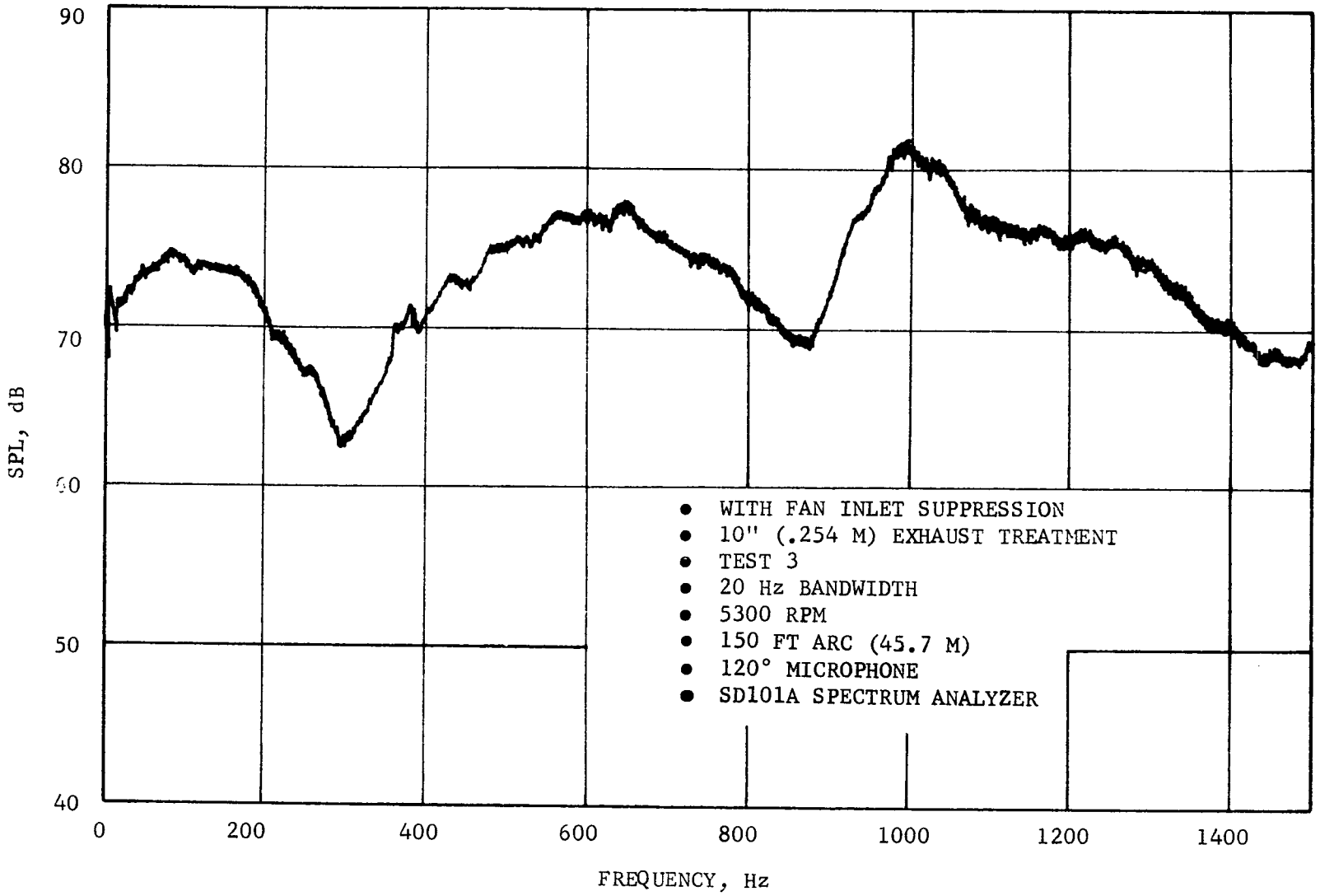

Figure 177. LF336/B Spectrum at 5300 RPM and 120 Degree Microphone from Test 3

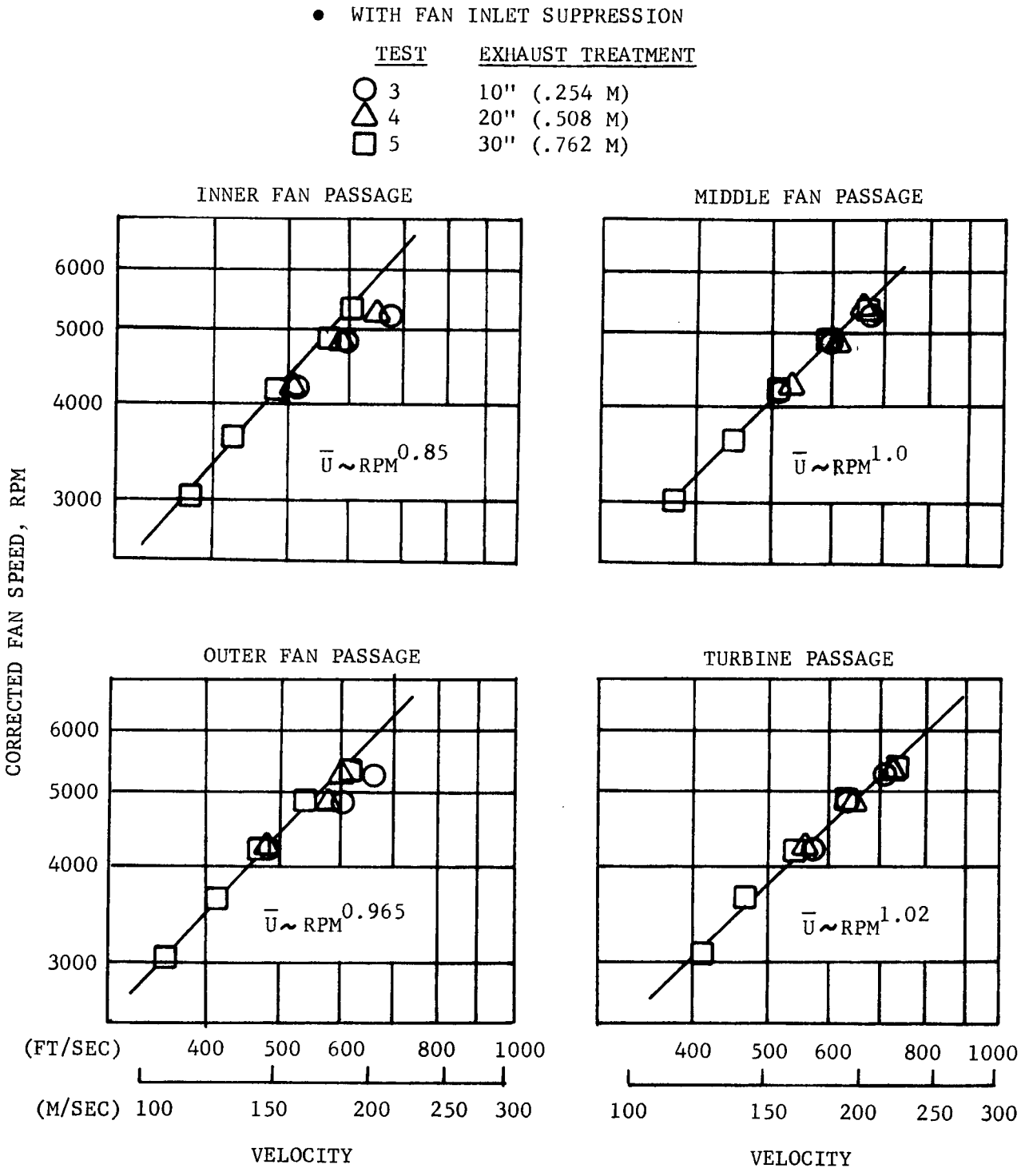

Figure 178. Variation of Suppressed LF336/B Velocities with Fan Speed

- 150 FT ARC (45.7 M)
- 120° MICROPHONE
- WITH FAN INLET SUPPRESSION

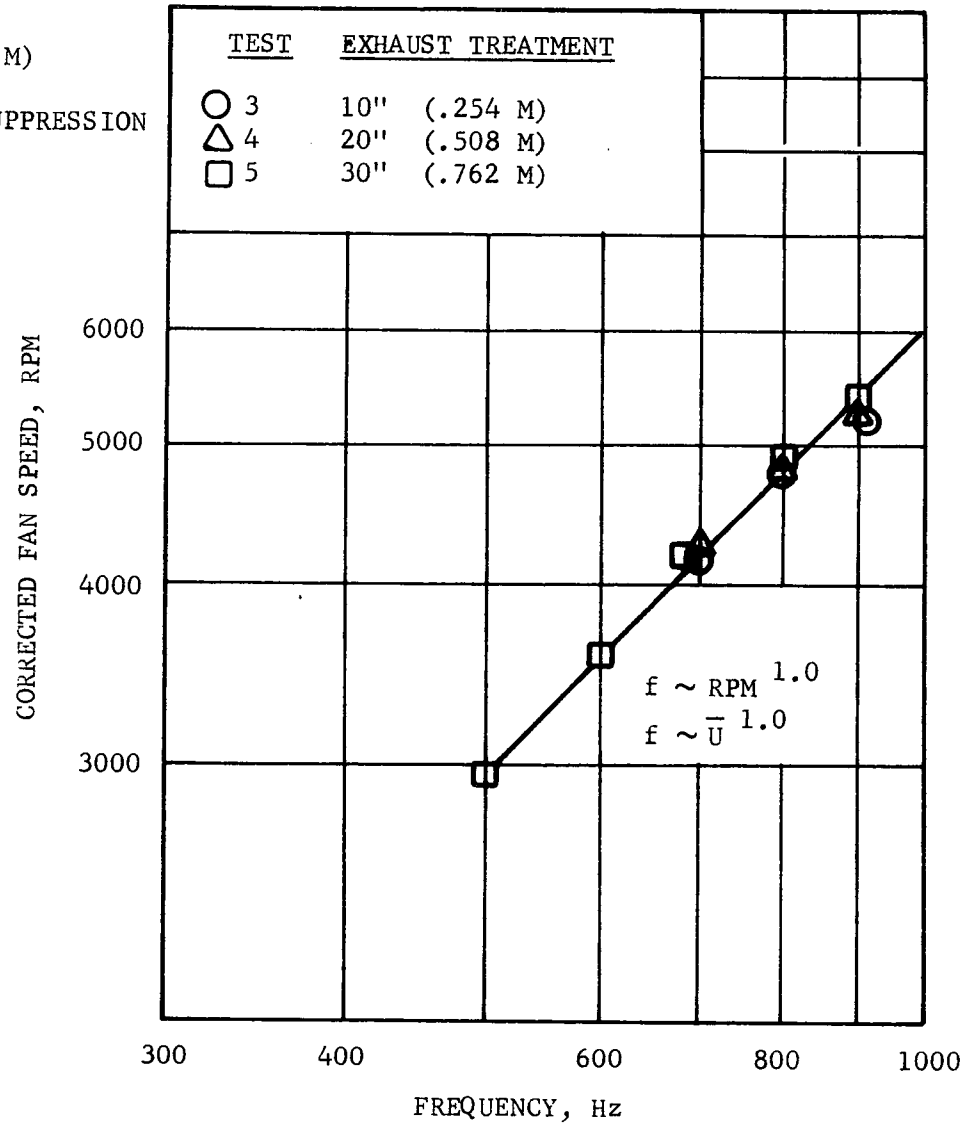

Figure 179. Variation in LF336/B Exhaust Tone Peak Frequency with Fan Speed

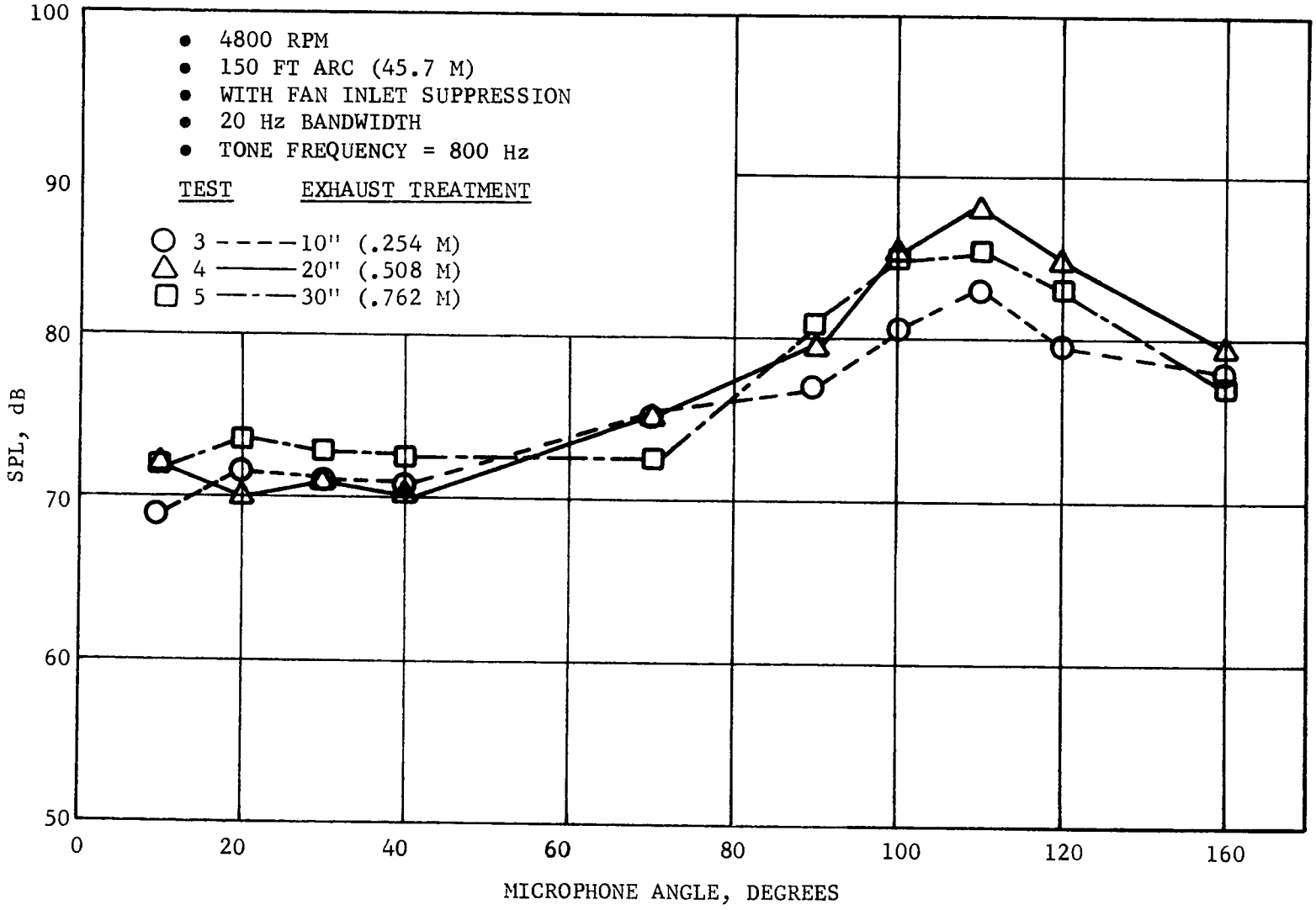

Figure 180. LF336/B Exhaust Tone Directivity

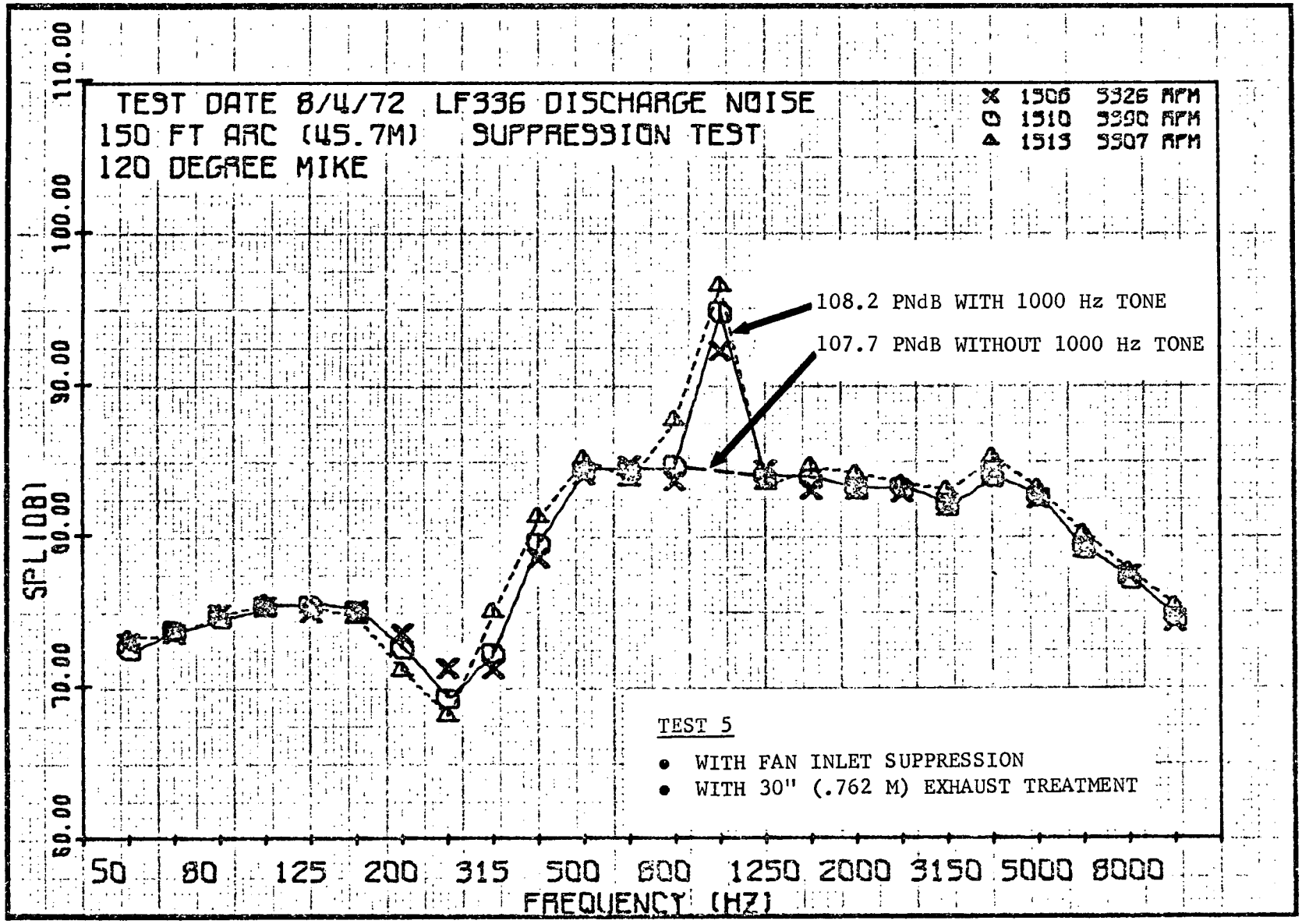

Figure 181. Effect of Exhaust Tone on Perceived Noise Levels

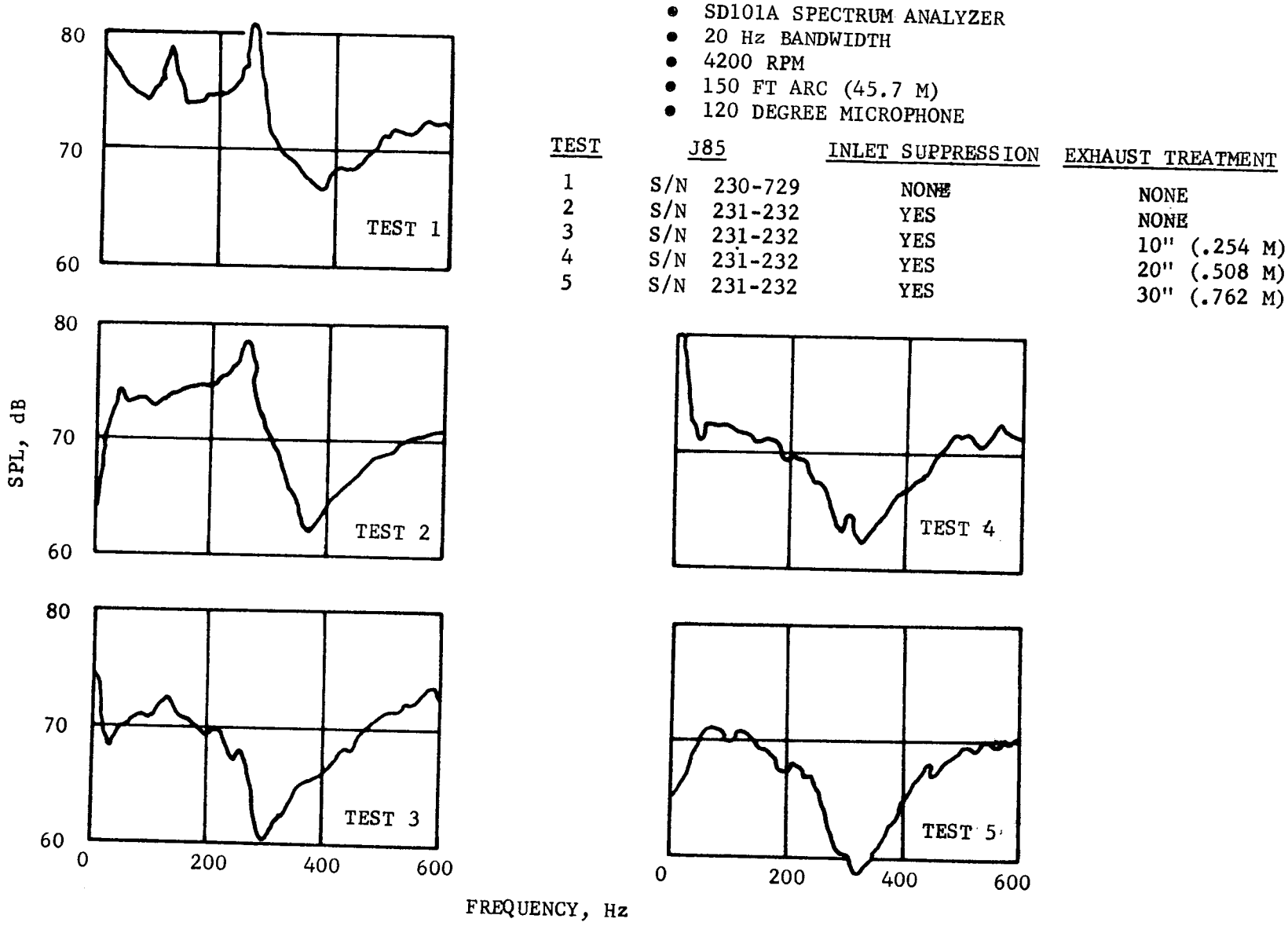

Figure 182. LF336/B Low Frequency Narrowbands at 4200 RPM and 120 Degree Microphone

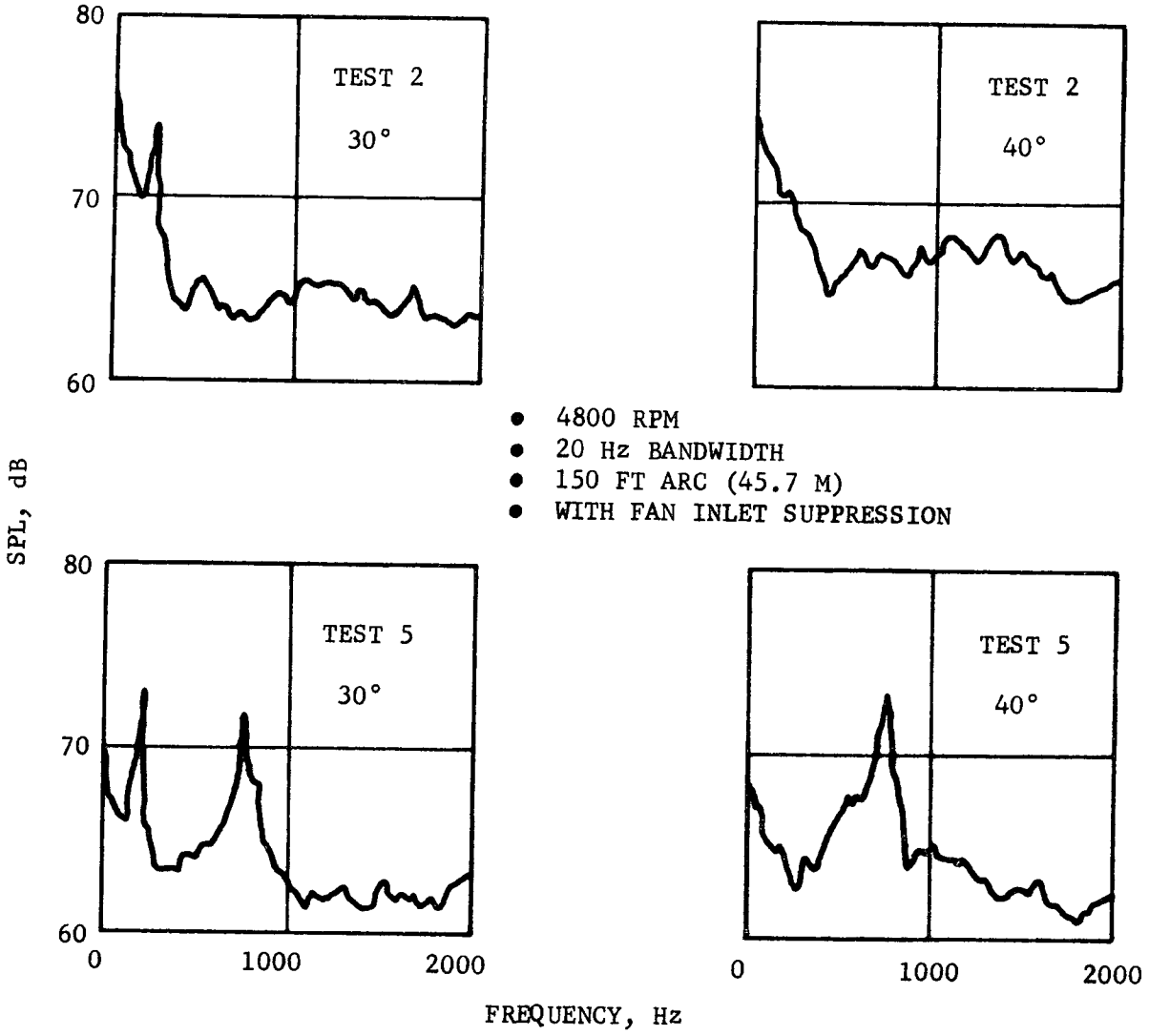

Figure 183. LF336/B Forward Quadrant Low Frequency Narrowbands at 4800 RPM

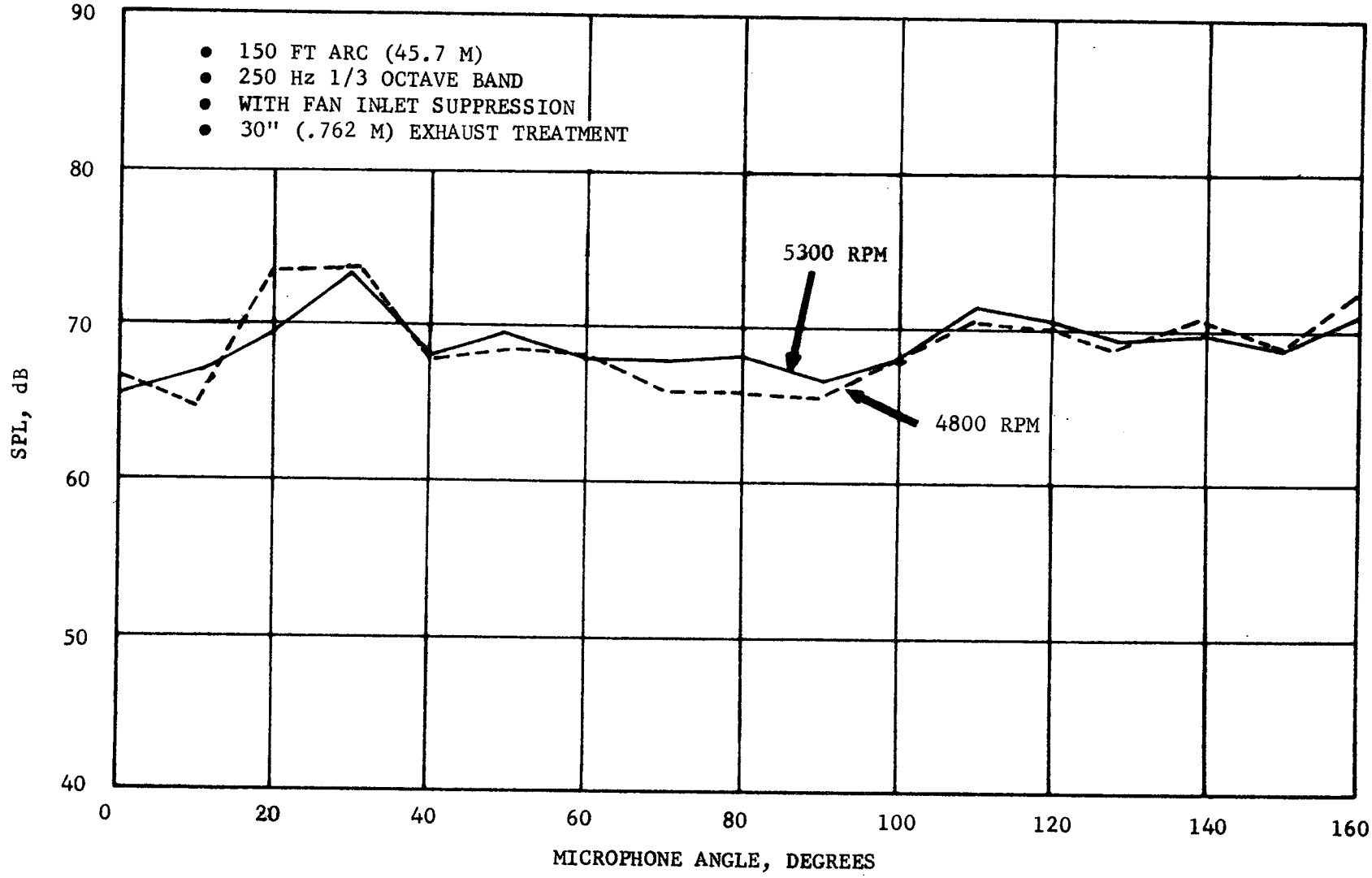

Figure 184. LF336/B 250 Hertz 1/3 Octave Band Sound Pressure Level Directivity Pattern

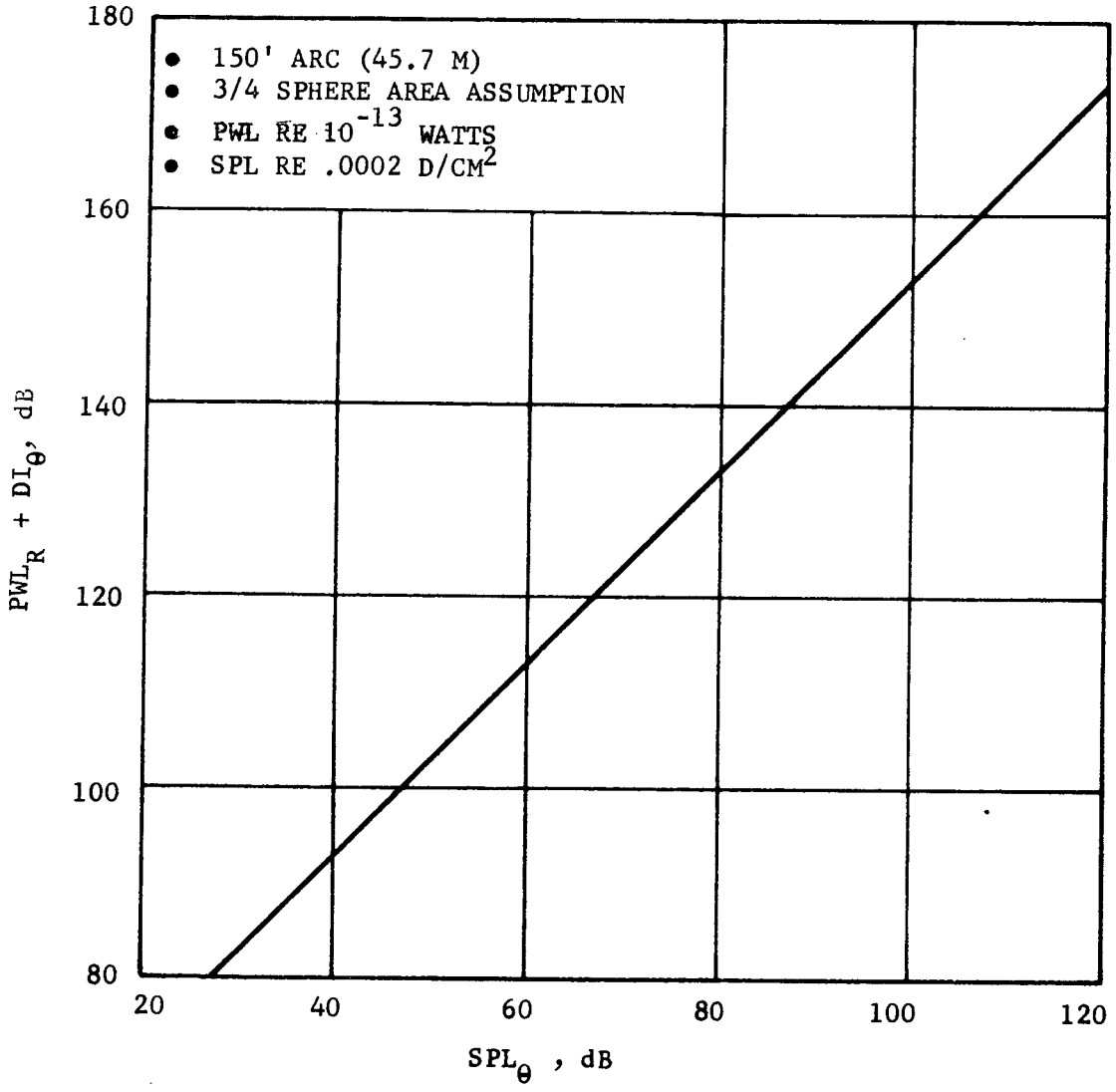

Figure 185. Relationship Between 150 foot (45.7 m) Sound Power Level, Directivity Index and Sound Pressure Level

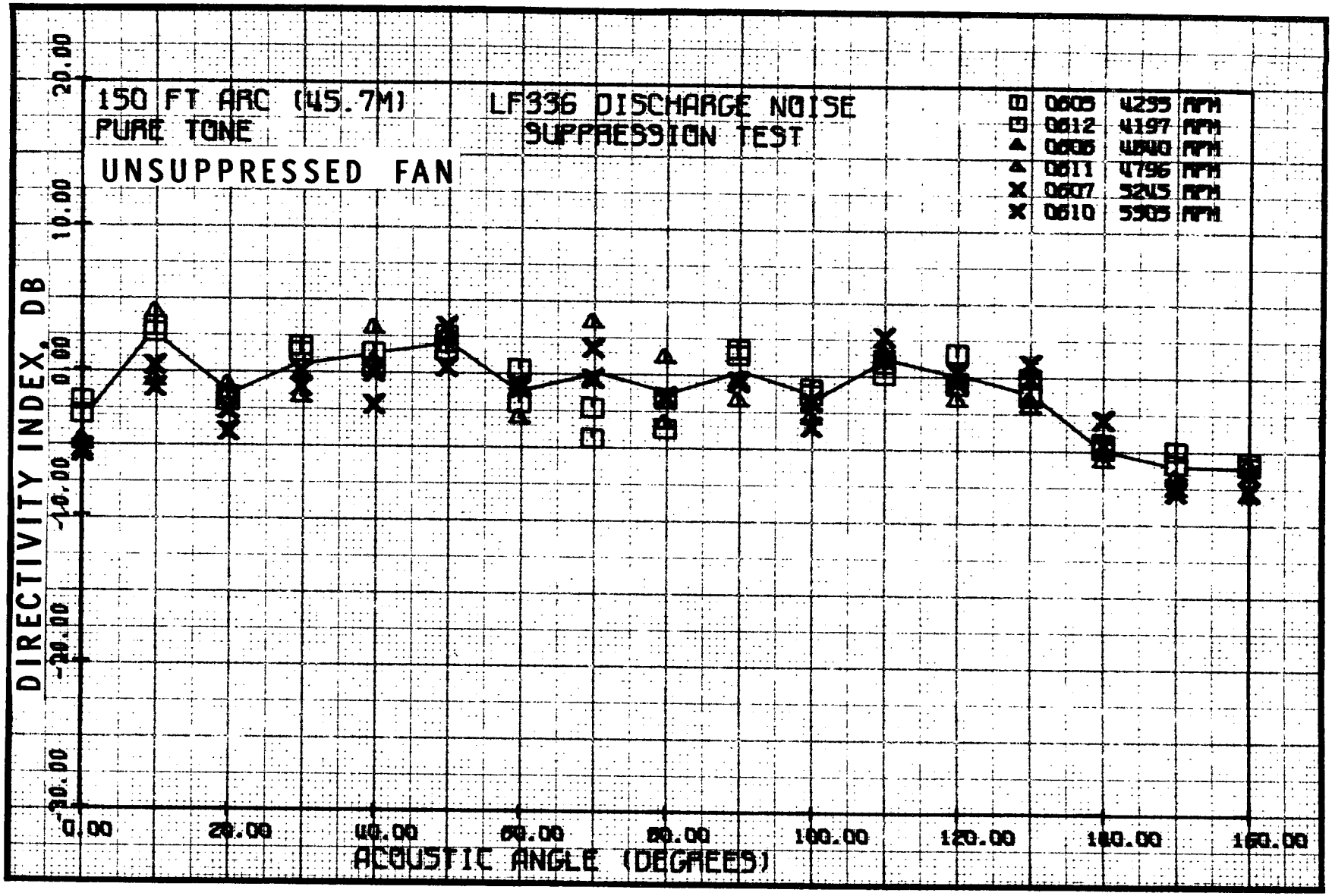

Figure 186. LF336/B Unsuppressed Pure Tone Directivity Indices

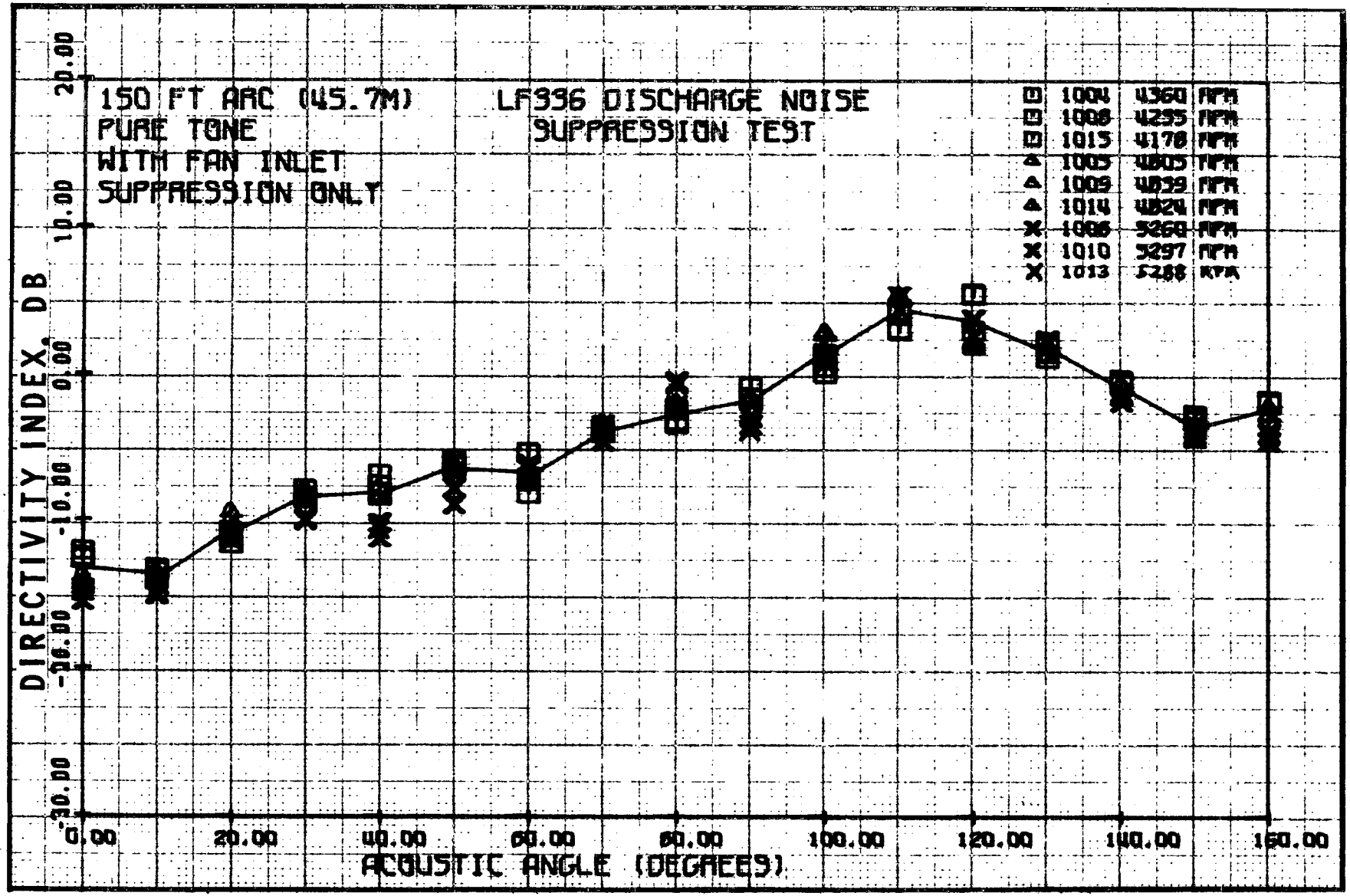

Figure 187. LF336/B Pure Tone Directivity Indices with Fan Inlet Suppression

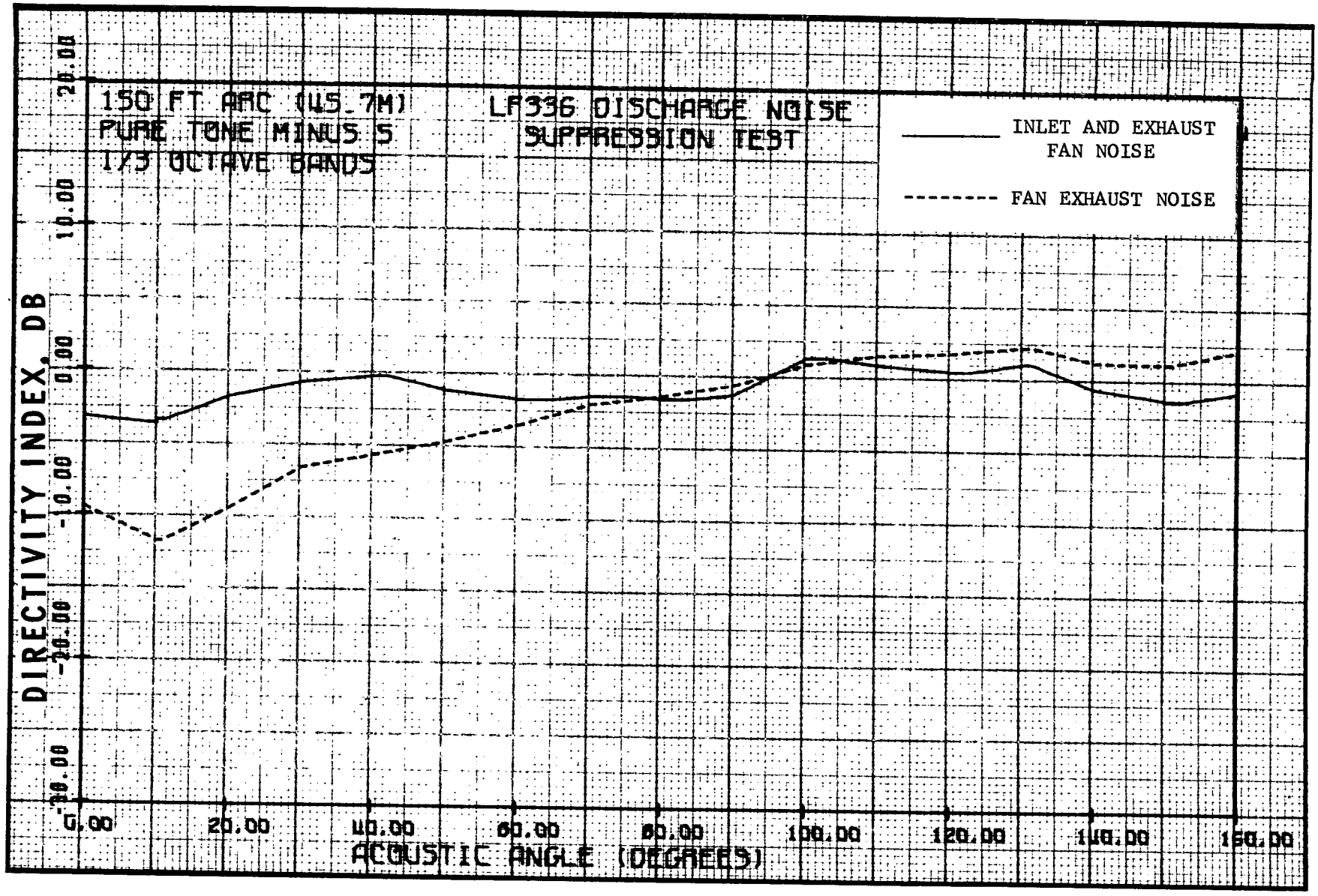

Figure 188. LF336/B Directivity Indices Five 1/3 Octave Bands below the Pure Tone Band

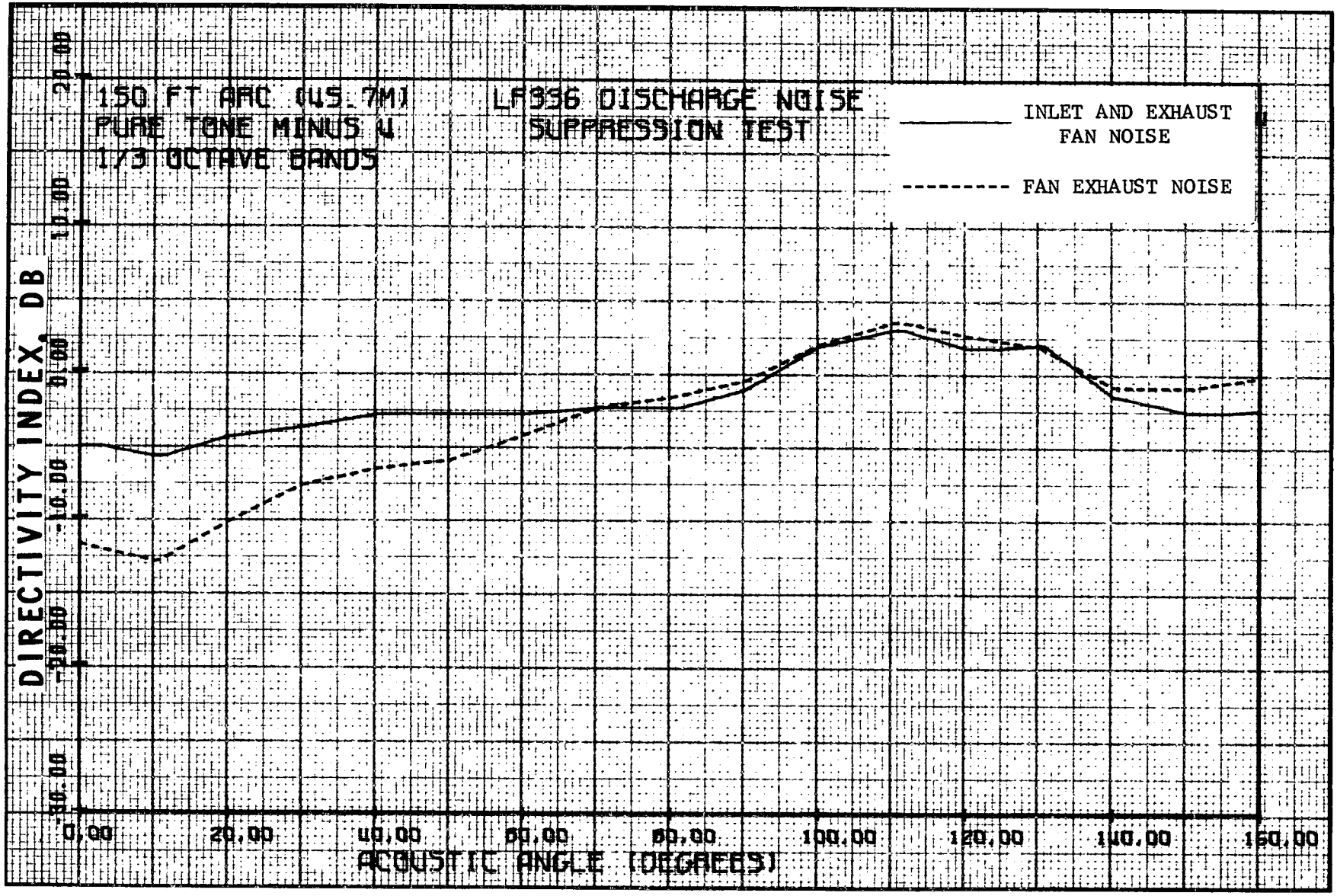

Figure 189. LF336/B Directivity Indices Four 1/3 Octave Bands below the Pure Tone Band

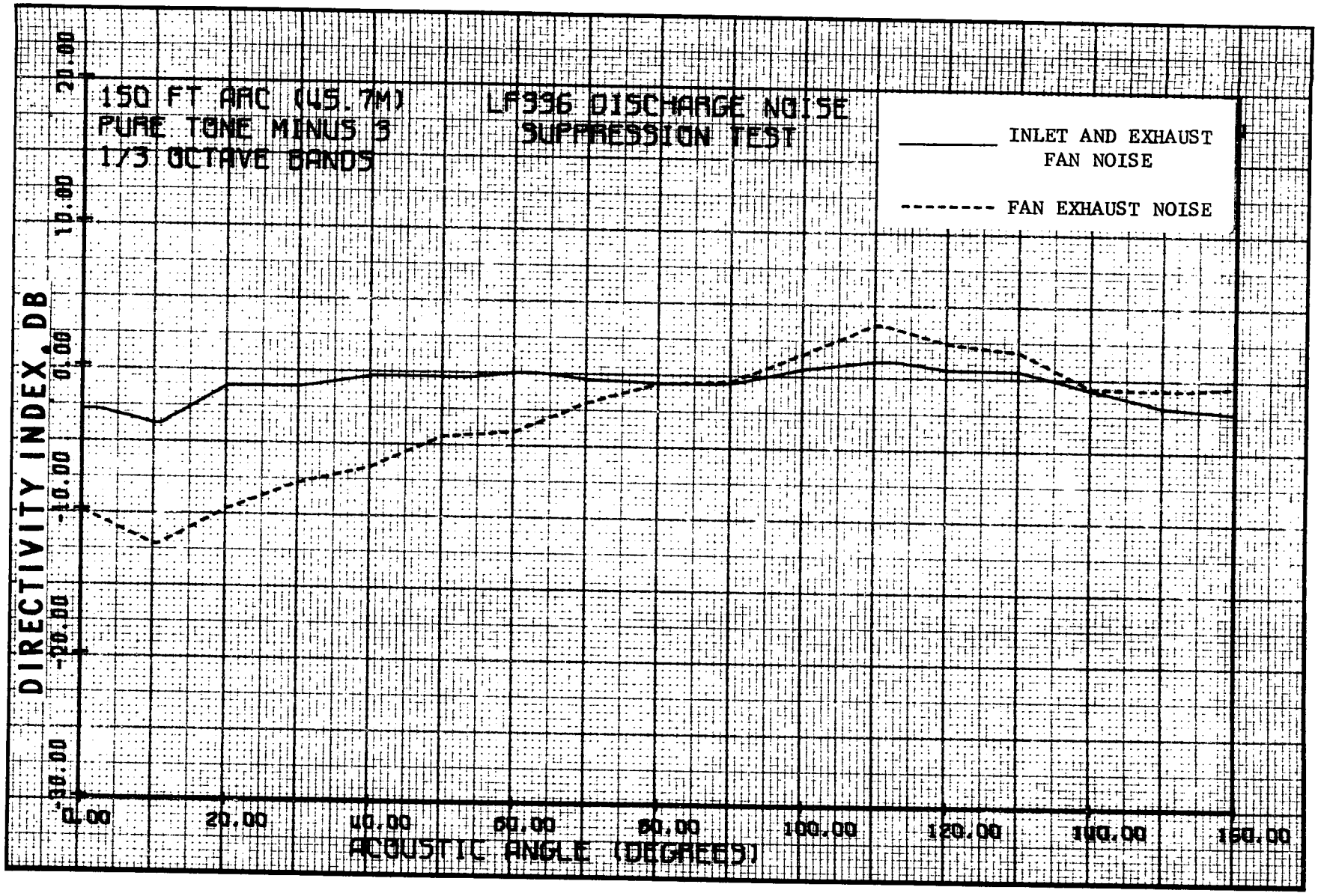

Figure 190. LF336/B Directivity Indices Three 1/3 Octave Bands below the Pure Tone Band

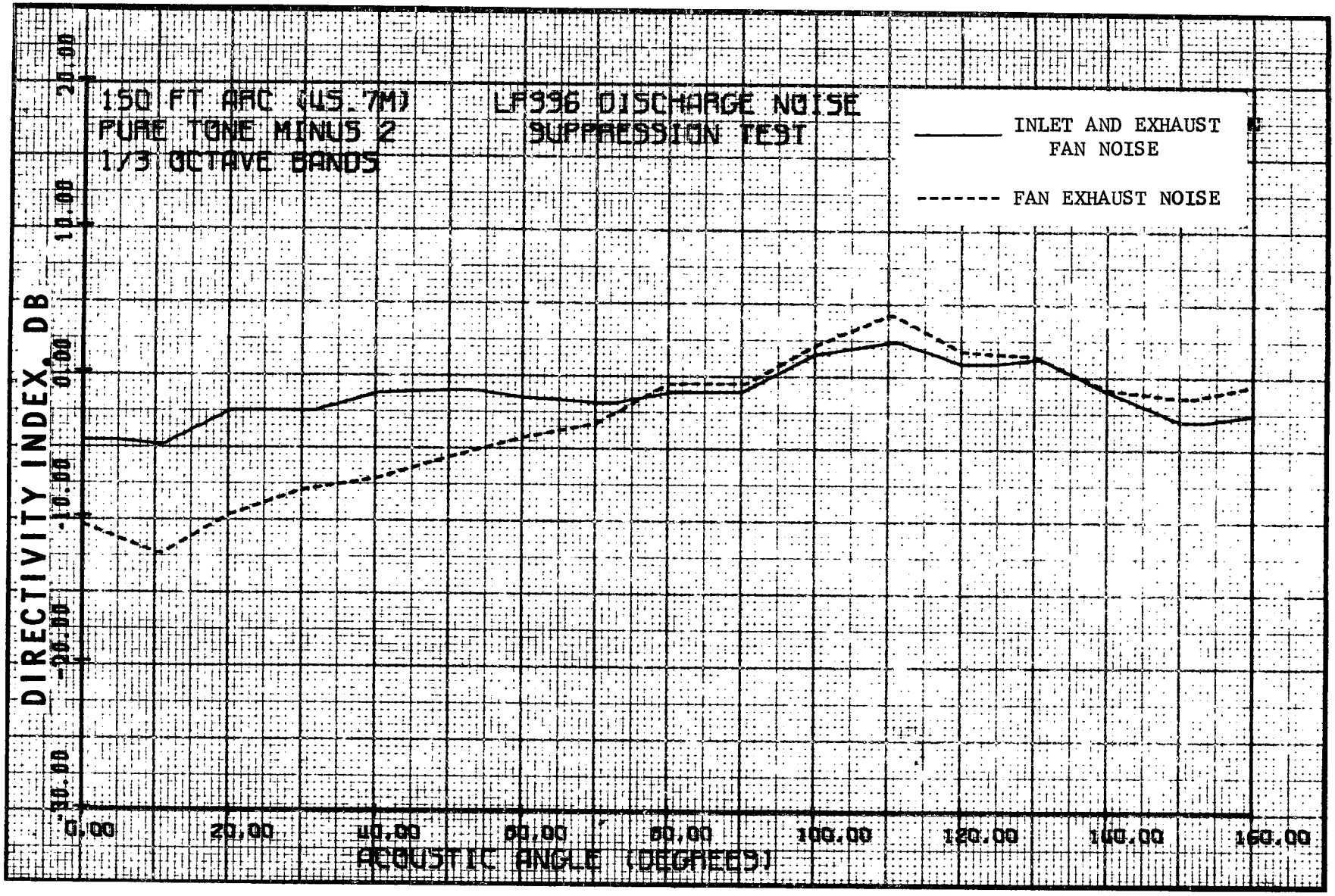

Figure 191. LF336/B Directivity Indices Two 1/3 Octave Bands below the Pure Tone Band

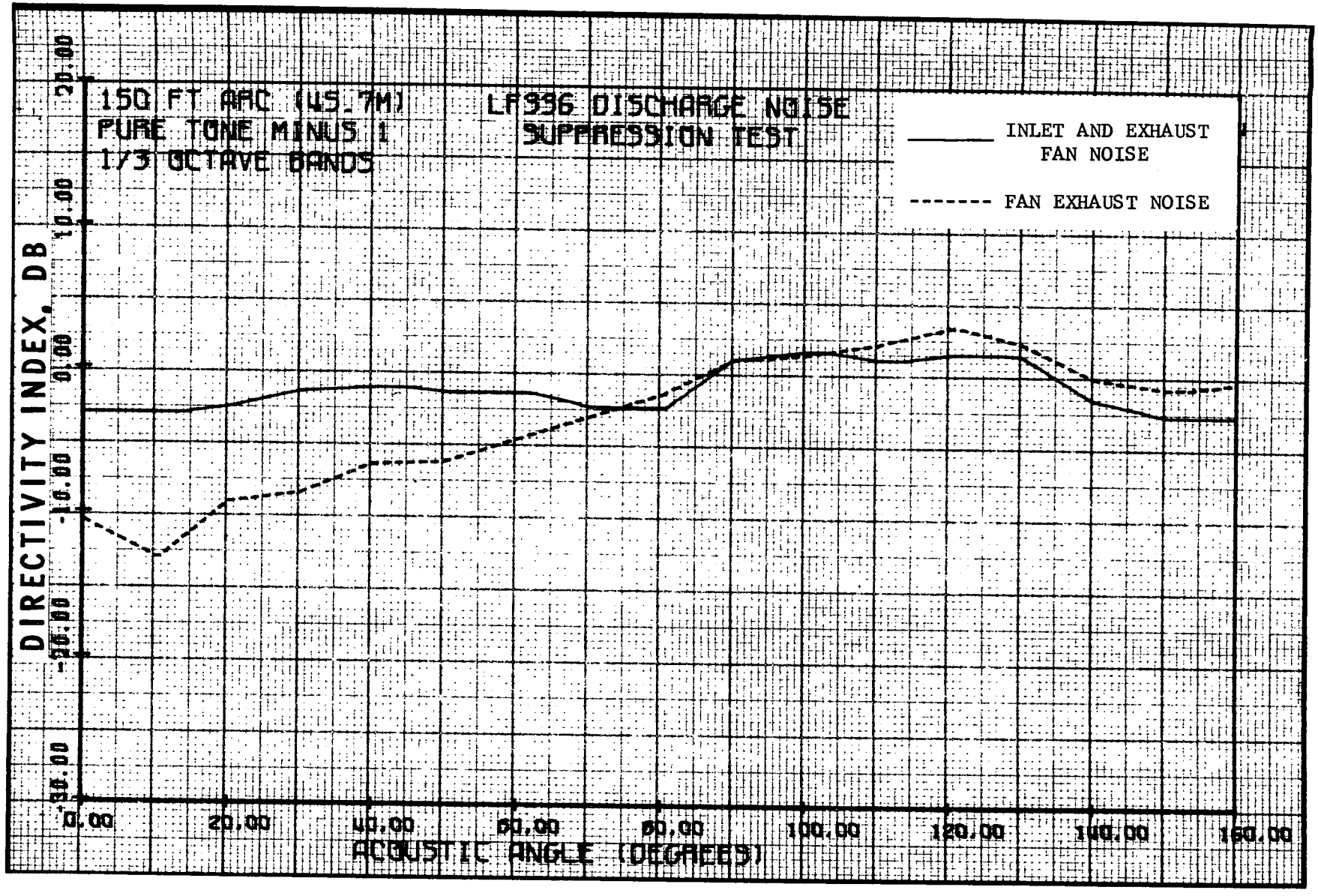

Figure 192. LF336/B Directivity Indices One 1/3 Octave Bands below the Pure Tone Band

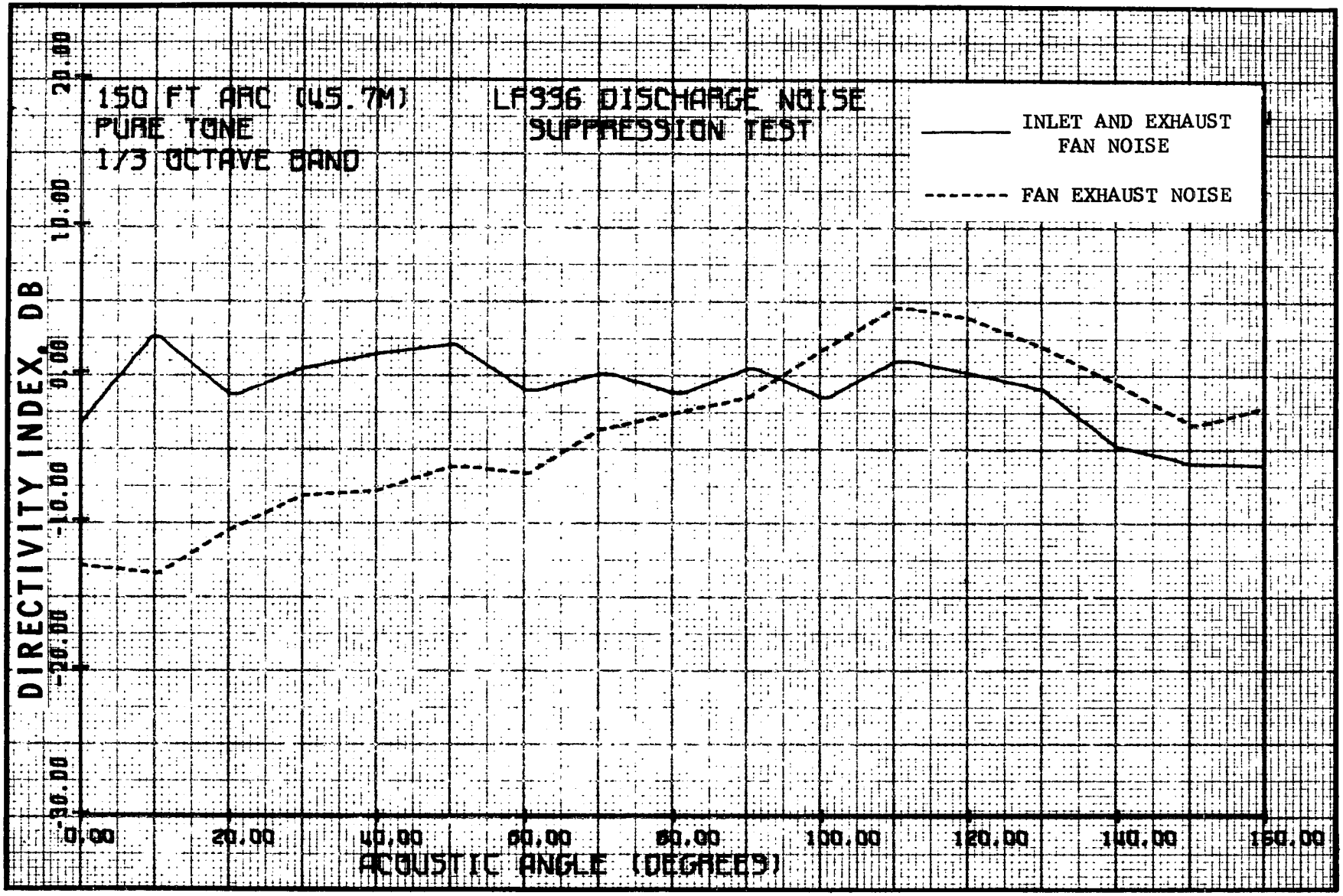

Figure 193. LF336/B Pure Tone Directivity Indices

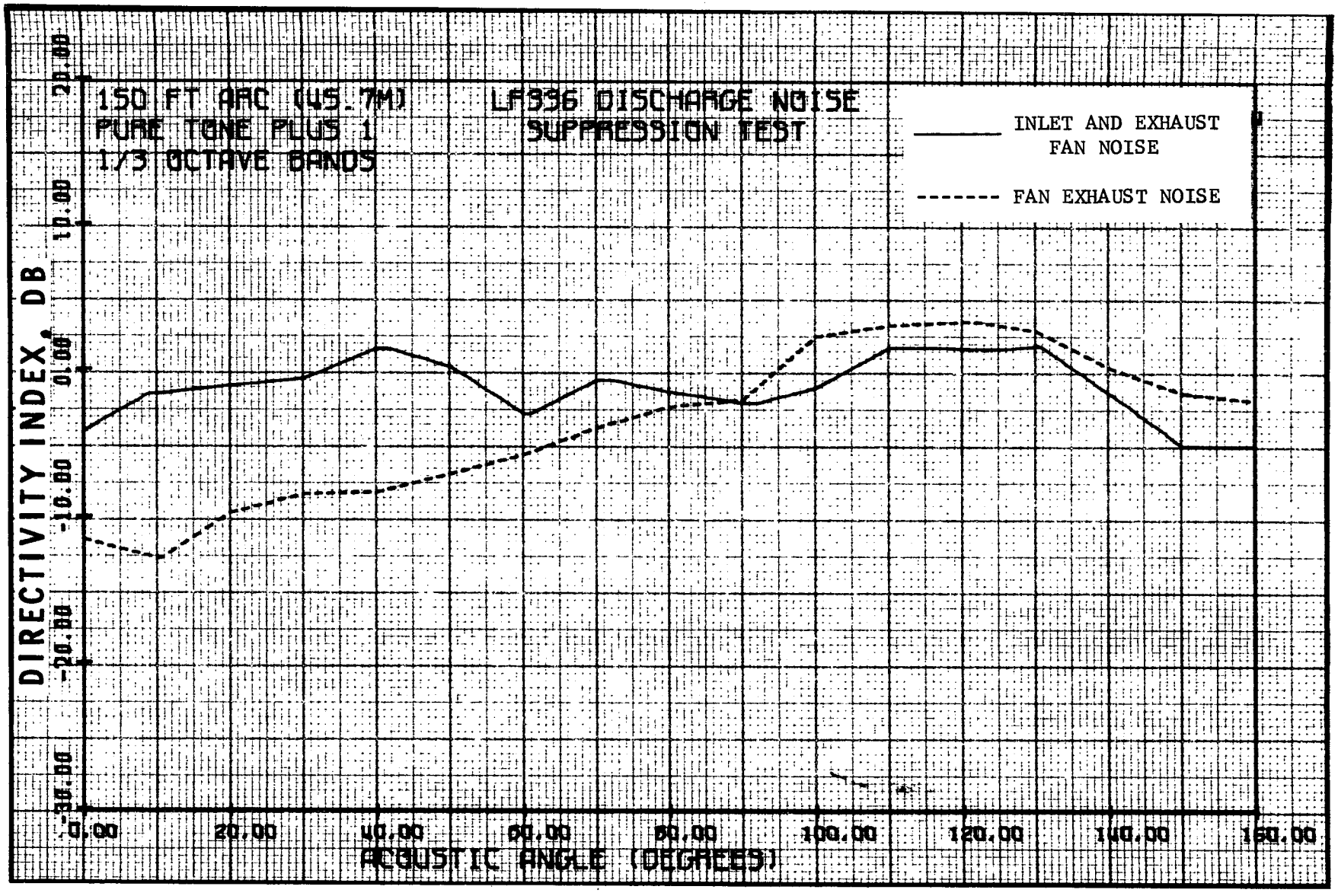

Figure 194. LF336/B Directivity Indices One 1/3 Octave Bands above the Pure Tone Band

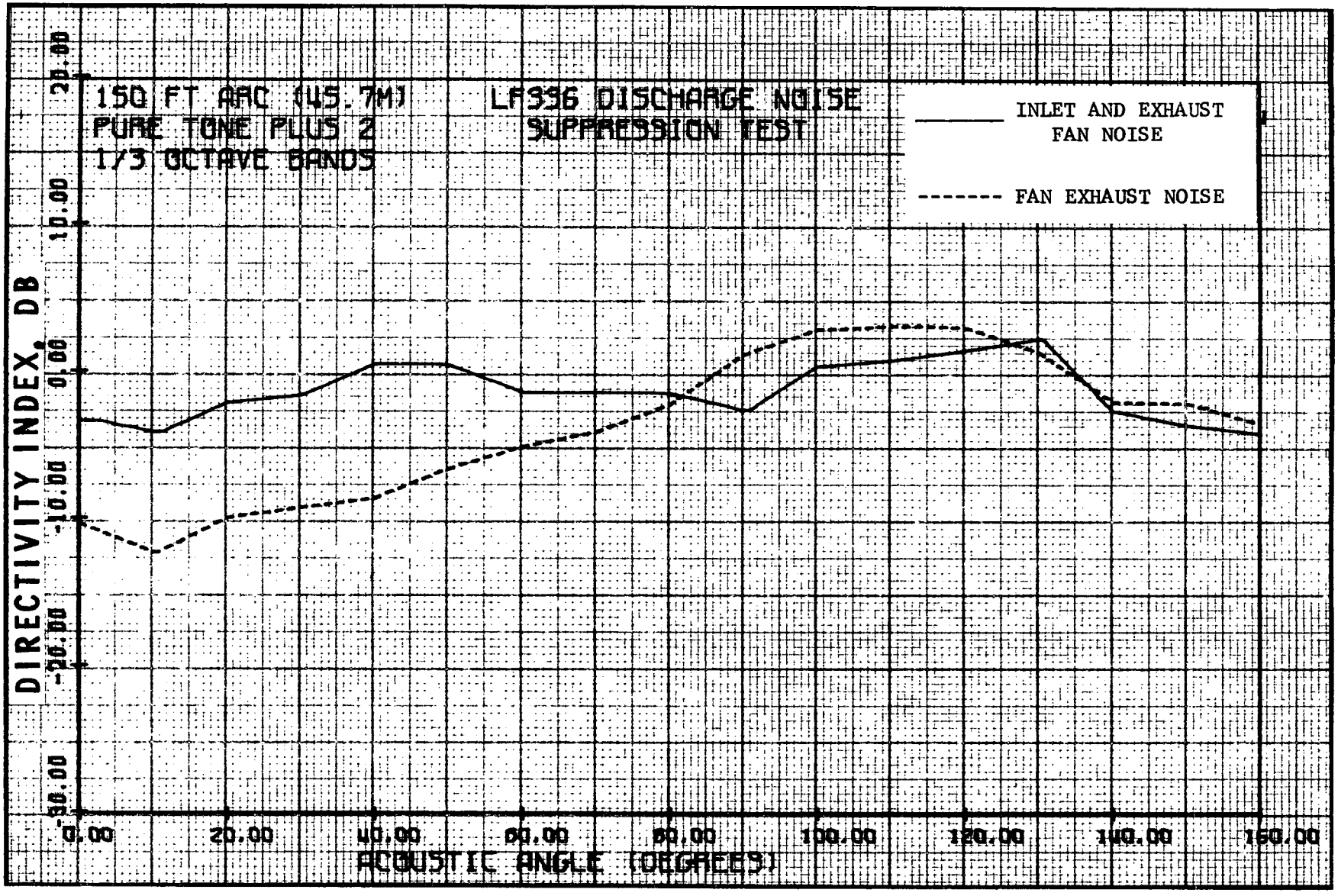

Figure 195. LF336/B Directivity Indices Two 1/3 Octave Bands above the Pure Tone Band

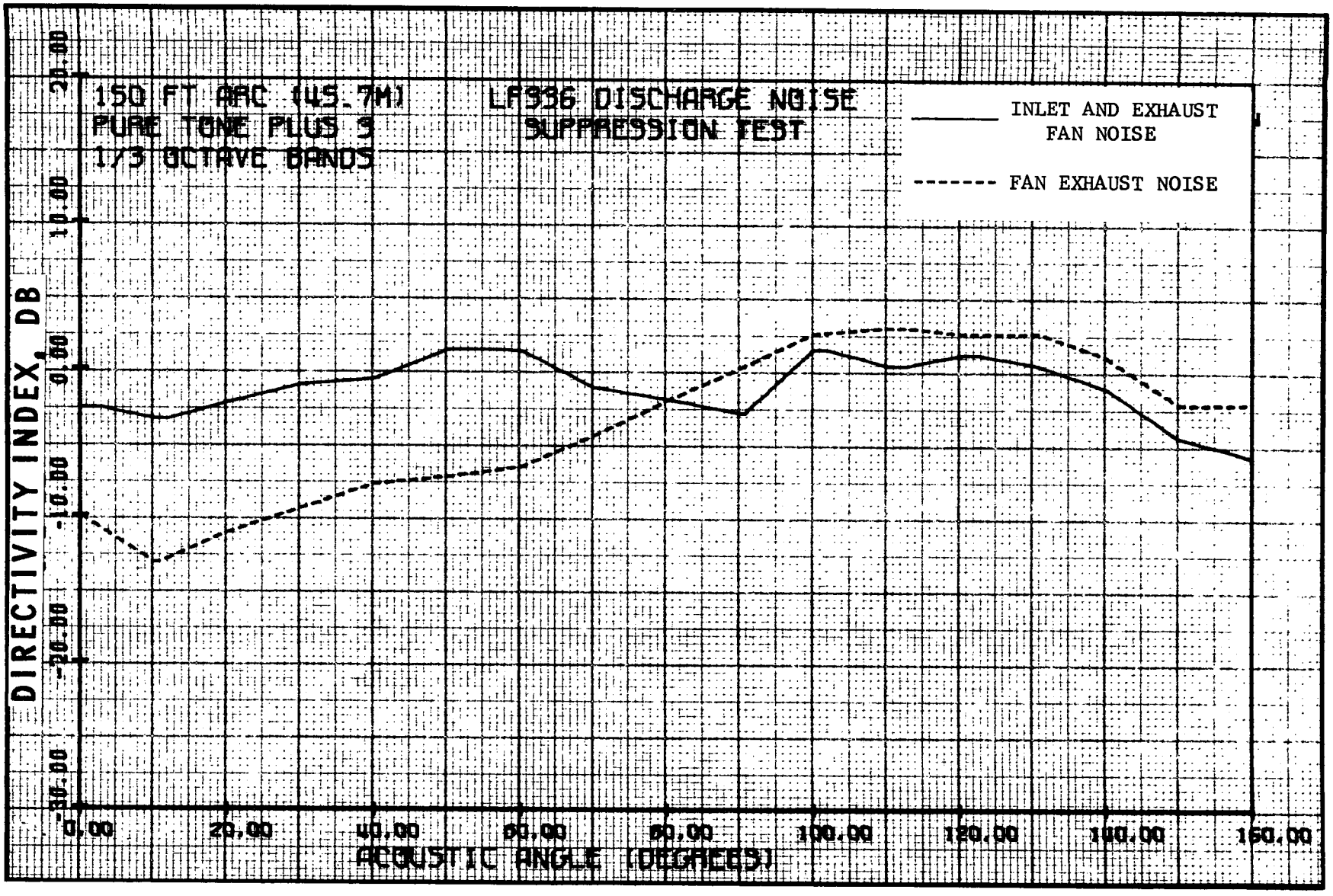

Figure 196. LF336/B Directivity Indices Three 1/3 Octave Bands above the Pure Tone Band

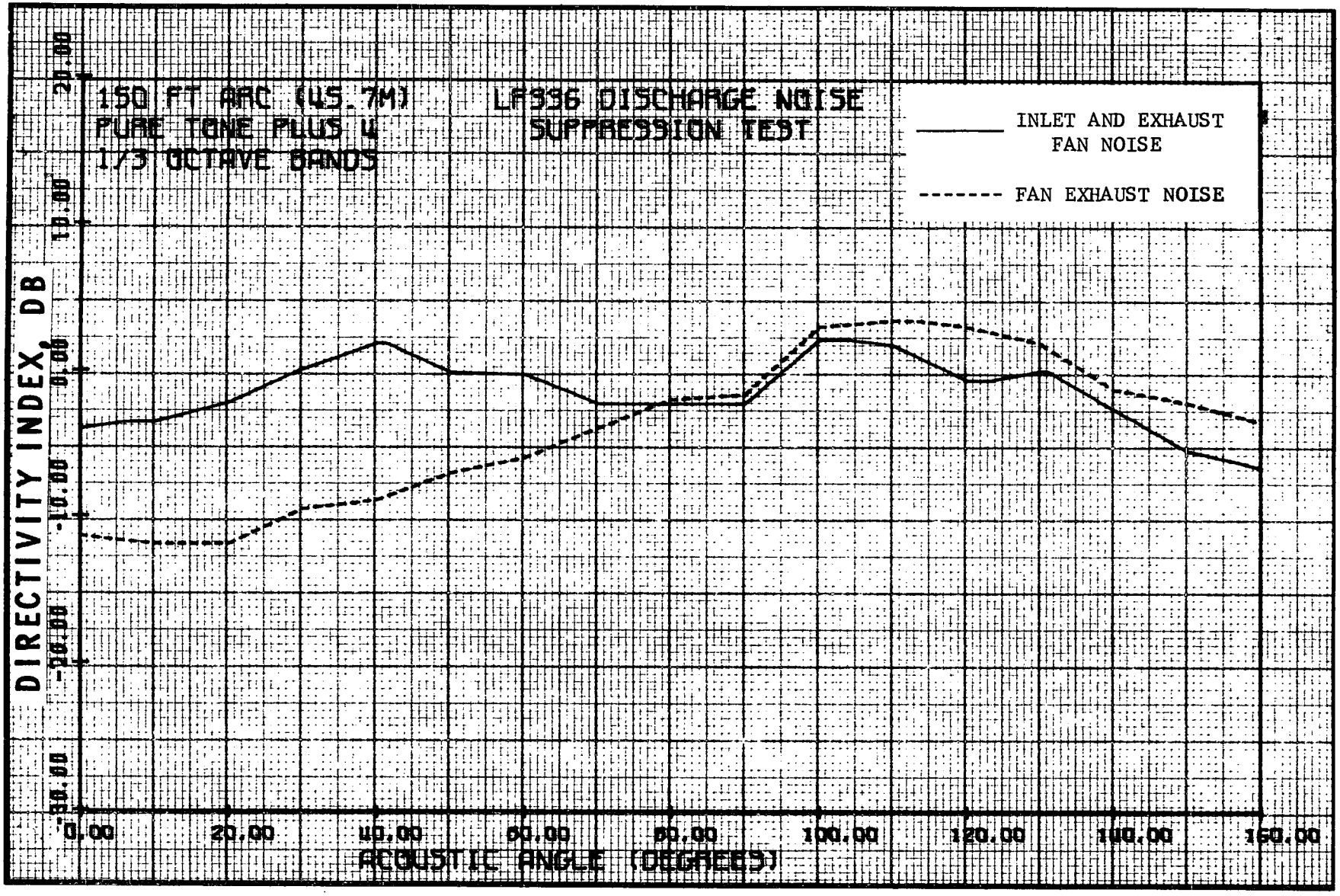

Figure 197. LF336/B Directivity Indices Four 1/3 Octave Bands above the Pure Tone Band

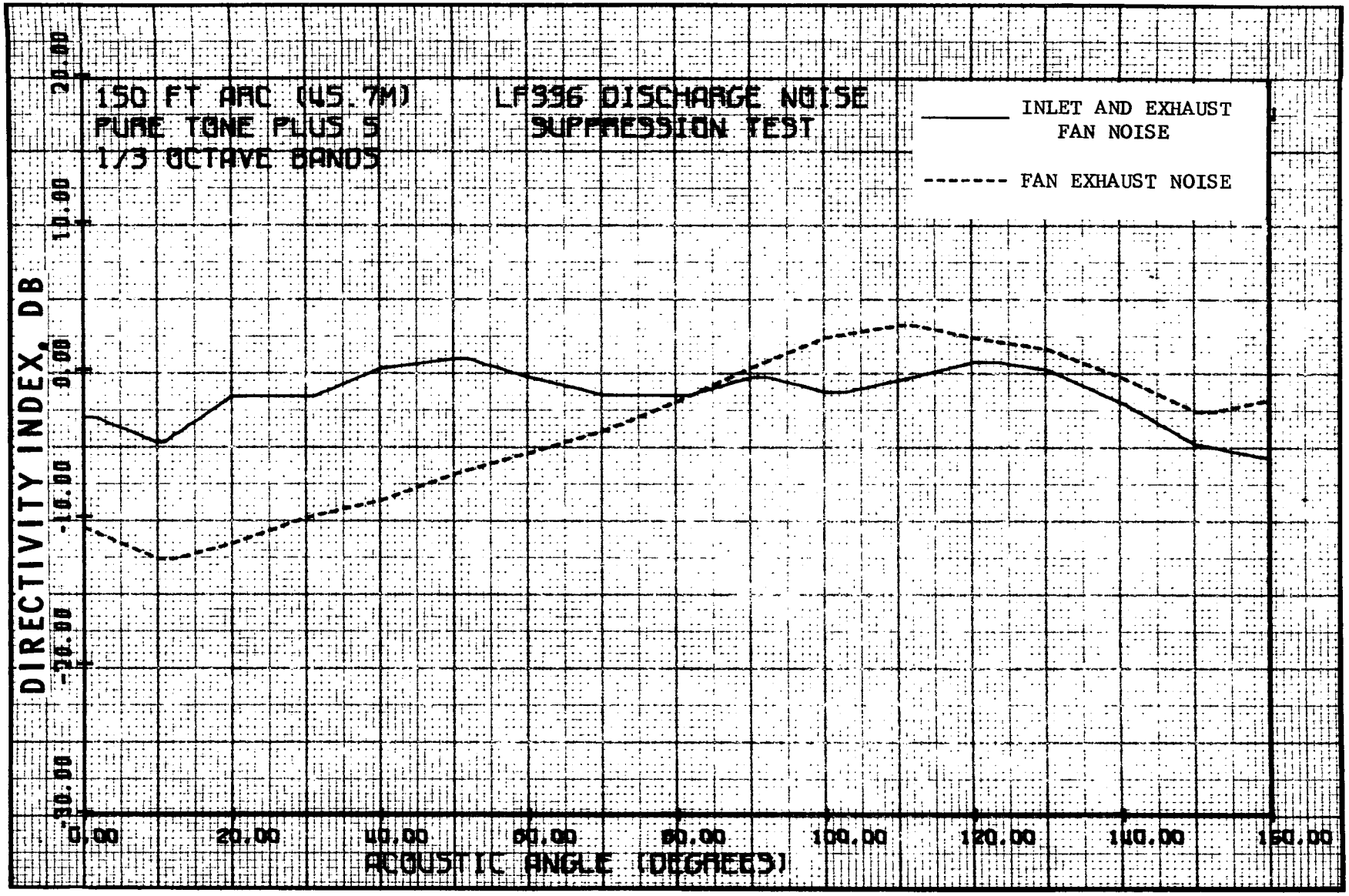

Figure 198. LF336/B Directivity Indices Five 1/3 Octave Bands above the Pure Tone Band